Crystal Engineering of Co-ordination Polymers (CPs) Derived from *Bis*-pyridyl amides and Analyzing Their Structural Transformations Triggered by External Stimulus

THESIS

Submitted in partial fulfillment of the requirements for the Degree of

Doctor of Philosophy

by

Kumari Suman ID - 2010PHXF422P

Under the Supervision of

Dr. Madhushree Sarkar

Birla Institute of Technology and Science Pilani, Pilani Campus
Pin - 333031 Rajasthan, INDIA
December 2016

Dedicated to My Son

Samar Malik

BIRLA INSTITUTE OF TECHNOLOGY AND SCIENCE

PILANI (RAJASTHAN)

CERTIFICATE

This is to certify that the thesis entitled **"**Crystal Engineering of Co-ordination Polymers (CPs) Derived from Bis-pyridyl amides and Analyzing Their Structural Transformations Triggered by External Stimulus**"** submitted by **Mrs. Kumari Suman** ID No **2010PHXF422P** for the award of Ph. D. Degree of the Institute embodies the original work done by him under my supervision.

Signature in full of the Supervisor:

Name in capital block letters: **Dr. MADHUSHREE SARKAR**

Designation: Assistant Professor

BITS Pilani, Pilani Campus

Date:

TABLE OF CONTENTS

TABLE OF CONTENTS

TABLE OF CONTENTS

TABLE OF CONTENTS

TABLE OF CONTENTS

TABLE OF CONTENTS

ACKNOWLEDGEMENTS

I would like to pay my gratitude and respect to my supervisor, Dr. Madhushree Sarkar for her invaluable guidance and continuous encouragement throughout my research work. I deeply thanks her for encouragement that carried me on through difficult times and for her insights and suggestions that helped to shape my research skills. Her inspiring guidance and constant motivation have helped me to understand better and remain optimistic during the course of my study. Although this eulogy is insufficient, I preserve an everlasting gratitude to her.

I put forward my thanks to Prof. Souvik Bhattacharyya, Vice-chancellor and Prof. A.K. Sarkar, Director, Birla Institute of Technology & Science, Pilani (BITS Pilani), Pilani Campus, for allowing me to pursue my research work successfully. I am immensely thankful to Deputy Directors and Deans of BITS Pilani for providing necessary facilities and financial support. I also express my sincere gratitude to Prof. S. K. Verma (Dean, ARD, BITS Pilani), for his constant support, timely help and encouragement. I sincerely thanks Prof. Hemant R Jadhav (Associate Dean, ARD, BITS Pilani) for his cooperation and constant guidance during each phase of my research work. I also express my thanks to the office staff of ARD, whose secretarial assistance helped me in submitting the various evaluation documents in time.

I am grateful to the members of my Doctoral Advisory Committee, Dr. Subit Kumar Saha and Dr. Saumi Ray for their great cooperation in refining my thesis. I sincerely thanks to Dr. Anil Kumar (Dean, WILP Division, Ex-Head of Dept.) and Head of Department of chemistry, Dr. Bharti Khungar for providing me all the departmental facilities. I am thankful to all the respectable faculty members of the Department of Chemistry, BITS Pilani for their generous help and support along with fruitful discussions during the different stages of my doctoral study. Thanks are also to all the office staff of the department for their help during my work. I am very much thankful to my lab-mates, Mr. Ashok Sharma, Mrs. Archana Choudhary, Ms. Moyana Das, Ms. Sushila Poonia, Ms. Pallavi Rao, Ms. Pragati, Mr. Fayaz Baig, Mr. Ramraju, Mr. Mir Nishar, Mr. Sachin choudhary, Mr. Anoop Mewar and all research scholars of the Department of

Chemistry. A special thanks to my friends Mrs. Neelam Jakhar, Mrs. Surmila Sheoran and Mrs. Saroj Poonia for their help and charming company.

I would like to thank my parents (Shri Raghuveer Singh and Smt. Prem Devi), father in-law (Shri Ranjeet Singh) and mother in-law (Smt. Vidya Devi) for their love, inspirations, support, and never-ending blessings. I am very much thankful to my brothers (Mr. Virendra Bhambhu and Mr. Jitendra Bhambhu) for their love & affection. I extend my heartfelt thanks to my husband, Mr. Rohit Malik for his love, motivation and accepting my decision in letting me pursue things with enormous encouragement. Without his love, encouragement, co-operation and sacrifice, successful achievement of this work would have only remained a dream.

My thanks are duly acknowledged to BITS Pilani and UGC for Basic Research Fellowship (UGC-BSR) for their financial support. Finally, I want to thanks Department of School Education, Haryana to permit me to complete this degree.

Kumari Suman

ABSTRACT

The thesis entitled – **"Crystal Engineering of Co-ordination Polymers (CPs) Derived from Bis-pyridyl amides and Analyzing Their Structural Transformations Triggered by External Stimulus"** deals with the synthesis of flexible reverse *bis*-pyridyl-*bis*-amide ligands having different alkyl spacer and their co-ordination polymers (CPs) with Cu(II) and Cd(II). The detailed structures of the co-ordination polymers are determined using single crystal XRD technique. The chapter 1 of thesis provides the literature survey on structure of the CPs, their post synthetic modification and various applications related to porous nature. The different networks of 4.4'-*Bi*pyridine and other bidentate ligands are discussed and the effect of introducing hydrogen bonding moiety in the ligand on the network geometry is analyzed. The intermolecular interactions *i.e.* hydrogen bonding, π-π interactions, co-ordinate bond interaction and their strength and role in organizing supramolecular geometry is also discussed. Chapter 2 deals with the instrumental techniques, used by us in our work for characterization of CPs.

Chapter 3 of thesis is about the synthesis CP of ligand **1a** with Cu(II) salts, where the ligand **1a** is a *bis*-pyridyl-*bis*-amide with ethyl spacer. The ligand **1a** formed 1D-looped chain network **(CP1)** with $Cu(PF_6)_2$, where the anion PF_6^- involved in hydrogen bonding with the amide and resulted in unavailability of space for guest inclusion in the loops. The exchange of PF_6^- ion with ClO_4^- ion resulted in the intake of aromatic guest molecules, which were monitored by IR and UV-Vis spectroscopy. The capability of the flexible ethyl spacer of **1a** to adjust the conformation according to the requirements of the other components of the networks is observed in this chapter. This resulted in reversible inclusion and removal of guest molecules triggered by the exchange of anions.

In Chapter 4, CPs of ligand **1b** with $Cu(ClO_4)_2$ resulted 2D network (**CP3**), which showed two-fold parallel interpenetration; whereas with $Cd(ClO_4)_2$ is a 1D network with rectangular loops (**CP4**). The metal metathesis of **CP4** with Cu(II) resulted in isomorphous replacement of the Cd(II) centre with that of Cu(II) and resulted **CP5**. Transmetallation reaction resulted in retaining the structural features of **CP4** even in case of flexible ligand. The CP formed *via* transmetallation

couldn't be synthesized from the direct reaction of *bis*(3-pyridyl)butanediamide and $Cu(ClO_4)_2$. The transmetallation kinetic studies are performed with AAS and WD-XRF.

In Chapter 5 co-ordination polymers (CPs) of ligand **1b** has been found to be directed by the anion of the starting metal salt: a 1D network with rectangular loops (**CP6**) for $CuSO_4$ and a 2D network having two-fold parallel interpenetration (**CP3**) for $Cu(ClO_4)_2$. In the 1D network a π•••π interaction between C=O groups of the amide is present while in the 2D network an amide-to-amide hydrogen bond is present. On the other hand, ligand **1b** with $Cu(C_6H_5COO)_2$ results in a 1D chain (**CP7**), where the benzoate units are also co-ordinated to the Cu(II) centers. The role of the counter anions (ClO_4^-, SO_4^{2-} and $C_6H_5COO^-$) towards the formation of the CPs was monitored through the competitive reactions, where the ligand was allowed to react with $Cu(NO_3)_2$ in the presence of other three counter anions at a time. Further, an understanding on the network stability was gained by studying the counter anion exchange reactions.

In chapter 6, photo physical properties and photo-catalytic activities are discussed, where the structure property relationship was studied. Finally, Chapter 7 gives the overall conclusion of the thesis and the future scope of the work.

LIST OF SYMBOLS & ABBREVIATIONS

α	Alpha
β	Beta
Å	Angstrom
θ	Theta
μ	nu
ε	Epslon
λ	Lambda
φ	psi
δ	Delta
ω	Omega
ν	mu
bipy	4,4'-Bipyridine
CPs	Co-ordination polymers
MOFs	Metal Organic Frameworks
1D	One Dimensional
2D	Two Dimensional
3D	Three Dimensional
SCSC	Single-Crystal-to-Single-Crystal
ISO	N-N'-bis-(pyridine-4-ylmethyl)isophthalamide
PSM	Postsynthetic Modification
PSD	Postsynthetic Deprotection

LIST OF SYMBOLS & ABBREVIATIONS

FT-IR	Fourier Transform Infrared
NMR	Nuclear Magnetic Resonance
XRD	X-Ray Differection
MeOH	Methanol
EtOH	Ethanol
n-PrOH	Propanol
DCM	Dichloromethane
DMF	Dimethylformamide
DMSO	Dimethylsulfoxide
TEA	Triethylamine
THF	Tetrahydrofuran
WD-XRF	Wavelength Dispersive X-ray Fluorescence
ED-XRF	Energy Dispersive X-ray Fluorescence
AAS	Atomic Absorption Spectroscopy
TGA	Thermo gravimetric Analysis
TG	Thermogravimetry
DTG	Differential Thermo Gravimetric
SEM	Scanning Electron Microscopy
5-AIP	5-aminoisophthalic
MB	Methylene Blue

LIST OF SYMBOLS & ABBREVIATIONS

LIST OF TABLES

LIST OF SCHEMES

LIST OF FIGURES

LIST OF FIGURES

LIST OF FIGURES

LIST OF FIGURES

LIST OF FIGURES

LIST OF FIGURES

Chapter 1

Introduction

1.1 Supramolecular Chemistry & Crystal Engineering

1.1.1 Supramolecular chemistry:

Supramolecular chemistry is defined as: "The chemistry of molecular assemblies and of the intermolecular bond" by Jean-Marie Lehn. He along with Donald J. Cram and Charles J. Pedersen were awarded Nobel Prize in 1987 for their pioneering work in this field.[1-5] Supramolecular chemistry, Chemistry beyond the molecule, is defined in terms of the non-covalent interaction between a 'host' and a 'guest' molecule. Figure 1.1 illustrates an analogy between molecular and supramolecular chemistry in terms of both structures and function according to Lehn.[6,7]

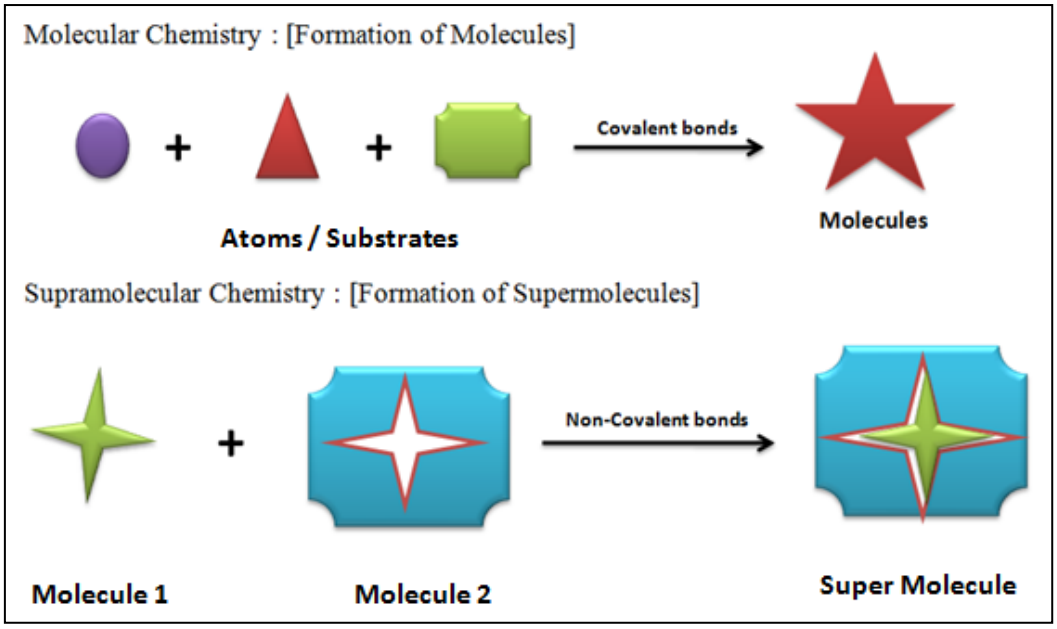

Figure 1.1: A schematic showing the formation of molecules and super molecule defined by Lehn [1-5]

Studies on crown-ethers marks the beginning of supramolecular chemistry while the development of selective "host-guest" complexes in particular, in which a host molecule recognizes and selectively binds certain guest, is an important milestone in this area. [8-10] Three decades later also supramolecular chemistry is an important, interdisciplinary branch of science. The riches of this area have been extended to polymer science [11], solid-state chemistry[12], and liquid-crystal[13] Researchers from the areas of physical, chemical, biological, computational & biochemical sciences have been benefitted from knowledge & resources in this area. The supramolecular chemistry has evolved as an interdisciplinary science with important applications in wide range of areas.

"Thus supramolecular chemistry involves investigating molecular systems in which the most important feature is that components are held together by weak intermolecular forces, not by covalent bonds".[14]

1.1.2 Crystal Engineering

In 1971, Schmidt used the term 'crystal engineering', while studying the photo-dimerisation reactions of cinnamic acids.[14] Later on in 1988, Desiraju defined 'crystal engineering' as "the understanding of intermolecular interactions in the context of crystal packing and the utilization of such understanding in the design of new solids with desired physical and chemical properties".[15] The concepts of crystal engineering are used in tailor - made the materials according to our requirement. The materials designed using the concepts of crystal engineering have potential applications in the areas of gas storage[16], separation and catalysis[17], sensors [18,19], host-guest chemistry[20,21], luminescence[22] photovoltaic cells[23] and semiconductors[24].

The primary task in crystal engineering is to predict the network architectures resulting from different building blocks. Supramolecular synthons,[25] which is defined as "a structural unit within a super molecule, which can be formed or assembled by known or conceivable synthetic operations involving intermolecular interactions", will lead to identify the recurring intermolecular interaction pattern between various functional groups. The Cambridge Structural Database (CSD) is an important research tool which gives us the survey of all reports on various compounds.[26,27] The information available in CSD includes compound name, journal reference, molecular formula, unit-cell parameters, space-group and symmetry operators, atomic coordinates and R-factors. This data is useful to understand the supramolecular synthons of various functional groups, geometrical constraints in the occurrence of any intermolecular interaction and to identify structure-property relationship. The information availed from CSD along with other databases is required to design the new materials with predefined properties.

1.2 Intermolecular Interactions in Supramolecular Chemistry

As crystal engineering deals with predicting and designing the structures of new materials, an understanding of intermolecular interactions is the most important part. In supramolecular chemistry, knowledge of non-covalent interactions is important to determine the structure of

the networks. Non-covalent interactions are structure directing and dictates the overall supramolecular architecture. The molecular aggregates and assemblies of higher complexities is the outcomes of all the intermolecular interactions. Most of these interactions are electrostatic in nature, when the contributing molecules are permanently charged species or polar in nature. Non-polar molecules can also generate significant non-bonded interactions, strength of which are less when compared to charged species. Some of the non-covalent interactions include: Hydrogen bonding, π•••π interactions, Dipole-Dipole, Ion-Dipole, Ion-Ion, Halogen-Halogen interactions, van der Waals and Hydrophobic interactions (Table 1.1).

Table 1.1 Types of Non-covalent Interactions

Interaction	**Strength (kJ mole^{-1})**	**Examples**
1. Hydrogen Bonding	120 – 4	Details are given in Table 1.2
2. π-π interactions	50 – 0.05	Benzene, Toluene (discussed in 1.3)
3. Dipole-Dipole	50 – 5	HCl, Small Ketones
4. Ion- Dipole	200 – 50	$[Ru(bipy)_3]^{+2}$
5. Ion-Ion	300 – 200	Tetrabutylammonium chloride
6. van der Waals	Depends on surface area < 5 (Variable)	Ar, Kr any other ideal gas packed in molecular crystal
7.Hydrophobic interactions	Depends on solvent - solvent interaction energy	Cyclodextrin inclusion compounds

1.2.1 Hydrogen Bonding Interaction

Hydrogen bond interaction is the most commonly occurring interaction in small molecules as well as in biological systems such as the nucleic acids, proteins and polysaccharides.[28] Hydrogen bond interaction is electrostatic interaction present between a hydrogen atom, which is covalently bonded to an electronegative atom e.g. N, O, F etc (Donor) and another electronegative atom (Acceptor). Thus the hydrogen atom is simultaneously attracted to two atoms i.e. the covalently attached atom which acts as the hydrogen donor and another electronegative atom which acts as hydrogen acceptor (Figure 1.2).

Definitions of hydrogen bond interactions were given by many researchers. Latimer and Rodebush, in 1920s suggested that “a free pair of electrons on one water molecule might be

able to exert enough force on hydrogen held by a pair of electrons on another water molecule to bind the two water molecules together".[29] Later on Pauling defined hydrogen bond as largely ionic in character and formed only between the most electronegative atom.[30]

Pimentel and Mc Clellan in 1960 examined about 2000 cases, where hydrogen bonding existed. Based on their study, they defined hydrogen bonding by stating that "a hydrogen bond exists if (1) there is evidence of a bond and (2) there is evidence that this bond sterically involves a hydrogen atom already bonded to another atom".[31] This definition didn't specify the chemical nature of the atoms, such as their electro negativities, polarities, net charges and hence it can include various weak hydrogen bonds such as C-H•••O, C-H•••N and so on. In 1989 Atkins defined as: A hydrogen bond is a link formed by a hydrogen atom lying between two strongly electronegative atoms.[32]

Steiner in 2002 modified definition of the hydrogen bond as: "X-H•••A interaction is called a hydrogen bond if: (1) it constitutes a local bond, and (2) X-H acts as proton donor to A and A is called the acceptor".[33] Hydrogen bond is characterized by four parameters namely d, D, θ and φ (Figure 1.2). D and d are the X•••A and H•••A distances, respectively, whereas θ and φ are the X-H•••A and B-A•••H angles, respectively, the angle φ accounts for the directionality of the hydrogen bond. For the formation of a hydrogen bond, the D and d should be less than the sum of the van der Waals radii of the atoms.[33]

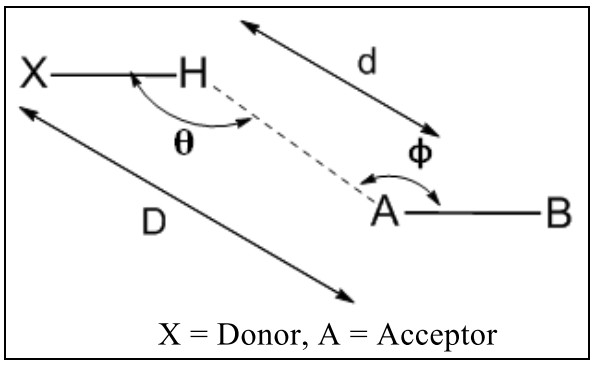

Figure 1.2: A schematic showing the formation of hydrogen bond.

Hydrogen bonding interactions can be classified based on their strength as: (1) very strong (2) strong and (3) weak hydrogen bonds [34] (Table 1.2). The strong hydrogen bonds are structure directing and due to the reproducibility in occurrence, structure prediction with the help of their known supramolecular synthons are quite reliable.

Table 1.2 Classification of hydrogen bonds based on strength.[34]

Types of hydrogen bonds	Bond Energy (kcal/mol)	Examples	D (X•••A)	d (H•••A)	θ range (°)	Lengthening of X-H bond [Å]	Effect on crystal packing
Very Strong	15-40	[F•••H•••F], $[N•••H•••N]^+$ P-OH•••O=P	2.2-2.5 Å	1.2-1.5 Å	170 -180	0.08-0.25 Å	High
Strong	4-15	O-H•••O=C N-H•••O=C O-H•••O-H	2.5-3.2 Å	1.5-2.2 Å	>130	0.02-0.08 Å	Distinctive
Weak	< 4	C-H•••O O-H•••π	<< H•••A	>3.2 Å	>90	< 0.02	Variable

The hydrogen bond interactions between the amide groups fall under this category. The amide groups are known to form self-complementary hydrogen bonds resulting in homomeric synthons. (Figure 1.3(a)). The presence of different functional groups can disturb the formation of homomeric synthons and result heteromeric synthons. For example, the presence of pyridyl moiety in amides can also involve in hydrogen bond formation (Figure 1.3(b)).

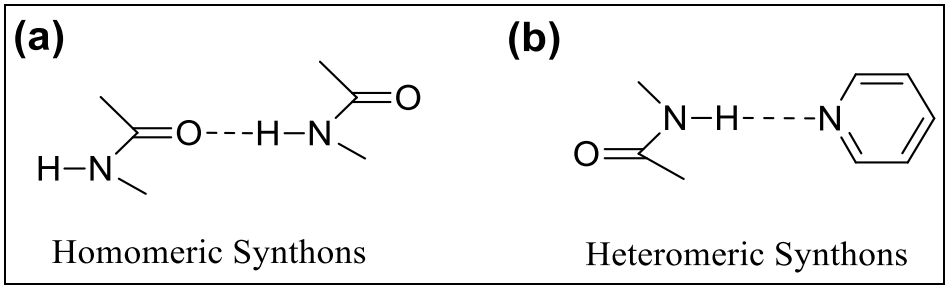

Figure 1.3 Supramolecular synthons of amide group (a) self complements (b) in presence of other functional group.

Hydrogen bond functionalities present in the co-ordination polymer (CPs) help in assembling the networks into higher dimensionality.[35-44] Assembling of co-ordination complexes and co-ordination polymers (CPs) *via* hydrogen bond interactions are widely reported by many researcher. Aakeröy *et al.* have used pyridyl-based ligands with certain functional groups e.g. carboxylic acids, amides and oximes, which are robust connectors for the formation of

hydrogen bonded networks in co-ordination complexes.[37-39] They have reported that a Ag(I) complex was propagated *via* self-complementary oxime•••oxime hydrogen-bond interaction.[39] Desiraju *et al.* and Braga *et al*. have introduced important results in the context of assembling the organometallic complexes *via* hydrogen bonds.[35,36,41,42] In the organometallic complexes of compounds containing carbonyl and amide, the hydrogen bond synthons present in the organometallic complexes were found to similar as that of the free compound. Hydrogen bond assembled transition metal macrocycle complexes were reported by Bazzicalupi *et al.*, where dizinc macrocyclic complex of Thymine and Uracil was assembled by intra and inter-molecular hydrogen bonding.[42] Goldberg *et al.* have studied the arrangements of metal-porphyrin building blocks *via* various hydrogen bonded interactions.[44]

1.2.2 π•••π Interactions

One of the important non-covalent interactions possible in aromatic molecules and also in compounds with π-bonds is the "π•••π stacking", or more generally "π•••π interactions". In biological systems, structures of proteins, DNA and RNA are stabilized by π•••π interactions and around 60 % of aromatic side chains in proteins participate in π•••π interactions. Hunter and Sanders in the early 1990s noted that the distribution of the electron density on most aromatic rings is such that it results in a quadrupole moment with partial negative charge above both aromatic faces and a partial positive charge around the periphery (Figure 1.4(a)).[45] But when any aromatic ring is attached with a electron-withdrawing groups, the polarization will take away the π-electron density from the aromatic core and thus creating a completely different electronic distribution. In this case, overall quadrupole moment results in relative electron deficiency in the central area (Figure 1.4(b)).

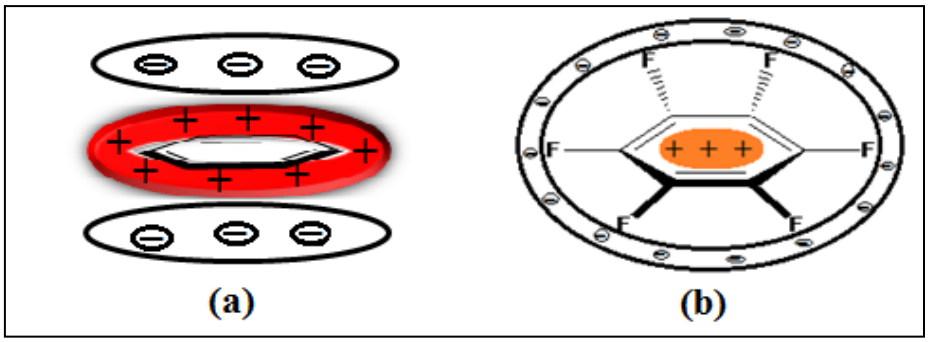

Figure 1.4: Schematic showing quadrupole moment (a) benzene (b) hexafluorobenzene, the polarity inverted due to difference in electronegativity of hydrogen and fluorine.

Face-to-face stacking will arise when 'electron deficient' aromatic centre is in close proximity with an electron-rich aromatic moiety. This is also called 'aromatic donor–acceptor interaction' as it involves a situation in which relatively electron-deficient and electron-rich aromatic molecules stack in an alternate fashion.[46,47]

The neutron diffraction spectroscopic studies on benzene and toluene have given information on aromatic π•••π interactions.[48] In solid benzene, the molecules interact and arrange predominantly in perpendicular edge-to-face arrangement. The perpendicular edge-to-face arrangements are of two types: Y-shaped and T-shaped and it is observed that Y-shaped is more stable. In solid toluene, the molecules stack in an off-centre parallel manner, where the methyl group of the adjacent molecule interacts with π-orbitals of the aromatic ring. Sherrill and Sinnokrot carried out comprehensive set of calculations for benzene and reported, T-shaped edge-to-face arrangement and parallel-offset dimers are nearly isoenergetic (Figure 1.5). Hunter *et al.* used double mutant to study the aromatic interactions in di-amides and observed T-shaped edge-to-face arrangement. They have further studied the substituent effect on π•••π stacking interaction.[49]

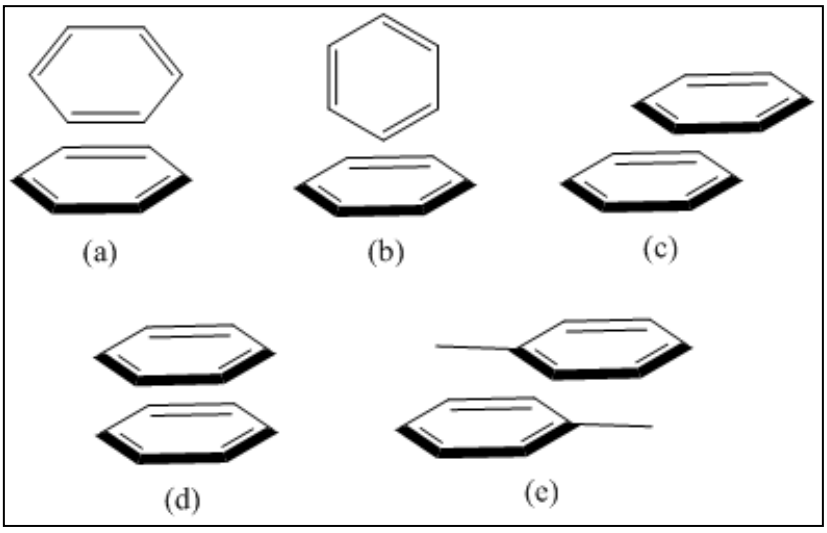

Figure 1.5: Aromatic stacking: (a) Perpendicular Y-shaped (b) Perpendicular T-shaped (c) Parallel-offset (d) Parallel face-centered (e) Parallel-offset for toluene.

Cai *et al.* reported π•••π interaction between aromatic ring of pyrazole in the Cu(II) co-ordination polymer.[50] Lalit *et al.* reported interpenetrated CP, where $Zn_4O(COO)_6$ cluster as a 6-connected node and tricarboxylic acid as a 3-connected node, the π•••π interaction resulted 2D network with (3,6)-connected topology.[51] The π•••π interaction between aromatic moiety and carbonyl moiety will depend on: (i) the dihedral angle (ω) between the

planes of >C=O and the aromatic ring & (ii) the distance (d) of carbonyl oxygen atoms from the aromatic centers (which should be 2.8 Å < d < 3.3 Å).[52,53] (Figure 1.6).

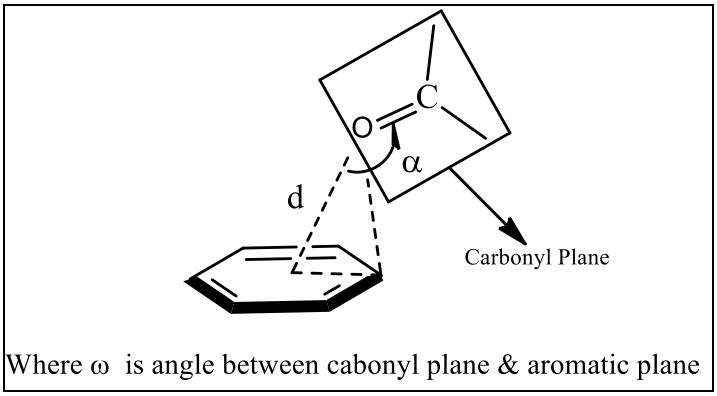

Figure 1.6: Schematic for π•••π interaction between >C=O and aromatic molecules.

Ramasubbu Sankararamakrishnan *et al.* did quantum mechanical calculations (Gaussian 03 suite of programs) by taking formaldehyde-benzene as model compound and reported the π•••π interactions in the >C=O•••aromatic centroid contacts. They varied the distance between the benzene centre and oxygen of formaldehyde in steps of 0.05 Å and plotted the potential energy at different **ω** values (Figure 1.7) and found ideal π•••π interaction is at 0°.

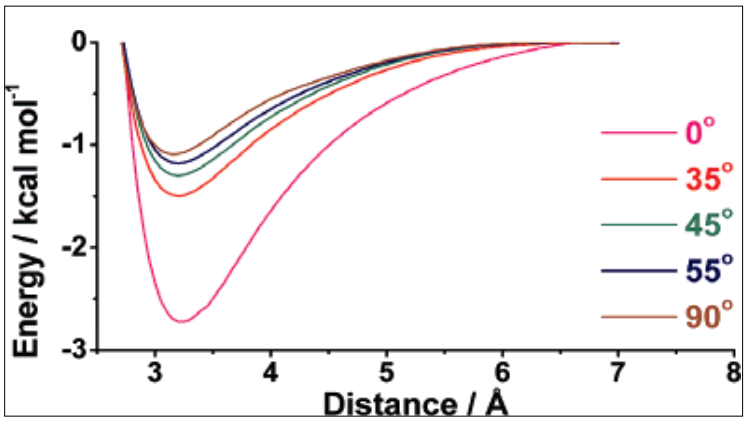

Figure 1.7: Potential energy plot for the benzene-formaldehyde complex.[51]

When ω = 0°, the carbonyl oxygen will be parallel to the aromatic plane and there is ideal π•••π interactions, but if ω = 90°, the >C=O group will have a head-on orientation towards the aromatic ring centroid and the interaction is referred as lp (lone pair) •••π-interactions between the lone pair of oxygen and π-electrons of the aromatic ring.[54] Mak *et al.* reported >C=O•••π-interactions in two Metal Organic Frameworks (MOF) of 2,6-pyridinediylbis(3-pyridinyl)methanone and Cu(II) with different anion NO_3^- and BF_4^-.

Table1.3 The variation of potential energy with ω, affecting the π•••π interaction [54]

Dihedral angle (ω)	Potential Energy kcal/mol	Type of Interaction
0°	-2.88	Ideal π•••π interaction
35°	-1.42	Between Ideal π•••π & lp•••π interaction
45°	-1.19	Between Ideal π•••π & lp•••π interaction
55°	-1.05	Between Ideal π•••π & lp•••π interaction
90°	-0.93	lp•••π interaction

They identified four different types of unconventional intermolecular >C=O•••π-interactions between carbonyl and pyridyl moieties.[54] Type-**I** is similar of the carbonyl-arene interaction in reported organic system, where the >C=O group is nearly parallel to the pyridyl ring.

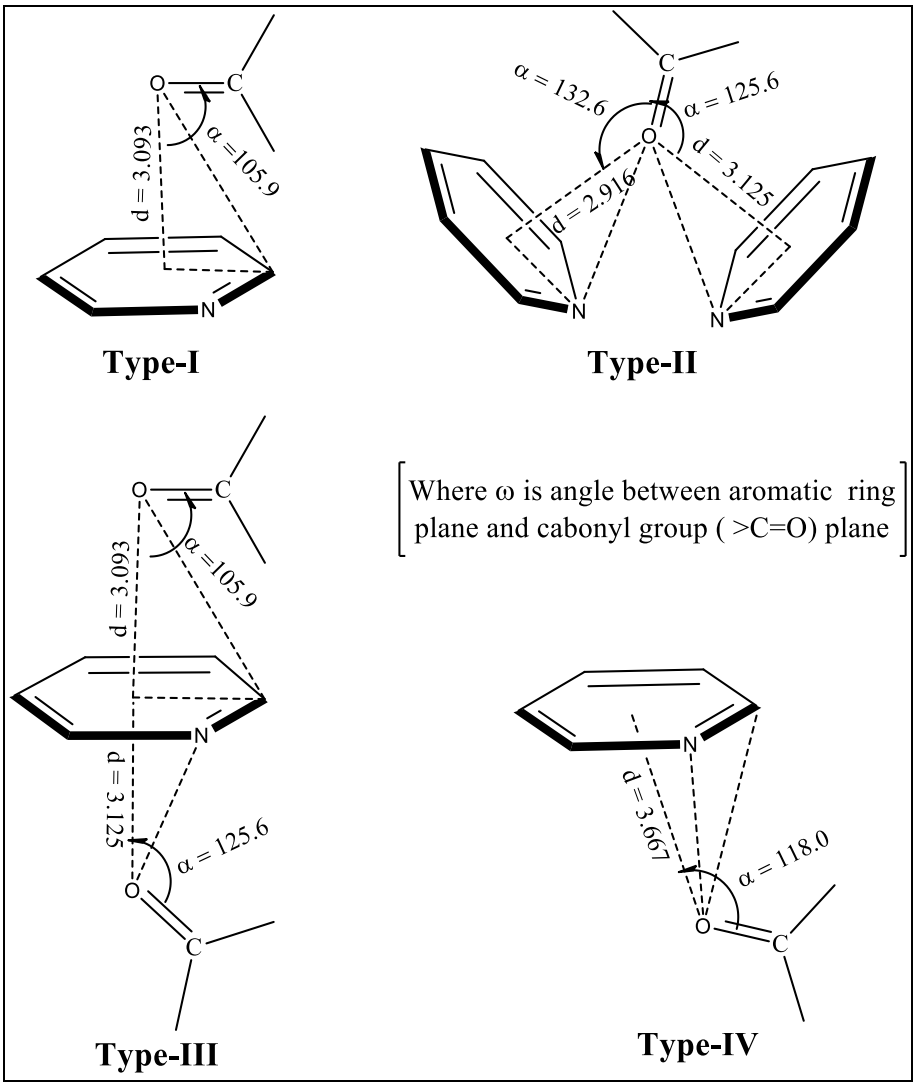

Figure 1.8: Classification of >C=O•••π (pyridyl) interactions in CPs.[54]

Type-**II** interaction as linker and formed layers and in Type-**III** interaction Type-**I** >C=O•••π-interactions shares one pyridyl ring with Type-**II**. In Type-**IV** >C=O•••π-interaction, the carbonyl group is attached to the pyridyl ring *via* an edge interaction.

1.2.3 Co-ordinate Bond Interactions

Co-ordinate bond interaction has a strength in the range of 30-70 kcal/mol and offers greater directionality and stability, which results in diverse structures of CPs.[55] Co-ordination polymers as the name suggests is a polymeric network involving metal ions and organic ligands. In the early 1990s, R. Robson and co-workers described 'node and spacer' approach to design the porous co-ordination polymers.[56] Around 2000, O. M. Yaghi's research group replaced metal ions with inorganic clusters, known as the secondary building units (SBUs) and introduced reticular chemistry.[57,58] Thus Metal Organic Frameworks (MOFs) is a special class of co-ordination polymers where the metal clusters are connected by organic linkers (usually carboxylates).

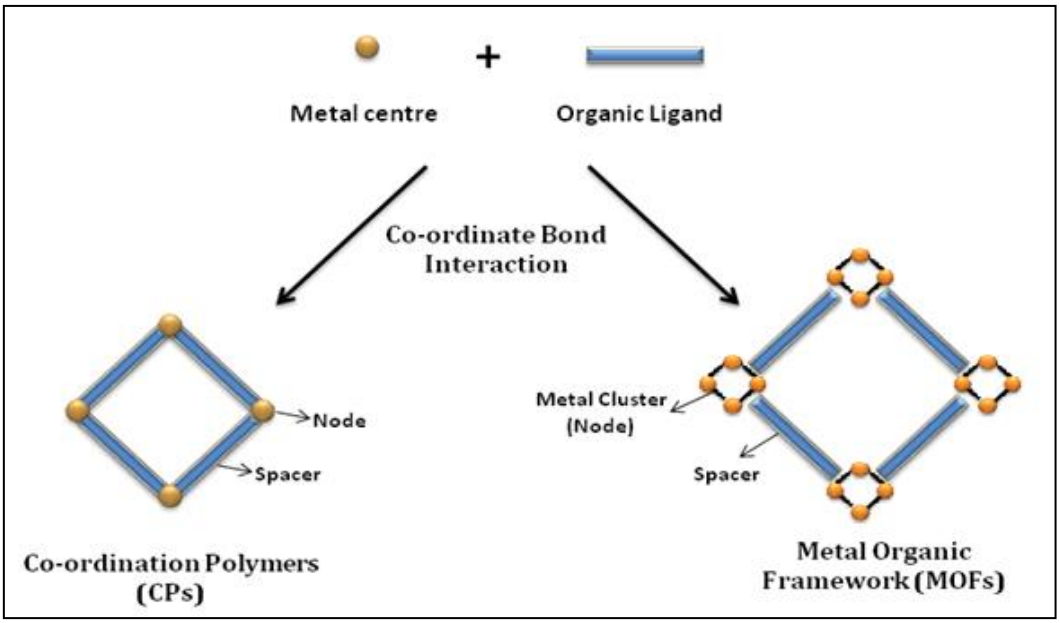

Figure 1.9: Co-ordinate bond between metal ions & organic ligand form Co-ordination Polymers (CPs) and Metal Organic Frameworks (MOFs)

The structure and properties of the materials resulting from co-ordinate bond interactions get further diversified on including the versatility of hydrogen bond interactions. In the co-ordination polymers, the frameworks are primarily dependent on the co-ordination preferences of the metal center and the functionalities of the ligand. Various other factors such as the metal to ligand ratio, counter anions, guest molecules and reaction conditions,

also play the structure directing roles.

1.3 Co-ordination Polymers (CPs) and Metal Organic Frameworks (MOFs): Structure

Although there are reports on CPs from late 1950s [58,59] and early 1960s, [60-63] the area of research on CP was boosted by the pioneering works of Robson and co-workers[56,64] followed by Kitagawa *et al.*[65,66] and Ferey *et al.*[67] Later on Yaghi *et al.*[57,58,68,69] explored Metal Organic Frameworks (MOFs) widely in area of gas storage, best known example being the structure of MOF−5, published in 1999 in Nature. The CPs and MOFs are exploited widely because of their porous nature. Their porosity is greater than 50% of the MOF crystal volume, surface area values is typically range from 1000 to 10,000 m^2/g.[70]

4,4′-Bipyridine is one of the most widely used ligands in construction of robust CPs. Derivatives of the 4,4′-Bipyridine ligand, consisting of various kinds of spacer units between two pyridine rings (Figure 1.10) are also utilized widely in designing, from one-, two-, and three dimensional (1D, 2D, and 3D) networks.

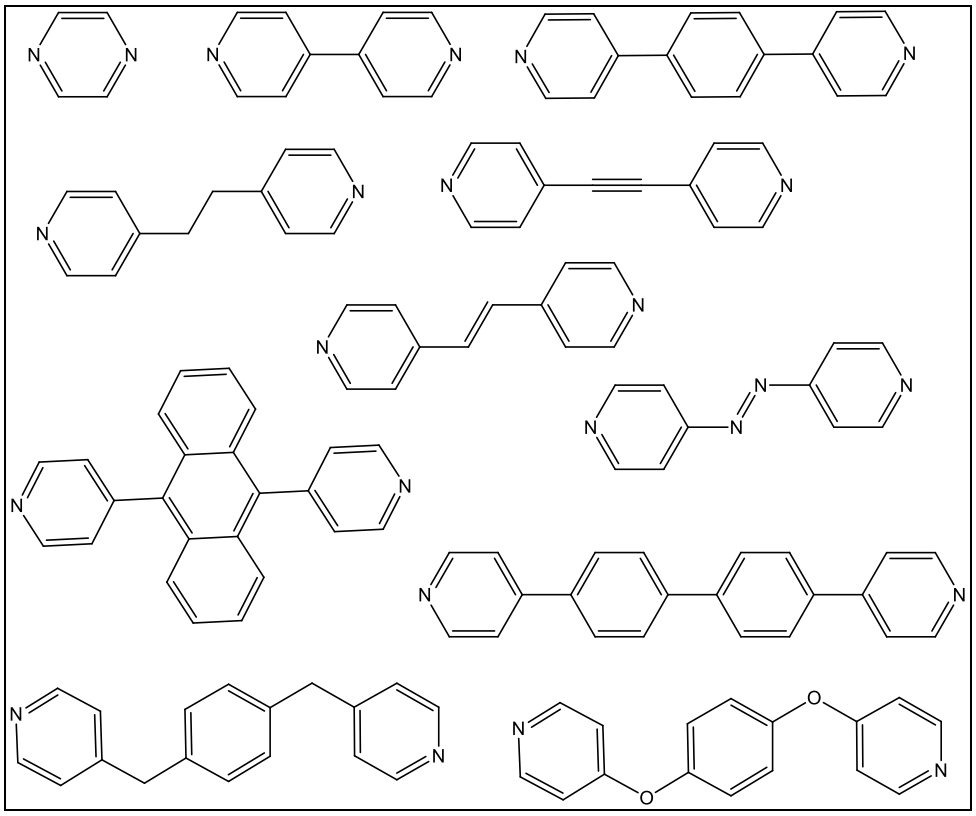

Figure 1.10: Schematic of the "rod like" *Bis*-pyridyl ligands with different spacer.

Large number of reports are on co-ordination polymers of these ligands with different Cu(I) or Cu(II), Ag(I), Cd(II), Zn(II), Co(II) and Ni(II) ions.[71-100]

1.3.1 One Dimensional (1D) Co-ordination Polymers (CPs)

The reaction conditions *i.e.* temperature, pressure, solvent used and solubility of the product formed influence the geometry and dimensionality of the network. The 1D CPs of 4,4′-bipyridine with transition metal atom resulted mainly due to competition of 4,4'-bipyridine with anions and other ligands, water, 2,2′-bipyridine *etc.* to co-ordinate to the metal centre.In 1982, X-ray structure of first co-ordination polymer of 4,4′-bipyridine was reported by Kubel *et al.* where the treatment of 4,4′-bipyridine with Co(dimethylglyoximate)$_2$ resulted in a 1D - Linear chain. In that CP, the Co(II) had octahedral geometry and 4,4′-bipy occupy the two co-ordination sites *trans* to each other to propagate the network in 1D (Figure 1.11).[71]

(1) 1D - Linear chain Network [71]

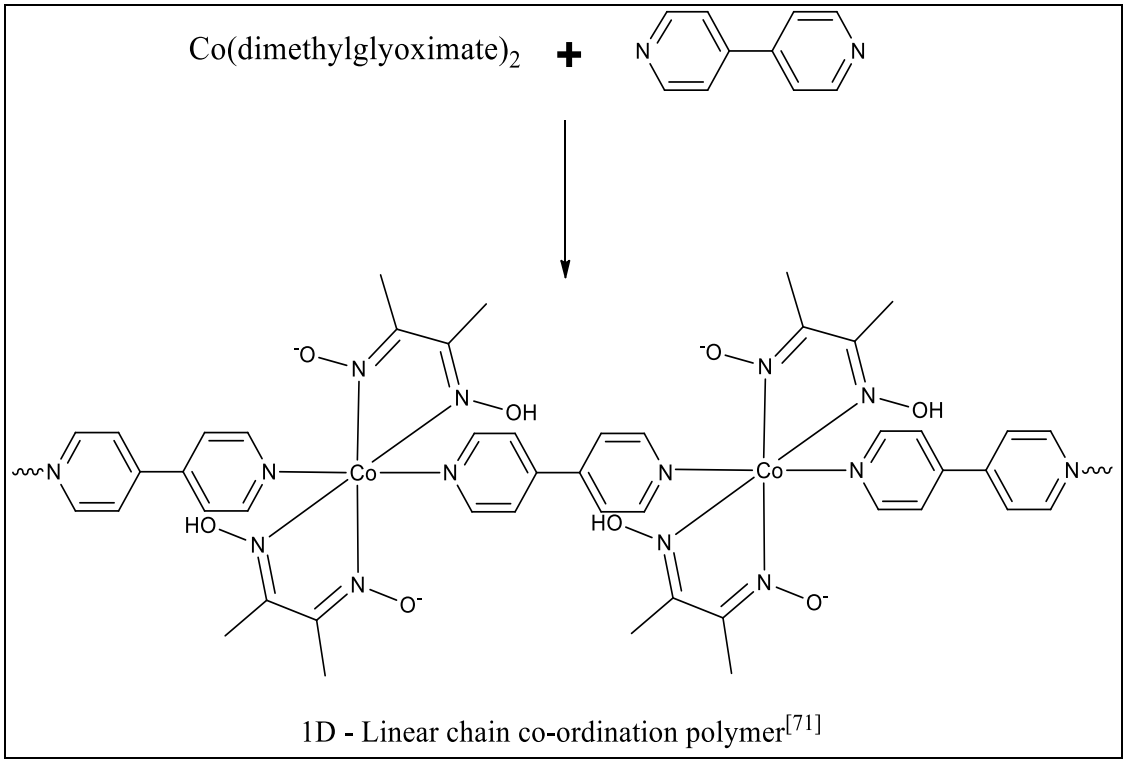

Figure 1.11: 1D-Linear Chain co-ordination polymer of 4,4′-bipy.[71]

In presence of bi-dentate chelating ligands - ethylenediamine or 2,2′-bipyridine as competing ligands with 4,4′-bipyridine, 1D - zig-zag chain results. The 4,4′-bipy occupy two *cis* sites of a metal atom having octahedral geometry, propagate the network. The one-dimensional co-

ordination polymers (CPs) include linear, zig-zag, helical, ladder, molecular antenna and railroad.[71-75] The linear, zig-zag and helical chains have 1 : 1 metal to ligand ratio, whereas the 1D-ladder, railroad and molecular antenna have metal to ligand ratio 1:1.5, 1:2.5 and 1:3, respectively.

(1) 1D - Zig-zag chain Network [72]

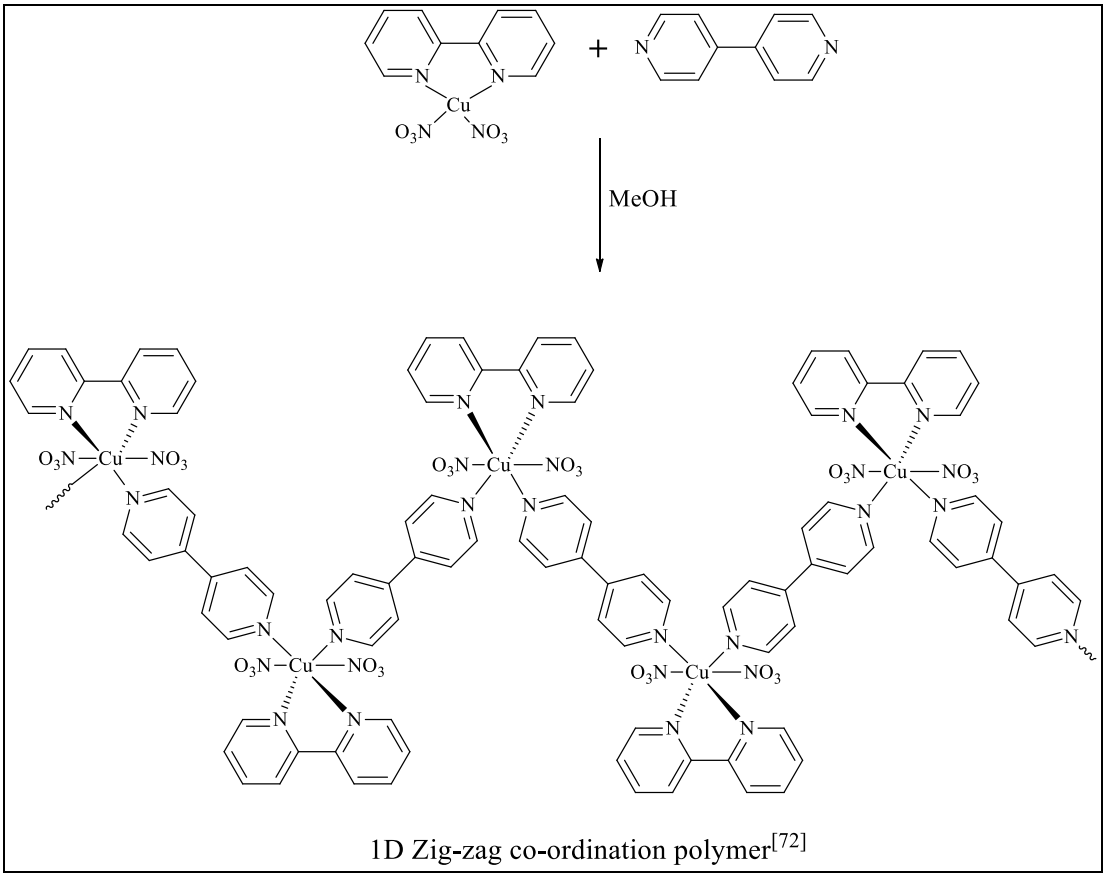

Figure 1.12: 1D - Zig-zag chain co-ordination polymer of 4,4′-bipy.[72]

The linear, zig-zag and helical chains possess the same metal to ligand ratio but there is a difference in the arrangement of the ligands to the metal centre. The linear chain is formed when the ligands are *trans* to each other whereas the zig-zag and helical chains are formed when they are *cis* to each other. When T-shaped metal co-ordination mode with respect to ligands (three co-ordinating sites of the metal ion occupied by ligands), results in the formation of 1D-ladder (Figure 1.14) and 1D railroad (Figure 1.15) whereas the square planar co-ordination mode forms1D-molecular antenna (Figure 1.13). The molecular antenna network formed only when 4,4′-bipyridine ligand present in excess and acting as monodentate as well as bidentate ligand and also as a guest molecules.

(2) 1D - Molecular Antenna Network [73]

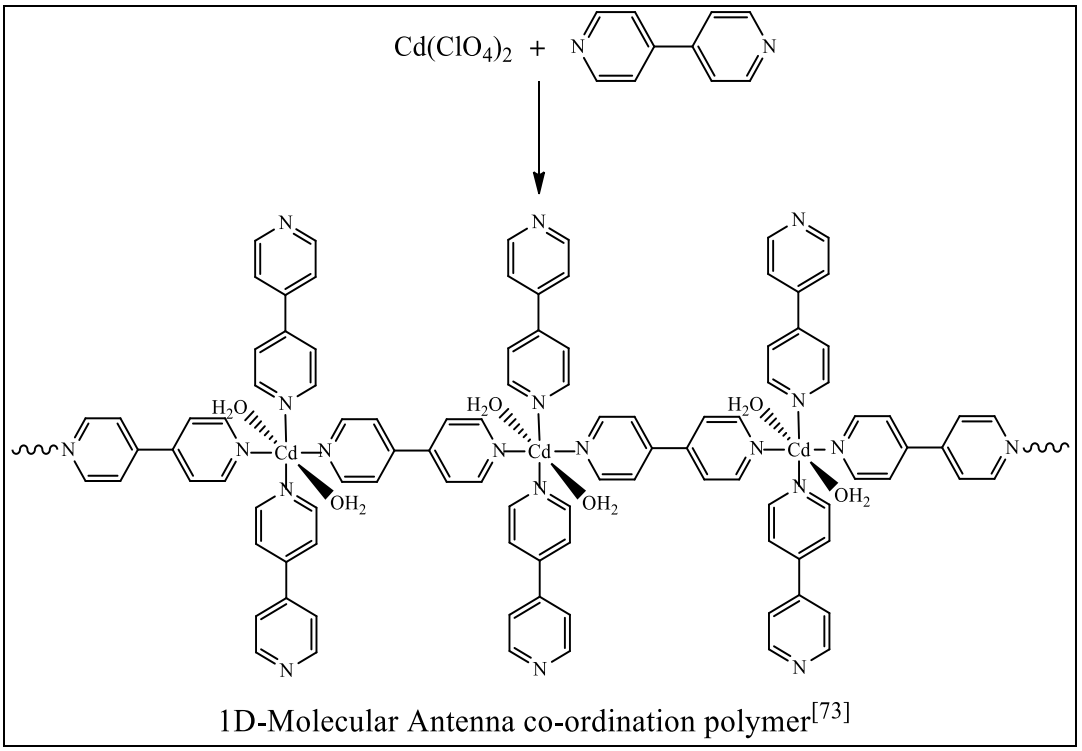

Figure 1.13: 1D – Molecular Antenna co-ordination polymer of 4,4′-bipy.[73]

(3) 1D -Molecular Ladder Network [74]

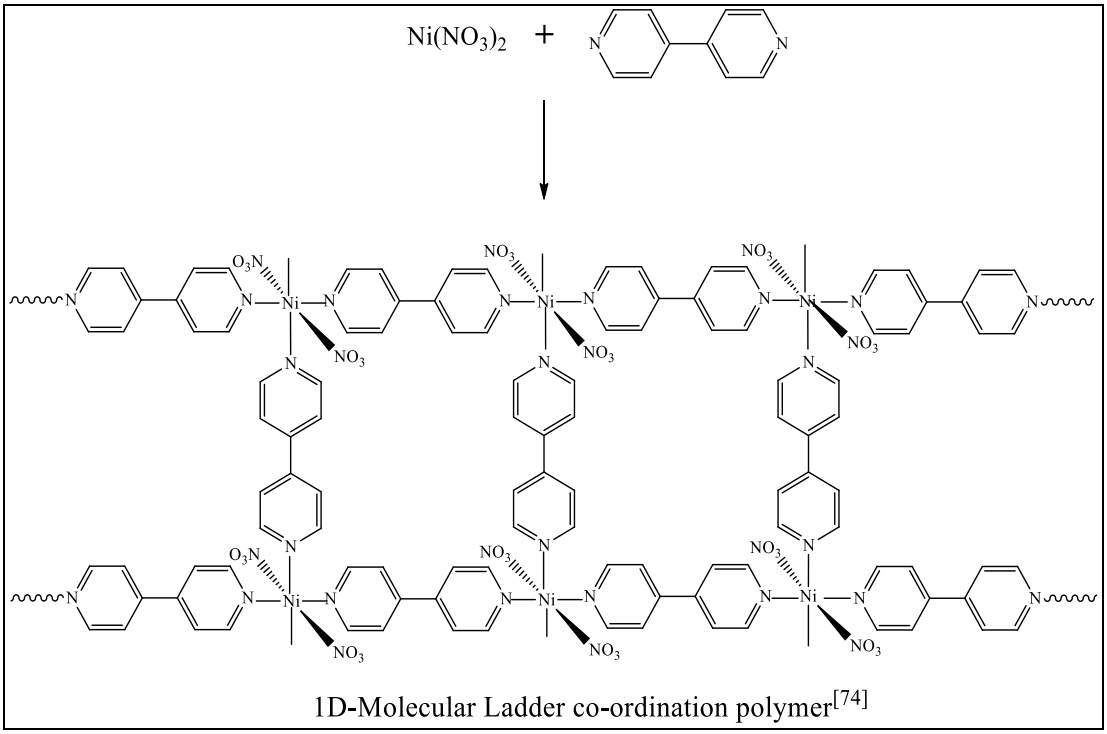

Figure 1.14: 1D - Molecular Ladder co-ordination polymer of 4,4′-bipy.[74]

(4) 1D - Railroad Network [75]

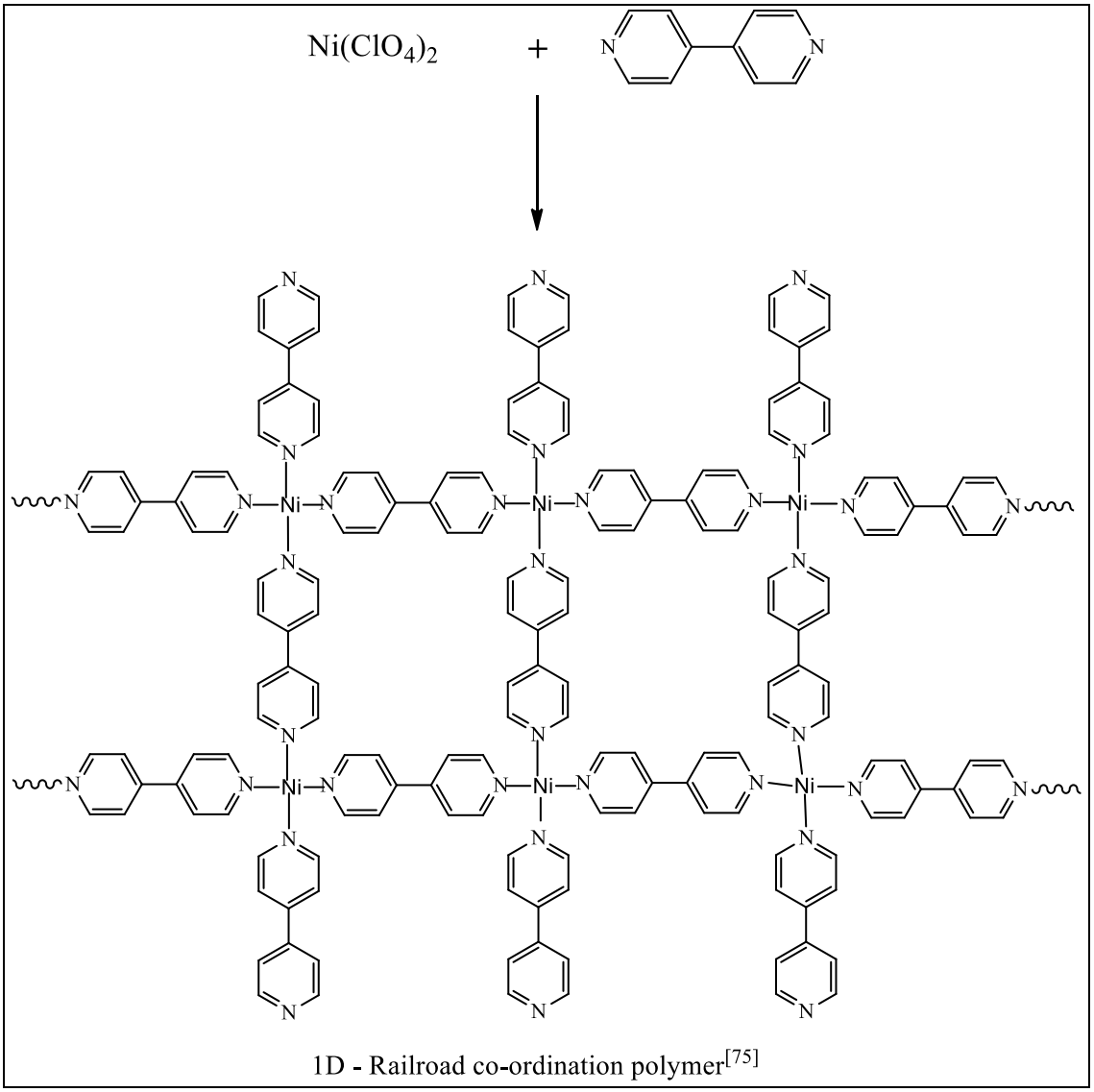

Figure 1.15: 1D - Railroad co-ordination polymer of 4,4′-bipy.[75]

1.3.2 Two Dimensional (2D) Co-ordination Polymers (CPs)

The geometries of the two-dimensional polymers of 4,4′-bipyridine (bipy) and its analogue include square grids [76-81], rectangular grids [82,83], honeycomb [84,85], bilayer [86,87], herringbone [88] and brick wall [89]. The square grids (Figure 1.16) and rectangular grids are four-connected networks whereas the bilayer, herringbone, brick wall and honeycomb networks are three-connected networks. Square grid networks are the well explored examples and are based upon 1: 2 metals to ligand ratio. There are many reports on the square grids which contain huge cavities to include the guest molecules. The metal centre in the network adopts

octahedral co-ordination mode with four ligands at the equatorial positions and two solvent/H_2O/counter anions at the axial positions.

(1) 2D – Square grid Network [77]

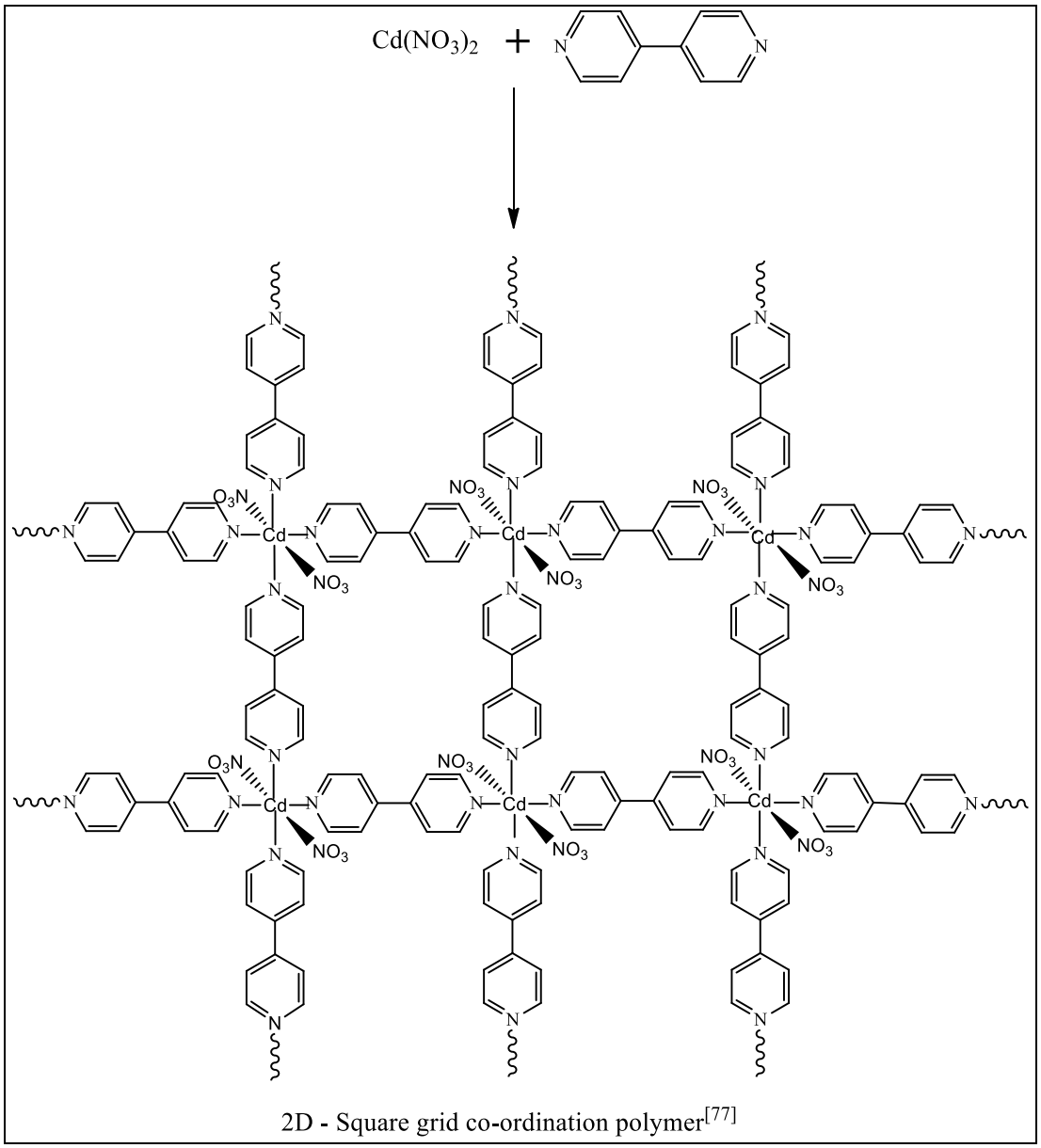

Figure 1.16: 2D – Square grid co-ordination polymer of 4,4'-bipy.[77]

The first square grid co-ordination polymer using 4,4′-bipyridine (bipy) was reported by Robson *et al.* in the crystal structure of $\{(Zn(bipy)_2(H_2O)_2)(SiF_6)\}_n$, but the networks were doubly interpenetrated (Figure 1.17(a)).[76] Later Fujita *et al.* reported the first non-interpenetrated or open square grid network with 4,4′-bipyridine (bipy) in the crystal structure

of $\{(Cd(bipy)_2(NO_3)_2)\bullet 2(o\text{-dibromobenzene})\}_n$ (Figure 1.17(b))[77]. In this CP, the guest molecules were included in the cavities of the network.

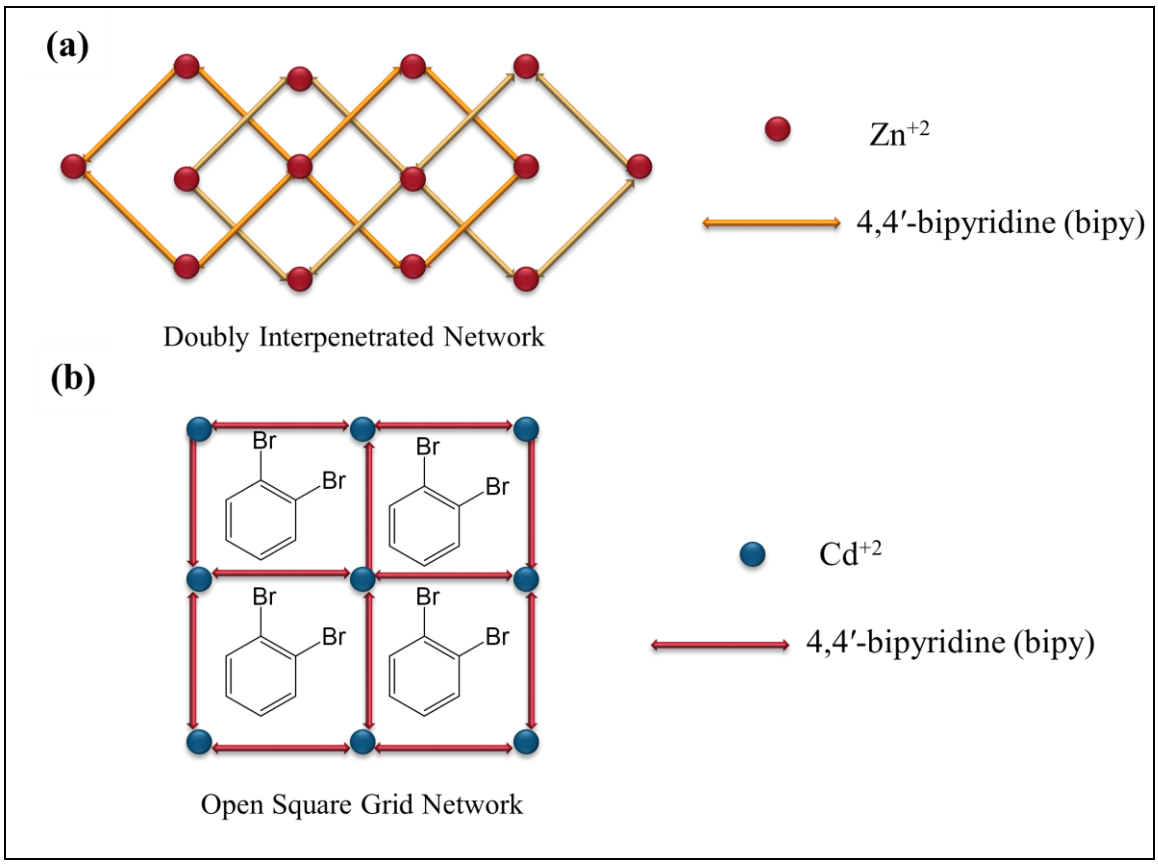

Figure 1.17: (a) Doubly interpenetrated network of $\{[Zn(bipy)_2(H_2O)_2][SiF_6]\}_n$[76] (b) Open network with guest molecules of $\{[Cd(bipy)_2(NO_3)_2.\ 2(o\text{-dibromobenzene})]\}_n$[77]

Subsequently, Zaworotko *et al.* have reported the square grid networks of bipy in the presence of various guest molecules such as benzene, pyrene, naphthalene, anisole, veratrole, and nitrobenzene. The use of longer analogue of bipy resulted in square grid networks containing larger cavities of dimensions 11×11 Å^2, 15×15 Å^2, 20×20 Å^2 and 25×25 Å^2.[78-82] Biradha *et al.* reported interpenetrated network in Cu(II) co-ordination polymer of *bis*-pyridyl-*bis*-amide ligand, where the layers were parallel interpenetrated.[83] Gong *et al.* reported interpenetrated CPs of Cd(II) and Zn(II) with *bis*-pyridyl-*bis*-amide ligand having phenyl spacer along with aromatic polycaboxylate.[84] Wang *et al.* studied interpenetrated CPs of Cu(II) with flexible *bis*-pyridyl-*bis*-amide ligand, different length alkyl spacer and meta- position of pyridyl-N.[85] Rectangular grids were obtained by taking two different ligands. The rectangular grids with neutral ligands are rare. Mak *et al.* have shown the formation of rectangular grid network of dimensions 6.8×11.1 Å^2 using pyrazine and 4,4'-

bipy with Cu(II).[86] Further Fujita *et al.* reported rectangular grids with bipy and longer analogues of bipy (Figure 1.18).[87]

(2) 2D – Rectangular grid Network [87]

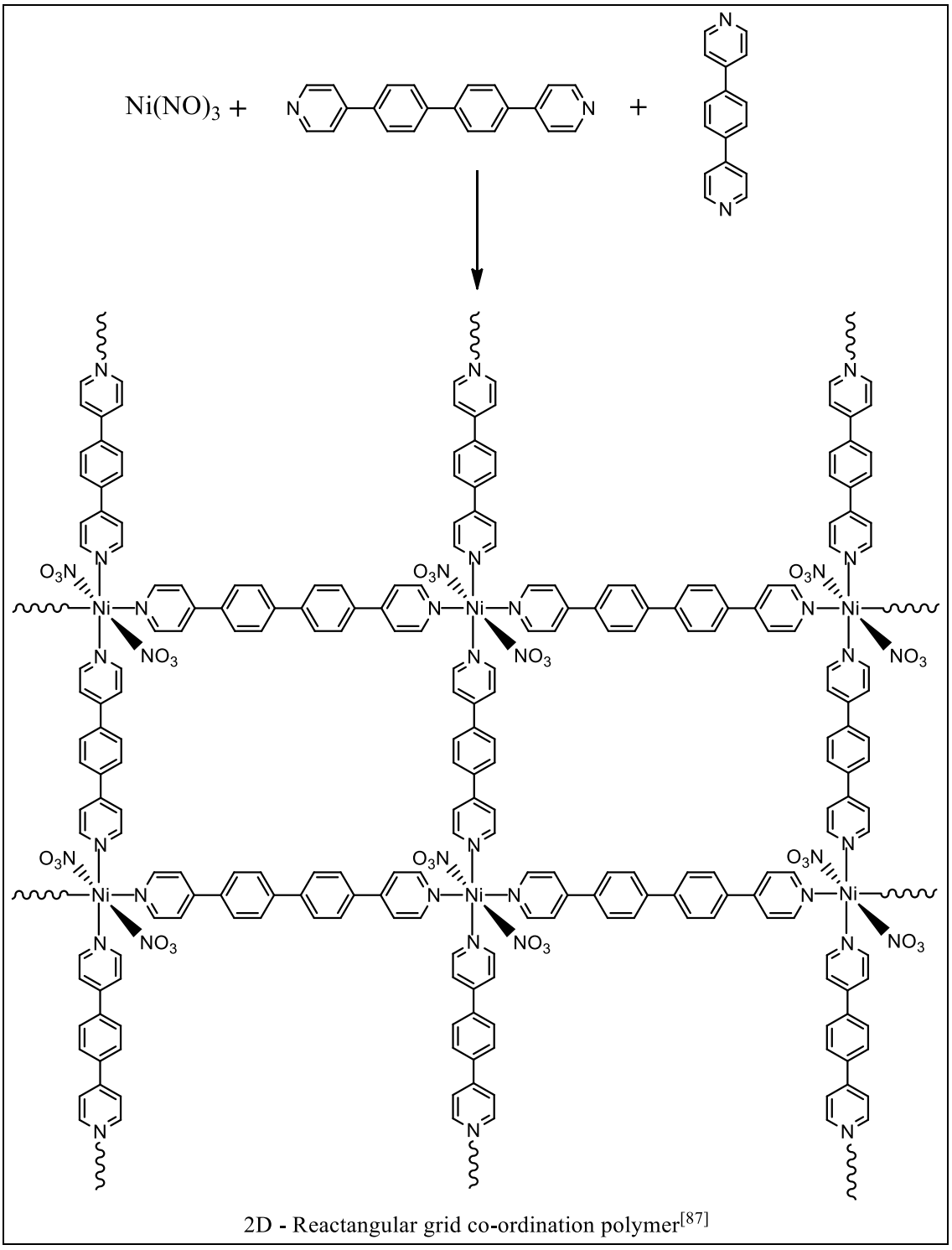

Figure 1.18: 2D – Rectangular grid co-ordination polymer of 4,4′-bipy.[87]

Honeycomb network is formed when the metal centre adopts trigonal geometry. The occurrence of honeycomb networks is rare as the trigonal and trigonal-bipyramidal co-ordination geometries of the metal centre is the requirement for its formation, which is relatively less in transition metal centers (Figure 1.19). Zaworotko *et al.* [88] and Yaghi *et al.*[89] have reported honeycomb network of Cu(II) with pyrazine and bipy, respectively.

(3) 2D – Honeycomb Network [88, 89]

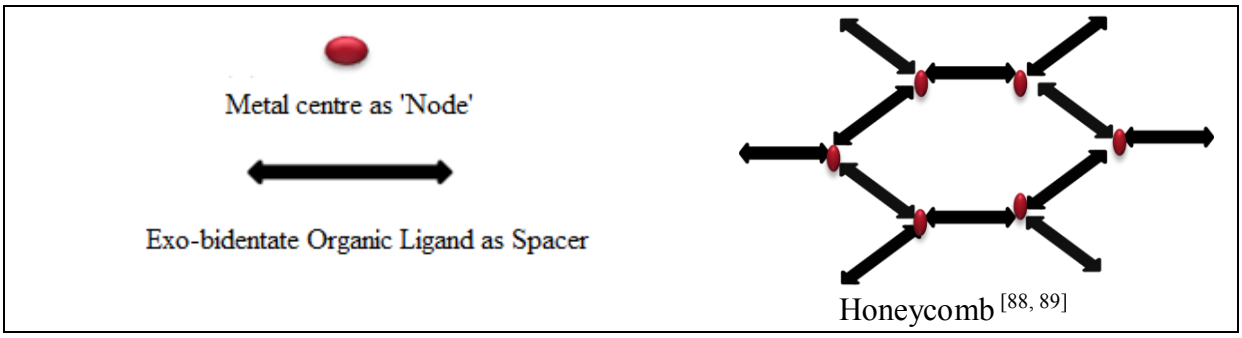

Figure 1.19: 2D – Honeycomb co-ordination polymer.[88, 89]

(4) 2D –Bilayer [90, 91], Herringbone Networks [92] and Brick wall [93]

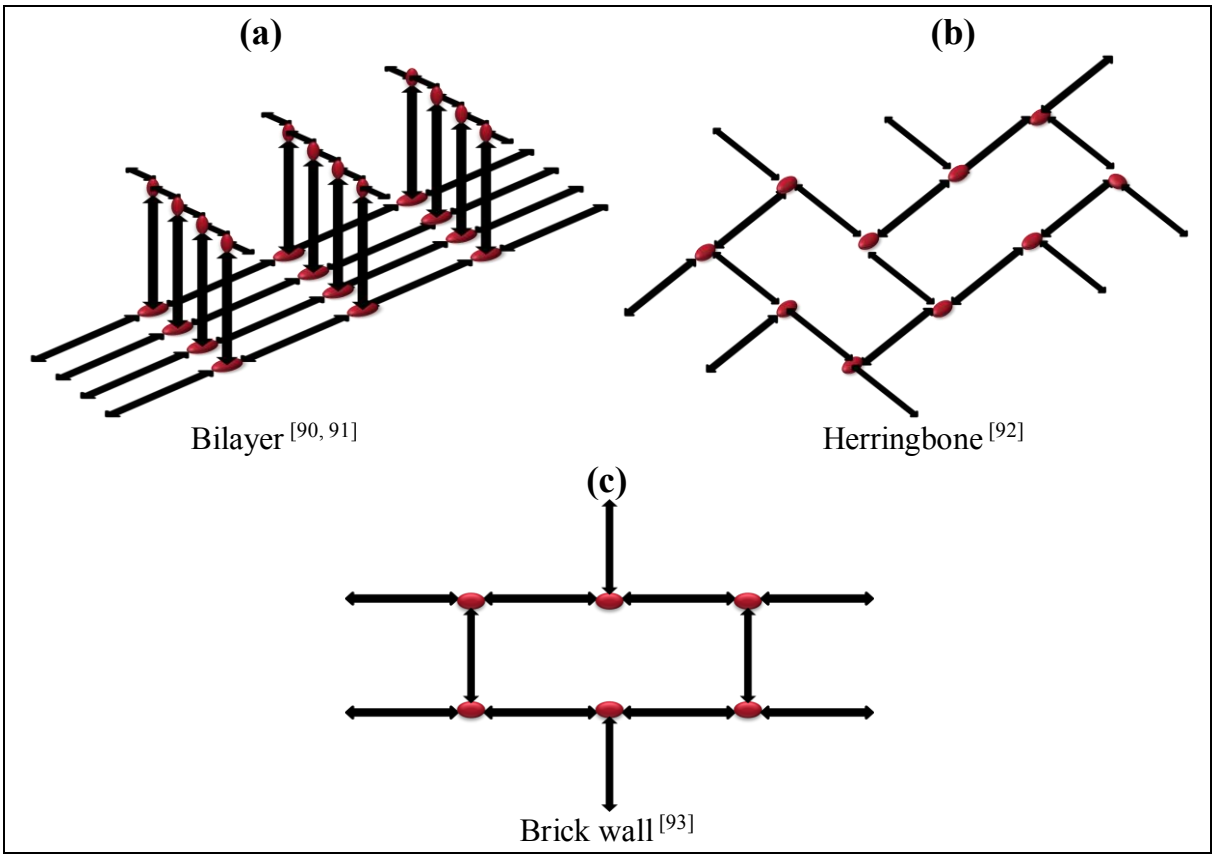

Figure 1.20: 2D - Bilayer [90, 91], Herringbone [92] and Brick wall [93] co-ordination polymer.

The bilayer network observed in CPs is different from the conventional bilayers of the lyotropic liquid crystals. In the conventional bilayers, the hydrophobic and hydrophilic layers are arranged in alternate fashion. In the bilayer networks of CPs, the two layers are identical and are separated by a spacer ligand. Both the layers of a bilayer contain a set of one-dimensional chains arranged in a parallel fashion and the chains in one layer make an approximate angle of 90° with those of the other layer (Figure 1.20 (a)).

Zaworotko *et al.* have reported the first bilayer co-ordination polymer with 1,2-bis(4-pyridyl)ethane and $Co(NO_3)_2$.[90,91] The brick wall and herringbone networks are propagated by T-shaped metal geometry. The herringbone network was reported by Lin *et al.*, where Zn(II) was reacted hydrothermally with 4,4′-bipy and pyridine-2,4,6-tricarboxylic acid (Figure 1.20 (b)).[92] An example of the brick wall network is reported with 4,4′-bipy and imidazole-4,5-dicarboxylic acid with $Cd(NO_3)_2$ (Figure 1.20 (c)).[93] However in this case the heterocyclic carboxylates ligand were also used.

1.3.3 Three Dimensional (3D) Co-ordination Polymers (CPs)

The three-dimensional networks with bidentate ligands can be broadly classified as the networks:

(i) propagated by three-connected nodes,[94-96]

(ii) networks propagated by four-connected nodes,[97,98]

(iii) linking of the 2D layers *via* anions[99,100]

In the three-dimensional networks that are propagated by three-connected nodes, the metal centre can adopt either T-shaped or trigonal co-ordination geometry. Among the various possible networks, the T-shaped geometry can lead to the formation of Lincoln Log networks which are reported with 4,4′-bipy and Ag(I) (Figure 1.21(b)).[94,96]

The most common network that is propagated by four-connected node is diamondoid network (Figure 1.21(c)). The diamondoid network was reported by Zaworotko *et al.*[97] and Ciani *et al.*[98] with 4,4′-bipy and Cu(I) and Ag(I), respectively. The linking of the two-dimensional metal-organic layers *via* anions can also result in 3D-networks. Zaworotko *et al.*[99] and Kitagawa *et al.*[100] have reported three-dimensional networks that are formed by linking the square grid networks of 4,4′-bipy and M(II) with SiF_6^-.

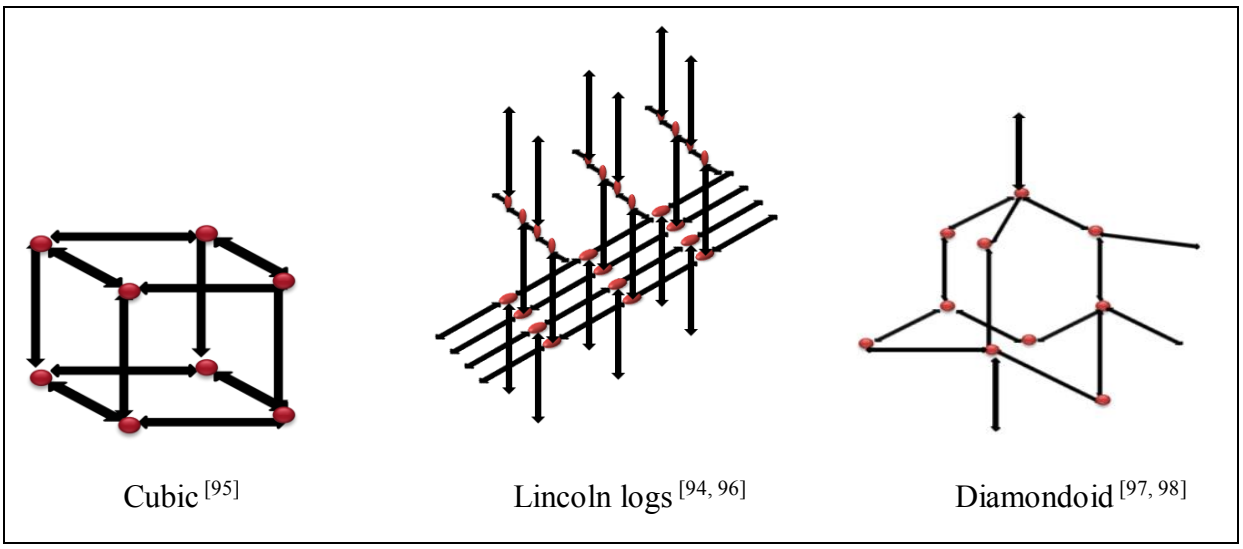

Figure 1.21: 3D - Cubic[95], Lincoln logs[94, 96] and Diamondoid[97, 98] co-ordination polymer.

1.4 Co-ordination Polymers (CPs) containing Hydrogen Bonding Functionalities

The CPs of metal ions and ligands containing hydrogen bonding functionalities such as: amides, urea's, diacids, hydroxyl *etc.* (Figure 1.22) result in wide range novel networks due to the participation of networks in various hydrogen bond interactions.

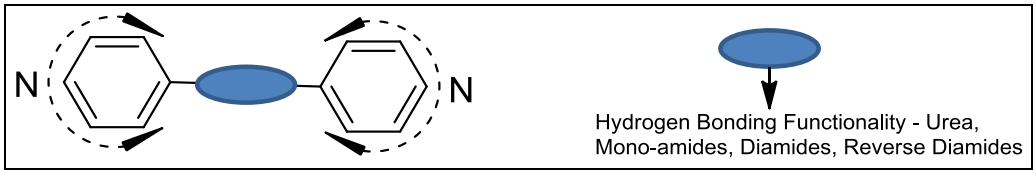

Figure 1.22: *Bis*-pyridyl ligands with hydrogen bond functionality in the spacer.

Aakeröy *et al.* reported the neutral complex, from isonicotinic acid and tetrachloroplatinate, where the O-H•••O hydrogen bond interaction resulted in square grid network.[101] As no counter-ions were present in the complex, the voids in the network were available for guest molecules. But interpenetrated resulted in the square planar complex of $Pt(isonicotinate)_2(isonicotinic\ acid)_2$, where three networks interpenetrated in perpendicular manner, resulting in decrease in cavity size (5 Å in diameter). Aakeröy *et al.* also used pyridyl-based ligands substituted with hydrogen bond functionalities to form CPs, where the pyridyl-N form co-ordinate bonds and the substituents carboxylic acids, carboxamide and oximes were involved in hydrogen bonding interactions to arrange the networks in 3D.

Goldberg and co-workers have synthesized many substituted porphyrin complexes that resulted in flat, grid-like 2D networks through amide–amide and acid–acid hydrogen bond interactions. [102] Aoyama and co-workers connected Zn(II) porphyrin units via the hydrogen bond interactions of by 3,5-dihydroxybenzene substituents and assembled into 2-D networks.[103]

1.4.1 Co-ordination Polymers of Urea

Introducing a urea moiety as the backbone of a CP, play a crucial role in shaping up the structures and functions. Urea itself generally displays 1D α - network *via* hydrogen bonding involving the carbonyl oxygen and two N–H atoms (Figure 1.23); it can also interact with various counter anions or solvent guest molecules. The *bis*-pyridyl ligands having urea as spacer can be of two types (Figure 1.23) as:

(i) *Bis*-pyridyl-*mono*-urea

(ii) *Bis*-pyridyl-*bis*-urea

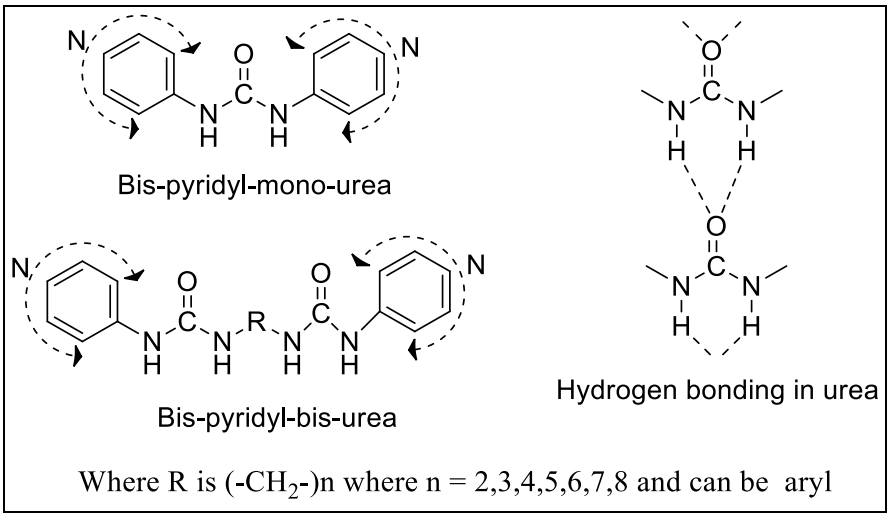

Figure 1.23: *Bis*-pyridyl ligands with urea moiety and hydrogen bonding in urea itself.

Some leading research groups have explored the CPs of these ligands and showed the effect of anion, metal centers, solvents, guest molecules and more importantly, the N-H•••O=C hydrogen bonding interactions with in the urea moieties while assembling their co-ordination polymers (CPs).[91–103] Fowler *et al*. reported that α-network of urea was conserved in CPs of *bis*-pyridyl-*mono*-urea ligands. Later, Crustacean *et al.*[104] and Dastidar *et al.*[105-109] extensively studied interesting CPs derived from this class of ligands.

The effect of positional isomerism in the CP was nicely demonstrated by Dastidar *et al.*[105], by using 1,3-di(pyridin-4-yl)urea and 1,3-di(pyridin-3-yl)urea with tetrahedral metal center Zn(II). One of the CP resulted in 5-fold diamondoid network in which urea moiety found to be involved in hydrogen bonding with the counter anion ClO_4^-, while other have (4,4) 2D grid architecture sustained by a complementary α hydrogen bonding network of urea (Figure 1.24).

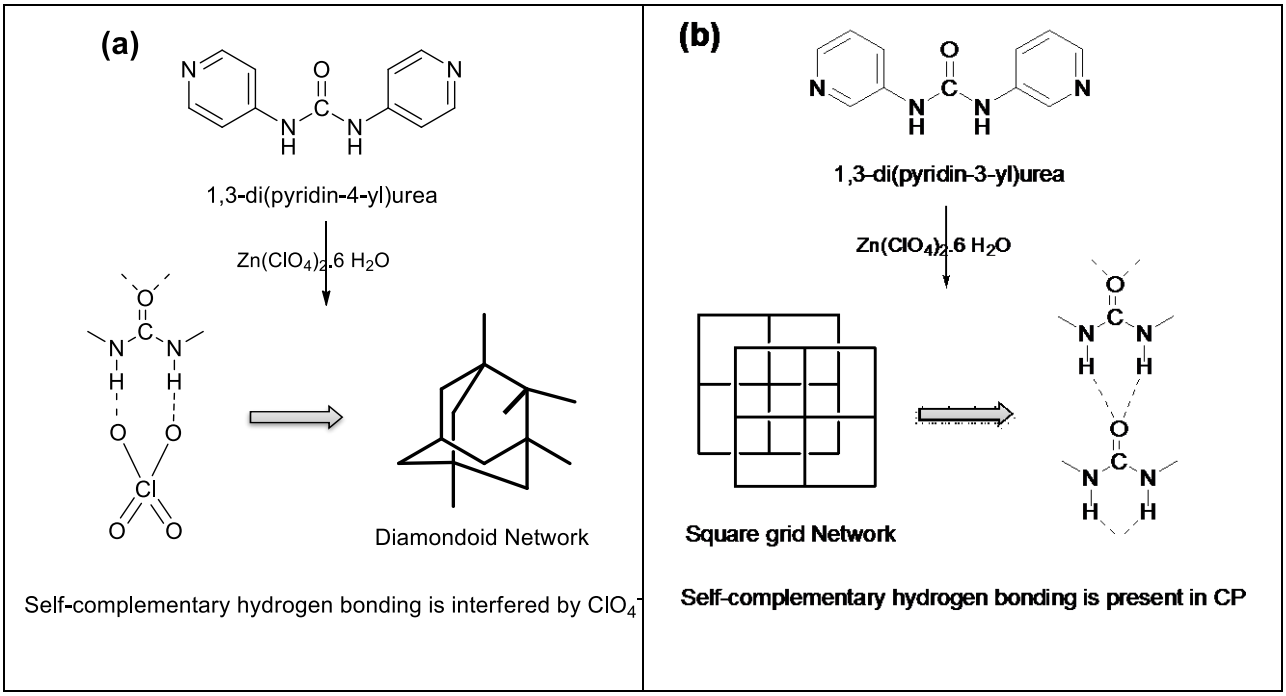

Figure 1.24: Effect of positional isomerism in structure of CP.[105]

Further the effect of counter anions *i.e.* Cl^-, OAc^- and SO_4^{-2} on the resultant supramolecular structures of CPs of Zn(II) salts were carried out using these ligands.[106] 1,3-Di(pyridin-3-yl) urea was used to study the effect of conformation dependent ligating topology and counter anion on the resultant supramolecular architecture of the CPs derived from Cu(II) salts having different counter anions such as ClO_4^-, $CF_3SO_3^-$, SiF_6^{-2}, SO_4^{-2} and NO_3^-.[107] For the SO_4^{-2} anion, urea–sulfate hydrogen bonding interactions generated micro porous assembly of nanorods. Further the CPs of these ligands with $Cd(NO_3)_2$ in polar solvents (nitrobenzene, methylsalicylate) and non-polar solvents (toluene, o-, m-, and p-xylene) were studied to observe the effect of solvents polarity on CP.[109] It was observed that polar solvents resulted in formation of CPs, where self-complementary hydrogen bond interactions were interfered with solvent or counter anions. CPs derived from ligands with two urea functionalities (*bis*-urea) was shown to N-H•••O hydrogen bonding of urea while in some cases it is interfered

with counter anions. One of the early reports on *bis*-pyridyl-*bis*-urea CPs was from Steed's group, in which two 1D CPs with $AgNO_3$ resulted under different reaction conditions, where the degree of folding of the 1D chains was different due to the hydrogen bonding interactions of the urea moiety with the counter anion and the solvents.[110] Steed's group for the first time, nicely exploited hydrogen bond interaction between urea and anion (nitrate) to stabilize Borromean Entanglement in CP of bis-urea ligands having ethyl spacer and $AgNO_3$.[111] An entanglement of three closed circuits (rings) where in all the circuits become separable just by breaking one of them, known as Borromean entanglement or Borromean ring. Borromean topology has inspired human beings over generations as evident its presence in history, arts and science (Figure 1.25).[112]

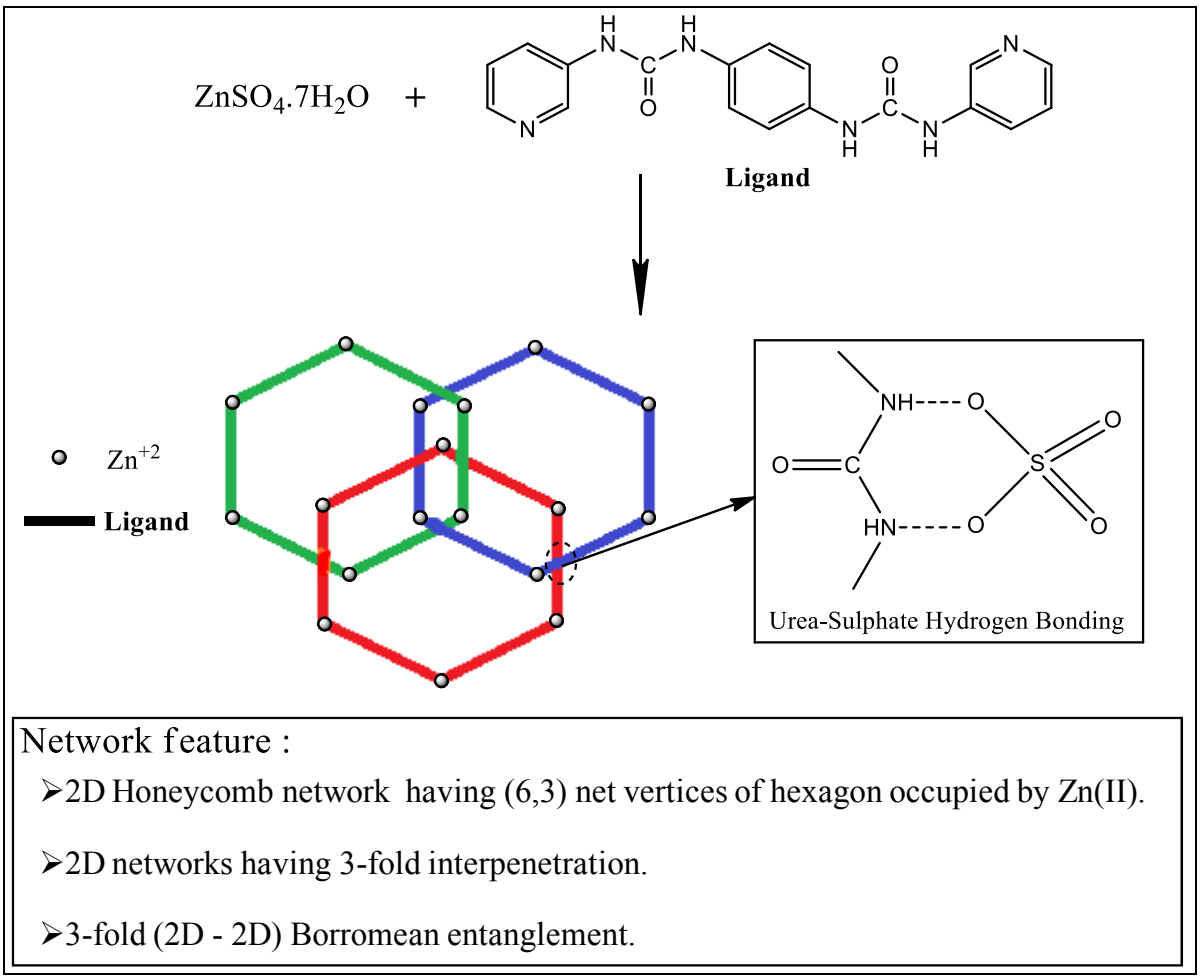

Figure 1.25: Borromean entanglement (topology) showed by Hexagonal Network[112].

Later on, *bis*-pyridyl-*bis*-urea ligand with aromatic backbone was exploited by Dastidar to generate Borromean wave CP of $ZnSO_4$, where hydrogen bond interaction between urea and

sulfate was responsible Borromean entanglement.[113] They further used the CPs in separation of anions, where the anion SO_4^{-2} was separated from a mixture of anions - (SO_4^{-2}, ClO_4^-, NO_3^- & $CF_3SO_3^-$). Steed *et al.* also reported effect of anion and the molar ratio (metal : ligand) on the formation of metallogel and crystalline co-ordination polymers.[114] A series of Ag(I) and Cu(II) metallogel of *bis* -urea was reported where it was observed Ag(I) with NO_3^- as anion resulted in crystalline CP while with BF_4^- resulted in a semi transparent metallogel. The explanation for this observation was based on the strong hydrogen bonding ability of urea with NO_3^- than that with BF_4^- (Figure 1.26).

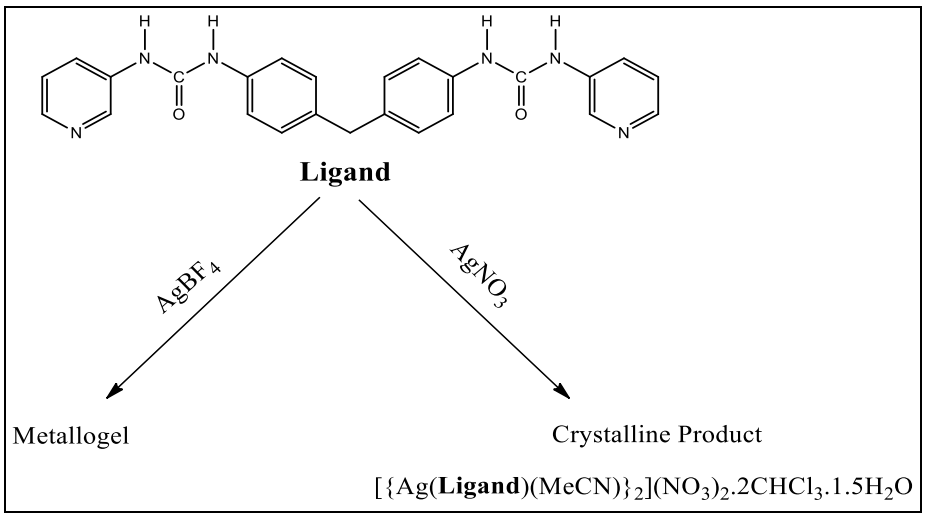

Figure 1.26: Effect of anion on CPs of Ag(I).[114]

Custelcean *et al.* reported a 2D co-ordination polymer of *bis*-urea and $NiSO_4$ in which SO_4^{-2} was entrapped within the interstitial space between two adjacent layers and also studied the selective separation of SO_4^{-2} from an aqueous solution containing F^-, Cl^-, Br^-, I^-, NO_3^-, ClO_4^- and SO_4^{-2}.[115] Dastidar *et al*. also used an analogous series of *bis*-pyridyl-*bis*-urea ligands, synthesized CPs and metallogel, which showed application in anion separation.[116]

1.4.2 Co-ordination Polymers of Amides

The *Bis*-pyridyl ligands with amide spacer can be classified into three main classes (Figure 1.27):

(i) *Bis*-pyridyl-*mono*-amide

(ii) *Bis*-pyridyl-*bis*-amide

(iii) Reverse *bis*-pyridyl-*bis*-amide

All these ligands have dual functional groups: pyridyl and amide; pyridyl nitrogen is co-ordinating site while the amide group participates in various hydrogen bonding interactions with the counter anions or guest molecules if present.[117-144]

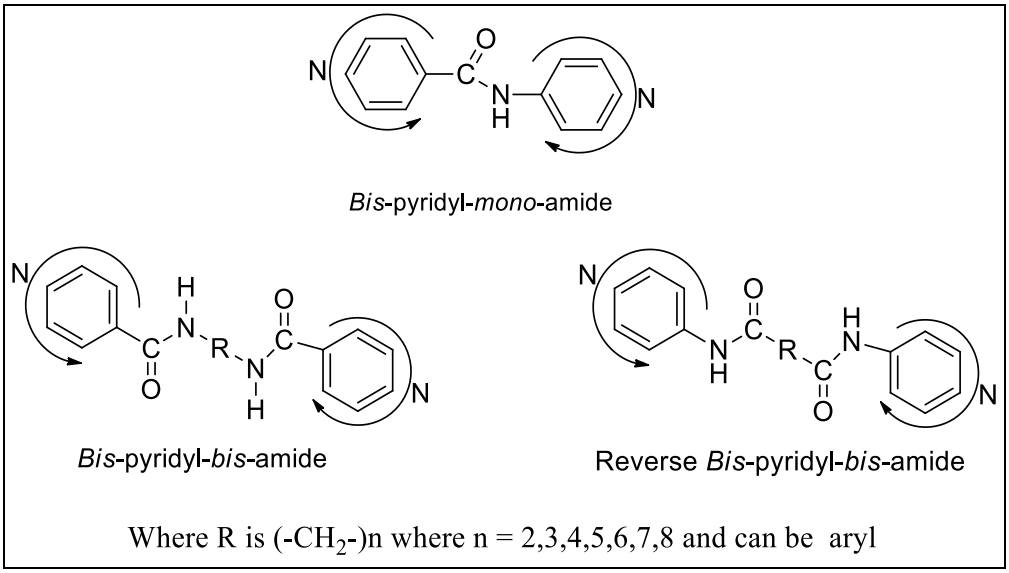

Figure 1.27: *Bis*-pyridyl ligands with amide spacer.

These ligands are flexible; have various ligating topologies and have an ability to adjust according to the geometrical requirements of a metal ion, which will influence the dynamic behaviors in CPs. The amide functional group is equipped with two types of hydrogen bonding sites: (i) the –N-H moiety acts as an electron acceptor (ii) the –C=O group acts as an electron donor.

1.4.2.1 Co-ordination Polymers of *Bis*-Pyridyl-*Mono*-Amide

Kitagawa and co-workers used the *bis*-pyridyl-*mono*-amide ligands to synthesize co-ordination polymer of Co(II), where the *bis*-pyridyl-*mono*-amide ligand acted as pillar to join the 2D polymeric sheets of the Co(II)-pyrazine dicarboxylate framework (Figure 1.28).[118]

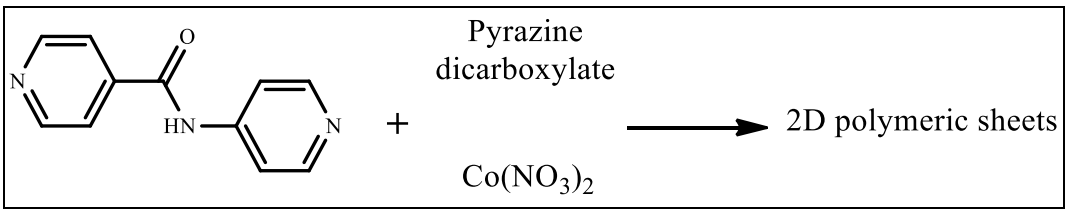

Figure 1.28: 2D-sheet of Co(II) of *bis*-pyridyl-*mono*-amide and pyrazine dicarboxylate.[118]

Puddephatt *et al.* reported molecular triangle by the supramolecular self-assembly of a *cis*-

blocked Pt(II) unit [[(bu_2-bpy)]Pt^{2+}; bu_2-bpy = 4,4′-di-tert-butyl-2,2′-bipyridine] and *bis*-pyridyl-*mono*-amide, where N-H•••O hydrogen bonding of amide helped the triangles to form stacked pairs while the counter anion triflate was found to be encapsulated within the triangular cavity (Figure 1.29).[119]

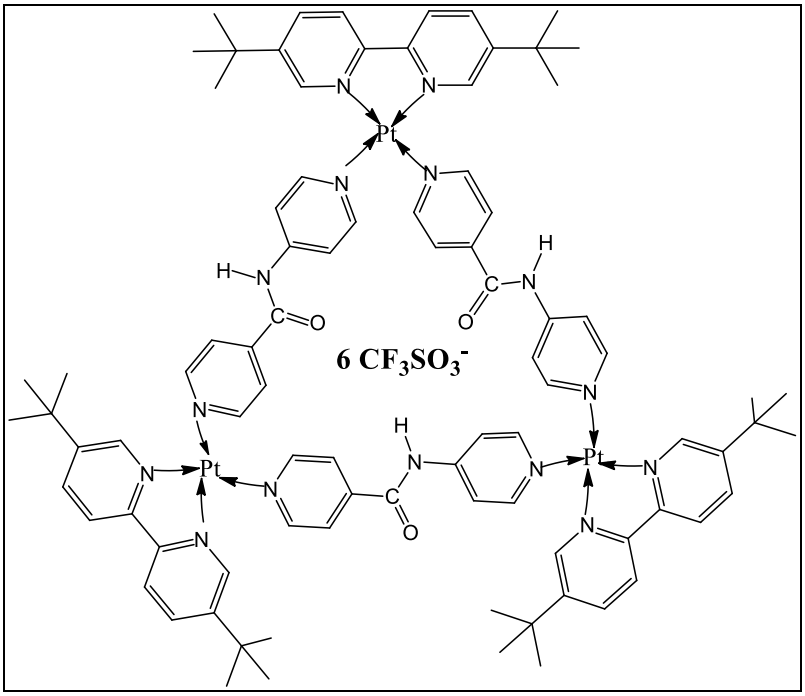

Figure 1.29: Molecular triangle of *cis*-blocked Pt(II) unit with encapsulated triflate anion.[119]

Ghosh and Mukherjee reported the first example of a nanoscopic Pt(II) based molecular rectangle, in which amide backbone was found to be involved in hydrogen bonding with the nitrate counter anion trapped within the rectangular cavity.[120] Kitagawa *et al.* reported a novel flexible (dynamic) porous co-ordination polymer of $Co(SCN)_2$ that showed interesting guest adsorption/desorption properties *via* the single-crystal-to-single-crystal (SCSC) process, but the apohost (CP without guest molecules) was amorphous in nature (Figure 1.30).[121]

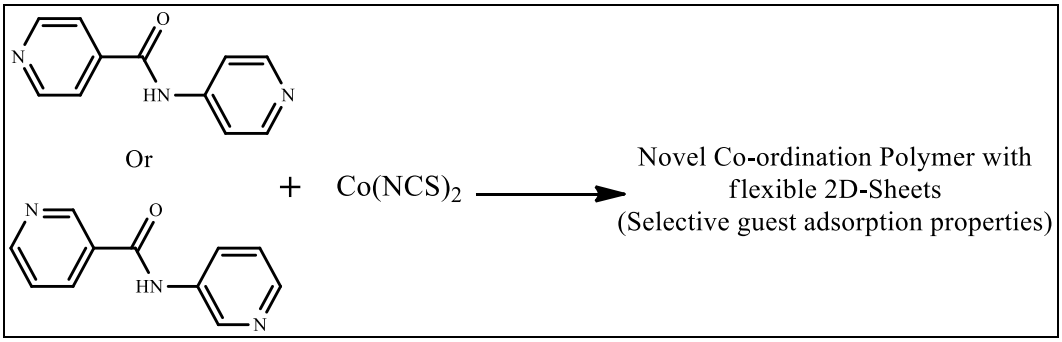

Figure 1.30: Co-ordination polymer of Co(II) with *bis*-pyridyl-*mono*-amide.[121]

Latter on 2004, they introduced the ethyl group in the backbone of *mono*-amide and showed reversible amorphous to crystalline adsorption/desorption behaviour in case of acetone as guest.[122] The amide moiety was often found to be involved in hydrogen bonding with the counter anions and/or the lattice included solvent molecules. Dastidar *et al.* reported counter anion free CPs of *mono*-amide along with carboxylates (fumarate, succinate and terephthalate) and depending on the mode of coordination of the carboxylates, 1D or 2D grid architectures were formed. [123-125] They have reported the 1D polymeric chain of Co(II) and Zn(II) with N-(4-pyridyl)isonicotinamide, where pyridyl-N co-ordinated to two adjacent metal ions.[123] The 1D-chains were further bridged *via* maleate resulted a 2D grid polymeric network (Figure 1.31).

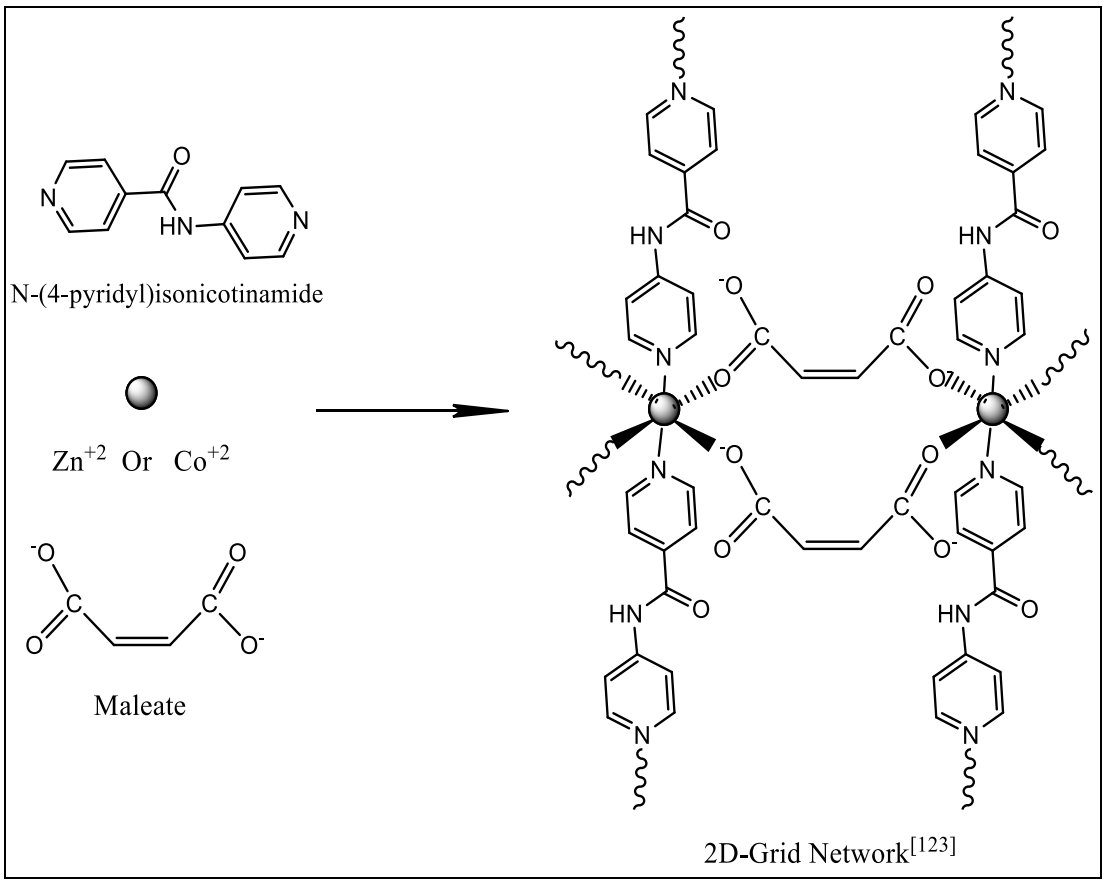

Figure 1.31: 2D-Grid network of Zn(II) and Co(II); maleate acts as bridging ligand.[123]

The effect of charging the N-position in pyridyl group was also observed when N-(3-pyridyl)isonicotinamide and maleate resulted in 1D zig-zag chain co-ordination polymer, where four co-ordination sites were occupied by four oxygen atoms of two maleate (Figure 1.32). These 1D chains are further self-assembled in a parallel fashion *via* hydrogen-bonding

interactions involving carboxylate oxygen atom and amide nitrogen atom.

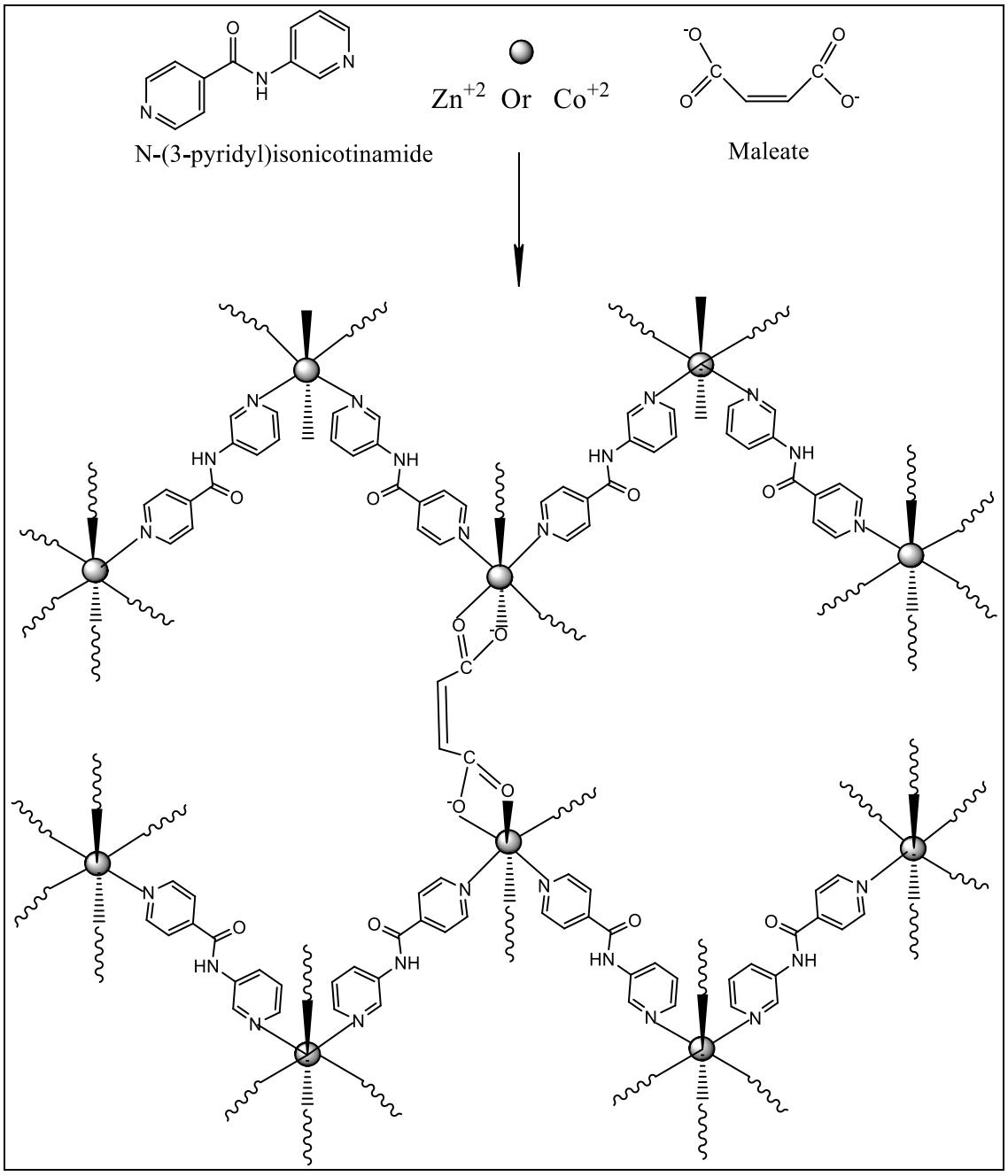

Figure 1.32: 1D Zig-zag chain network of N-(3-pyridyl)isonicotinamide with Co(II) and Zn(II).[125]

The use of phthalate instead of maleate in the CP of Co(II) and N-(4-pyridyl)isonicotinamide resulted in 1D chains, where phthalate anion acted as chelating ligand.[124] While in the CP of Co(II) and N-(3-pyridyl)isonicotinamide, the phthalate anion was co-ordinated in a mono-dentate fashion and resulted 1D zig-zag chains. Further they studied the effect of solvent on

CP of Co(II) and N-(3-pyridyl)isonicotinamide along with sodium fumarate.[125] When methanol was used as solvent, 1D zig-zag chains were obtained, where the chains were packed *via* solvate water molecule but when acetonitrile was used as solvent, ladder like framework was obtained where unco-ordinated fumarate were located between the parallel arrays of the ladder.

1.4.2.2 Co-ordination Polymers of Diamides

Introduction of two amide groups in bis-pyridyl ligand might encourage the hydrogen bonding backbone to participate in self-complementary amide•••amide even in the presence of anions and solvents. Dastidar, Biradha, Wang, Puddephatt are leading research groups explored the co-ordination polymers of pyridyl based diamides ligands having different spacer lengths, with different transition metals and lanthanides.

Biradha *et al*. studied the crystal structure of a series of bis(4-pyridinecarboxamido)alkane and bis(3-pyridinecarboxamido)alkane derivatives in terms of hydrogen bond network of the amide functionalities.[126] These have aliphatic (flexible) or aromatic (semi-rigid) spacer. The structural diversities are more in case of aliphatic spacer ligands because of different possibilities of alkyl chain conformation. These ligands have following characteristic features, that make them unique:[127-137]

1. The ease of synthesis of different isomeric structures of ligands by varying positions of N atoms in the pyridyl rings (ortho, meta or para) and $–(CH_2)_n–$ backbones (n = 0, 1, 2, 3, 4, 5, 6, 8 or 10).
2. The spacer $–(CH_2)_n-$ have A (*anti*) and G (*gauche*) conformations (Figure 1.33) and various other possibilities around -C-C-C- bonds, thus have flexibility to adopt a variety of co-ordination environment of different metal ions leading the formation of novel topologies.

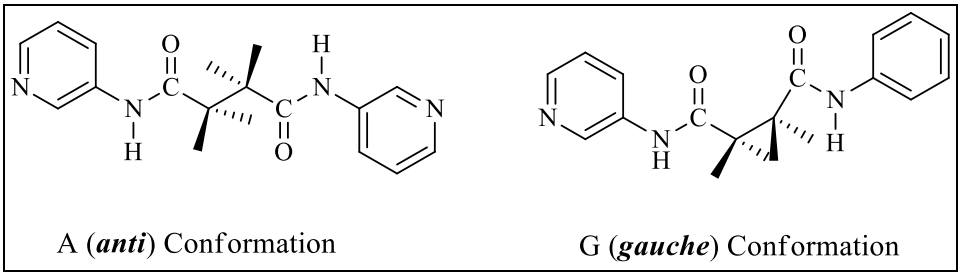

Figure 1.33: A **(*anti*)** and G **(*gauche*)** conformations of ethyl spacer.

3. The two carboxamide functional groups (−CO–NH– or –NH–CO–) have important role in assembling networks *via* hydrogen bonding and also have various possible conformations depending on the orientation of the C=O or N-H groups (Figure 1.34).

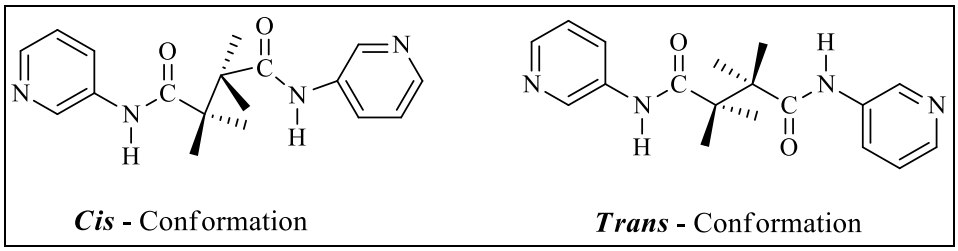

Figure 1.34: ***Cis*** and ***Trans*** conformation due to the orientation of the C=O or N-H groups.

4. The differences in the orientations of the pyridyl-N and amide-O atom further increase the flexibility of ligand topology. when both atoms have same orientation than *Sny* conformation and opposite orientation the conformation is *Anti* (Figure 1.35).[135]

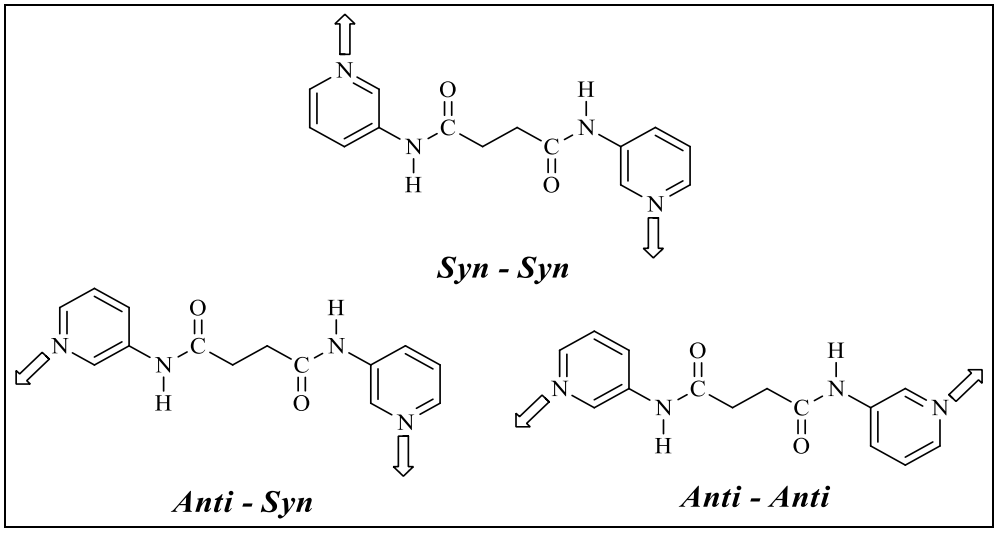

Figure 1.35: ***Anti*** and ***Syn*** due to the orientation of the C=O or N-H groups.

1.4.2.2.1 Co-ordination Polymers of *Bis*-Pyridyl-*Bis*-Amides

Biradha *et al*. reported crystal structure of a series of bis(4-pyridinecarboxamido)alkane and bis(3-pyridinecarboxamido)alkane derivatives, which were found to have β-sheet, doubly interpenetrated (4,4)-network and herringbone networks *via* N-H•••N hydrogen bonding.[138] They further exploited these amide based ligands to generate 2D-coordination networks (interpenetrated and non-interpenetrated) of (4,4)-topology with secondary building units of

CuI (Cu_2I_2 and Cu_4I_4) (Figure 1.36).[139]

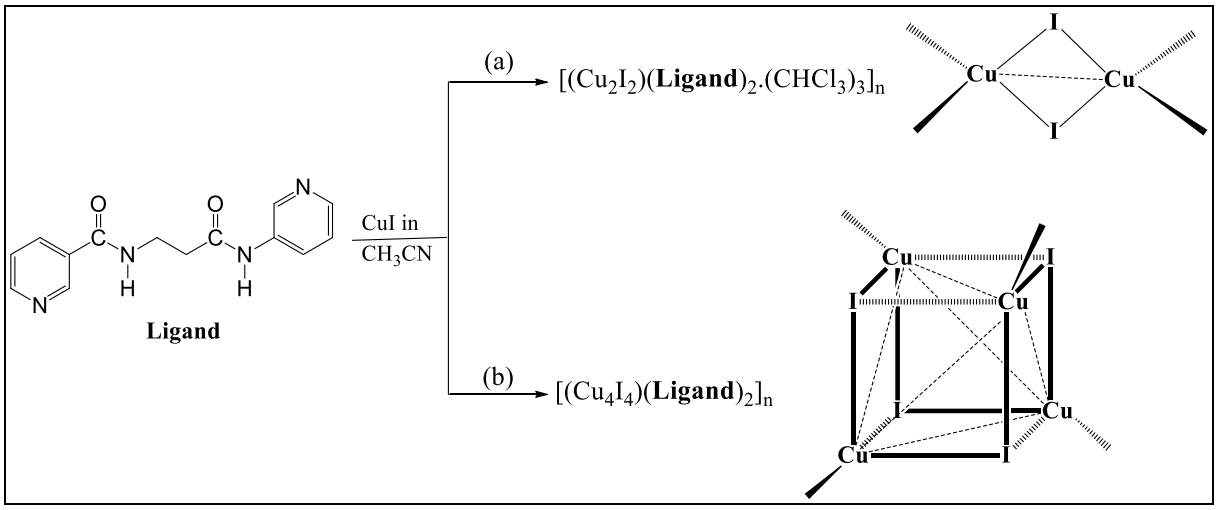

Figure 1.36: Co-ordination polymers of secondary building units of CuI.[139]

M. Sarkar studied the effect of network recognition, transformations, and exchange dynamics of guests and anions and showed how 1D-chain, which has rectangular cavities, was transformed into a pseudo-diamondoid network upon exchange of ClO_4^- with PF_6^- anions (Figure 1.37).[140,141]

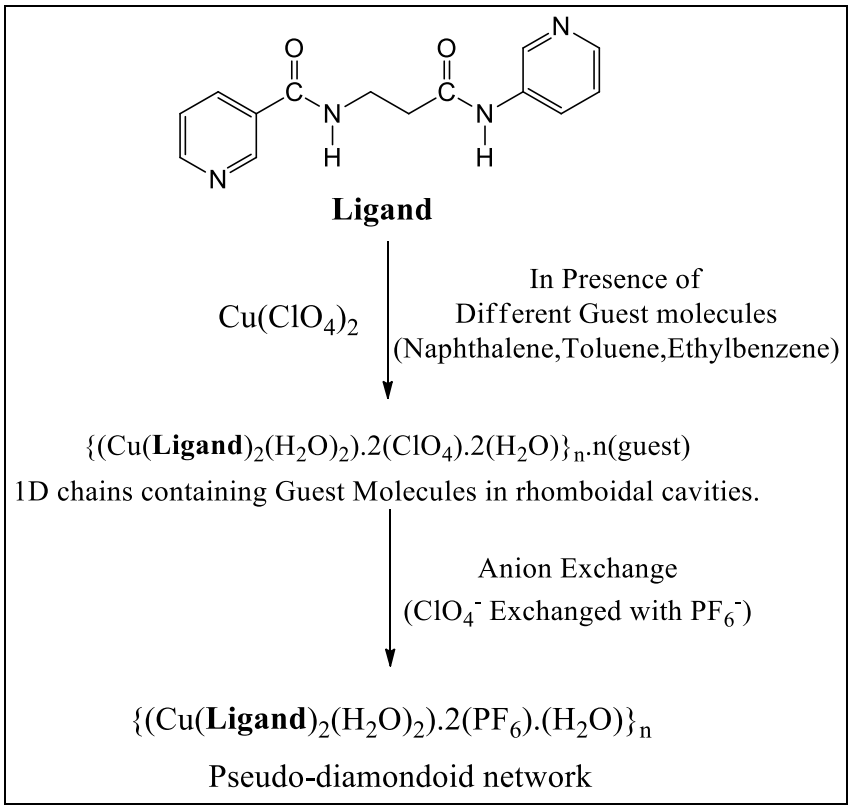

Figure 1.37: Structural transformation resulting on anion exchange.[141]

Extensive studies on the ligands with aromatic and aliphatic backbone reported by Biradha *et al.*[138-141] Puddephatt *et al.*,[142, 143] and Hosseini *et al.*[144] and Puddephatt *et al*. showed 1D co-ordination polymer of N-(2-(cyclohexa-2,4-dienecarboxamido)phenyl)-benzamide with gold (Au), which were assembled into a 3D architecture *via* self-complementary amide•••amide hydrogen bonding. [143] The conformation and hydrogen bonding between the co-ordinated ligands were so similar to those in the free ligand. Hosseini *et al.* reported effect of positional isomerism dependent ligating topology and hydrogen bonding backbone when ligands N,N'-(1,4-phenylene)di-isonicotinamide and N,N'-(1,4-phenylene)di-nicotinamide were reacted separately with $HgCl_2$.[144]

1.4.2.2.2 Co-ordination Polymers Reverse *Bis*-Pyridyl-*Bis*-Amides

N-N′-bis-(pyridine-4-ylmethyl)isophthalamide (**ISO**) was the first *bis*-pyridyl-*bis*-amide, formed a 0D dinuclear cage-like complex with $Cu(NO_3)_2$ as well as $Co(NO_3)_2$ where the metal centers adopts an octahedral geometry (Figure 1.38).[145,146]

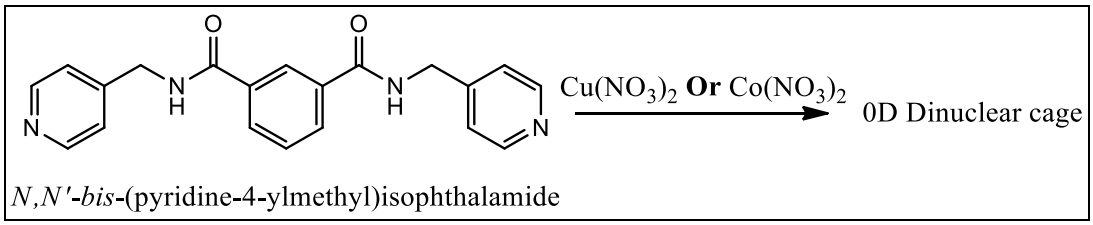

Figure 1.38: Formation of 0D dinuclear cage with Cu(II) or Co(II).[145,146]

The effect of ligating topology and counter anion on the resultant supramolecular array of the CPs was reported for the N^1,N^3-di(pyridin-3-yl)isophthalamide ligand, where it was reacted with $Cd(NO_3)_2$ and $CdSO_4$, under identical reaction conditions (Figure 1.39).[147]

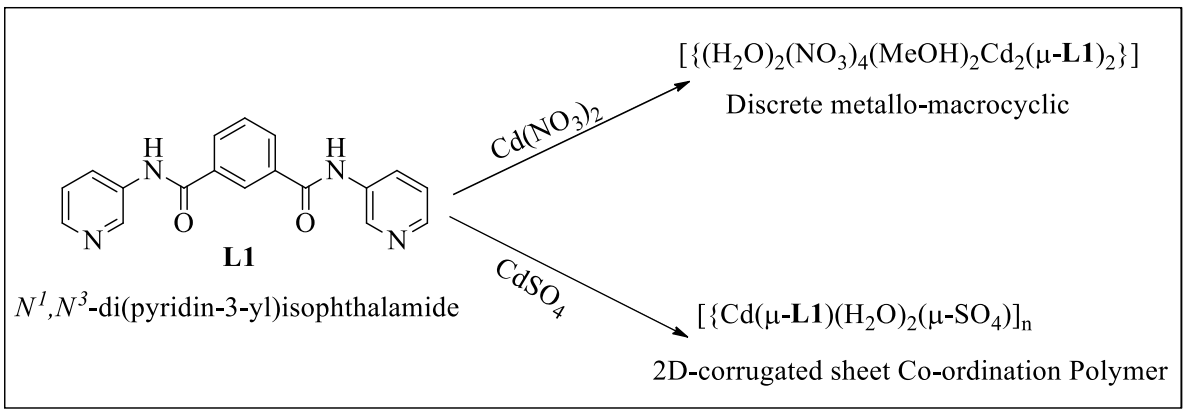

Figure 1.39: Effect of anion in forming different networks.[147]

It was found that the U-shaped ligating topology and mono-co-ordination of the counter anion NO_3^- were responsible for metallamacrocycle with $Cd(NO_3)_2$, while with $CdSO_4$ linear ligating topology and bridging of sulphate (SO_4^{-2}) ions resulted in a 2D corrugated sheet. Anion exchange, encapsulation and separation are important applications of CPs.[148] Thus using N^1,N^3-di(pyridin-3-yl)isophthalamide ligand along with different Cu(II) salts resulted in metallacryptands obtained, where various counter anions such as SO_4^{-2}, SiF_6^{-2}, ClO_4^- were encapsulated within the cryptand cage, which were held by amide•••counter anion hydrogen bonding (Figure 1.40).[149]

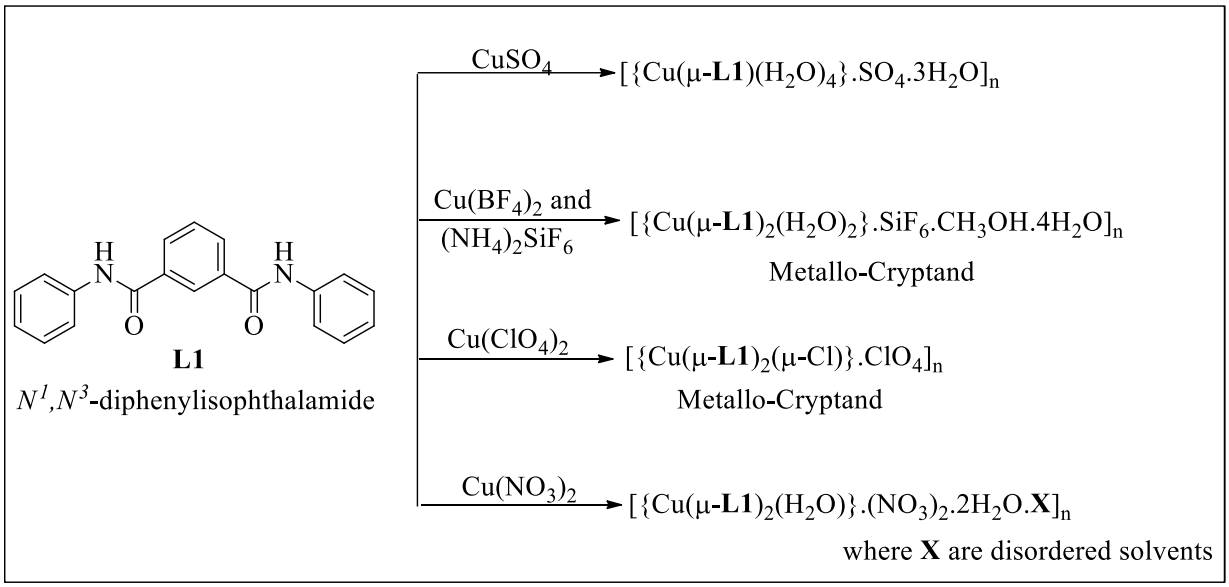

Figure 1.40: Effect of anions on Cu(II) co-ordination polymers.[149]

The nuclear waste tank have anion SO_4^-, as contamination, could be separated from a complex mixture of SO_4^{2-}, ClO_4^- and NO_3^- in the form of Cu (II) metallocryptand. Biradha *et al.* reported chiral 2D CPs of Cu(II) ions of (4,4)-topology in the presence of different anions like SO_4^{2-}, SiF_6^{2-} and NO_3^-.[150] Further they studied the molecular recognition of the organic materials (ligand) in the CPs of *bis*-pyridyl-*bis*-amide and reverse-*bis*-pyridyl-*bis*-amide with $Cu(SCN)_2$ in the presence of various guests such as DMF, nitrobenzene, benzonitrile, 1,4-dihalobenzenes, phenanthrene, biphenyl, anthracene, 9-anthraldehyde and pyrene.[151] Recently, a series of co-ordination polymers of Co(II)/Ni(II)/Cu(II)/Zn(II) and Cd(II) were constructed from semi-rigid *bis*-pyridyl-*bis*-amide and benzenetricarboxylic acid under hydrothermal conditions (Figure 1.41).[152]. Their fluorescence sensing properties and the photocatalytic activities were investigated.

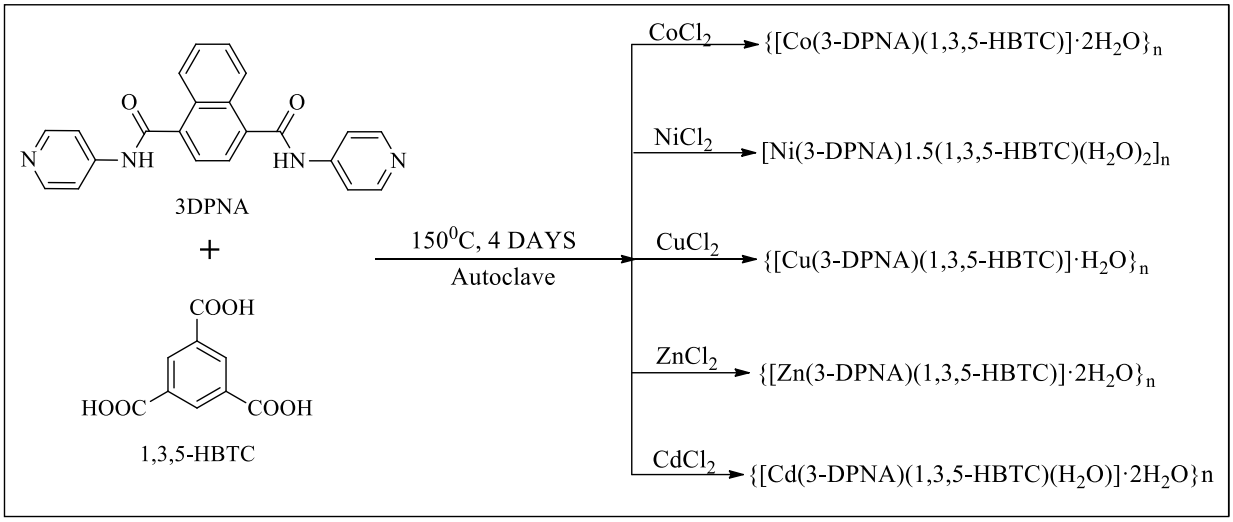

Figure 1.41: A series of co-ordination polymers of Co(II)/Ni(II)/Cu(II)/Zn(II) and Cd(II).[152]

Xiu-Li Wang *et al.* reported the CPs of rigid, semi-rigid and flexible *bis*-pyridyl-*bis*-amide and polycarboxylates. By taking a semi-rigid ligand N,N′-bis(pyridin-3-yl)cyclohexane-1,4-dicarboxamide and polycarboxylates, they synthesized Co(II) and Cu(II) CPs, where they studied the electrochemical behaviors and the solid state fluorescent properties.[153] In the CPs of N,N'-di(3-pyridyl)octanediamide and dicarboxylate, they investigated the role of polycarboxylates in assembling the MOFs of Co(II) and Cu(II).[154]

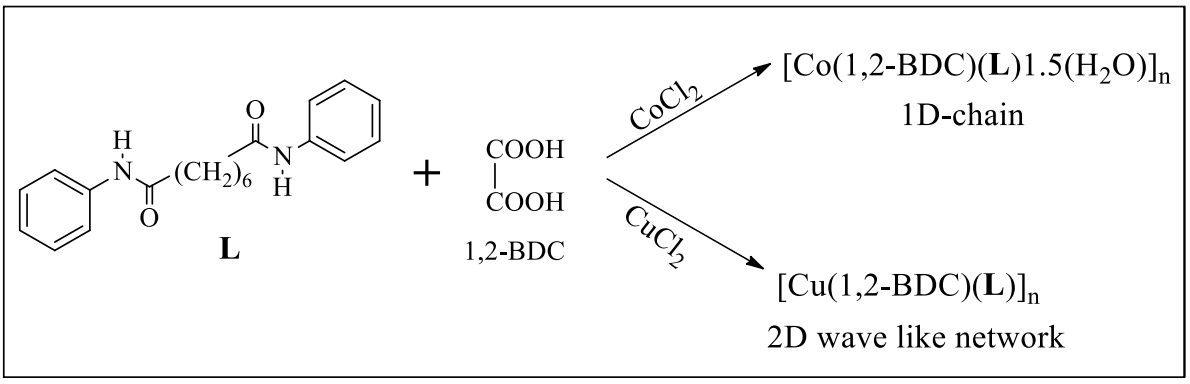

Figure 1.42: Role of dicarboxylate in assembling CPs.[154]

1.5 Postsynthetic Modification (PSM) in Co-ordination polymers

The post-synthetic approaches should be a more controllable synthetic strategy to generate desirable materials because we have the knowledge about the structure and properties of the precursor materials. The modifications on those precursor materials will direct the construction of a designed structure.

Postsynthetic Modification (PSM) can be categorized as:

(a) covalent PSM

(b) dative PSM (co-ordinate PSM)

(c) postsynthetic deprotection (PSD)

Covalent and co-ordinate postsynthetic modifications (PSMs) have been well developed and proved to be a general and facile synthetic strategy toward new functionalized CPs.[155] The direct synthesis of CPs with desired functionalities is often difficult to achieve and dependent on many parameters such as the various co-ordination geometries of the metal center, nature and ligating topologies of the ligands used, metal-to-ligand ratio, nature of the counter anions and various experimental conditions such as solvent, temperature and crystallization methods.[156-158] The post-synthetic approaches are useful when direct methods to synthesize the CPs do not give the expected product in a crystalline form, desired framework topology or function. The post-synthetic modifications of CPs involving exchange of free guest molecules, counter ions or the removal of free/weakly bound solvent molecules have been studied frequently.[159-165]

The CPs derived from hydrogen bond functionalized ligands have the possibility of forming varied hydrogen bond synthons within the networks and have the ability to recognize counter anions and various guest molecules *via* hydrogen bonding interactions.[166,167] The pyridyl based exo- bidentate ligands bearing amide moieties are able to form co-ordination networks and can further assemble into higher dimensional architectures *via* hydrogen bond interactions. The amide-based ligands have been exploited by some of the leading research groups to form CPs, where the networks recognize each other by amide-to-amide hydrogen bonding.[169,170] Nevertheless, continuous effort should be devoted to improve our understanding of CPs *via* "pre-design" as well as post-synthetic modification strategies. The backbone capable of forming hydrogen-bonds involving amides will provide the network recognition process required for forming robust supramolecular architecture while the flexibility in the spacer will give enough opportunity to change the geometry in the event of variation in any of the other components in the CPs. Thus post-synthetic modifications of pre-assembled CPs derived from hydrogen bond functionalized ligands are important because they offer better control over the structures of the porous materials.

Some leading research groups demonstrated 'Metathesis' the replacement or exchange of integral parts (metal ions[171-173] or organic ligands[174-177]) of the CPs without altering their basic structure or topology. Metal metathesis *i.e.* exchange of metal ion (transmetallation[179]) is a type of co-ordinative PSMs, which can be proceed *via* single-crystal-to-single-crystal (SCSC) transformation.[179-186] Although this proved quite challenging, involves simultaneous breaking and formation of several co-ordinate bonds between the ligands and the leaving/incoming metal ions in the solid state. Metal metathesis is an attractive strategy for the incorporation of catalytically active metal center in the framework which is difficult or some time may not be possible - to achieve through direct synthesis. Most of the literature reports are on incomplete and irreversible transmetallation or partial exchange of the framework metal ion which are irreversible in nature.

Kim's group reported first complete and reversible transmetallation in co-ordination polymers of a water-stable tricarboxylate system, where Cd^{+2} ions in the Cd_4O metal nodes exchanged with Pb^{+2} ions in a single-crystal to single-crystal transformation.[179] Zaworotko *et.al.* reported metal-ion exchange in cationic CPs of Cd(II) involving a porphyrin moiety (meso-tetra(N-methyl-4-pyridyl)porphine tetratosylate) encapsulated in the anionic framework of biphenyl-3,4',5-tricarboxylate with $CdCl_2$.[180] They immersed single crystal of Cd(II) co-ordination polymer in methanoic solution of $MnCl_2$, after one week Cd from the cationic part exchanged by Mn, but complete replacement took one month time. Mn have two different oxidation states -in the porphyrin and anionic framework which are +3 and +2 respectively. Structural integrity and single crystallinity maintained even after the exchange but unit cell parameters were reduced because of smaller size of Mn metal. Gargi Mukherjee and Kumar Biradha reported co-ordination polymer of benzene-1,3,5-triyltriisonicotinate ligand with salts of Cu(II), Co(II), Cd(II) and Zn(II) containing ClO_4^-, PF_6^-or SbF_6^- as counter ions in the presence of different aromatic guest molecules.[181] Their CPs showed metal metathesis reactions, where metal exchanged from Zn(II) to Cu(II), Cd(II) to Cu(II), Cu(II) to Cd(II) *via* a SCSC fashion. A number of similar metal ion exchange reactions have been successfully carried out without destroying the framework structures or while maintaining single crystallinity.[182-189]

Huang *et al.* have studied the fluorescence properties on pre- and post-metal ion exchanged CPs and found that the central metal ions have great influence on the fluorescence signal and

play a more important role than their skeleton structures.[184] Zhou and co-workers have demonstrated the robustness and enhanced gas adsorption properties achieved when a Zn_2-paddlewheel in a MOF was substituted by a Cu_2-paddlewheel.[185] The redox-active properties of co-ordination polymers makes them good catalysts but not an easy task because cations in lower oxidation states are not stable, oxidized. Brozek and Dinca have shown that the post-synthetic metal metathesis of $[Zn_4O(1,4\text{-benzenedicarboxylate})_3]_n$ resulted in MOFs with redox reactivity.[186] Liangjun *et al.* synthesized a Zn(II) co-ordination polymer using a methyl-functionalized ligand, having zig-zag pores with pore diameters of ≈0.7 nm, which could be favorable for CO_2 traps. On solvothermal metal metathesis, isomorphic structure but more stable Cu(II) co-ordination polymer produced having a permanent porosity for this framework. They also investigated the influence of the reaction temperatures on the metal metathesis process; slow at room temperature but on increasing the temperatures complete replacement occurred.[187]

Grancha *et al.* reported SCSC transmetallation in the three-dimensional (3D) framework of formula $Mg^{II}_2\{Mg^{II}_4[Cu^{II}_2\text{-}(Me_3mpba)_2]_3\}\cdot 45H_2O$ where Me_3mpba^{4-} is N,N′-2,4,6-trimethyl-1,3-phenylenebis(oxamate)). The complete exchanged of the Mg^{+2} ions by Co^{+2} and Ni^{+2} ions took seven days and generate two co-ordination networks having higher structural stability and enhanced gas sorption and magnetic properties.[188] Recently Soana *et al.* synthesized an extremely flexible and robust anionic Cd- co-ordination polymer, where metal metathesis resulted in 16 new iso-structural CPs of transition metals, lanthanide and main group metal ions have been obtained, out of which 11 of them were characterized with single crystal X-ray structures determined.[189] The extent of metal exchange can be studied by elemental analyses by inductively coupled plasma atomic emission spectroscopy (ICP-AES), EDX analyses and SXRD refinement and Cd : M (exchanged metal) ratio determined. After post-synthetic modification the new obtained CPs exploited for the separation of organic dyes based on their charges and the lanthanides shows brilliant luminescence.

1.6 Aim of the Present Study

The synthesis of co-ordination polymers with robust and flexible network but can undergo reversible structural modifications in response to external stimulus, has always been a major challenge. The approaches that can be used to generate flexible sort of framework include: (i) using flexible building units (e.g. alkyl chains) connected with strong interactions (e.g. co-

ordination bonds); (ii) using stiff building units (e.g. phenyl group) connected with weaker interactions (e.g. hydrogen bonds, van der Waals interactions, π–π stacking); (iii) using a combination of flexible building units (e.g. alkyl chains) and weaker interactions (e.g. hydrogen bonds, van der Waals interactions, π-π stacking).

The main objective of the present thesis is to obtain flexible co-ordination polymers and to observe the structural transformation on changing the external conditions. Generating flexible CPs will also lead us to achieve the following targets: (i) Wide range of novel topological architectures of the CPs, where the assembling of the frameworks *via* various non-covalent interactions will be explored; (ii) Flexible nature of CPs induced by guest molecules will be explored; (iii) Structure properties relationship of the CPs**.**

1.7 References

[1] Lehn, J., M. *Pure Appl. Chem* **1978**, *50*, 871–892.

[2] Lehn, J.-M. *Angew. Chem. Int. Ed. Engl.* **1988**, *27* (1), 89-112.

[3] Cram, D. J. *Angew. Chem. Int. Ed. Engl.* **1988**, *27* (8), 1009-1020.

[4] Pedersen, C. J. *Angew. Chem. Int. Ed. Engl.* **1988**, *27* (8), 1021-1027.

[5] Lehn, J. M. *Supramolecular chemistry: Concepts and perspectives, 1st* edition (Weinheim: VCH) **1995**.

[6] Steed, J. W.; Atwood, J. L. *Supramolecular chemistry* (Chichester: Wiley) **2000**.

[7] Steed, J. W.; Atwood, J. L. *Supramolecular Chemistry, 2nd edition*, **2009**, John Wiley & Sons, Ltd.

[8] Cram, D. J. *Angew. Chem. Int. Ed. Engl.* **1986**, *25* (12), 1039-1057.

[9] Cook, T. R.; Zheng, Y.-R.; Stang, P. J. *Chem. Rev.* **2013**, *113* (1), 734-777.

[10] Qu, D.-H.; Wang, Q.-C.; Zhang, Q.-W.; Ma, X.; Tian, H. *Chem. Rev.* **2015**, *115* (15), 7543-7588.

[11] Ikkala, O.; ten Brinke *Science* **2002**, *295* (5564), 2407-2409.

[12] Hollingsworth, M. D. *Science* **2002**,*295* (5564), 2410-2413.

[13] Kato, T. *Science* **2002**, *295* (5564), 2414-2418.

[14] Schmidt, G. M. J. *Pure Appl. Chem*, **1971**, *27*(4), 647-678.

[15] Desiraju, G. R. Crystal *Engineering: The Design of Organic Solids*, Elsevier, Amsterdam **1989**.

[16] Liu, J.; Thallapally, P. K.; McGrail, B. P.; Brown, D. R.; Liu, J. *Chem. Soc. Rev.* **2012**, *41* (6), 2308-2322.

[17] Hasegawa, S.; Horike, S.; Matsuda, R.; Furukawa, S.; Mochizuki, K.; Kinoshita, Y.; Kitagawa, S. *J. Am. Chem. Soc.* **2007**, *129* (9), 2607-2614.

[18] Chen, B.; Wang, L.; Zapata, F.; Qian, G.; Lobkovsky, E. B. *J. Am. Chem. Soc.* **2008**, *130* (21), 6718-6719.

[19] Chen, B.; Wang, L.; Xiao, Y.; Fronczek, F. R.; Xue, M.; Cui, Y.; Qian, G. *Angew. Chem. Int. Ed. Engl.* **2009**, *48* (3), 500-503.

[20] McGuire, C. V.; Forgan, R. S. *Chem. Commun.* **2015**, *51* (25), 5199-5217.

[21] Devic, T.; Horcajada, P.; Serre, C.; Salles, F.; Maurin, G.; Moulin, B.; Heurtaux, D.; Clet, G.; Vimont, A.; Grenèche, J.-M.; Ouay, B. L.; Moreau, F.; Magnier, E.; Filinchuk, Y.; Marrot, J.; Lavalley, J.-C.; Daturi, M.; Férey, G. *J. Am. Chem. Soc.* **2010**, *132* (3), 1127-1136.

[22] Bauer, C. A.; Timofeeva, T. V.; Settersten, T. B.; Patterson, B. D.; Liu, V. H.; Simmons, B. A.; Allendorf, M. D. *J. Am. Chem. Soc.* **2007**, *129* (22), 7136-7144.

[23] Lee, D. Y.; Kim, E.-K.; Shin, C. Y.; Shinde, D. V.; Lee, W.; Shrestha, N. K.; Lee, J. K.; Han, S.-H. *RSC Adv.* **2014**, *4* (23), 12037-12042.

[24] Silva, C. G.; Corma, A.; Garcia, H. *J. Mater. Chem.* **2010**, *20* (16), 3141-3156.

[25] Desiraju, G. R. *Angew. Chem. Int. Ed. Engl.* **1995**, *34* (21), 2311-2327.

[26] Allen, F. H.; Kennard, O. *Chem. Des. Automation News*, **1993**, *8* (1), 31-37.

[27] Hamilton, W. C.; Ibers, J. A. *Hydrogen Bonding in Solids*, Benjamin, New York, **1968**, 188.

[28] Taylor, R.; Kennard, O. *Acc. Chem. Res.* **1984**, *17* (9), 320-326.

[29] Latimer, W. M.; Rodebush, W. H. *J. Am. Chem. Soc.* **1920**, *42* (7), 1419-1433.

[30] Linus; Pauling *The Nature of Chemical Bond and the Structure of Molecules and Crystals – An Introduction to Modern Structural Chemistry*, Oxford University Press, London, **1940**.

[31] Pimentel, G.C.; McClellan, A.L. *The Hydrogen Bond*, Freeman, San Francisco, **1960**.

[32] Atkins, P. *General Chemistry*, Scientific American Books, New York, **1989**

[33] Steiner, T. *Angew. Chem. Int. Ed. Engl.* **2002**, *41* (1), 48-76.

[34] Desiraju, G. R. *The Weak Hydrogen Bond in Structural and Chemical Biology*, Oxford University Press, Oxford, **1999**.

[35] Braga, D.; Grepioni, F.; Biradha, K.; Pedireddi, V. R.; Desiraju, G. R. *J. Am. Chem. Soc.* **1995**, *117* (11), 3156-3166.

[36] Braga, D.; Grepioni, F.; Desiraju, G. R. *Chem. Res.* **1998**, *98* (4), 1375-1406.

[37] Aakeroy, C. B. *Chem. Commun.* **1998**, (10), 1067-1068.

[38] Aakeröy, C. B.; Beatty, A. M.; Leinen, D. S. *Angew. Chem. Int. Ed. Engl.* **1999**, *38*(12), 1815-1819.

[39] Aakeroy, C. B.; Beatty, A. M.; Leinen, D. S. *CrystEngComm* **2002**, *4* (55), 310-314.

[40] Braga, D.; Grepioni, F. *Coord. Chem. Rev.* **1999**, *183* (1), 19-41.

[41] Braga, D.; Grepioni, F. *Acc. Chem. Res.* **2000**, *33* (9), 601-608.

[42] Bazzicalupi, C.; Bencini, A.; Berni, E.; Bianchi, A.; Ciattini, S.; Giorgi, C.; Paoletti, P.; Valtancoli, B. *Eur. J. Inorg. Chem.* **2001**, *2001* (3), 629-632.

[43] Beatty, A. M. *CrystEngComm* **2001**, (51), 243-255.

[44] Goldberg, I. *Chem. Commun.* **2005**, (10), 1243-1254.

[45] Hunter, C. A.; Sanders, J. K. M. *Angew. Chem. Int. Ed. Engl.* **1990**, *112* (14), 5525-5534.

[46] Williams, J. H.; Cockcroft, J. K.; Fitch, A. N. *Angew. Chem. Int. Ed. Engl.* **1992**, *31* (12), 1655-1657.

[47] Claessens, C. G.; Stoddart, J. F. *J. Phys. Org. Chem.* **1997**, *10* (5), 254-272.

[48] Sinnokrot, M. O.; Sherrill, C. D. *J. Phys. Chem. A* **2006**, *110* (37), 10656-10668.

[49] Cockroft, S. L.; Hunter, C. A.; Lawson, K. R.; Perkins, J.; Urch, C. J *J. Am. Chem. Soc.* **2005**, *127* (24), 8594-8595.

[50] Cai, H.; Guo, Y.; Li, J.-G *Acta Crystallogr. Sect. C* **2013**, *69* (1), 8-10.

[51] Rajput, L.; Hong, S.; Liu, X.; Oh, M.; Kim, D.; Lah, M. S. *CrystEngComm* **2011**, *13* (23), 6926-6929.

[52] Egli, M.; Sarkhel, S. *Acc. Chem. Res.* **2007**, *40* (3), 197-205.

[53] Jain, A.; Purohit, C. S.; Verma, S.; Sankararamakrishnan, R. *J. Phys. Chem. B* **2007**, *111* (30), 8680-8683.

[54] Wan, C.-Q.; Chen, X.-D.; Mak, T. C. W. *CrystEngComm* **2008**, *10* (5), 475-478.

[55] Hoskins, B. F.; Robson, R. *J. Am. Chem. Soc.* **1990**, *112* (4), 1546-1554.

[56] Eddaoudi, M.; Li, H. L.; Yaghi, O. M. *J. Am. Chem. Soc*. **2000**, *122* (7), 1391-1397.

[57] Yaghi, O. M.; O'Keeffe, M.; Ockwig, N. W.; Chae, H. K.; Eddaoudi, M.; Kim, J. *Nature* **2003**, *423* (6941), 705-714.

[58] Kinoshita, Y.; Matsubara, I.; Higuchi, T.; Saito, Y. *Bull. Chem. Soc. Jpn.* **1959**, *32* (11), 1221-1226.

[59] Knobloch, F. W.; Rauscher, W. H. *J. Polym. Sci.* **1959**, *38* (133), 261-262.

[60] Aleksandr, A. B.; Matveeva, N. G. *Russ. Chem. Rev.***1960**, *29* (3), 119-128.

[61] Block, B. P.; Rose, S. H.; Schaumann, C. W.; Roth, E. S.; Simkin, J. *J. Am. Chem. Soc.* **1962**, *84* (16), 3200-3201.

[62] Kubo, M.; Kishita, M.; Kuroda, Y. *J. Polym. Sci.* **1960**, *48* (150), 467-471.

[63] Tomic, E. A. *J. Appl. Polym. Sci.* **1965**, *9* (11), 3745-3752.

[64] Batten, S. R.; Hoskins, B. F.; Robson, R. *J. Am. Chem. Soc.* **1995,** *117* (19), 5385-5386.

[65] Kitagawa, S.; Matsuyama, S.; Munakata, M.; Emori, T. *Dalton Trans.* **1991**, (11), 2869-2874.

[66] Kitagawa, S.; Kawata, S.; Nozaka, Y.; Munakata, M. *Dalton Trans.* **1993**, (9), 1399-1404.

[67] Riou, D.; Ferey, G. *J. Mater. Chem.* **1998**, *8* (12), 2733-2735.

[68] Li, H.; Eddaoudi, M.; O'Keeffe, M.; Yaghi, O. M. *Nature* **1999**, *402* (6759), 276-279.

[69] Long, J. R.; Yaghi, O. M. *Chem. Soc. Rev.* **2009**, *38* (5), 1213-1214.

[70] Ferey, G. *Chem. Soc. Rev.* **2008**, *37* (1), 191-214.

[71] Kubel, F.; Strähle, J. *Z. Naturforsch.* **1982**, *37b*, 272-275.

[72] Chawla, S. K.; Hundal, M. S.; Kaur, J.; Obrai, S. *Polyhedron* **2001**, *20* (17), 2105-2111.

[73] Seidel, R. W.; Goddard, R.; Zibrowius, B.; Oppel, I. M. *Polymers* **2011**, *3* (3), 1458-1474.

[74] Fletcher, A. J.; Cussen, E. J.; Bradshaw, D.; Rosseinsky, M. J.; Thomas, K. M. *J. Am. Chem. Soc.* **2004**, *126* (31), 9750-9759.

[75] Yaghi, O. M.; Li, H.; Groy, T. L. *Inorg. Chem.* **1997,** *36* (20), 4292-4293.

[76] Gable, R. W.; Hoskins, B. F.; Robson, R. *Chem. Commun.* **1990**, (23), 1677-1678.

[77] Fujita, M.; Kwon, Y. J.; Washizu, S.; Ogura, K. *J. Am. Chem. Soc.***1994**, *116* (3), 1151-1152.

[78] Biradha, K.; Fujita, M. *Dalton Trans.* **2000**, (21), 3805-3810.

[79] Biradha, K.; Hongo, Y.; Fujita, M. *Angew. Chem. Int. Ed.* **2000**, *39* (21), 3843-3845.

[80] Biradha, K.; Aoyagi, M.; Fujita, M. *J. Am. Chem. Soc.* **2000**, *122* (10), 2397-2398.

[81] Biradha, K.; Fujita, M. *J. Inclusion Phenom. Mol. Recognit. Chem.* **2001**, *41* (1-4), 201-208.

[82] Pschirer, N. G.; Ciurtin, D. M.; Smith, M. D.; Bunz, U. H. F.; zur Loye, H.-C. *Angew. Chem. Int. Ed.* **2002**, *41* (4), 583-585.

[83] Sarkar, M.; Biradha, K. *Cryst. Growth Des.* **2007**, *7* (7), 1318-1331.

[84] Gong, Y.; Li, J.; Qin, J.; Wu, T.; Cao, R.; Li, J. *Cryst. Growth Des.* **2011**, *11* (5), 1662-1674.

[85] Wang, X.-L.; Luan, J.; Sui, F.-F.; Lin, H.-Y.; Liu, G.-C.; Xu, C. *Cryst. Growth Des.* **2013**, *13* (8), 3561-3576.

[86] Biradha, K.; Fujita, M. *Chem. Commun.* **2001**, (1), 15-16.

[87] Tong, M.-L.; Chen, X.-M.; Yu, X.-L.; Mak, T. C.W. *Dalton Trans.* **1998**, (1), 5-6.

[88] MacGillivray, L. R.; Subramanian, S.; Zaworotko, M. J. *Chem. Commun.* **1994**, (11), 1325-1326.

[89] Yaghi, O. M; Li, G. *Angew. Chem. Int. Ed. Engl.* **1995**, *34* (2), 207-209.

[90] Hennigar, T. L.; MacQuarrie, D. C.; Losier, P.; Rogers, R. D.; Zaworotko, M. J. *Angew. Chem. Int. Ed. Engl.* **1997**, *36* (9), 972-973.

[91] Atencio, R.; Biradha, K.; Hennigar, T. L.; Poirier, K. M.; Power, K. N.; Seward, C. M.; White, N. S.; Zaworotko, M. J. *Cryst. Eng.* **1998**, *1* (3–4), 203-212.

[92] Lin, J.; Wen, L.; Zang, S.; Su, S.; Lu, Z.; Zhu, H.; Meng, Q. *Inorg. Chem. Commun.* **2007**, *10* (1), 74-76.

[93] Lu, W.-G.; Jiang, L.; Feng, X.-L.; Lu, T.-B. *Cryst. Growth Des.* **2006**, *6* (2), 564-571.

[94] Robinson, F.; Zaworotko, M. J. *Chem. Commun.* **1995**, (23), 2413-2414.

[95] Yaghi, O. M.; Li, H. *J. Am. Chem. Soc.***1995**, *117* (41), 10401-10402.

[96] Yaghi, O. M.; Li, H. *J. Am. Chem. Soc.***1996**, *118* (1), 295-296.

[97] MacGillivray, L. R.; Subramanian, S.; Zaworotko, M. J. *Chem. Commun.* **1994**, (11), 1325-1326.

[98] Carlucci, L.; Ciani, G.; Proserpio, D. M.; Sironi, A. *Chem. Commun.***1994**, (24), 2755-2756.

[99] Subramanian, S.; Zaworotko, M. J. *Angew. Chem. Int. Ed. Engl.* **1995**, *34* (19), 2127-2129.

[100] Noro, S.-i.; Kitagawa, S.; Kondo, M.; Seki, K. *Angew. Chem. Int. Ed. Engl.* **2000**, *39* (12), 2081-2084.

[101] Aakeröy, C. B.; Beatty, A. M.; Leinen, D. S. *Angew. Chem. Int. Ed.* **1999**, 38 (12), 1815-1819.

[102] Krishna Kumar, R.; Goldberg, I. *Chem. Commun*. **1998**, (14), 1435-1436.

[103] Kobayashi, K.; Koyanagi, M.; Endo, K.; Masuda, H.; Aoyama, Y. *Chem. Eur. J.* **1998**, *4* (3), 417-424.

[104] Custelcean, R.; Haverlock, T. J.; Moyer, B. A. *Inorg. Chem.* **2006**, *45* (16), 6446-6452.

[105] Kumar, D. K.; Jose, D. A.; Das, A.; Dastidar, P. *Inorg. Chem.* **2005**, *44* (20), 6933-6935.

[106] Kumar, D. K.; Das, A. *CrystEngComm* **2006**, *8* (11), 805-814.

[107] Kumar, D. K.; Das, A.; Dastidar, P. *New J. Chem.* **2006**, *30* (9), 1267-1275.

[108] Kumar, D. K.; Das, A.; Dastidar, P. *Cryst. Growth Des.* **2007**, *7* (2), 205-207.

[109] Kumar, D. K.; Das, A.; Dastidar, P. *Cryst. Growth Des.* **2007**, *7* (10), 2096-2105.

[110] Applegarth, L.; Goeta, A. E.; Steed, J. W. *Chem. Commun.* **2005**, (18), 2405-2406.

[111] Byrne, P.; Lloyd, G. O.; Clarke, N.; Steed, J. W. *Angew. Chem. Int. Ed.* **2008,** *47* (31), 5761-5764.

[112] Carlucci, L.; Ciani, G.; Proserpio, D. M. *CrystEngComm* **2003**, *5* (47), 269–279.

[113] Adarsh, N. N.; Dastidar, P. *Cryst. Growth Des.* **2010**, *10* (2), 483-487.

[114] Applegarth, L.; Clark, N.; Richardson, A. C.; Parker, A. D. M.; Radosavljevic-Evans, I.; Goeta, A. E.; Howard, J. A. K.; Steed, J. W. *Chem. Commun.* **2005**, (43), 5423-5425.

[115] Custelcean, R.; Sellin, V.; Moyer, B. A. *Chem. Commun.***2007,** (15), 1541-1543.

[116] Adarsh, N. N.; Kumar, D. K.; Dastidar, P. *Curr. Sci.* **2011**, *101* (7), 869-880.

[117] Banerjee, S.; Adrash, N. N.; Dastidar, P. *CrystEngComm* **2013**, *15* (2), 245-248.

[118] Kitagawa, S.; Uemura, T.; Uemura, K.; Arakawa, M.; Tanabe, S. JP2004323455A, **2004.**

[119] Qin, Z.; Jennings, M. C.; Puddephatt, R. J. *Chem. Commun.* **2001**, (24), 2676-2677.

[120] Ghosh, S.; Mukherjee, P. S. *Dalton Trans.* **2007,** (24), 2542-2546.

[121] Uemura, K.; Kitagawa, S.; Kondo, M.; Fukui, K.; Kitaura, R.; Chang, H.-C.; Mizutani, T. *Chem. Eur. J.* **2002**, *8* (16), 3586-3600.

[122] Uemura, K.; Kitagawa, S.; Fukui, K.; Saito, K. *J. Am. Chem. Soc.* **2004**, *126* (12), 3817-3828.

[123] Kumar, D. K.; Das, A.; Dastidar, P. *Cryst. Growth Des.***2006**, *6* (8), 1903-1909.

[124] Kumar, D. K.; Das, A.; Dastidar, P. *J. Mol. Struct.* **2006**, *796* (1–3), 139-145.

[125] Kumar, D. K.; Das, A.; Dastidar, P. *CrystEngComm* **2007**, *9* (10), 895-901.

[126] Rajput, L.; Biradha, K. *Cryst. Growth Des*. **2007**, *7* (12), 2376-2379.

[127] Rajput, L.; Biradha, K. *CrystEngComm* **2009**, *11* (7), 1220-1222.

[128] Rajput, L.; Biradha, K. *New J. Chem.* **2010**, *34* (11), 2415-2428.

[129] Rajput, L.; Chernyshev, V. V.; Biradha, K. *Chem. Commun.* **2010**, *46* (35), 6530-6532.

[130] Saha, S.; Rajput, L.; Joseph, S.; Mishra, M. K.; Ganguly, S.; Desiraju, G. R. *CrystEngComm* **2015**, *17* (6), 1273-1290.

[131] Rajput, L.; Kim, D.; Lah, M. S. *CrystEngComm* **2013**, *15* (2), 259-264.

[132] Rajput, L.; Hong, S.; Liu, X.; Oh, M.; Kim, D.; Lah, M. S. *CrystEngComm* **2011**, *13* (23), 6926-6929.

[133] Rajput, L.; Banerjee, R. *Cryst. Growth Des.* **2014**, *14* (6), 2729-2732.

[134] Rajput, L.; Biradha, K.*Cryst. Growth Des*. **2009**, *9* (1), 40-42.

[135] Rajput, L.; Biradha, K. *Cryst. Growth Des*. **2009**, *9* (9), 3848-3851.

[136] Rajput, L.; Biradha, K. *Cryst. Growth Des*. **2007**, *7* (12), 2376-2379.

[137] Oh, M.; Rajput, L.; Kim, D.; Moon, D.; Lah, M. S. *Inorg. Chem.* **2013**, *52* (7), 3891-3899.

[138] Sarkar, M.; Biradha, K. *Cryst. Growth Des*. **2006**, *6* (1), 202-208.

[139] Sarkar, M.; Biradha, K. *Chem. Commun.* **2005**, (17), 2229-2231.

[140] Sarkar, M.; Biradha, K. *Cryst. Growth Des*. **2006**, *6* (8), 1742-1745.

[141] Sarkar, M.; Biradha, K. *Cryst. Growth Des*. **2007**, *7* (7), 1318-1331.

[142] Burchell, T. J.; Eisler, D. J.; Jennings, M. C.; Puddephatt, R. J. *Chem. Commun.* **2003**, (17), 2228-2229.

[143] Burchell, T. J.; Puddephatt, R. J. *Inorg. Chem.* **2005**, *44* (10), 3718-3730.

[144] Pansanel, J.; Jouaiti, A.; Ferlay, S.; Wais Hosseini, M.; Planeix, J.-M.; Kyritsakas, N. *New J. Chem.* **2006**, *30* (1), 71-76.

[145] Cheng, P.-C.; Yeh, C.-W.; Hsu, W.; Chen, T.-R.; Wang, H.-W.; Chen, J.-D.; Wang, J.-C. *Cryst. Growth Des*. **2012**, *12* (2), 943-953.

[146] Barbour, L. J.; Orr, G. W.; Atwood, J. L. *Nature* **1998**, *393* (6686), 671-673.

[147] Adarsh, N. N.; Kumar, D. K.; Dastidar, P. *Inorg. Chem. Commun.* **2008**, *11* (6), 636-642.

[148] Akine, S.; Miyashita, M.; Piao, S.; Nabeshima, T. *Inorg. Chem. Front.* **2014**, *1* (1), 53-57.

[149] Adarsh, N. N.; Tocher, D. A.; Ribas, J.; Dastidar, P. *New J. Chem*. **2010**, *34* (11), 2458-2469.

[150] Rajput, L.; Biradha, K. *Cryst. Growth Des.* **2009**, *9* (9), 3848-3851.

[151] Rajput, L.; Biradha, K. *New J. Chem*. **2010**, *34* (11), 2415-2428.

[152] Wang, X.; Le, M.; Lin, H.-Y.; Luan, J.; Liu, G.-C.; Sui, F.-F.; Chang, Z.-H. *Inorg. Chem. Front.* **2015**, *2* (4), 373-387.

[153] Wang, X.-L.; Mu, B.; Lin, H.-Y.; Yang, S.; Liu, G.-C.; Tian, A.-X.; Zhang, J.-W. *Dalton Trans.* **2012**, *41* (36), 11074-11084.

[154] Wang, X.-L.; Sui, F.-F.; Lin, H.-Y.; Xu, C.; Liu, G.-C.; Zhang, J.-W.; Tian, A.-X. *CrystEngComm* **2013**, *15* (36), 7274-7284.

[155] Cohen, S. M., *Chem. Rev.* **2012**, *112* (2), 970-1000.

[156] Batten, S. R.; Neville, S. M.; Turner, D. R. *Coordination Polymers: Design, Analysis and Application*, RSC Publishing, **2009.**

[157] Hong, M.-C.; Chen, L. *Design and Construction of Coordination Polymers,* John Wiley & Sons, **2009.**

[158] Stock, N.; Biswas, S. *Chem. Rev*. **2012**, *112* (2), 933-969.

[159] Kitagawa, S.; Uemura, K. *Chem. Soc. Rev.* **2005**, *34* (2), 109-119.

[160] Chen, C.-L.; Beatty, A. M. *J. Am. Chem. Soc.* **2008**, *130* (51), 17222-17223.

[161] Cao, M.-L.; Mo, H.-J.; Liang, J.-J.; Ye, B.-H. *CrystEngComm* **2009**, *11* (5), 784-790.

[162] Hao, H.-Q.; Lin, Z.-J.; Hu, S.; Liu, W.-T.; Zheng, Y.-Z.; Tong, M.-L. *CrystEngComm* **2010**, *12* (7), 2225-2231.

[163] Chen, B.; Xiang, S.; Qian, G. *Acc. Chem. Res.* **2010**, *43* (8), 1115-1124.

[164] Aguado, S.; Bergeret, G.; Titus, M. P.; Moizan, V.; Nieto-Draghi, C.; Bats, N.; Farrusseng, D. *New J. Chem*. **2011**, *35* (3), 546-550.

[165] Sharma, M. K.; Bharadwaj, P. K. *Inorg. Chem.* **2011**, *50* (5), 1889-1897.

[166] Aakeroy, C. B.; Beatty, A. M.; Leinen, D. S.; Lorimer, K. R. *Chem. Commun.* **2000**, (11), 935-936.

[167] Adarsh, N. N.; Kumar, D. K.; Suresh, E.; Dastidar, P. *Inorg. Chim. Acta* **2010**, *363* (7), 1367-1376.

[168] Adarsh, N. N.; Dastidar, P. *Chem. Soc. Rev.* **2012**, *41* (8), 3039-3060.

[169] Sarkar, M.; Biradha, K. *Cryst. Growth Des.* **2007**, *7* (7), 1318-1331.

[170] Mi, L.; Hou, H.; Song, Z.; Han, H.; Xu, H.; Fan, Y.; Ng, S.-W. *Cryst. Growth Des.* **2007**, *7* (12), 2553-2561.

[171] Mi, L.; Hou, H.; Song, Z.; Han, H.; Fan, Y. *Chem. Eur. J.* **2008**, *14* (6), 1814-1821.

[172] Wang, X.-J.; Li, P.-Z.; Liu, L.; Zhang, Q.; Borah, P.; Wong, J. D.; Chan, X. X.; Rakesh, G.; Li, Y.; Zhao, Y. *Chem. Commun.* **2012**, *48* (83), 10286-10288.

[173] Han, S.; Ma, Z.; Hopson, R.; Wei, Y.; Budil, D.; Gulla, S.; Moulton, B. *Inorg. Chem. Commun.* **2012**, *15*, 78-83.

[174] Galet, A.; Munoz, M. C.; Real, J. A. *Chem. Commun.* **2006**, (41), 4321-4323.

[176] Burnett, B. J.; Barron, P. M.; Hu, C.; Choe, W. *J. Am. Chem. Soc.* **2011**, *133* (26), 9984-9987.

[177] Kim, M.; Cahill, J. F.; Fei, H.; Prather, K. A.; Cohen, S. M. *J. Am. Chem. Soc.* **2012**, *134* (43), 18082-18088.

[178] Lalonde, M.; Bury, W.; Karagiaridi, O.; Brown, Z.; Hupp, J. T.; Farha, O. K. *J. Mater. Chem.* **2013**, *1* (18), 5453-5468.

[179] Das, S.; Kim, H.; Kim, K. *J. Am. Chem. Soc.* **2009**, *131* (11), 3814-3815.

[180] Zhang, Z.; Zhang, L.; Wojtas, L.; Nugent, P.; Eddaoudi, M.; Zaworotko, M. J. *J. Am. Chem. Soc.* **2012**, *134* (2), 924-927.

[181] Mukherjee, G.; Biradha, K. *Chem. Commun.* **2012**, *48* (36), 4293-4295.

[182] Liu, T.-F.; Zou, L.; Feng, D.; Chen, Y.-P.; Fordham, S.; Wang, X.; Liu, Y.; Zhou, H.-C. *J. Am. Chem. Soc.* **2014**, *136* (22), 7813-7816.

[183] Song, X.; Jeong, S.; Kim, D.; Lah, M. S. *CrystEngComm* **2012**, *14* (18), 5753-5756.

[184] Huang, S.; Li, X.; Shi, X.; Hou, H.; Fan, Y. *J. Mater. Chem.* **2010**, *20* (27), 5695-5699.

[185] Yao, Q.; Sun, J.; Li, K.; Su, J.; Peskov, M. V.; Zou, X. *Dalton Trans.* **2012**, *41* (14), 3953-3955.

[186] Brozek, C. K.; Dincă, M. *J. Am. Chem. Soc.* **2013**, *135* (34), 12886-12891.

[187] Li, L.; Xue, H.; Wang, Y.; Zhao, P.; Zhu, D.; Jiang, M.; Zhao, X. *ACS Appl. Mater. Interfaces* **2015**, *7* (45), 25402-25412.

[188] Grancha, T.; Ferrando-Soria, J.; Zhou, H.-C.; Gascon, J.; Seoane, B.; Pasán, J.; Fabelo, O.; Julve, M.; Pardo, E. *Angew. Chem. Int. Ed.* **2015**, *54* (22), 6521-6525.

[189] Seth, S.; Savitha, G.; Moorthy, J. N. *J. Mater. Chem.* **2015**, *3* (45), 22915-22922.

Chapter 2

Experimental Techniques

The chapter discusses the detailed experimental techniques used to achieve the objectives of the present thesis. The experimental techniques include synthesis and characterization of organic compounds; various crystallization techniques to obtain good quality crystals of CPs, their characterization, analysis and property studies. The characterization techniques utilized here include: Elemental analysis, FT-IR, NMR, Single Crystal XRD, PXRD. Thermal analysis and photo-physical properties of the organic compounds and their CPs were studied. The instrumentation details and basic principles of various techniques are discussed in this chapter.

2.1 Synthesis of organic ligands or organic linkers

Organic ligands were synthesized by following procedures:

(i) One-step synthesis by reacting diacid and amine in the presence of triphenylphosphite using pyridine as solvent.

(ii) Condensation of diacid chloride with pyridyl amines.

2.1.1 Synthesis of ligands by using diacids

3-Amino pyridine was added to a pyridine solution of dicarboxylic acid, while stirring the solution triphenylphosphite was added (2:1 molar ratio triphenylphosphite: dicarboxylic acids). The mixture was refluxed for 5 hours.[1,2]

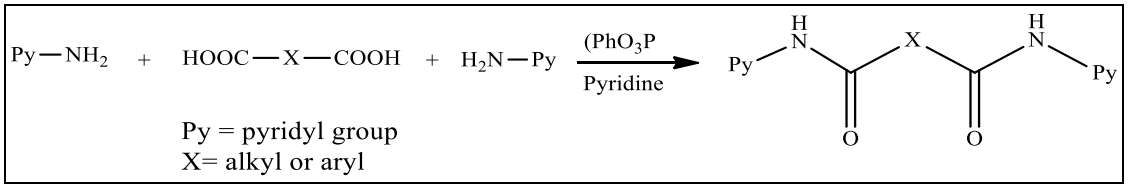

Scheme 2.1: Synthesis of the organic ligands having amide spacers using diacids.[1,2]

The solution was reduced by distilling out the pyridine, and a white precipitate was obtained. The solid was filtered, washed with water, and dried under vacuum. The compounds are soluble in EtOH, n-PrOH and insoluble in other common organic solvents such as $CHCl_3$, DCM, Acetone, CH_3CN and aromatics. All the compounds have been recrystallized from 1:1 mixture of EtOH and water. The melting point of each solid powder was recorded by thin capillary tube and % yield calculated. The compounds were characterized by FT-IR, ^{1}H-NMR, ^{13}C-NMR.

2.1.2 Synthesis of ligands by using diacid chlorides

Amino pyridine and Triethylamine (TEA) in tetrahydrofuran (THF) was cooled to 0°C, and the corresponding di-acidchloride was added drop wise with continuous stirring. The whole mixture was stirred overnight, and resulted in milky white solution.[3] The resulting solid was filtered, washed with water, and dried under vacuum. Melting point of each white powder was noted and % yield was calculated. The compounds were characterized by FT-IR, ^{1}H-NMR, ^{13}C-NMR.

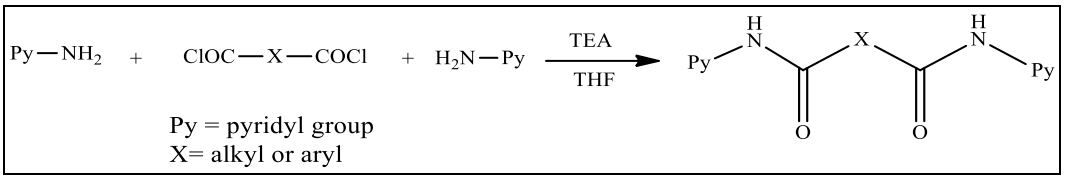

Scheme 2.2: Synthesis of the organic ligands having amide spacers using diacid chlorides.

2.2 Synthesis of co-ordination polymers (CPs)

Co-ordination polymers (CPs) are usually obtained by using pre-designed linkers or organic ligands, which either is commercially available or synthesized prior to use. We adopted various procedures to derive CPs from the synthesized ligands. The main aim here was to obtain the product in perfectly crystalline form suitable for characterization by Single Crystal X-Ray Diffraction (SXRD). Usually, the mixing of ligands with metal salts immediately forms precipitate. This precipitate can be dissolved either by heating or by adding some solvents and slow evaporation may result in the formation of crystalline product. But in most of the cases, the direct mixing results in the formation of insoluble powders, which cannot be characterized by Single Crystal XRD.

Three techniques are utilized for synthesizing the co-ordination polymers (CPs) in perfectly crystalline form.

2.2.1 Layering Technique [4]

The layering technique is most widely used for synthesising CPs in crystalline form. It depends on the slow diffusion of the components from one solvent to another. The solvents of different densities were taken for this purpose. Solvent of lower density is slowly layered over the solvent of higher density (Figure 2.1).

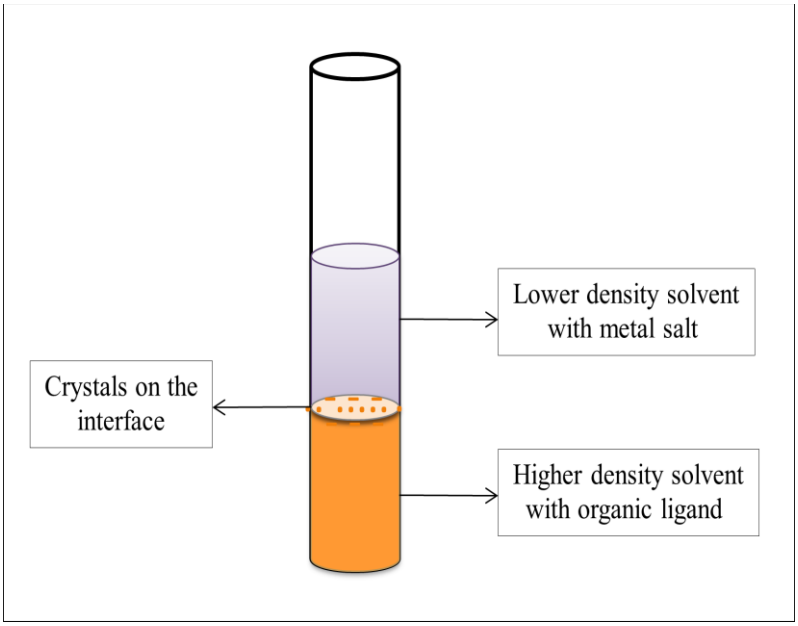

Figure 2.1: Schematic showing layering technique for crystallization of co-ordination polymers (CPs).

The following solvents were used in the present thesis:

(a) Protic solvents: H_2O, MeOH, EtOH.

(b) Non-aromatic organic solvents: CH_2Cl_2, $CHCl_3$, CCl_4, CH_3CN, Acetone, Tetrahydrofuran (THF), Dimethylformamide (DMF), Dimethyl sulfoxide (DMSO).

(c) Aromatic organic solvents: Nitrobenzene, Benzonitrile, Acetophenone, Toluene, Xylene, Ethyl benzene, Benzene.

(d) Solid aromatic compounds dissolved in non-aromatic solvents: Naphthalene, Anthracene, Dihydroxybenzenes, 1, 4-Dibromobenzene dissolved in non-aromatic solvents ($CHCl_3$, CCl_4 etc.).

2.2.2 Hydrothermal or Solvothermal Synthesis [5]

Most of the reported CPs have been synthesized using hydrothermal or solvothermal synthetic conditions, by using sealed Teflon-lined autoclaves (Figure 2.2). In this method many reaction parameters should be considered as - composition of the reactants, temperature and pressure, concentration, reaction time, pH value and solubility *etc.*[6] Both ligand and metal salt are kept in a Teflon coated sealed autoclave tube and usually water is used as the solvent in most of the synthesis.

In solvothermal synthesis, solvents other than water are employed process. Selection of the solvent is very important, since some metal salts and/or organic ligands have very low solubility or are even insoluble in a given solvent. In some cases, to increase the solubility, mixture of two or three solvents used and ultrasonic pretreatment may be also helpful.

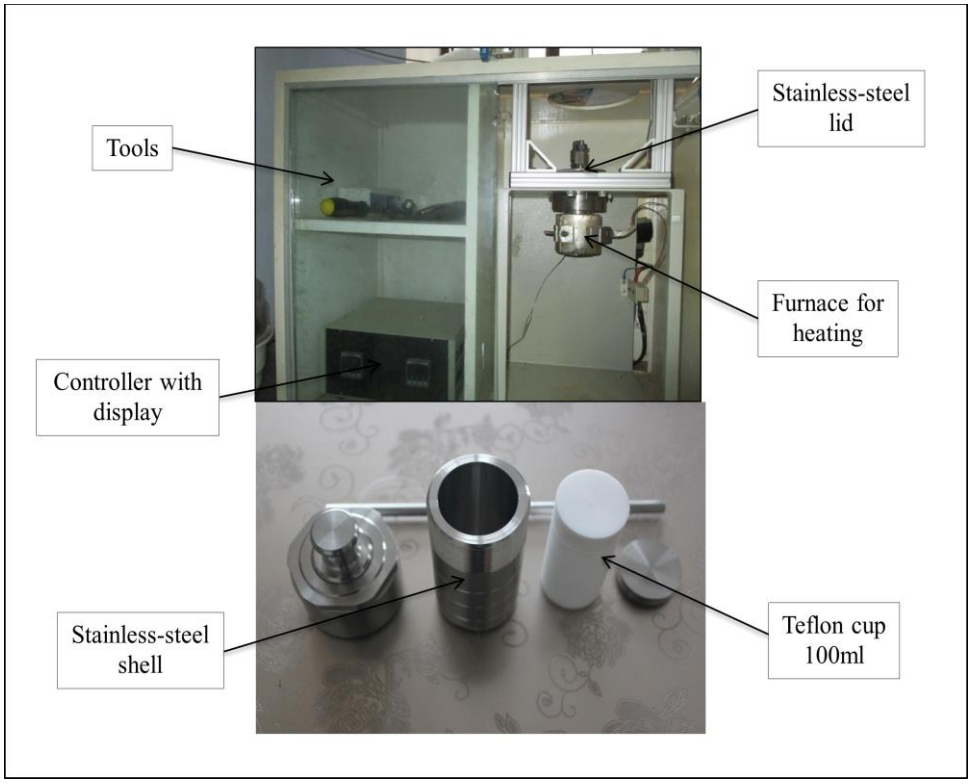

Figure 2.2: Photograph of autoclave used for hydrothermal synthesis.

Solvents play crucial roles as the structure directing, templating, and pore-filling agents during the formation of CPs. It is a non-equilibrium process and may give rise to metastable products; the cooling rate after completion of reaction is an important parameter or slow cooling give rise to good quality crystals. Compared to the solution reactions, hydrothermal techniques plays an important role in preparing robust and stable CPs because the solubility of the reactants increases in these methods which makes the reaction more likely to occur.[7]

2.2.3. Microwave-Assisted Synthesis

Microwave irradiation has been not only used in the synthesis organic molecules[8] but also inorganic materials, organic - inorganic hybrid materials CPs. More recently, it has been observed that microwave assisted synthesis technique on CPs saves reaction time by providing porous materials within a few minutes[9], offers phase selectivity and provides

facile morphology control.[10] Microwave are electromagnetic radiation of wavelengths 1 mm to 1 m (300 MHz to 300 GHz), which is between radio and infrared waves.[11] The molecules with permanent dipole moments rotate to align themselves with the alternating electric field of electromagnetic radiation. Water or ionic liquids with a high dipole moment are the best solvents for microwave assisted synthesis. The main advantage of microwave heating is its energy efficiency. Energy is generated directly throughout the bulk of the material instead of by conduction from the external surface. The reactions performed by using microwave ovens are specifically designed for chemical synthesis, which allow control over the various parameters (*e.g.*, irradiation power, time of the reaction, temperature inside the vessels, among other parameters).

2.3 Characterization Techniques

The instrumental technique used for characterization of organic ligands and property analysis of the CPs are summarized below.

2.3.1 Infrared Spectroscopy

Infrared spectroscopy (IR spectroscopy) deals with the infrared region of the electromagnetic spectrum, photon energies associated with this part of the infrared (from 1 to 15 kcal/mole) are not large enough to excite electrons, but may induce vibrational excitation of covalently bonded atoms and groups.[19] A molecule can vibrate in many ways; each way is called a vibrational mode. In order for a vibrational mode to be "IR active," the gross selection rule is that during vibration there must be changes in the dipole moment.[18,20] The vibrational motion of diatomic molecule can be compared to the physical model of a vibrating spring system (Figure 2.3).

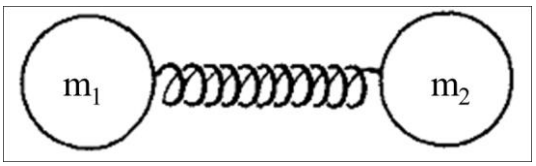

Figure 2.3: Diatomic molecule, where the bond as a spring and the atoms as rigid spheres.

The associated with its vibration wavenumber can be described by Hooke's Law

$$\bar{\nu} = \frac{1}{2\pi}\sqrt{\frac{k}{\mu}} \qquad \text{Where} \qquad \mu = \frac{m_1.m_2}{m_1+m_2}$$

where, $\bar{\nu}$ is vibrational wavenumber, k is force constant (which describes the stiffness of the spring or bond), μ is reduced mass, m_1 and m_2 are two masses of atoms having covalent bond. The band positions in the IR spectrum are presented in wavenumber ($\bar{\nu}$) which is proportional to the energy of vibration.

$$E = h\nu = \frac{hc}{\lambda} = hc\bar{\nu}$$

where h is Planck's constant, 6.626×10^{-34} joules-sec.

IR spectrum is a graph of infrared light absorbance (or transmittance) on the vertical axis *vs.* wavenumber on the horizontal axis.

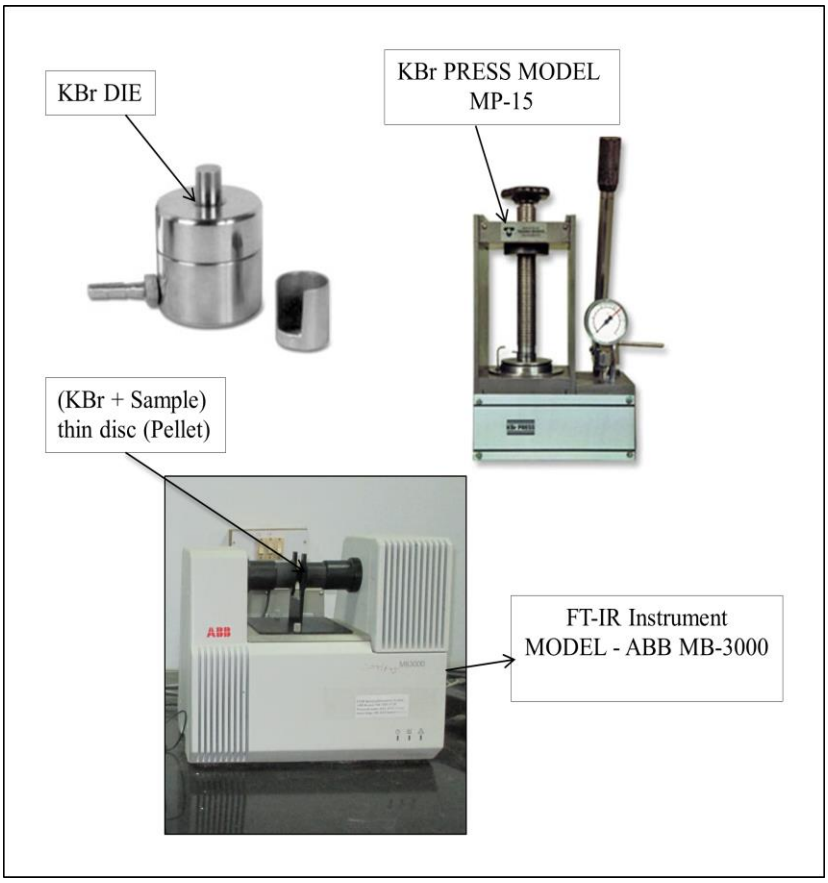

Figure 2.4: Photograph of the Fourier Transform Infrared (FT-IR) spectrometer assembly.

The spectra do not normally display separate absorption signals for each fundamental vibrational modes of a molecule; the number of observed absorptions may be increased by additive and subtractive interactions leading to combination tones and overtones of the fundamental vibrations. In present thesis work, we have used IR spectroscopy for qualitative

analysis. We have recorded FT-IR spectra of bis-pyridyl-bis-amide ligands and their CPs using KBr pellets on ABB Bomen MB-3000 Fourier transform infrared (FT-IR) spectrometer (Figure 2.4). Analysis of the position, shape and intensity of peaks in this spectrum reveals details about the molecular structure of the sample. Signal intensities (height) are usually denoted by the following abbreviations: w (weak), m (medium), s (strong), v (variable). A broad signal shape is sometimes indicated by br. and it's absorption frequency is given as a single approximation value (≈) rather than a range**.**

2.3.2 Nuclear Magnetic Resonance (NMR) Spectroscopy [16]

Proton and carbon-13 nuclear magnetic resonance (^{1}H-NMR and ^{13}C-NMR) spectra of all ligands are measured on a 400 MHz NMR spectrometer (Bruker AVANCE III) equipped with BBFO probe and auto-sampler, using $CDCl_3$ and DMSO-d_6 as solvents (Figure 2.5).

Figure 2.5: Photograph of 400 MHz NMR spectrometer (Bruker AVANCE III)

Chemical shifts (δ) were reported in parts per million (ppm) using deuterated solvent peak. Data are reported as follows: chemical shifts, multiplicity (s = singlet, d = doublet, t = triplet, q = quartet, dd = doublet of doublets, m = multiplet), coupling constants (J) and integration.

NMR technique applicable to any kind of sample that contains nuclei possessing spin e.g. ^{1}H or ^{13}C, placed in a magnetic field absorb electromagnetic radiation at a frequency characteristic of the isotope. The resonant frequency, energy of the absorption, and the intensity of the signal are proportional to the strength of the magnetic field.[17]

2.3.3 Ultraviolet – Visible (UV-Vis) Spectroscopy

The UV-Vis spectroscopy is used in analytical chemistry for the quantitative calculation of different analytes, such as transition metal ions, highly conjugated organic compounds, biological macromolecules. The range in UV-Vis spectroscopy absorption spectroscopy, is between 190 nm to 800 nm which is divided into the ultraviolet (UV, 190-380 nm) and visible (Vis, 380-800 nm) regions. Since the absorption of ultraviolet or visible radiation by a molecule leads to transition between the electronic energy levels of the molecule, it is also often called as electronic spectroscopy. Molecules having π-electrons or non-bonding electrons (n-electrons), called highest occupied molecular orbitals (HOMO) can absorb the energy excited to higher anti-bonding molecular orbitals called lowest unoccupied molecular orbital (LUMO).[21]

UV-Vis spectroscopy can be used to determine the concentration of organic compound having high degree of conjugation dissolved in suitable solvent.[22] The solvent polarity and pH can affect the absorption spectrum of an organic compound. According to Lambert-Beer's Law - Absorbance (A) of an absorbing species in a solution is directly proportional to the concentration (c) of the species and its molar extinction coefficient (ε) at the measuring wavelength λ and is given by the equation -

$$A = log\ (I_0/I) = \varepsilon.c.l$$

where, I_0 and I are the intensities of the incident and transmitted light, respectively, and l is the path length for the light beam passing through the sample. The sample is usually kept in a quartz cuvette of 1cm path length.

In the present thesis, UV-Vis was measured: (i) Shimadzu Spectrophotometer with model UV-2450 and (ii) JASCO model V-650 (Figure 2.6). The wavelength range covered in both the spectrophotometers is 200-1100 nm, tungsten (W-lamp) for the 1100 to 350 nm region and a deuterium (D_2-lamp) for the 350-200 nm region. The light sources Si-photodiodes are used as the light detectors.

The minimum wavelength resolution for the two spectrophotometers is 0.2 nm and lowest absorbance measurable is ~0.005.

Figure 2.6: Photograph of the UV-Vis spectrophotometers (a) Shimadzu with model UV-2450 (b) JASCO with model V-650

2.3.4 Structural Determination of CPs by X-ray crystallography

In 1912, Max von Laue discovered that crystalline substances act as three-dimensional diffraction gratings for X-ray wavelengths similar to the spacing of planes in a crystal lattice.[23] X-ray crystallography is a common technique used for identifying the atomic and molecular structure of crystalline solids. In this technique, crystalline solids diffract a beam of incident X-rays into many specific directions, is analogous to diffraction of light by droplets of water, producing rainbow. The X-rays diffraction pattern is different for different crystals, depending on the crystal lattice and the atomic arrangement in it. By measuring the angles and intensities of these diffracted beams, a crystallographer can produce a three-dimensional (3D) picture of the density of electrons within the crystalline solids. By which various other information; positions of the atoms in the crystal, chemical bonds between the atoms and their disorder and can be determined. To analysis structure of our CPs we used two types of X-ray diffraction spectroscopy:

1. Single Crystal X-ray Diffraction Spectroscopy

2. Powder X-ray Diffraction Spectroscopy

In both the techniques X-rays are generated by a cathode ray tube, filtered to produce monochromatic radiation, collimated to concentrate and directed toward the sample. The

interaction of the incident rays with the sample produces constructive interference and resulted diffracted ray.

According to Bragg's Law [24,25]

$$2d \sin\theta = n\lambda$$

This relates the wavelength of electromagnetic radiation with diffraction angle and lattice spacing in crystalline solids. These diffracted X-rays are then detected, processed and counted. By changing the geometry of the incident rays, the orientation of the crystal and the detector, all possible diffraction directions of the lattice should be attained. Hence key component of diffraction is the angle between the incident and diffracted rays.

2.3.4.1 Single Crystal X-ray Diffraction (SXRD)

Single-crystal X-ray Diffraction is analytical technique which provides us information about the internal lattice of crystalline solids, including unit cell dimensions, bond-lengths, bond-angles etc. X-ray diffractometers consist of three basic elements - an X-ray tube, a sample holder, and an X-ray detector. X-rays are generated in a cathode ray tube by heating a filament to produce electrons and accelerating the electrons toward a target. Molybdenum is the most common target material for single-crystal diffraction, Mo Kα radiation = 0.7107Å. For analysis, the sample should be selected from unfractured, optically clear crystals using a petro graphic microscope. Crystals can be broken off a larger sample and the best fragment selected. Samples should be between 30 and 300 microns, with ideal crystals averaging 150-250 microns in size. The data have been collected and phase problem must be solved to find the unique set of phases that can be combined with the structure factors to determine the electron density and, therefore, the crystal structure. Once the initial crystal structure is solved, various steps can be done to attain the best possible fit between the observed and calculated crystal structure. The final structure solution will be presented with an R value, which gives the percentage variation between the calculated and observed structures.

2.3.4.2 Powder X-ray Diffraction (PXRD)

In PXRD, X-rays are generated within a sealed tube under vacuum; current is applied that heats a filament within the tube; higher the current, greater the number of electrons emitted from the filament. A high voltage, 15-60 kilovolts is applied within the tube. This high voltage accelerates the electrons to hit a target, commonly made of Cu and X-rays are

produced. These X-rays are collimated and directed on-to the sample, which is fine powder (typically to produce particle sizes of less than 10 microns). A detector detects the X-ray signal; the signal is then processed either by a microprocessor or electronically, converting the signal to a count rate. In an X-ray powder diffractogram; the peaks represent positions where the X-ray beam has been diffracted by the crystal lattice. Since we know lambda (λ) and measure theta (θ), the diffraction pattern is represented as intensity vs. 2θ. Bragg's Law is used to convert observed 2θ positions to d_{hkl}. The characteristic set of d-spacings generated in a typical X-ray scan provides a unique "fingerprint" of the mineral present in the sample. When properly interpreted, by comparison with standard patterns and measurements, this "fingerprint" allows for identification of the material. A well-defined sharp peak pattern is usually obtained in case of crystalline/polycrystalline solids.

Figure 2.7: Photograph of by X-ray powder diffractometer (RIGAKU MiniFlex II).

However, for amorphous/glassy solids, where there is no long-range periodic structure, halo patterns are observed instead of well defined Bragg peaks. In a typical PXRD pattern of a crystalline sample, (i) position of the peaks refers to particular sets of planes, (ii) any shift with broadening in peak position may correspond to the lattice strain, (iii) intensity of the peaks correspond to the planar density, and (iv) full width at half maximum (β) of the peak infer the crystalline size (Debye-Scherrer Formula). In the present study, structure of the crystalline CPs having different anions, different guest molecules were compared by X-ray

powder diffractometer of RIGAKU MiniFlex II (Figure 2.7) with a typical Cu K_α radiation (λ = 1.54 Å) at room temperature and operated at a voltage of 30kV and filament current of 30 mA. The fine ground powder form of samples was required for characterization.

2.3.5 Wavelength Dispersive X-ray Fluorescence (WD-XRF) Spectroscopy

Wavelength Dispersive X-ray Fluorescence (WD-XRF) is one of the best analytical techniques used for elemental analysis in all kinds of the samples - liquids, solids or loose powders.[28] When materials are exposed to short-wavelength X-rays, ionization of their component atoms may take place. X-rays can be energetic enough to expel tightly held electrons from the inner orbitals of the atom. The removal of an electron in this way makes the electronic structure of the atom unstable, and electrons in higher orbitals "fall" into the lower orbital to fill the hole left behind. In falling, energy is released in the form of a photon, the energy of which is equal to the energy difference of the two orbitals involved. Thus, the material emits radiation, which has energy characteristic of the atoms present. All the elements in the sample are excited simultaneously, emitted characteristic radiation of different energies. These emitted radiations from the sample are diffracted into different directions by an analyzing crystal or monochrometer. The wavelength of this fluorescent radiation can be calculated from Planck's Law, $\Delta E = h\nu = \frac{hc}{\lambda} = hc\bar{\nu}$.

The fluorescent radiation can be analyzed by sorting the wavelengths of the radiation (wavelength-dispersive analysis). The intensity of each characteristic radiation is directly related to the amount of each element in the material. The sample is normally prepared as a flat disc, typically of diameter 20–50 mm. For obtaining sample disc, materials should be finely grounded, pressed into a tablet, and glasses should be casted to the required shape. In order to reduce the effect of surface irregularities, the sample is usually spun at 5–20 rpm. The spectral lines used for chemical analysis are selected on the basis of intensity, and we may calculate % of each element present in material.

Energy Dispersive X-ray Fluorescence Spectroscopy (ED-XRF) is a technique used for elemental analysis.[29] The resolution of WD-XRF techniques lies between 5 eV and 20 eV, whereas ED-XRF systems provide resolutions ranging from 150 eV to 300 eV or more, depending on the type of detector used. The WD-XRF has excellent accuracy and precision, simple and fast sample preparation and elements ranging from Beryllium (Be) to Uranium

(U) in the concentration range from 100 % down to the sub-ppm-level can be analyzed. The instrument details of used Wavelength Dispersive X-Ray Fluorescence (WD-XRF) which were used in the present thesis are S8 TIGER, Make: Bruker, Germany; with X-Ray tube of 4KW with 'Rhodium' target and a high voltage/tube current. 60 kv/64 mA

2.3.6 Atomic Absorption Spectroscopy (AAS)

Atomic Absorption Spectroscopy (AAS) is used for the quantitative determination of a particular element (the analyte) in a sample to be analyzed. This technique makes use of absorption spectrometry to assess the concentration of over 70 different elements in solution or directly in solid samples. It requires standards with known analyte content to establish the relation between the measured absorbance and the analyte concentration.

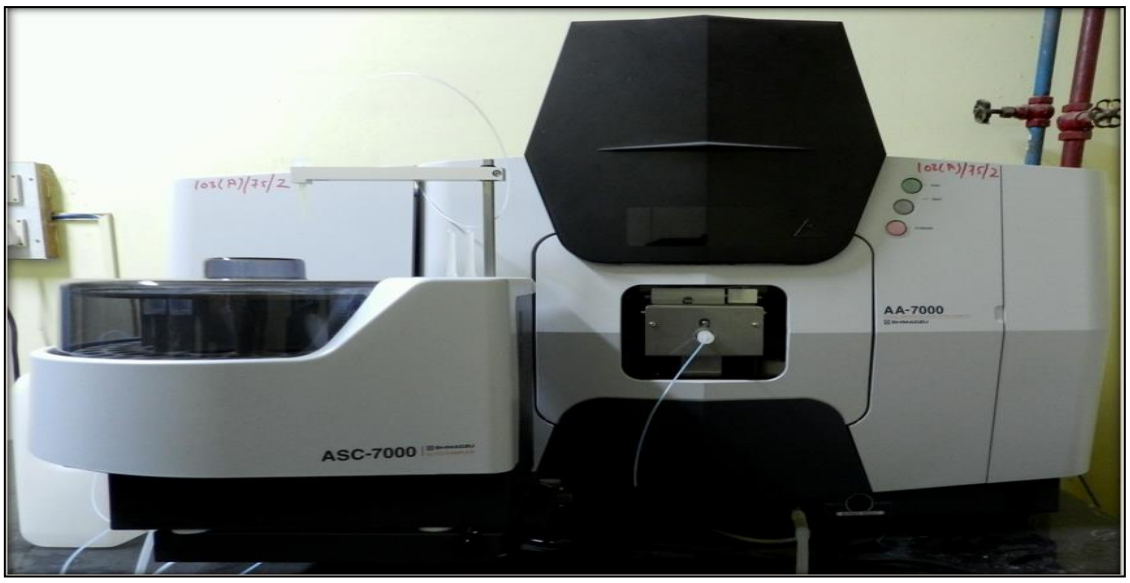

Figure 2.8: Photograph of the AA-7000 model of Shimadzu.

To analyze a sample for its atomic constituents, it has to be atomized (converted into ground state free atoms in the vapour state) by the atomizers most commonly flames atomizers. The electrons of the atoms in the atomizer can be promoted to higher orbitals (excited state) for a short period of time (nano seconds) by absorbing a defined quantity of energy (radiation of a given wavelength). This wavelength, is specific to a particular electron transition in a particular element, and the width of an absorption line is only of the order of a few picometers (pm), which gives the technique its elemental selectivity. Increase in the number of atoms in the light path, increases the amount of light absorbed also increase. By measuring the amount of light absorbed, a quantitative determination of the amount of analyte can be

done. The use of special light sources and careful selection of wavelengths allow the specific determination of individual elements.

In present study, we used AA-7000 model of Shimadzu (Figure 2.8), where two types of flames can be used -

1. Air-acetylene flame with a temperature of about 2300 °C
2. Nitrous oxide (N_2O)-acetylene flame with a temperature of about 2700 °C.

The latter flame, offers a more reducing environment, being ideally suited for analytes having high affinity to oxygen. Liquid or dissolved samples are typically used with flame atomizers. The sample solution is fed into the instrument and the unknown concentration (ppm) of each element present in our sample is directly displayed on the calibration curve.[30]

2.3.7 Thermo Gravimetric Analysis (TGA)

Thermo gravimetric Analysis (TGA) is a thermal event in which changes in physical and chemical properties of the materials are measured as a function of increasing temperature.[31] All thermal actions don't bring about a change in the mass of the sample (for example melting, crystallization or glass transition) but some compounds exhibit a phase change by process viz. desorption, absorption, sublimation, vaporization, oxidation, reduction and decomposition.

TGA instrument consist a sample pan, supported by a high precision balance. The pan resides in a furnace and a known amount of a starting material between 2 and 50 mg should be placed (initial weight) should cover bottom of the pan called initial weight. Knowing the initial weight of the starting material and the total weight of inclusions, such as ligands, structural defects, or side-products of reaction, which are liberated upon heating, stoichiometric ratio can be used to calculate the % weight loss of the substance in a sample. The results from TGA may be presented by –

1. Weight loss (or % weight loss) versus temperature (or time) curve, called the Thermogravimetry (TG).

Or

2. Rate of weight loss versus temperature curve, called the differential thermo gravimetric (DTG).

TGA can be used to evaluate the thermal stability of MOFs, over a temperature range. The MOF is thermally stable up to a temperature if there will be no mass change observed or no slope in the TGA trace. During heating of MOFs following processes takes place - release the adsorbed species, chemical reactions and at the end thermal decomposition which indicates that the material is no longer thermally stable.[32] The TGA instrument used in the present thesis is Perkin Elmer Thermo Gravimetric Analyzer of model TGA – 4000 (Figure 2.9).

Fig. 2.9: Photograph of Perkin Elmer Thermo Gravimetric Analyzer of model TGA – 4000.

2.3.8 Elemental Analysis

Elemental analysis is quantitative determination of elements in a compound.[33] The most common type of elemental analysis is for carbon, hydrogen and nitrogen (CHN) analysis, is accomplished by combustion analysis. In this technique, a sample is burned in an excess of oxygen and the combustion products: CO_2, H_2O, and NO_x (nitric/nitrous oxides) are collected. The masses of these combustion products used to calculate the composition of the unknown sample; we used this technique for our CPs.

The sample under test is weighed, 2 to 5 mg and wrapped in a tin capsule and inserted into a furnace held at 1200 °C. A steady stream of an unreactive gas (e.g., helium) is passed through the furnace and a burst of pure oxygen gas is added as the sample capsule is inserted into the oven. As the sample burns, the temperature rises to approximately 1700 °C. The furnace has catalyst (Cr_2O_3) that complete combustion of the sample and Copper turnings which ensure

that any nitrogen (nitric/nitrous oxides) in the sample is reduced to N_2, is an un-reactive gas. The leaving gas stream includes the analytically important species CO_2, H_2O und N_2. Finally the gas mixture is brought to a defined pressure/volume state and passed to a gas chromatographic system to separate the species, called zone chromatography. In this technique, a staircase type signal is registered whose step height is proportional to the substance amount in the mixture. The detection limit for carbon and nitrogen at sample amounts of 2 to 5 mg was found to be at about 0.05 weight % (500 ppm). The elemental analyzer used in the present work is Thermo Finnigan, Italy, Model FLASH EA 1112 series CHN analyzer consists of the system unit, a MAS 200 auto sampler for solid samples, and a Windows compatible computer with Eager 300 software. Oxygen combusts solid samples when ignited and the gases are carried by helium. The first furnace was set to 950 °C and holds a chromium (III) oxide column which oxidizes carbon into carbon dioxide, and nitrogen into nitrogen gas plus nitrogen oxides. The second furnace, set to 850 °C, holds copper wires, which reduce nitrogen oxides to nitrogen gas. The carbon dioxide and nitrogen gases flow through a magnesium perchlorate column which removes water before the gases enter the gas chromatograph column at 50 °C. The N_2 gas flows faster, followed by carbon dioxide thus separated by their retention rates. The gases are sensed by the thermal conductivity detector (TCD) to produce a chromatograph. These curves are integrated and used to calculate the weight percent of nitrogen and carbon in the sample.

2.3.9 Scanning Electron Microscopy (SEM) and Energy Dispersive X-ray (EDX) Spectroscopy

Scanning electron microscopy (SEM) is one of the most versatile and well known analytical techniques where a focused beam of high energy electrons used to scan the surface of any solid specimen (e.g. CPs in our study)[34] and largely magnified image is produced. A beam of electrons is produced at the top of the microscope by an electron gun (Figure 2.10).

The electromagnetic lenses (condenser and objective lenses) focus the electron beam which is scanned across the sample to produce an image. The emitted signals (secondary electron, backscattered electron etc.) due to the interaction of electron beam and sample are detected. In present work we examined our samples by FEI-Nova Nano SEM 450 (Field emission scanning electron microscopy (FE-SEM) type instrument). FE-SEM uses a field emission cathode that provides even narrow probing electron beams. Thus it improves the resolution

and minimizes sample charging and damage. The function of the electron beam gun is to provide a large and stable current in a beam.

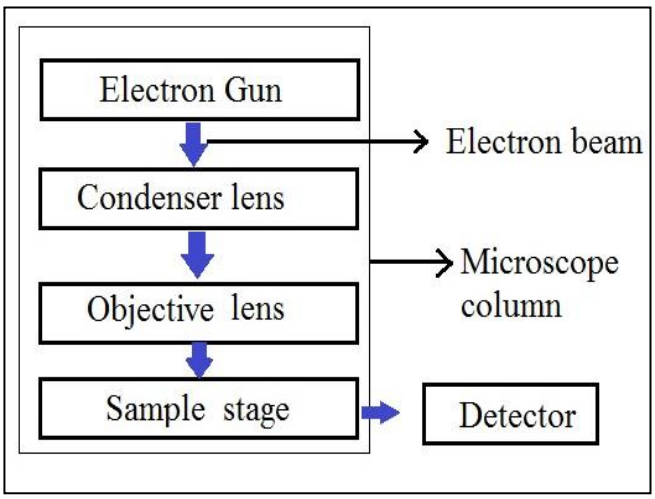

Figure 2.10: Schematic diagram of a typical scanning electron microscope (SEM).

There are essentially two classes of emission source: (i) thermionic emitter and (ii) field emitter. The main difference between the conventional SEM and the FE-SEM is because of different emitters used to produce the electron beam. In conventional SEM, thermionic emitters use electrical current to heat up a filament; the two most common materials used for filaments are Tungsten (W) and lanthanum hexaboride (LaB_6). When the heat is enough to overcome the work function of the filament material, the electrons can escape from the material itself. Thermionic sources have relative low brightness, evaporation of cathode material and thermal drift during operation. Field Emission is one way of generating electrons that avoids these problems. A Field Emission Gun (FEG); also called a cold cathode field emitter, does not heat the filament. The emission is reached by placing the filament in a huge electrical potential gradient. The FEG is usually a wire of Tungsten (W) fashioned into a sharp point.

The interaction of an electron beam with a sample produces a variety of emissions including X-rays; these X-rays can be used to determine the abundance of specific elements in the sample. This technique is known as Energy Dispersive X-ray Spectroscopy (EDX). The X-rays generated are from a region about 2 microns in depth and thus EDX is not a surface science technique. The elemental ratios can be determined from the spectra and hence this data can be used to examine the level of elements in the co-ordination polymer structures.

2.3.10 Fluorescence spectroscopy

In the present work, Shimadzu RF-5301PC scanning spectrofluorimeter (Figure 2.11) was used. The spectrofluorophotometer irradiates a sample with excitation light and measures the fluorescence from the irradiated sample.

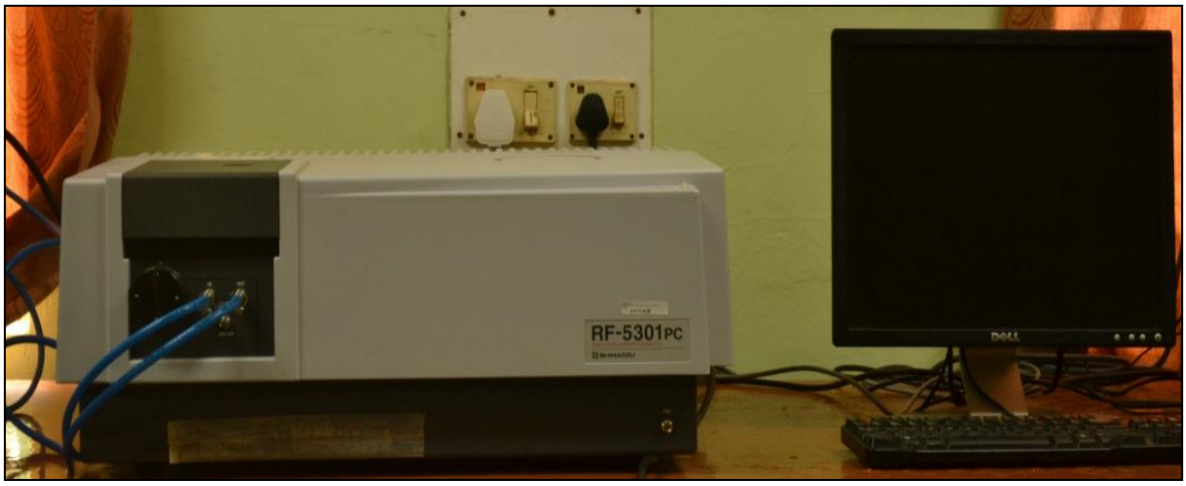

Figure 2.11: Photograph of the spectrofluorophotometer of Shimadzu model RF-5301PC.

This instrument is equipped with the light source of 150W Xenon lamp. The lamp housing is provided with ozone self-decomposition. The excitation monochromator isolates a band of a particular wavelength from the light from the Xenon lamp to obtain excitation light. Since brighter excitation light will contribute to higher sensitivity of the spectrofluorophotometer, the excitation monochromator incorporates a diffraction grating with a large aperture to collect the largest possible amount of light. The monochromator is of blazed holographic concave diffraction grating (F/2.5 for both excitation and emission sides) with the measurable scan range of 220-750 nm. The emission monochromator selectively receives fluorescence emitted from the sample and the photomultiplier tube measures the intensity of the fluorescence. The monochromator has a diffraction grating whose size is the same as that of the excitation monochromator to collect the greatest possible amount of light.

A light beam from the xenon lamp is incident upon the excitation monochromator. From the excitation monochromator, part of the beam is directed to the monitor detector through the beam splitter. All the drive components including the wavelength motor and slit control motor are operated according to signals from the internal computer. On the other hand, output signals from the monitor detector and fluorescence measurement detector (photomultiplier)

are fed to the A/D converter and the internal computer for processing, and then output data is sent to the personal computer.

The detector in this system consists of photomultiplier tube for both photometry (R3788-02) and monitor (R212-14) sides. Generally, the Xenon lamps used on spectrofluorimeter are characterized by very high emission intensity and an uninterrupted radiation spectrum. However, their tendency to unstable light emission will result in greater signal noise if no countermeasure is incorporated. In addition, the non-uniformity in the radiation spectrum of the Xenon lamp and in the spectral sensitivity characteristics of the photomultiplier tube (these criteria are generally called instrument functions) causes distortion in the spectrum. To overcome these factors, the photomultiplier tube monitors a portion of excitation light and feeds the resultant signal back to photomultiplier tube for fluorescence scanning. This scheme is called the light-source compensation system. It also has variable slit width facility (1.5/3/5/10/15/20 nm) with the wavelength accuracy of $\pm$ 1.5 nm.

2.4 References

[1] Sarkar, M.; Biradha, K. *Cryst. Growth Des.* **2006**, *6* (1), 202-208.

[2] Rajput, L.; Singha, S.; Biradha, K. *Cryst. Growth Des.* **2007**, *7* (12), 2788-2795.

[3] Banihashemi, A.; Eghbali, M. *J. Polym. Sci. A Polym. Chem.* **1976**, *14* (11), 2659-2664.

[4] Bridle, C.; Lomer, T. R. *Acta. Crystallogr.* **1965**, *19* (3), 483-484.

[5] Rowsell, J. L. C.; Yaghi, O. M. *Micropor. Mesopor. Mat.* **2004**, *73* (1–2), 3-14.

[6] Demazeau, G. *J. Mater. Sci.* **2008,** *43* (7), 2104-2114.

[7] Zhao, X.-X.; Ma, J.-P.; Dong, Y.-B.; Huang, R.-Q.; Lai, T. *Cryst. Growth Des.* **2007**, *7*(6), 1058-1068.

[8] Larhed, M.; Moberg, C.; Hallberg, A. *Acc. Chem. Res.* **2002**, *35* (9), 717-727.

[9] Jhung, S. H.; Yoon, J. W.; Hwang, J.-S.; Cheetham, A. K.; Chang, J.-S. *Chem. Mater.* **2005**, *17* (17), 4455-4460.

[10] Hwang, Y. K.; Chang, J.-S.; Park, S.-E.; Kim, D. S.; Kwon, Y.-U.; Jhung, S. H.; Hwang, J.-S.; Park, M. S. *Angew. Chem. Int. Ed.* **2005**, *44* (4), 556-560.

[11] Klinowski, J.; Almeida Paz, F. A.; Silva, P.; Rocha, J. *Dalton Trans.* **2011**, *40* (2), 321-330.

[12] Wang, Z.; Cohen, S. M. *Chem. Soc. Rev.* **2009**, *38* (5), 1315-1329.

[13] Chui, S. S. Y.; Lo, S. M. F.; Charmant, J. P. H.; Orpen, A. G. *Science* **1999**, *283* (5405), 1148-1150.

[14] Mukherjee, G.; Biradha, K. *Chem. Commun.* **2012**, *48* (36), 4293-4295.

[15] Tanabe, K. K.; Cohen, S. M. *Chem. Soc. Rev.* **2011**, *40* (2), 498-519.

[16] Akitt, J. W. *NMR and chemistry: an introduction to modern NMR spectroscopy*, Chapman & Hall, London; New York, **1992**.

[17] Sanders J. K. M.; Hunter, B. K. *Modern NMR spectroscopy: a guide for chemists,* Oxford University Press, New York, **1993**.

[18] Harris, D. C.; Bertolucci, M. D. *Symmetry and Spectroscopy: An Introduction to Vibrational and Electronic Spectroscopy.* New York. Dover Publications, INC **1993**.

[19] Christain, G. D. *Analytical Chemistry,* 5th ed. New York. John Wiley & Sons, INC. **1994**.

[20] Drago, R. S. *Physical Methods,* 2nd ed. Mexico. Saunders College Publishing **1992**.

[21] Griffith, J. S.; Orgel, L. E. *Q. Rev. Chem. Soc.* **1957**, *11* (4), 381-393.

[22] Kunkely, H.; Vogler, A. *Inorg. Chem.Commun.* **2001**, *4*, 692.

[23] Eckert, M. *Ann. Phys.* **2012**, *524* (5), A83-A85.

[24] Bragg, W. H.; Bragg, W. L. *Proc. R. Soc. A* **1913**, *88* (605), 428-438.

[25] Bragg, W. L. *Proceedings of the Cambridge Philosophical Society,* **1913**, *17*, 43–57.

[26] *CrysAlis PRO (oxford Diffraction),* Oxford Diffraction Ltd., Yarton, Oxfordshire, England, **2010**.

[27] Sheldrick, G. M. *Acta Crystallogr., Sect. A: Found. Crystallogr.* **2008**, *A64*, 112-122.

[28] Beckhoff, B.; Kanngießer, B.; Langhoff, N.; Wedell, R.; Wolff, H. *Handbook of Practical X-Ray Fluorescence Analysis*, Springer, **2006**

[29] Nielson, K. K.; Sanders, R. W.; Evans, J. C. *Anal. Chem.* **1982**, *54* (11), 1782-1786.

[30] Wang, Y.; Xie, J.; Wu, Y.; Hu, X. *Microchim. Acta.* **2014**, *181* (9-10), 949-956.

[31] Coats, A. W.; Redfern, J. P. *Analyst* **1963**, *88* (1053), 906-924.

[32] Bae, Y.-S.; Dubbeldam, D.; Nelson, A.; Walton, K. S.; Hupp, J. T.; Snurr, R. Q. *Chem. Mater.* **2009**, *21* (20), 4768-4777.

[33] Kanoo, P.; Gurunatha, K. L.; Maji, T. K. *J. Mater. Chem.* **2010**, *20* (7), 1322-1331.

[34] Masoomi, M. Y.; Morsali, A.; Junk, P. C. *CrystEngComm* **2015**, *17* (3), 686-692.

Chapter 3

Swelling and Shrinking of Network Cavities in Response to Anion Exchange: Reversible Intake and Release of Aromatic Guest Molecules

3.1 Introduction:

CPs based on pyridyl based exo-bidentate ligand **1a** (Scheme 3.1), where the pyridyl moieties are separated by amide functional groups and an ethyl spacer, are exploited by some of the leading research groups to form CPs. In most of the CPs, the networks form self complementary amide-to-amide hydrogen bonds.[1-5] Scheme 3.1 shows the possible supramolecular synthons of the di-amide functional groups: (i) β-Sheet[1-5], (ii) 4,4 – Network[3-5], (iii) α-Sheet[6].

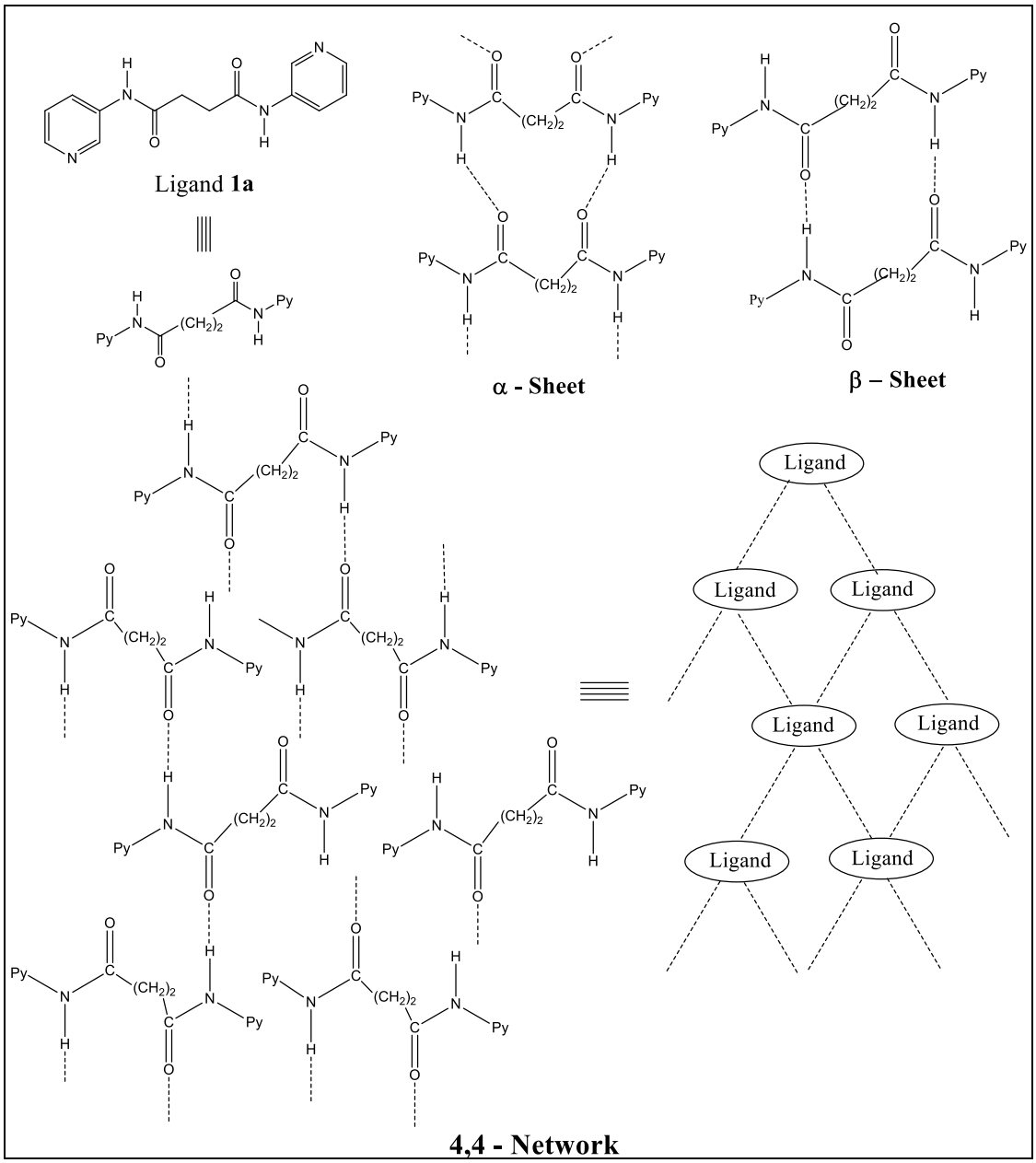

Scheme 3.1: Ligand **1a** having possible amide-to-amide hydrogen bonding patterns in CPs[1-5].

The preference for one supramolecular synthon over the other depends on the combination of various factors such as energetic, steric and proximity of the functional groups and the final supramolecular array will be a result of the balance between all the intermolecular interactions. The presence of ethyl spacer in ligand **1a** will enhance the possibilities of novel network architectures and interesting properties as it can bend and twist with a large degree to satisfy the co-ordination requirement of metal ions. Further, the meta-positioning of the pyridyl-N atoms, gives flexibility and swing over ligating topologies (Figure 3.1).

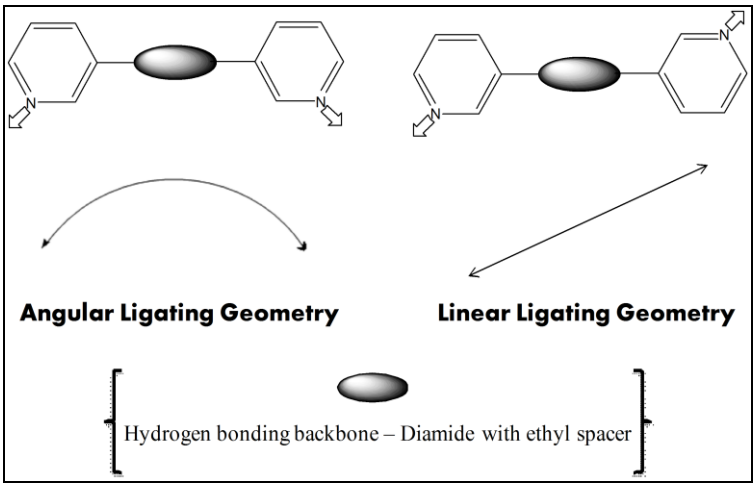

Figure 3.1: Varied ligating geometries in ligand **1a** due to meta-position of pyridyl-N.

In one-dimensional (1D), where the metal ion is co-ordinated at least with two ligands,[7] the alternate arrangement of metal ion and organic ligands leads to formation of various kinds of polymeric chains such as zig-zag, linear, sinusoidal, looped, concavo-convex, helix, ladder-like chains.[8-13] 1D networks are frequently observed with bidentate ligands in the presence of other competing ligands such as counter anions, H_2O or solvents. In case of flexible bidentate ligand, 1D looped chain may be observed if the ligand attains an arc like geometry (Figure 3.2). These cavities may show interesting porous properties such as guest inclusion and exchange.

Biradha *et al.* synthesized CPs of **1a** with $Cu(SCN)_2$ using DMF and methanol as solvent.[14] Two types of crystal were resulted in the same reaction flask both were 1D chains with octahedral coordination environment around Cu(II). The difference between them lies in the 3D arrangement and guest absorption where amide-to-amide self-complementary hydrogen bonds are absent, the amide N-H involved in hydrogen bonding with guest molecules. In one

CP, DMF molecules occupies 32% volume of the crystal lattice, forms hydrogen bond with amide N–H and stays in between the layers. The crystal packing is *via* weak hydrogen bonds such as C–H•••O between carbonyl group and pyridine C–H groups. In the other CP, 1D-chains form a 2D-layer *via* N–H•••S hydrogen bonds between amide N–H and SCN^- and the amide carbonyl joins these layers *via* bifurcated C–H•••O hydrogen bonds with pyridine C–H groups.

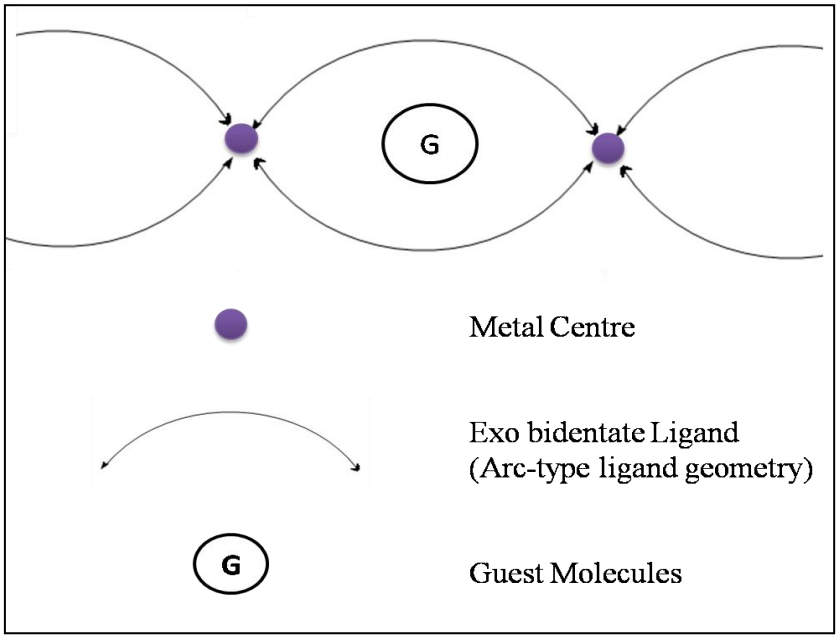

Figure 3.2: Schematic showing 1D-chain with cavities for guest inclusion.

Biradha *et al.* further performed same reaction in presence of nitrobenzene, which resulted crystalline product, where Cu(II) center has octahedral co-ordination in which the equatorial sites are occupied by two pyridine units of the ligand **1a** and two N-atoms of SCN^- while at the axial sites two S-atoms of SCN^- anion *via* bridging. The network resulted in cavities of dimensions 16.91 Å × 17.59 Å, which are filled by nitrobenzene molecules and the DMF molecules are present in between the layers *via* N–H•••O hydrogen bonds. These layers packed *via* C–H•••O hydrogen bonds between amide carbonyl and pyridine C-H with interlayer separation of 9.445 Å, the guest molecules DMF and nitrobenzene accounts for 53% of volume in the total crystal lattice.

Dastidar *et al.* introduced hydroxyl groups into the backbone of ethyl spacer in ligand **1a**, which were involved in hydrogen bonding with the hydroxyl groups of the neighboring molecules.[15] In the resulting CP of the modified ligand, self complementary amide-to-amide

hydrogen bonds was absent. They further explored the gelation properties of this ligand using both polar and non-polar solvents. The CPs displayed only hydrogelation properties at pH below 7.0, otherwise protonation of the pyridyl-N atom occurred and disruption of the hydrogen bonding started. There are many reports on CPs of ligand **1a** along with polycarboxylates. Wang *et al.* reported three Cu(II) CPs of ligand **1a** with aromatic polycarboxylates: Nitroisophthalic acid, 1,2-Benzenedicarboxylic acid and 1,3,5-Benzenetricarboxylic acid.[16] Ligand **1a** and Nitroisophthalic acid with Cu(II) formed 2D polymeric layer containing a tri-flexural helical chain with three types of 1D helical chains. In this CP, co-ordination environment of Cu(II) centre has two pyridyl-N from two different ligands and four carboxylate oxygen atoms from two acid ligands. The bridging of adjacent Cu(II) ions *via* **1a** resulted in 1D left-handed and right-handed helix chains *i.e.* left-[Cu-**1a**]$_n$ and right-[Cu-**1a**]$_n$. Both carboxyl groups of Nitroisophthalic acid are deprotonated and co-ordinated with Cu(II) ions from adjacent left-handed and right-handed [Cu-**1a**]$_n$ chains to form a new left-handed helix chain due to the twist of carboxyl groups. All the three helical chains are in a vertical arrangement and shares Cu(II) ions to form a 2D polymeric layer, a rare structure in CPs history. These 2D layers are further packed to form 3D network *via* hydrogen bonding and π-π stacking. Ligand **1a** with benzenedicarboxylic acid form 2D wave like polymeric layer, where **1a** connects two adjacent Cu(II) ions and form 1D [Cu-**1a**]$_n$ sinusoidal chain. Benzenedicarboxylic acid also bridges two adjacent Cu(II) ions and form 1D V-shaped chain. The non covalent interactions between 1D [Cu-**1a**]$_n$ sinusoidal chain and 1D V-shaped chain resulted in 2D-wave like polymeric layer with grids of different sizes. Further extension to 3D-network resulted *via* hydrogen bonding between N-H of amide and carboxyl oxygen. Benzenetricarboxylic acid and **1a** formed 2D double-layer co-ordination polymer, where **1a** bridges two adjacent Cu(II) ions and form 1D [Cu-**1a**]$_n$ zig-zag chain. Benzenetricarboxylic acid act as chelating ligand *i.e* two oxygen of one carboxyl group coordinate to one Cu(II) ion and also bidentate bridging ligand connecting two adjacent Cu(II) ions to form 1D-double chain. These two different types of 1D chains, linked to each other to form a 2D double-layer structure which further packed *via* N–H•••O hydrogen-bonding and face-to-face π-π stacking.

Wang *et al*. have also reported CPs of **1a** with Cu(II) and Co(II) along with dicarboxylic and tricarboxylic acids; where Cu(II) CP resulted in a 2D network and hydrogen bond interactions assembled them into a 3D array.[17] In Co(II) CP the ligand **1a** served as a

bridging ligand resulting in an overall 3D framework with binodal (3,8)-connected topological structure was observed, when 5-aminoisophthalic (5-AIP) acid was used. But while using 1,3-benzenedicaboxylic acid, Co(II) CP generated a 2-fold interpenetrated 3D architecture, where ligand **1a** served as a bridging ligand.

In this chapter, we will discuss the synthesis, characterization and crystal structure analysis of CPs of **1a** with different metal salts. The flexible ethyl chain along with various ligating topologies has resulted in forming different network geometries by varying reaction conditions (in the present chapter: changing the counter anion).

(i) **Role of counter anions:** PF_6^- and ClO_4^- were selected for forming CPs in the present chapter. PF_6^- and ClO_4^- differ in shape, size and coordinating ability; (a) PF_6^- has octahedral geometry while ClO_4^- has tetrahedral geometry. (b) PF_6^- is bigger in size than ClO_4^-, having six F atoms which are more electronegative than O atom. A study on tri-amide based receptor showed that the binding affinity of the anion PF_6^- is more than ClO_4^-.[11] In amide-based MOFs, PF_6^- have shown higher probability to interfere in self-complementary amide-to-amide hydrogen bond than ClO_4^-.[4,12]

(ii) **Effect of ethyl spacer:** Analyzing the possible conformations/geometry of ligand **1a** and comparing with some of the reported CPs and the effect of counter anions in modulating the flexible ethyl chain.

(iii) **Guest inclusion properties:** Analyzing the aromatic guest inclusion properties of the CPs. Further calculation of number of guest molecules present in cavity will be done.

3.2 Experimental section

3.2.1 General

Melting points of organic ligands were determined in open capillary tubes on a MPA120-Automated Melting Point apparatus. Proton and carbon-13 nuclear magnetic resonance (^{1}H-NMR and ^{13}C-NMR) spectra of all ligands are measured on a 400 MHz Bruker NMR spectrometer; using DMSO-d_6 as solvent and the chemical shifts are expressed in ppm. Data are reported as follows: chemical shifts, multiplicity (s = singlet, d = doublet, t = triplet, q = quartet, dd = doublet of doublets, m = multiplet), coupling constants (Hz), and integration. The IR spectra were recorded using KBr pellets on FT-IR ABB Bomen MB-3000. UV-Vis absorption spectra were recorded in Shimadzu Spectrophotometer with model UV-2450.

Elemental analyses were obtained with a Thermo Finnigan, Italy, Model FLASH EA 1112 series.

Powder X-ray diffraction (PXRD) data were recorded with a Rigaku miniflex II, λ = 1.54, Cu Kα. 3-Amino pyridine, succinic acid and triphenylphosphite were purchased from Sigma-Aldrich. All other reagents and solvents were purchased from S. D. Fine, India and used without further purification unless otherwise specified.

3.2.2 Synthesis of Ligand Bis-(3-pyridyl)ethanediamide 1a:

The ligand **1a** was synthesized according to a literature procedure (Scheme 3.2).[5] 3-Amino pyridine (2 mmol) was added to 40 mL of a pyridine solution of succinic acid (1 mmol), and the solution was stirred for 15 min. To this solution, triphenyl phosphite (2 mmol) was added, and the mixture was refluxed for 5 h. The volume of the solution was reduced to 5 mL by distilling out the pyridine, and a white precipitate was obtained. The solid was filtered, washed with water, and dried under vacuum.

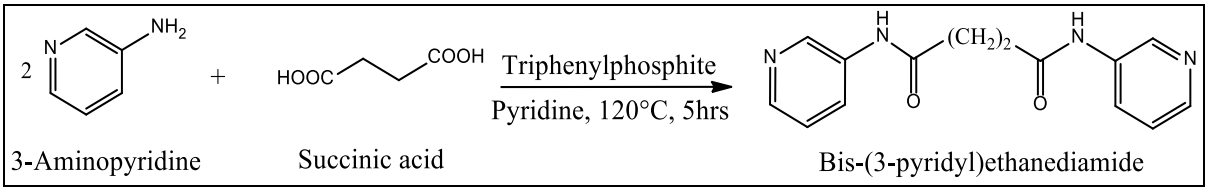

Scheme 3.2: Synthesis of Ligand **1a.**

For the white powder, calculated % yield and melting point noted. Further it was characterized by using FT-IR, ^{1}H-NMR and ^{13}C-NMR.

Analytical data of the synthesized ligand 1a:

Yield: 70%. Melting point: 195–198 °C.

FT-IR (cm^{-1}): 3301(w), 3232(m), 3178(m), 3116(m), 3039(s), 2954(vs), 2908(vs), 1689(vs), 1612(s), 1589(vs), 1550(vs), 1473(s), 1419(vs), 1326(vs), 1272(s), 1157(vs), 1126(m), 1033(m), 948(w), 856(s), 802(s), 694(s), 617(m) (Appendix-1 Figure A1); ^{1}H-NMR (400 MHz, DMSO) δ (ppm) 10.26 (s, 1H), 8.74 (d, J = 2.3 Hz, 1H), 8.24 (dd, J = 4.6, 1.2 Hz, 1H), 8.04 (ddd, J = 8.3, 2.4, 1.5 Hz, 1H), 7.33 (dd, J = 8.3, 4.7 Hz, 1H), 2.71 (s, 2H) (Figure 3.3); ^{13}C-NMR (400 MHz, DMSO) δ (ppm) 171.41, 144.40, 141.01, 136.36, 126.26, 124.11, 31.32 (Figure 3.4).

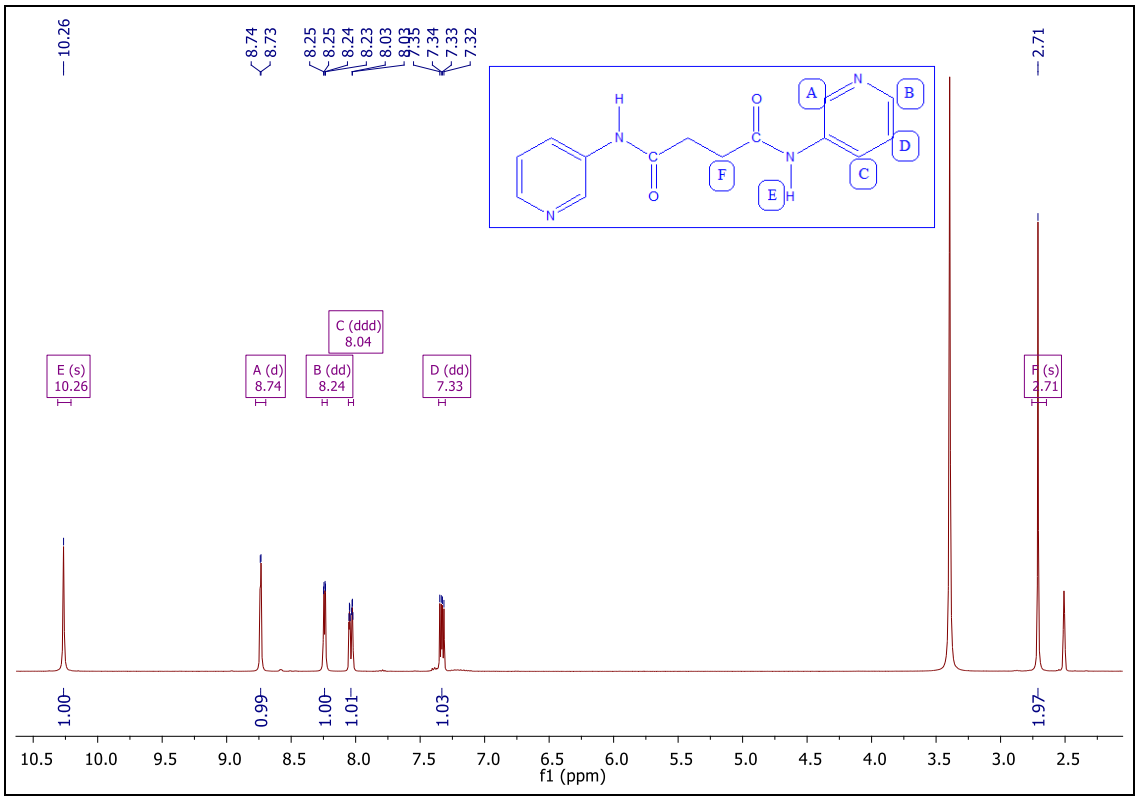

Figure 3.3 ^{1}H-NMR spectrum of Ligand **1a.**

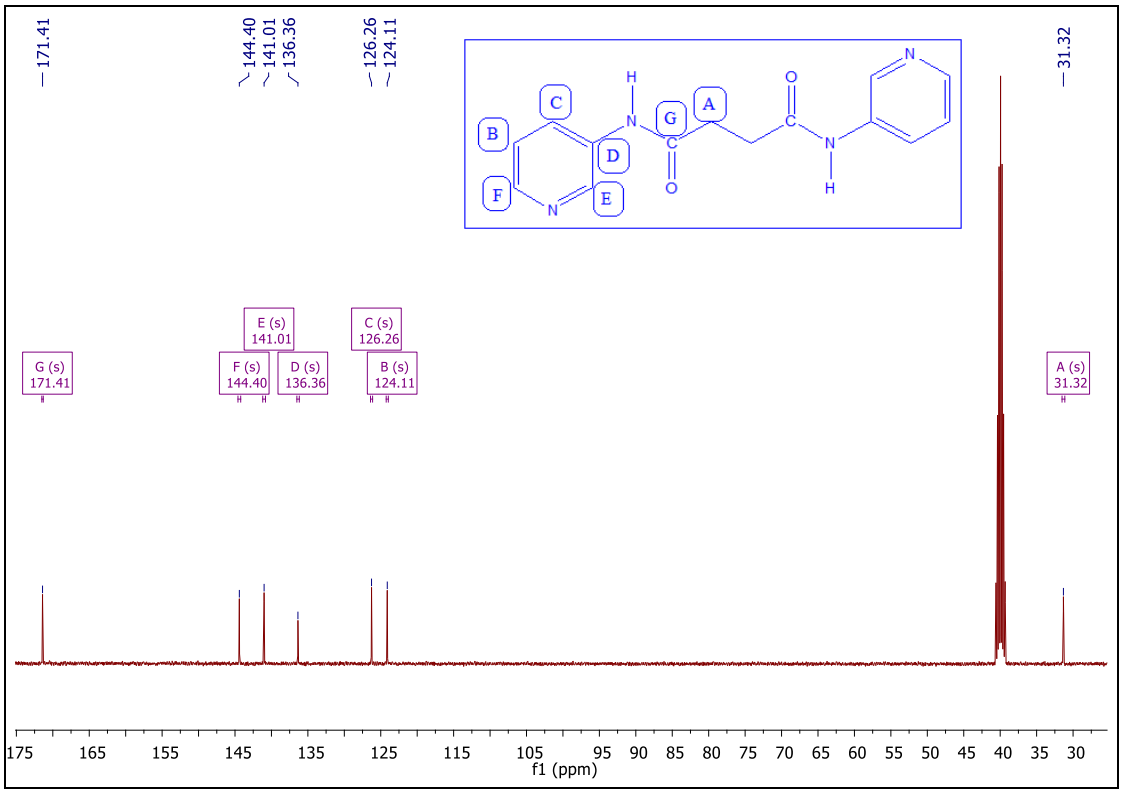

Figure 3.4: ^{13}C-NMR spectrum of Ligand **1a.**

3.2.3 Synthesis of Co-ordination Polymer CP1; [catena-poly[diaquabis-μ-{N, N'-bis(3-pyridyl)ethanediamido}copper (II) hexaflurophosphate]

A solution of NH_4PF_6 (65.2 mg, 0.4 mmol) in 2 mL water was added to a stirred solution of the ligand **1a** (54 mg, 0.2 mmol) in 5 mL of (1 : 1) water–ethanol solution. An ethanolic solution (2 mL) of $Cu(NO_3)_2.3H_2O$ (25 mg, 0.1 mmol) was layered over the ligand solution. Blue colored crystals were formed after 1 week in 70% yield. Good quality crystals were collected for SXRD and were also characterized by elemental analysis, FT-IR (Appendix-1 Figure A2) and PXRD (Appendix-1 Figure A3).

The above reaction was also performed by taking 5ml of aromatic solvents (nitrobenzene, benzonitrile and *p*-xylene). These reactions also resulted in **CP1**; aromatic solvents were not present in the network.

*Analytical data of the synthesized co-ordination polymer1 (**CP1**):* Molecular Formula: $C_{28}H_{32}CuF_{12}N_8O_6P$; Molecular weight = 930.08. Elemental analysis: Calculated: C 36.16 %, H 3.47 %, N 12.05 % ; Found: C 35.38 %, H 3.46 %, N 12.28 %. FT-IR (cm^{-1}): 3386(s), 3280(m), 3185(w), 3109(w), 3073(w), 3054(w), 1688(vs), 1612(m), 1535(vs), 1488(s), 1419(m), 1334(m), 1288(m), 1195(m), 1149(w), 1110(w), 1064(w), 972(w), 826(vs), 702(m), 617(m), 547(s) (Appendix-1 Figure A2)

3.2.4 Synthesis of co-ordination polymers (CP2a-c) by anion exchange reaction

The anion exchange reactions were performed by immersing the crystals of **CP1** (0.05 mmol) in ethanol solution (5 mL) of $NaClO_4$ (0.2 mmol). To this, 5 mL of nitrobenzene/benzonitrile/p-xylene was added. After three days, the crystals were characterized by FT-IR (Appendix-1 Figure A4, A6 and A8) and powder XRD (Appendix-1 Figure A5, A7 and A9).

CP2a: FT-IR (cm^{-1}): 3325(s), 3101(w), 3070(w), 1681(s), 1612(m), 1527(vs), 1488(s), 1411(m), 1334(vs), 1288(m), 1195(w), 1065(s), 972(w), 810(w), 702(w), 617(s), 555(m). (Appendix-1 Figure A4)

CP2b: FT-IR (cm^{-1}): 3409(w), 3325(m), 3070(m), 2229(s), 1689(s), 1604(w), 1542(s), 1488(s), 1450(m), 1411(w), 1334(w), 1288(m), 1249(w), 1064(s), 756(vs), 686(vs). (Appendix-1 Figure A6)

CP2c: FT-IR (cm^{-1}): 3325(s), 3101(w), 3070(w), 1689(s), 1612(w), 1544(vs), 1488(s), 1411(m), 1334(m), 1288(m), 1248(w), 1195(w), 1064(vs), 972(w), 925(w), 810(m),702(s), 617(s). (Appendix-1 Figure A8)

3.2.5 Synthesis of Apohost CP2

CP2a, **CP2b** and **CP2c** was washed thoroughly with $CHCl_3$ and then keeping under vacuum for 4–5 h. Whole guest molecules were washed out with chloroform, the network was still stable named **Apohost CP2** characterized by FT-IR and powder XRD.

FT-IR (cm^{-1}) data: 3325(m), 3101(w), 3070(w), 1681(vs), 1612(m), 1542(vs), 1488(s), 1411(m), 1334(m), 1288(m), 1195(m), 1064(vs), 972(w), 925(w), 810(m), 702(s), 617(s) (Appendix-1 Figure A10). Powder XRD pattern of **Apohost CP2** shown in (Appendix-1 Figure A11).

3.2.6 Anion exchange reaction of CP2a–c with NH_4PF_6

The anion exchange reactions were performed by immersing the crystals of **CP2a**, **CP2b** or **CP2c** (0.05 mmol) in ethanol solution (5 mL) of NH_4PF_6 (0.2 mmol). To this, 5 mL of nitrobenzene/benzonitrile/p-xylene was added.

After three days, the crystals were characterized by FT- IR (Appendix-1 Figure A12, A13 and A14) and PXRD (Appendix-1 Figure A15, A16 and A17). After all exchanges the FT-IR spectras and PXRD pattern are similar, shows the formation of same compound after all exchanges.

3.3 X-Ray crystallography

The single crystal data were collected on a Xcalibur, Sapphire3 X-ray diffractometer that uses graphite monochromated Mo Kα radiation (λ = 0.71073 Å) by the ω-scan method.[23] The structures were solved by direct methods and refined by least square methods on F^2 using SHELX-97.[24] Non-hydrogen atoms were refined anisotropically and hydrogen atoms were fixed at calculated positions and refined using a riding model.

The crystal data and structure refinements of **CP1** are summarized in Table 3.1 (CCDC 912609). ORTEP (Appendix-1 Figure A18)

Table 3.1 The crystal structure data of Co-ordination Polymer **CP1**

CP1	
Empirical formula	$C_{28}H_{32}CuN_8O_6P_2F_{12}$
Formula Wt.	930.10
Crystal system	Triclinic
Space group	$P\bar{1}$
a/Å	8.8145(3)
b/Å	9.5878(3)
c/Å	11.3029(3)
α / °	82.786(2)
β/ °	70.994(3)
γ/ °	86.460(2)
V/Å^3	895.78(5)
Z	1
D_{calcd}/g cm^{-3}	1.724
Final R	R_1 = 0.0392; wR_2 = 0.1025

3.4 Results and discussion

3.4.1 Crystal structure analysis of CP1

CP1 crystallizes in triclinic space group $P\bar{1}$. The asymmetric unit contains one unit of **1a**, half of Cu(II), one coordinated H_2O molecule and one PF_6^-. The crystal structure of **CP1** reveals that Cu(II) has a distorted octahedral geometry as four units of **1a** occupy the equatorial positions (Cu–N: 2.031 Å, 2.095 Å) and two H_2O molecules occupy the axial positions (Cu–O: 2.427 Å). The analysis of the geometry of the **1a** in **CP1** reveals the following points (Figure 3.6):

1. The ethyl chain adopts *anti* conformation.
2. The two amide planes within a ligand are oriented at an angle of 86°.

3. The pyridyl-Ns of a ligand are pointing in the same direction and the two pyridyl planes make an angle of 80.36° with each other.

All these factors resulted in arc-like geometry of the ligand. Further, the angle between amide plane and the pyridyl plane are 28.13° and 23.91° (Figure 3.5), which is compatible with the requirement for amide-to-amide hydrogen bond in absence of any other interfering components.[20]

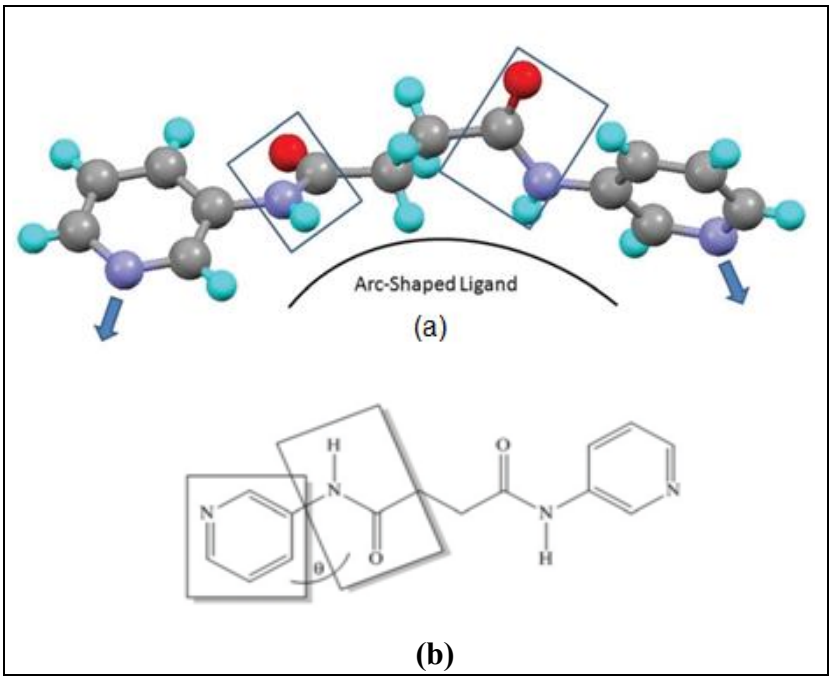

Figure 3.5: (a) Arc-shaped geometry of the ligand **1a** in **CP1.** (b) The interplanar angle between the pyridyl and amide planes.

In **CP1**, amide-to-amide hydrogen bond is not present and this may be due to the interference of counter anion PF_6^- in self-complementary amide-to-amide bond. The network of **CP1** can be described as a 1D-looped chain with elliptical cavities, which have longest axis of 14.687 Å and shortest axis being 7.088 Å.

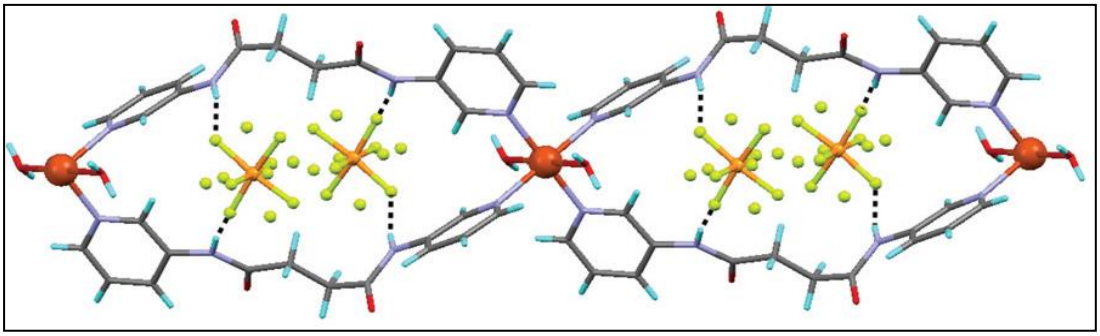

Figure 3.6: Hydrogen bonding interactions of PF_6^- anion with N–H of amide group.

As shown in (Figure 3.6) each PF_6^- anion is simultaneously involved in hydrogen bond interactions with the N–H of the amide groups present in the same loop (N-H•••F 2.247Å, 3.004Å, 165.88°).The N-H•••F hydrogen bond interactions direct the ethyl spacer to adopt the *anti* conformation so that the ligand adopts less curvature compared to that in *gauche* conformation. The hydrogen bond interactions of the amide C=O and coordinated H_2O molecules assembled the chains into higher dimensions (Figure 3.7(a)). The hydrogen bonding interactions of anion PF_6^- with the N–H of the amide groups resulted "slipped" assembling of the looped chains thereby reducing the channel space (Figure 3.7(b)).

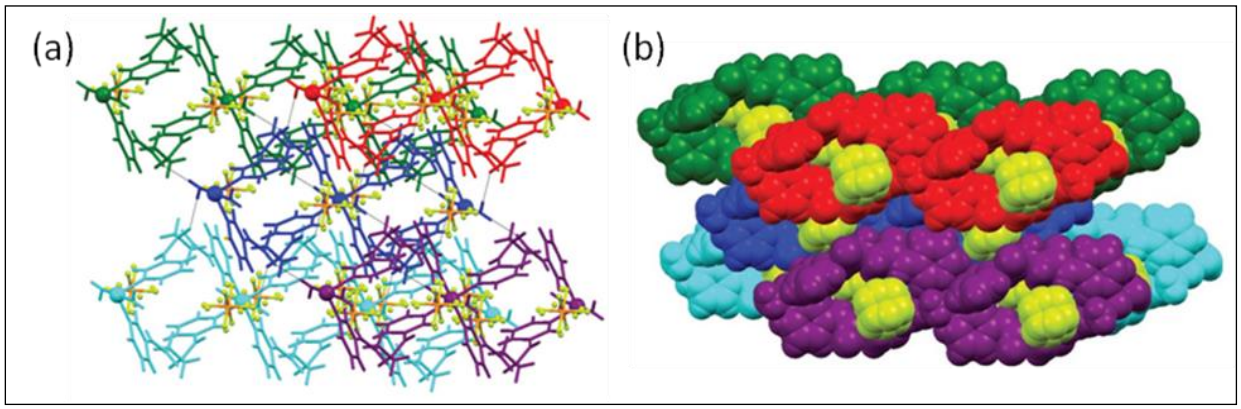

Figure 3.7 (a) Assembling of the 1D - chains *via* (water)O–H···O=C of amide hydrogen bonds; different chains are represented in different colors (b) Space filling representation of the slipped arrangement of the chain and PF_6^- forbid the formation of channels.

Biradha and co-workers have reported a 1D-looped chain derived from the reaction of *N,N′*-(ethane-1,2-diyl)diisonicotinamide with $Cu(ClO_4)_2$, where aromatic molecules are included in the loops[18] (Scheme 3.3). In that structure, the ethyl chain adopted *gauche* conformation and thus the more cavity size (10.0 Å × 13.8 Å) along with the stacking of the looped chains resulted in channels which were sufficient to include the bigger aromatic molecules as guest.

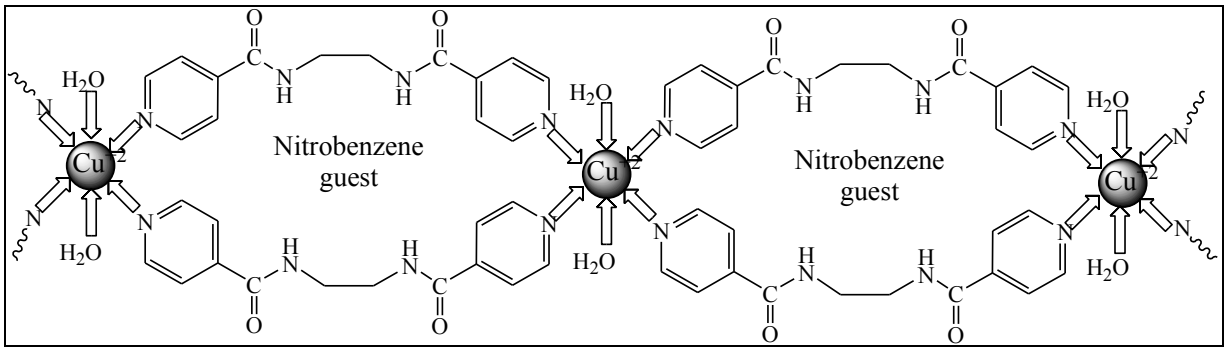

Scheme 3.3: Schematic showing Cu(II) co-ordination polymer of *N,N′*-(ethane-1,2-diyl)diisonicotinamide

3.4.2 Anion exchange reaction of CP1 with $NaClO_4$

The reaction of **CP1** with $NaClO_4$ in different aromatic solvents resulted in formation of CPs (Nitrobenzene: **CP2a**; Benzonitrile: **CP2b**; *p*-Xylene: **CP2c**). The CPs were amorphous materials characterized by IR, powder XRD and solid state UV-Vis spectroscopy.

IR spectra of **CP2a**, **CP2b** and **CP2c** showed very strong peak at 1064 cm^{-1}, which confirm the presence of anion ClO_4^-. The absence of PF_6^- anion peak at 826 cm^{-1} in **CP2a**, **CP2b** and **CP2c**, verify the complete exchange of PF_6^- with ClO_4^-. The presence of aromatic solvents in **CP2** is also confirmed by IR spectroscopy. The IR spectra of **CP2a** show peak at 1334 cm^{-1} which confirms nitrobenzene, whereas a peak at 2229 cm^{-1} in **CP2b** corresponds to C≡N and shows the presence of benzonitrile (Figure 3.8).

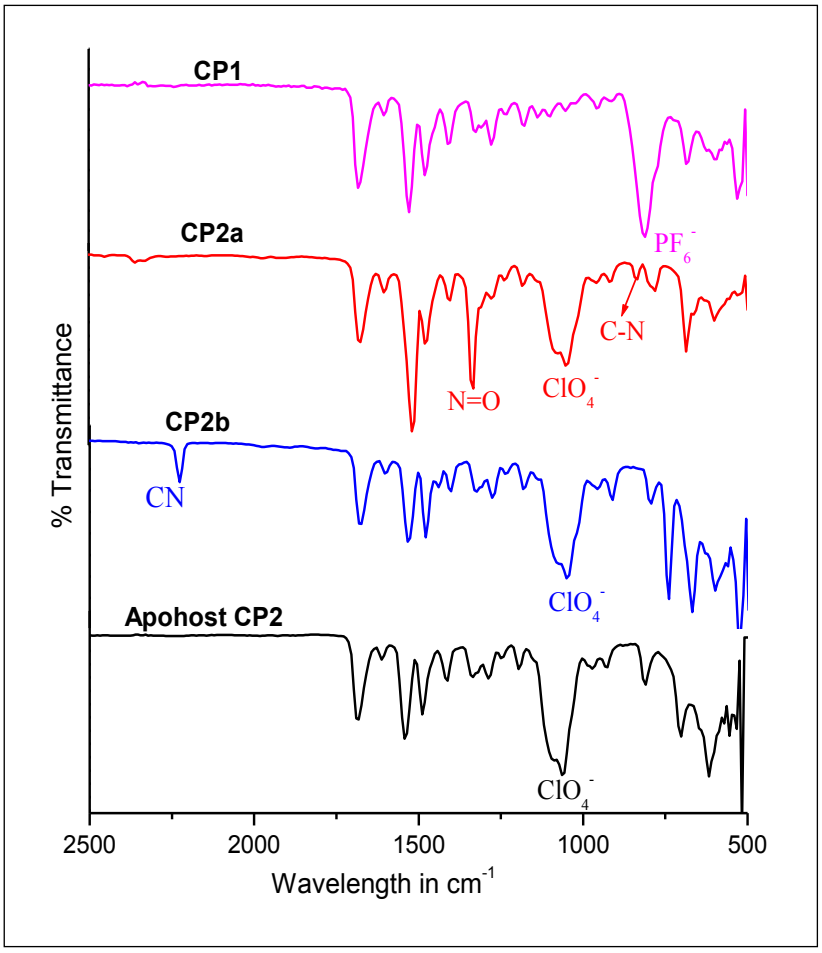

Figure 3.8: FT-IR of **CP1**, **CP2a**, **CP2b** and **Apohost CP2**.

The powder XRD patterns of the **CP2a–c** confirms that the network structures of **CP2a-c** are same, while the differences in the powder XRD pattern of **CP1** and **CP2** suggest that

structural transformation have occurred due to anion exchange (Figure 3.9). The powder XRD pattern of Apohost **CP2** is similar to **CP2a-c** shows the network stability after guest removal.

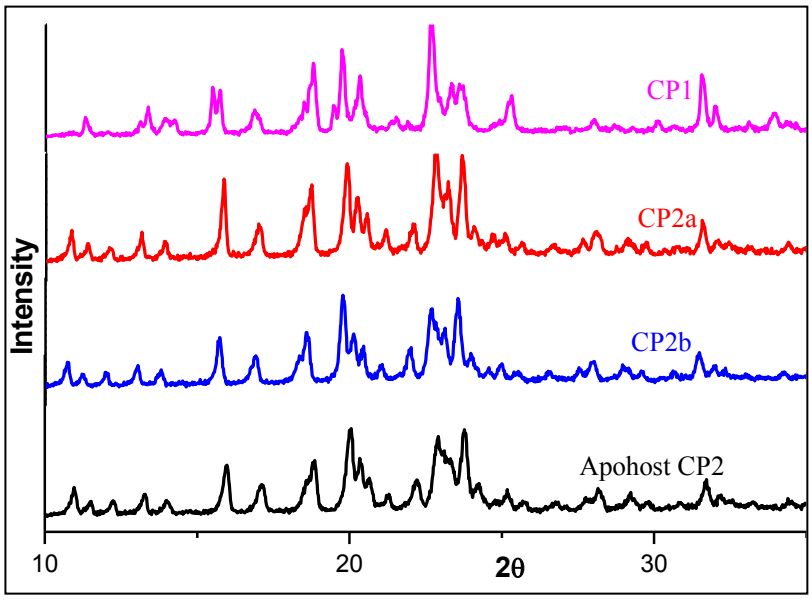

Figure 3.9 The powder XRD pattern showing the anion exchange and presence of guest molecules and stability of network after guest removal.

3.4.3 UV-Vis absorption spectra

The solid state UV absorption spectra of the ligand **1a**, **CP1,** apohost **CP2** and **CP2a-c** were recorded at room temperature (Figure 3.10 and 3.11). The free ligand **1a** exhibits absorption in the range of 200–300 nm with maxima at 200, 250 and 290 nm**.** The 200 nm peak of **1a** was because of $\pi \rightarrow \pi^*$ transition. The ligand have lone pair of electrons (non-bonding electrons) on carbonyl-O and pyridyl-N; showed $n \rightarrow \pi^*$ transition. In case of ligand **1a** the absorption peak at 250 nm was due to $n \rightarrow \pi^*$ transitions of the non-bonding electrons of carbonyl-O. The non-bonding electrons of the pyridyl-N showed absorption peak at 290 nm because of $n \rightarrow \pi^*$ transition on uv-light absorption.

The **CP1** exhibits an absorption peak at 198 nm and weak absorptions in the range of 250–400 nm with peaks at 292 and 360 nm. The apohost **CP2** exhibits an absorption peak at 200 nm and weak absorptions in the range 250–400 nm with peaks at 295 and 375 nm. The absorption peaks for **CP1** and apohost **CP2** are different from those of **1a** indicating that they may be ascribed to the metal-to-ligand charge-transfer (MLCT).[34-36] **CP2a** shows intense peak at 254 nm (Figure 3.11), which is shows the presence of nitrobenzene in the network.

"Free" nitrobenzene shows a strong absorption band at 262 nm. The presence of benzonitrile in **CP2b** is also confirmed by the solid state UV-Vis spectra, it shows intense peaks at 219 nm, 258 nm, 274 nm and 297 nm (Figure 3.11). The "free" benzonitrile have peaks at 240 nm, 264nm, 278 nm, 300 nm.

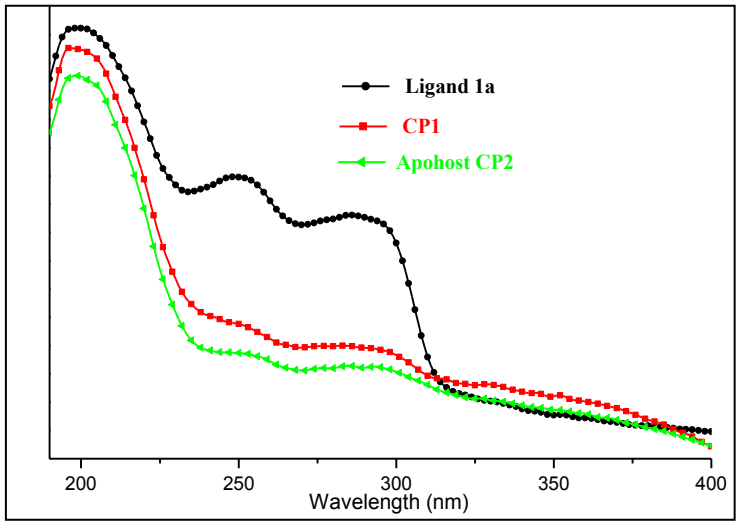

Figure 3.10 Solid state UV absorption spectra of the free organic ligand **1a**, co-ordination polymer **CP1,** apohost **CP2**.

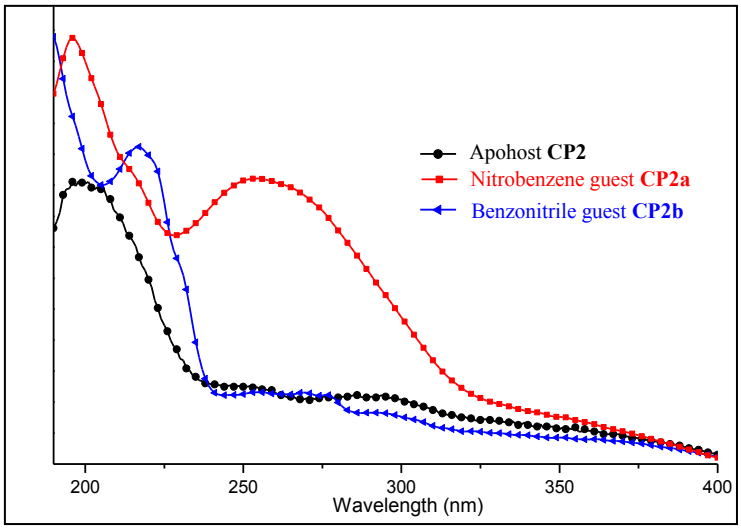

Figure 3.11 Solid state UV absorption spectra of apohost **CP2**, **CP2a**, **CP2b** showing presence of guest molecules.

3.4.4 Quantitative Estimation of Guest Molecules in CP2

UV-Vis spectroscopy was used to determine the amount of nitrobenzene & benzonitrile present in **CP2a** and **CP2b**. Guest molecules present in a given weight of **CPs** were extracted

in chloroform and using calibration plots concentration were determined.

3.4.4.1 Quantitative Estimation of Nitrobenzene in CP2a

To estimate nitrobenzene in **CP2a**, calibration curve of nitrobenzene was plotted at λ_{max} = 262 nm for nitrobenzene. For this UV spectra of known concentration of nitrobenzene *i.e.* 1µM, 2µM, 3µM, 4µM, 5µM, 6µM, 7µM, 8µM, 9µM, 10µM were recorded and a plots of absorbance *vs* wavelength and was obtained (Figure 3.12(a)). Then plotted a graph absorbance *vs* concentration at its λ_{max}= 262 nm (Figure 3.12(b)). From the slope of the curve the ε value calculated which is 26400 L mol^{-1} cm^{-1}.

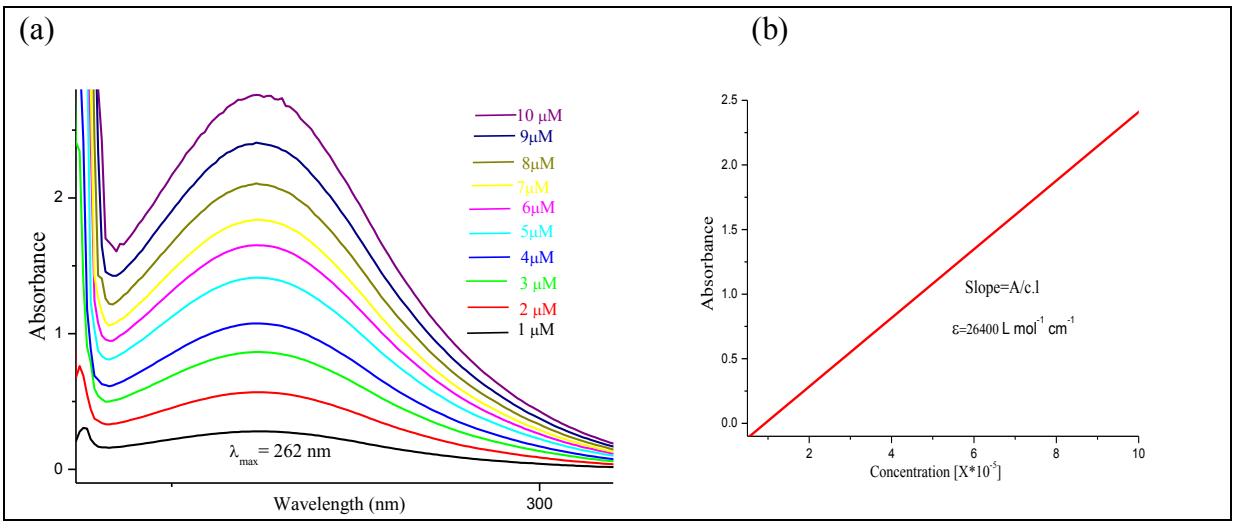

Figure 3.12: (a) UV-Vis Spectra of known concentrations of nitrobenzene (λ_{max} = 262 nm) (b) Calibration plot of nitrobenzene (Absorbance vs. Concentration)

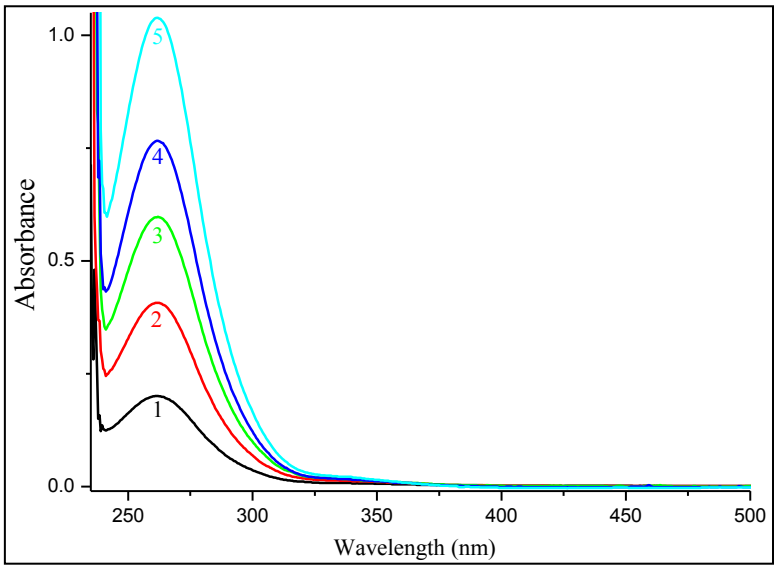

Figure 3.13: UV plot of extracted nitrobenzene in chloroform from known amount of **CP2a.**

Five sets of known weight of **CP2a** were taken, each in 10 ml of chloroform and stirred overnight at RT. Then UV-Vis spectra were recorded for these five sets of extracted nitrobenzene in chloroform (Figure 3.13).

For Plot-**1**,

0.00337 gm of **CP2a** was taken and nitrobenzene was extracted in 10 ml of chloroform and the concentration of nitrobenzene was determined using Lambert-Beer's Law as follows:

According to Lambert-Beer's Law,

$$A = \varepsilon . c . l \quad \text{Or} \quad c = \frac{A}{\varepsilon . l}$$

The **Apohost CP2** consists of network without any guest molecules, its molecular weight will include: 1 Cu^{+2} + 2 Ligand **1a** + 2 Coordinated H_2O + 2 ClO_4^-.

Molecular weight of **Apohost CP2** = 63.5 + (2 ×270) + (2 × 18) + (2 × 99.5) = 838.5 gm.

The **CP2a** consists of nitrobenzene in the cavity. Let **x** molecules of nitrobenzene are there per Cu(II) in **CP2a**.

Molecular weight of **CP2a** = 838.5 + **x .** Nitrobenzene = (838.5 + 123.11 **. x**) gm

Thus {0.00337/(838.5 + 123.11 **. x**)} moles of **CP2a** have 0.761 × 10^{-5} moles of nitrobenzene.

One mole of **CP2a** have **x** moles of nitrobenzene.

Using simple mathematical calculations :

$$\frac{0.761 \text{ x } 10^{-5}}{0.00337 / (838.5 + 123.11.\mathbf{x})} = \mathbf{x}$$

$$\frac{0.761 \text{ x } 10^{-5}.(838.5 + 123.11.\mathbf{x})}{0.00337} = \mathbf{x}$$

$$0.761 \text{ x } 10^{-5}.(838.5 + 123.11.\mathbf{x}) = \mathbf{x}.0.00337$$

$$0.761 .(838.5 + 123.11.\mathbf{x}) = \mathbf{x}.0.00337 \text{ x } 10^{5}$$

$$638.0985 + 93.6867.\mathbf{x} = 337 .\mathbf{x}$$

$$243.3133 .\mathbf{x} = 638.0985$$

$$\mathbf{x} = \frac{638.0985}{243.3133}$$

$$\mathbf{x} = 2.6225$$

Thus number of nitrobenzene present in cavity of co-ordination polymer **CP2a** were 2.6225 molecules per Cu(II) ion. Similarly, concentration of nitrobenzene was calculated for each set and it was found that there are approximately 2–3 molecules of nitrobenzene present per Cu(II) in **CP2a** (Table 3.2).

Table 3.2: Showing the concentration of nitrobenzene present in constant weight of co-ordination polymer CP2a.

Plot no.	Wt. of CP2a Taken	Nitrobenzene conc. (molar) $c=A/\varepsilon.l$	No. of Molecules of Nitrobenzene present per Cu(II) ion
1	0.00337 gm	0.761×10^{-5}M	2.622538
2	0.00475 gm	0.154×10^{-5} M	2.720126
3	0.00712 gm	0.207×10^{-5} M	2.439228
4	0.00952 gm	0.290×10^{-5} M	2.555777
5	0.01190 gm	0.393×10^{-4} M	2.770815

3.4.4.2 Quantitative Estimation of Benzonitrile in CP2b

Similarly, benzonitrile from **CP2b** was extracted in chloroform and the concentration of benzonitrile in the extract was determined. First the calibration curve of benzonitrile is plotted at λ_{max} = 264 nm for benzonitrile.

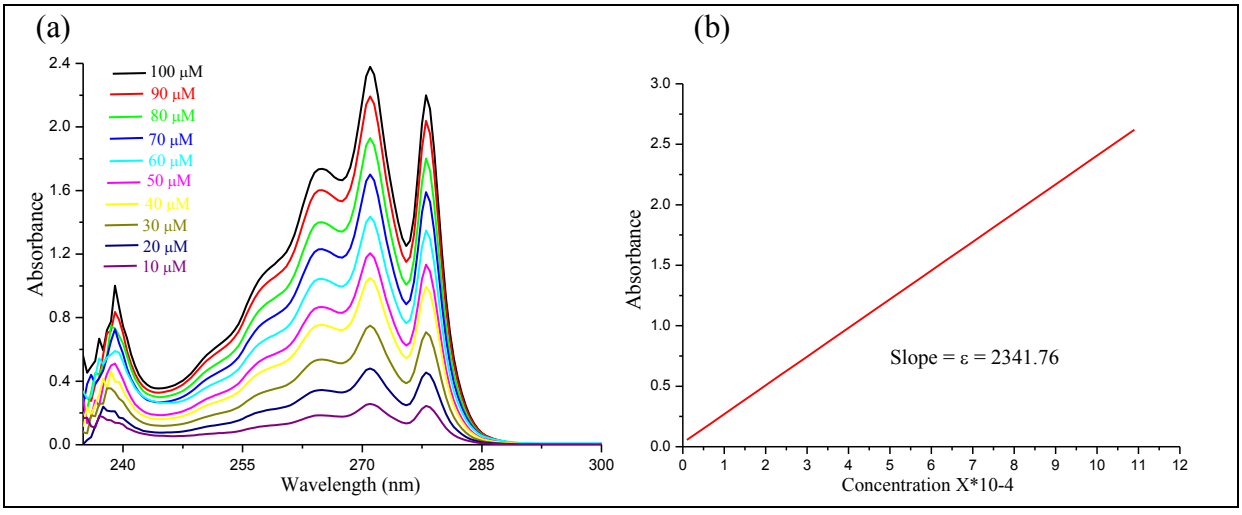

Figure 3.14: (a) UV-Vis Spectra of known concentrations of Benzonitrile (Absorbance *vs* Wavelength) (b) Calibration plot of Benzonitrile (Absorbance *vs* Concentration)

UV spectra of known concentration of benzonitrile *i.e.* 10µM, 20µM, 30µM, 40µM, 50µM, 60µM, 70µM, 80µM, 90µM, 100µM recorded and plotted a graph absorbance *vs* wavelength (Figure 3.14). Five sets of known weight **CP2b** were taken, each in 10 ml of chloroform and stirred overnight at RT. Then UV-Vis spectra were recorded for these five sets of extracted benzonitrile in chloroform (Figure 3.15).

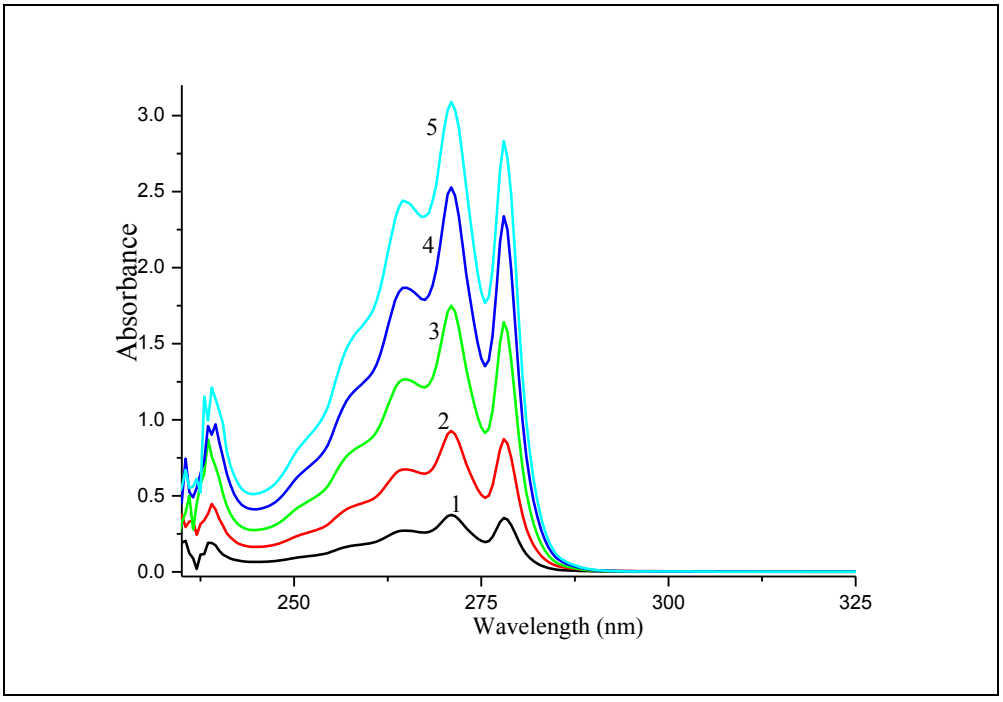

Figure 3.15: UV-plot of extracted benzonitrile in chloroform from known amount of **CP2b.**

Using Lambert-Beer's Law, concentration of benzonitrile was calculated for each set and it was found that there are approximately 2–3 molecules of benzonitrile present per Cu(II) in **CP2b** as shown in (Table 3.3).

Table 3.3: Showing the concentration of benzonitrile present in constant weight of CP2b

Plot no.	Wt. of CP2b Taken	Benzonitrile conc. (molar) c=$A / \varepsilon.l$	No. of Molecules of Benzonitrile
1	0.00850 gm	1.7×10^{-5}M	2.11235
2	0.01065 gm	2.2×10^{-5}M	2.20049
3	0.01252 gm	2.7×10^{-5} M	2.32488
4	0.01679 gm	3.3×10^{-5} M	2.03914
5	0.01800 gm	3.9×10^{-5} M	2.33892

3.4.5 Ligand geometry:

Biradha *et al.* reported the crystal structure of this ligand **1a**, where amide-to-amide hydrogen bonds are absent, the amide N-H is involved in N-H•••N hydrogen bonds with pyridyl-nitrogen. The asymmetric unit contain only half molecule and the ethyl chains exhibit a perfect *anti* conformation, almost planar and angle between the pyridyl and amide plane *i.e.* θ is 0°.[19]

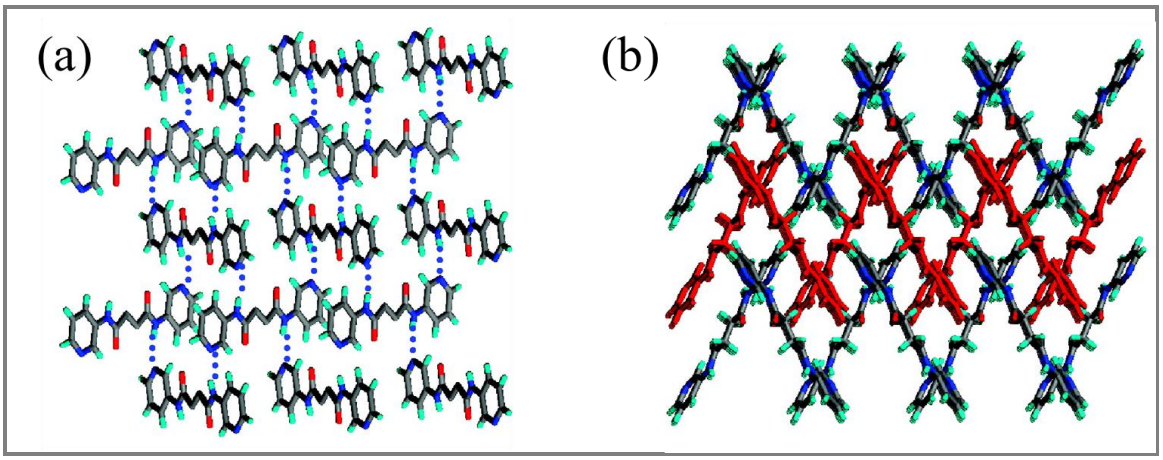

Figure 3.16: The crystal structures of ligand **1a** corrugated 2D layers (a) N–H···N hydrogen bonds (b) packing central layers were red in colour.[19]

This confirmation may be blamed for the inhibition of amide-to-amide hydrogen bonds. The molecules form a corrugated 2D layer *via* N-H•••N hydrogen bonds. The amide carbonyl (>C=O) group is involved in C-H•••O hydrogen bonds with neighboring layers (Figure 3.16).[19]

The ligand **1a** is flexible due to *meta* position of pyridyl nitrogen and ethyl spacer, the possible conformations are depicted in (Figure 3.17). The geometry of the ligand in **CP1** is conformation **3**, where the ligand adopts slightly arc-type geometry. But in order to accommodate bigger aromatic guest molecules, the curvature of the ligand should be more than that in case of *anti* conformation of the ethyl spacer. So we are predicting that the geometry of the ligand may have changed from *anti* to *gauche* in order to accommodate the aromatic guest molecules in **CP2a–c**. From the schematic we can see that the *gauche* conformation of the ethyl spacer results increasing the curvature of the ligand which can provide accommodation to the aromatic guest molecules. This dynamic structural transformation of the co-ordination polymer resulted on changing the counter anions.

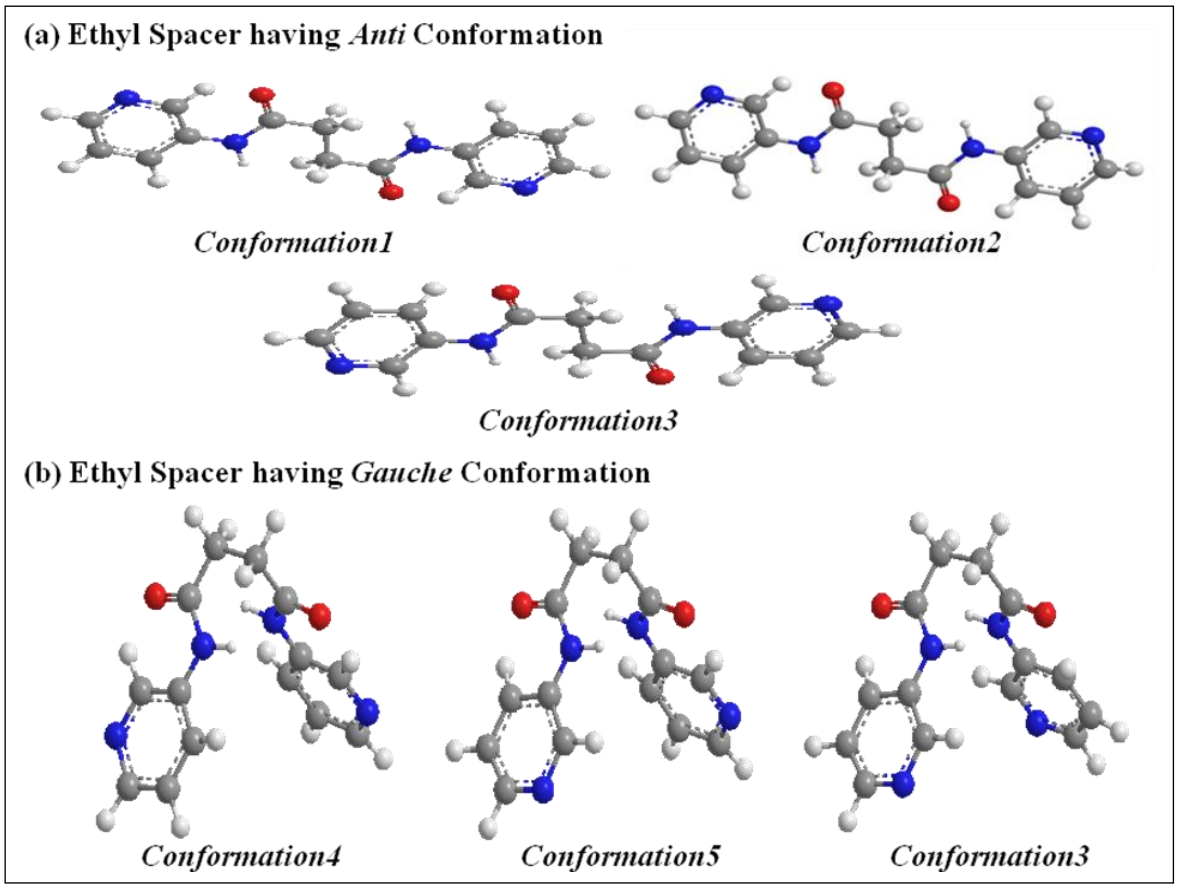

Figure 3.17: Schematic showing some of the possible Conformations of ligand **1a** (*ChemDraw Ultra 12.0*)

3.5 Conclusion

Ligand **1a** is flexible due to ethyl spacer and *meta* position of pyridyl-N, may change confirmation according to the requirement *i.e.* external environment around it. In the above study the geometry of anion is major structure directing factor. The PF_6^- having octahedral geometry *i.e.* the symmetrical arrangement of F^- around P makes it feasible to interact simultaneously with the two N–H of the same loop, which is not possible in ClO_4^- because of its tetrahedral geometry. The interaction of PF_6^- simultaneously with two N–H resulted the flexible ethyl chain to adopt *anti* conformation so that the distance between the two N–H groups within a loop is reduced. This resulted in unavailability of space for aromatic guest inclusion in the loops. By introducing ClO_4^- anion in place of PF_6^- resulted in changing the environment of the **CP** and this change is accommodated by simultaneous adjustment of the hydrogen bond interaction and the flexible framework. We wind up our results as reversible inclusion and removal of guest molecules triggered by the exchange of anions.

3.6 References

[1] Rajput, L.; Biradha, K. *Chem. Eng. Commun*. **2009**, *11* (7), 1220-1222.

[2] Sarkar, M.; Biradha, K. *Chem. Commun.* **2005**, (17), 2229-2231.

[3] Sarkar, M.; Biradha, K. *Cryst. Growth Des.* **2006**, *6* (8), 1742-1745.

[4] Sarkar, M.; Biradha, K. *Cryst. Growth Des.* **2007**, *7* (7), 1318-1331.

[5] Rajput, L.; Biradha, K. *New J. Chem.* **2010**, *34* (11), 2415-2428.

[6] Ma, L.; Abney, C.; Lin, W. *Chem. Soc. Rev.* **2009**, *38* (5), 1248-1256.

[7] Uemura, T.; Yanai, N.; Kitagawa, S. *Chem. Soc. Rev.* **2009**, *38* (5), 1228-1236.

[8] Rowsell, J. L. C.; Yaghi, O. M. *Micropor. Mesopor. Mat.* **2004**, *73* (1–2), 3-14.

[9] MacGillivray, L. R., *Metal-organic frameworks: design and application*, John Wiley & Sons: **2010**.

[10] McKinlay, A. C.; Morris, R. E.; Horcajada, P.; Férey, G.; Gref, R.; Couvreur, P.; Serre, C. *Angew. Chem. Int. Ed. Engl.* **2010**, *49* (36), 6260-6266.

[11] Farrusseng, D. *Metal-Organic Frameworks: Applications from Catalysis to Gas Storage*, Wiley: New York, **2011**.

[12] Suh, M. P.; Park, H. J.; Prasad, T. K.; Lim, D.-W. *Chem. Rev.* **2012**, *112*(2), 782-835.

[13] Zaworotko, M. J. *Chem. Commun.* **2001**, (1), 1-9.

[14] Rajput, L.; Biradha, K. *New J. Chem.* **2010**, *34* (11), 2415-2428.

[15] Adarsh, N. N.; Tocher, D. A.; Ribas, J.; Dastidar, P. *New J. Chem.* **2010**, *34* (11), 2458-2469.

[16] Wang, X.-L.; Luan, J.; Sui, F.-F.; Lin, H.-Y.; Liu, G.-C.; Xu, C. *Cryst. Growth Des.* **2013**, *13* (8), 3561-3576

[17] Wang, X.-l.; Sui, F.-f.; Lin, H.-y.; Zhang, J.-w.; Liu, G.-C. *Cryst. Growth Des.* **2014**, *14* (7), 3438-3452.

[18] Sarkar, M.; Biradha, K. *Cryst. Growth Des.* **2007**, *7* (7), 1318-1331.

[19] Rajput, L.; Singha, S.; Biradha, K. *Cryst. Growth Des.* **2007**, *7* (12), 2788-2795.

[20] Sarkar, M.; Biradha, K. *Cryst. Growth Des.* **2006**, *6* (1), 202-208.

[21] Wenzel, M.; Hiscock, J. R.; Gale, P. A. *Chem. Soc. Rev.* **2012**, *41* (1), 480-520.

[22] Blondeau, P.; van der Lee, A.; Barboiu, M. *Inorg. Chem.* **2005**, *44* (16), 5649-5653.

[23] *CrysAlis PRO (oxford Diffraction),* Oxford Diffraction Ltd., Yarton, Oxfordshire, England, **2010**.

[24] G. M. Sheldrick *Acta Crystallogr., Sect. A: Found. Crystallogr*. **2008**, *A64*, 112-122.

[25] K. Peter, C. Vollhardt and N. E. Schore, *Organic Chemistry: Structure and Function*, 3rd ed. W. H. Freeman and Company, New York, **2003**.

[26] Ohkoshi, S.-i.; Tokoro, H.; Hozumi, T.; Zhang, Y.; Hashimoto, K.; Mathonière, C.; Bord, I.; Rombaut, G.; Verelst, M.; Cartier dit Moulin, C.; Villain, F. *J. Am. Chem. Soc.* **2006**, *128* (1), 270-277.

[27] Stadler, A.-M.; Puntoriero, F.; Campagna, S.; Kyritsakas, N.; Welter, R.; Lehn, J.-M. *Chem. Eur. J.* **2005**, *11* (13), 3997-4009.

Chapter 4

Post-synthetic Modification of CP *via* Metal-Metathesis

4.1 Introduction

In the previous chapter, CP of ligand **1a** with $Cu(ClO_4)_2$ was discussed, where 1D- looped chain networks were observed. The ligand **1a** in **CP1** and **CP2** formed arc like geometry which resulted in cavities capable for including guest molecules. The chemical properties shape and size of the cavities of a network can be tuned by introducing or modifying the spacers. In the present chapter, we will discuss the CP of ligand **1b**, which has enhanced spacer length. On increasing the spacer length, the resulting CP is expected to have more empty space for guest inclusion (Figure 4.1).

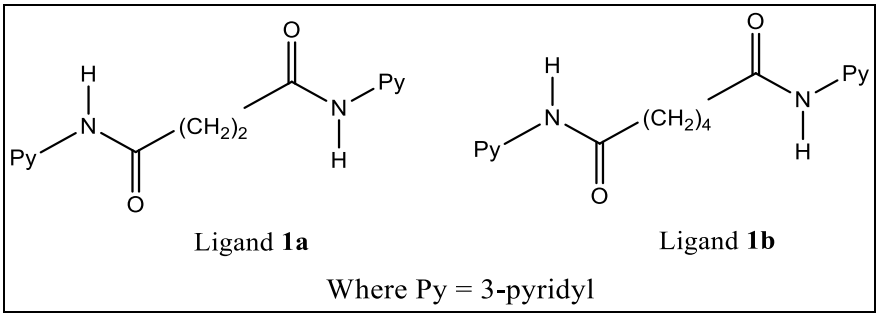

Figure 4.1: The flexible *exo*-bidentate having *bis*-pyridyl-*bis*-amide moiety.

In the absence of proper guest molecules, the empty spaces in the networks are filled by themselves by the phenomena called self-interpenetration or self-entanglements. Such interpenetrations are frequently observed aspect in coordination polymers. Interpenetration of the networks due to the presence of large empty spaces in the networks interferes in formation of porous CPs.

The term interpenetration was introduced by Wells, where it was described as the phenomena in which the motifs "cannot be separated without breaking links".[1] The interpenetration of the 2D networks of (4,4)-topology can be classified into two broad categories: parallel and perpendicular/inclined.[2,3] When the mean planes of the individual nets are parallel, the mode of the interpenetration is parallel. The perpendicular/inclined interpenetration occurs when the mean planes of the nets are exactly perpendicular or slightly inclined to each other. The perpendicular interpenetration can be further categorized into three types: parallel/parallel, diagonal/diagonal and parallel/diagonal. The term 'parallel' in this case refers to a structure in which a spacer of the ligand of one layer passes through the cavity of the other and the term 'diagonal' refers to a structure in which a node of one layer is within the cavity of the other.

(Figure 4.2)

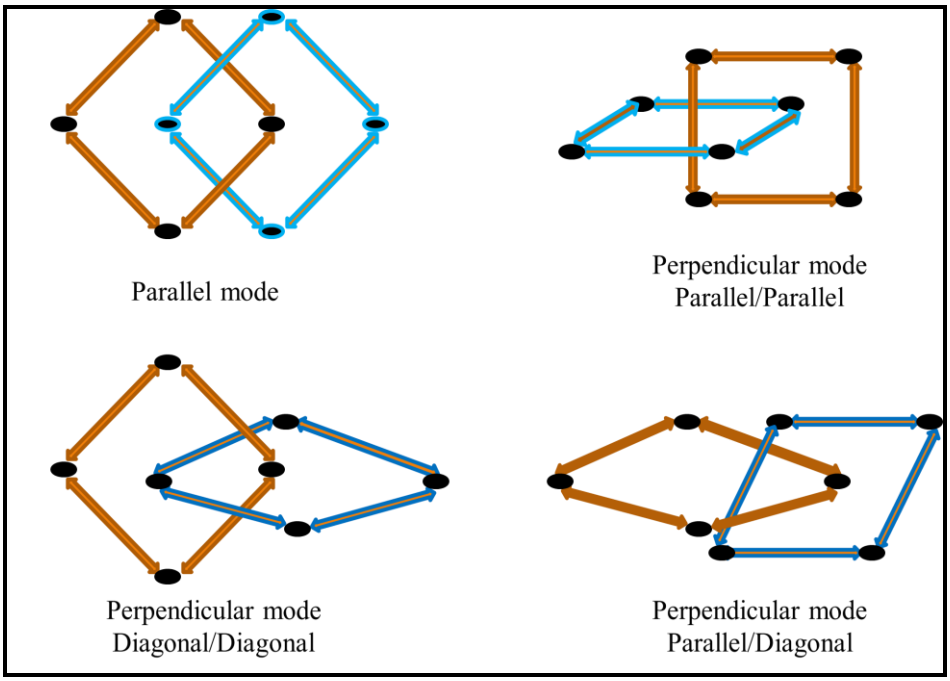

Figure 4.2: Types of interpenetration in 2D networks of (4,4)-topology structures.

In this chapter, we will discuss synthesis and structural aspects of the CPs of Ligand **1b** with different metal centers Cu(II) and Cd(II) to determine the role of the metal centre in forming the CPs. Ligand **1b** with $Cu(ClO_4)_2$ resulted in 2D network of (4,4)- topology having two-fold parallel interpenetration but with $Cd(ClO_4)_2$ it formed 1D-looped chains. Post synthetic Modification (PSM) reactions were carried out which resulted in synthesis the new Cu(II) 1D-chain CP.

The less reactive metal cation of any CP can be replaced by the more reactive metal cation, the process called 'transmetallation' or 'metal-metathesis'. Post synthetic Modification (PSM) *via* metal metathesis is a very talented approach to functionalize CPs because new metal cations can be introduced to the framework without destroying or altering the initial structural integrity and even single crystallinity. We know in a co-ordination polymer (CP) crystal the metal nodes are in equilibrium with metal cations in the solvent. Thus metal metathesis; introduction of new metal cations to the crystals is by exchanging them from the solution with the metal nodes in the crystals. However, the process of metal-metathesis was not homogeneous; it was reported that the outer shell of the crystals exchanged first, leading to a core-shell hetero structure.[4] This was explained by a difference of flexibility in the

framework; the diffusion of the metal ions through the pore is time taking process. The framework of a Co-ordination Polymer is more flexible in the outer parts than it is in the middle of the crystal. For metal metathesis often methanol is chosen as the solvent, as it gives higher exchange rates than other polar solvents, *i.e* acetone or other higher alcohols. Because size of methanol molecule is small and it will form smaller hydration shell around the dissolved metals and counter ions. This allows faster diffusion and closer interaction with the framework of a crystalline coordination polymer. Water has not been a good solvent because most CPs dissolved in water. Transmetallation have been further determined by several factors controlling the thermodynamics and the kinetics of the reaction, such as choice of solvent, concentration of soaking solution and reaction temperature. The thermodynamic stability of the daughter CP relative to the parent is most important factor to explore the metal metathesis.

The Irving-Williams series for the relative stabilities of octahedral complexes of transition metals [5]:

$$Mn^{2+} < Fe^{2+} < Co^{2+} < Ni^{2+} < Cu^{2+} > Zn^{2+}$$

According to this series, octahedral complexes of Cu(II) have maximum stability which drops down to Zn(II) since its d^{10} electronic configuration do not experience additional crystal field stabilization. Yao *et al.*[6] and Song *et al.*[7] independently conducted transmetallation experiments and established a thermodynamic stability order in CP's metal nodes - Cu(II) > Ni(II) > Co(II) ≈ Zn(II) which is in good agreement with the Irving–Williams series.

Gargi *et al.* synthesized fifteen iso-structural (2D-layered) co-ordination polymers of a pyridine based tripodal ligand (Benzene-1,3,5-triyltriisonicotinate) with metal ions (Zn^{+2}, Co^{+2}, Cu^{+2}, Cd^{+2}), in presence of different guest molecules (pyrene, phenanthrene, triphenelene, 9-anthraldehyde, nitrobenzene, styrene, chlorobenzene etc.) having general formula - $\{[M(L)_2(H_2O)_2]. 2(anion). Guest.2(H_2O)\}_n$. They performed transmetallation study on these CPs; Zn(II) to Cu(II), Cd(II) to Cu(II) and Cu(II) to Cd(II) have been studied by immersing the crystals of complexes in the MeOH solution of targeted metal salt. The result of the study indicated that the compound could be rapidly transmetallated with Cu^{2+} or Cd^{2+}, the Cd^{2+} nodes subsequently able to be transmetallated to Cu^{2+}; transmetallation of Cu^{2+} to Cd^{2+}, proceeded very slowly; whereas the transmetallation of Cu^{2+} to Zn^{2+} proved not feasible.[8] We exchanged the Cd(II) ion with more reactive Cu(II) ion which resulted a 1D-

chain co-ordination polymer. This chapter will focus on the synthesis and the post-synthetic cation exchange The kinetic study of this transmetallation have been monitored by field emission scanning spectroscopy (FE-SEM), energy dispersive X-ray (EDX) and atomic absorption spectroscopy (AAS) at various intervals. From AAS, the total time taken for complete metal exchange can be determined.

4.2 Experimental section

4.2.1 General

Infra-red spectra were recorded on a FT-IR ABB Bomen MB-3000. Elemental analyses were obtained with a Thermo finnigan, Italy, Model FLASH EA 1112 series. Powder X-ray diffraction (XRD) data were recorded with a Rigaku miniflex II, $\lambda = 1.54$ Å, Cu Kα. Atomic absorption spectra (AAS) was measured using AA-7000, Shimadzu. Wavelength dispersive X-ray fluorescence (WD-XRF) was measured using a S8 TIGER, Make: Bruker, Germany with X-ray tube of 4 kW, "Rhodium" target and a high voltage/tube current: 60 kV per 64 mA.

4.2.2 Synthesis of Ligand 1b

Ligand **1b** was synthesized according to a previously reported procedure.[9] 3-Amino pyridine (2 mmol) was added to 40 ml of a pyridine solution containing adipic acid (1 mmol), and the resultant solution was stirred for 15 min. To this solution triphenyl phosphite (2 mmol) was added and the reaction mixture refluxed for 5 h. The volume of the solution was reduced to 5 ml by removing the pyridine by distillation and a white precipitate was obtained. The solid was filtered, washed with water, and dried under vacuum.

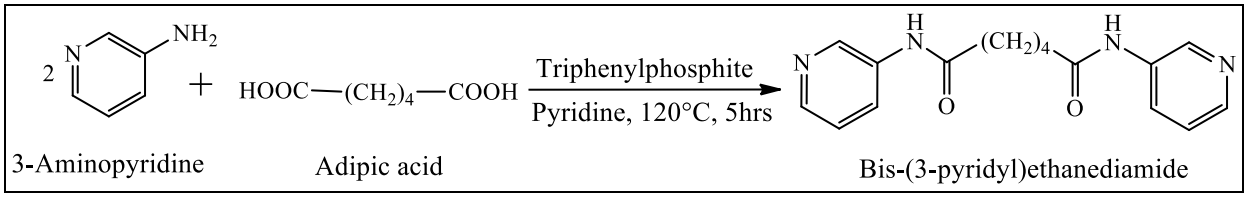

Scheme 4.1: Synthesis of Ligand **1a.**

Yield: 70%. Mp: 216–220 °C. FT-IR (KBr, cm^{-1}): 3301 (w), 3247 (m), 3178 (m), 3108 (m), 3039 (m), 2947 (vs), 2917 (s), 2875 (m), 1690 (vs), 1580 (vs), 1550 (s), 1478 (m), 1419 (vs), 1378 (m), 1281 (vs), 1157 (s), 1132 (w), 1034 (m), 943 (m), 910 (w), 856 (w), 810 (s), 735 (w), 701 (m), 625 (w), 578 (w) (Appendix-1 Figure A19).

^{1}H NMR (400 MHz, DMSO) δ (ppm) 10.14 (s, 1H), 8.73 (d, J = 0.4 Hz, 1H), 8.24 (dd, J = 4.7, 1.5 Hz 1H), 8.03 (dd, J = 2.5, 1.5 Hz 1H), 7.36 – 7.27 (m, 1H), 2.38 (t, J = 5.8 Hz, 2H), 1.66(t, J = 0.4 Hz, 2H) (Figure 4.3).

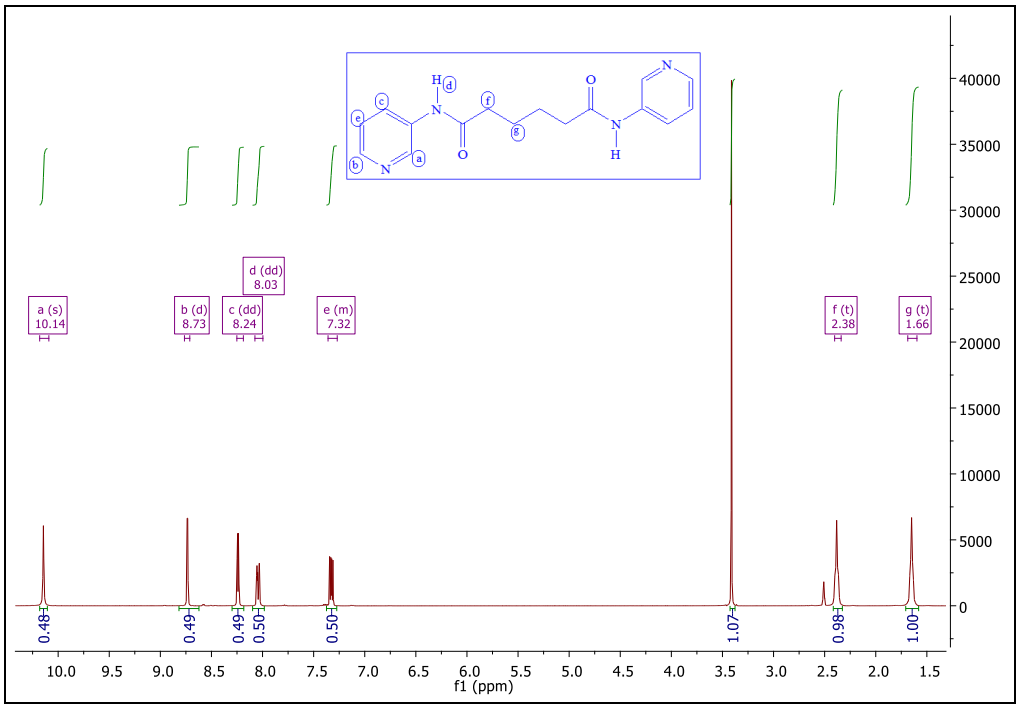

Figure 4.3: ^{1}H-NMR spectrum of Ligand **1b**

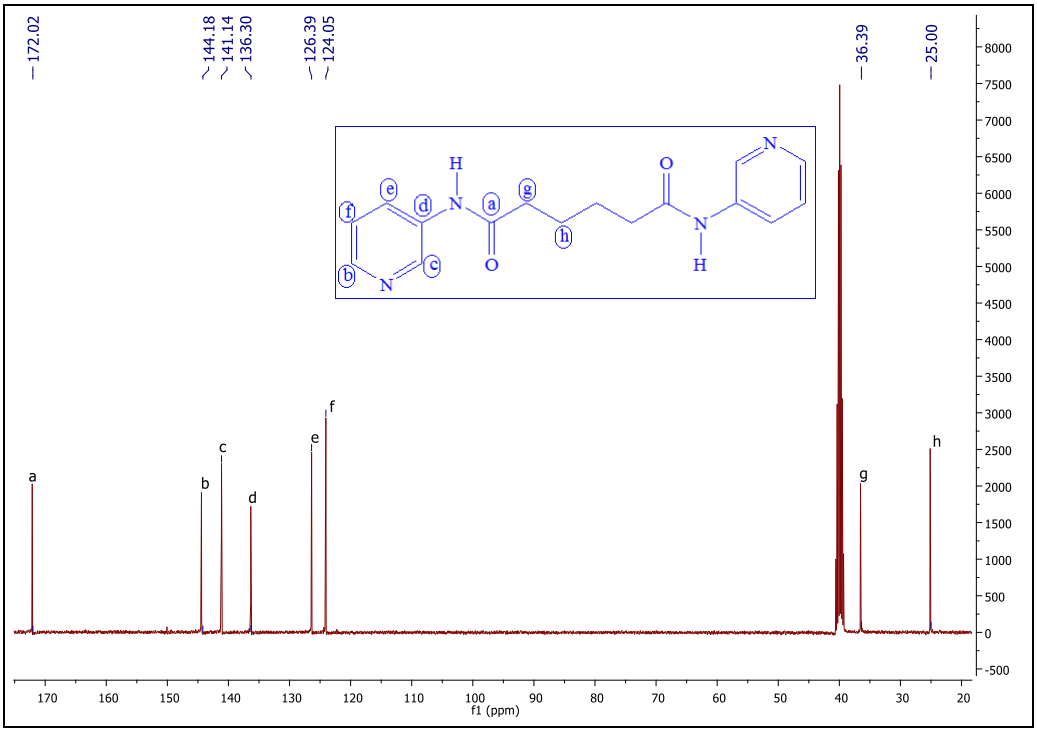

Figure 4.4: ^{13}C-NMR spectrum of **1b**

^{13}C NMR (400 MHz, DMSO) δ (ppm) 172.02, 144.18, 141.14, 136.30, 126.39, 124.05, 36.39, 25.00 (Figure 4.4).

4.2.3 Synthesis of Co-ordination Polymer CP3, $\{[Cu(1b)_2(H_2O)_2](ClO_4)_2.2(H_2O)\}_n$

Ligand **1b** (596 mg, 2.0 mmol) was dissolved in 15 ml of a 1 : 1 mixture of water–ethanol. To the above solution, 10 ml of an ethanolic solution of $Cu(ClO_4)_2$ (370.1 mg, 1.0 mmol) was added. The resulting blue precipitate was dissolved by adding a few drops of water. The solution was filtered and kept for slow evaporation.

Blue-colored crystals were formed after 8–10 days in 80% yield. FT-IR (KBr, cm^{-1}): 3564 (s), 3278 (s), 3201 (w), 3101 (w), 2931 (w), 2862 (w), 1674 (s), 1612 (w), 1589 (w), 1550 (vs), 1488 (m), 1427 (s), 1365 (w), 1296 (m), 1242 (w), 1195 (w), 1103 (vs), 956 (w), 918 (w), 810 (m), 702 (m), 624 (m), 555 (w) (Appendix-1 Figure A20). PXRD pattern of the co-ordination polymer **CP3** was shown in (Appendix-1 Figure A21). Anal. calcd (%) for $C_{32}H_{44}CuCl_2N_8O_{16}$: C, 41.27 %; H, 4.72 %; N 12.03 %. Found: C, 41.27 %; H, 4.55 %; N, 11.63 %.

4.2.4 Synthesis of Co-ordination Polymer CP4, $\{[Cd(1b)_2(H_2O)_2](ClO_4)_2.2(H_2O)\}_n$

A microwave-assisted technique was used wherein ligand **1b** (59.6 mg, 0.2 mmol) and $Cd(ClO_4)_2.6H_2O$ (41.94 mg, 0.1 mmol) was added to 5 ml of a 1 : 1 mixture of water–ethanol mixture in a specially designed microwave test tube. The reaction mixture was irradiated for 10 minutes at 90 °C at a medium stirring rate and 100 psi pressure.

White crystals suitable for single crystal XRD were formed after the solution was allowed to stand at RT for 1 day in 70% yield. FT-IR (KBr, cm^{-1}): 3865 (s), 3841 (s), 3741 (vs), 3672 (m), 3649 (m), 3618 (m), 3564 (w), 3317 (vs), 1674 (vs), 1527 (vs), 1481 (s), 1419 (s), 1326 (w), 1288 (m), 1164 (w), 1103 (vs), 956 (w), 802 (w), 771 (s), 702 (w), 624 (m), 563 (m) (Appendix-1 Figure A22). PXRD pattern of the co-ordination polymer **CP3** was shown in (Appendix-1 Figure A23). Anal. calcd (%) for $C_{32}H_{44}CdCl_2N_8O_{16}$: C, 39.22 %; H, 4.53 %; N 11.43 %.Found: C, 41.69 %; H, 4.57 %; N, 10.69 %.

The calculated percentages are based on the molecular formula from the single crystal XRD. **CP4** was crystallized from ethanol. If we include the free ethanol molecules, we can account for the observed elemental percentage (Table 4.1).

Table 4.1: Elemental Analysis of **CP4** based on different approximation

Found	C % 41.69	H % 4.57	N % 10.69
Calculated: Chemical Formula: $C_{32}H_{44}CdCl_2N_8O_{16}$ 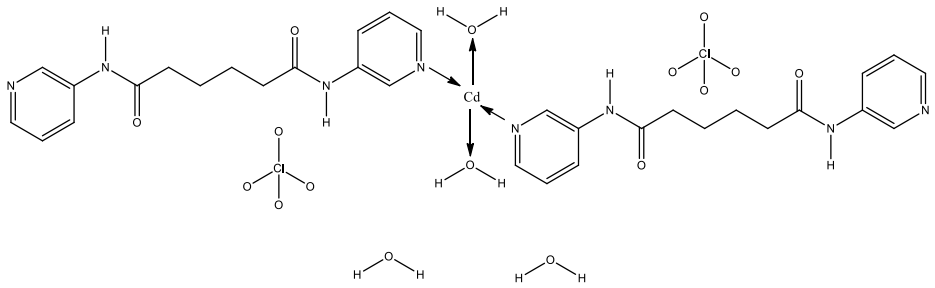	C % 39.22	H % 4.53	N % 11.43
Calculated: Chemical Formula: $C_{36}H_{52}CdCl_2N_8O_{16}$ 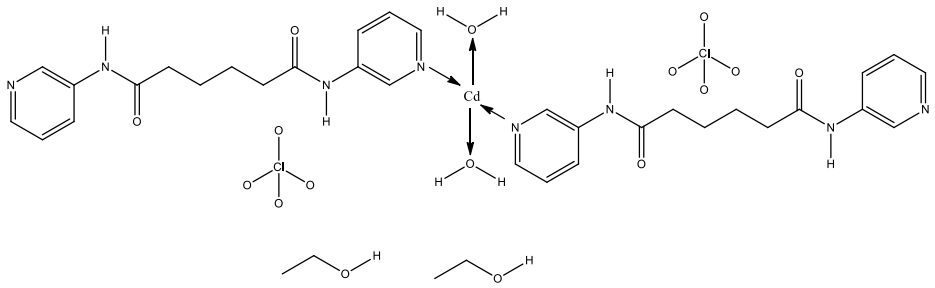	C % 41.73	H % 5.06	N % 10.81

4.2.5 Synthesis of Co-ordination Polymer CP5

A metal-metathesis reaction was performed on co-ordination polymer **CP4** wherein crystals of **CP4** were immersed into a 0.1 M ethanolic solution of $Cu(ClO_4)_2$. The white crystals slowly turned to blue crystals, termed as **CP5.** The crystals were analyzed by FT-IR, PXRD, AAS and WD-XRF spectroscopy.

FT-IR (KBr, cm^{-1}): 3564 (s), 3278 (s), 3201 (w), 3101 (w), 2931 (w), 2862 (w), 1674 (s), 1612 (w), 1589 (w), 1550 (vs), 1488 (m), 1427 (s), 1365 (w), 1296 (m), 1242 (w), 1195 (w), 1103 (vs), 956 (w), 918 (w), 810 (m), 702 (m), 624 (m), 555 (w) (Appendix-1 Figure A24). PXRD pattern of the Co-ordination Polymer **CP5** was shown in (Appendix-1 Figure A25). We assumed that only Cd(II) ions of **CP4** were replaced by Cu(II) Anal. calcd (%) for $C_{32}H_{44}CuCl_2N_8O_{16}$: C, 41.27 %; H, 4.72 %; N 12.03 %. Found: C, 41.97 %; H, 3.95 %; N, 11.73 %.

4.3 Single crystal X-ray crystallography

Single crystal data for **CP3** and **CP4** were obtained on a Xcalibur, Sapphire 3 X-ray diffractometer that uses graphite monochromatized Mo Kα radiation (λ = 0.71073 Å) using the ω-scan method.[10] The structures were solved by direct methods and refined by least square methods on F^2 using SHELX-97.[11] The crystal data and structure refinements of **CP3** and **CP4** are summarized in Table 4.2.

Table 4.2: Crystal structure data of Co-ordination Polymers **CP3** & **CP4.**

CP	CP3	CP4
Empirical formula	$C_{32}H_{44}Cl_2CuN_8O_{16}$	$C_{32}H_{44}Cl_2CdN_8O_{16}$
Formula Wt.	931.19	980.05
Crystal system	Orthorhombic	Triclinic
Space group	$P2_12_12$	$P\bar{1}$
a(Å)	11.3423(3)	9.0727(2)
b(Å)	19.2826(7)	9.0760(2)
c(Å)	9.5549(3)	15.3648(3)
α (°)	90	106.099(2)
β (°)	90	90.817(2)
γ (°)	90	93.146(2)
Volume(Å^3)	2089.74(11)	1213.17(4)
Z	2	1
Density (g/cm^3)	1.480	1.341
Temperature (K)	296(2)	296(2)
Theta(^{0}) range for data Collection	3.50 to 24.98	3.51 to 25.0
R_{int}	0.0428	0.0411
Reflection with $I > 2\sigma(I)$	2989	3982
No. of parameters refined	270	255
Final R (with $I > 2\sigma(I)$)	$R_1{}^a$ = 0.0679; $wR_2{}^b$ = 0.1726	$R_1{}^a$ = 0.0595; $wR_2{}^b$ = 0.1679
GOF on F^2	0.972	1.023

$^aR_1 = \Sigma||F_0| - |F_c|| / \Sigma|F_0|$. ^{b} $wR_2 = [\Sigma w(F_0^2 - F_c^2)^2 / \Sigma w(F_0^2)^2]^{1/2}$ where $w = 1/[\sigma^2(F_0^2) + (aP)^2 + bP]$, $P = (F_0^2 + 2F_c^2)/3$.

In both structures, the disorder in the perchlorate group was modeled (one of the oxygens over two positions for **CP3** and two of the oxygens over two positions (each) to obtain the lowest residual factors and optimum goodness of fit with convergence of refinement). Non-hydrogen atoms were refined anisotropically except the disordered perchlorate oxygens (O4/O4′) in **CP3** and the lattice water molecule (O2w) and the disordered perchlorate oxygens (O5/O5A and O6/O6A) in **CP4**. In the final difference Fourier maps there were no significant peaks >1 e $Å^{-3}$. All hydrogen atoms except for the water molecule (O2w) in the asymmetric unit of **CP4** were placed in ideal positions and refined as riding atoms with individual isotropic displacement parameters. ORTEP of **CP3** and **CP4** are shown in (Appendix-1 Figure A-26, A-27)

4.4 Results and discussion

4.4.1 Structural Description of CP3 and CP4

The geometry's of ligand **1b** in **CP3** and **CP4** gives insight into the flexiblity of the ligand to assemble according to the requirement of the other components in the CPs.

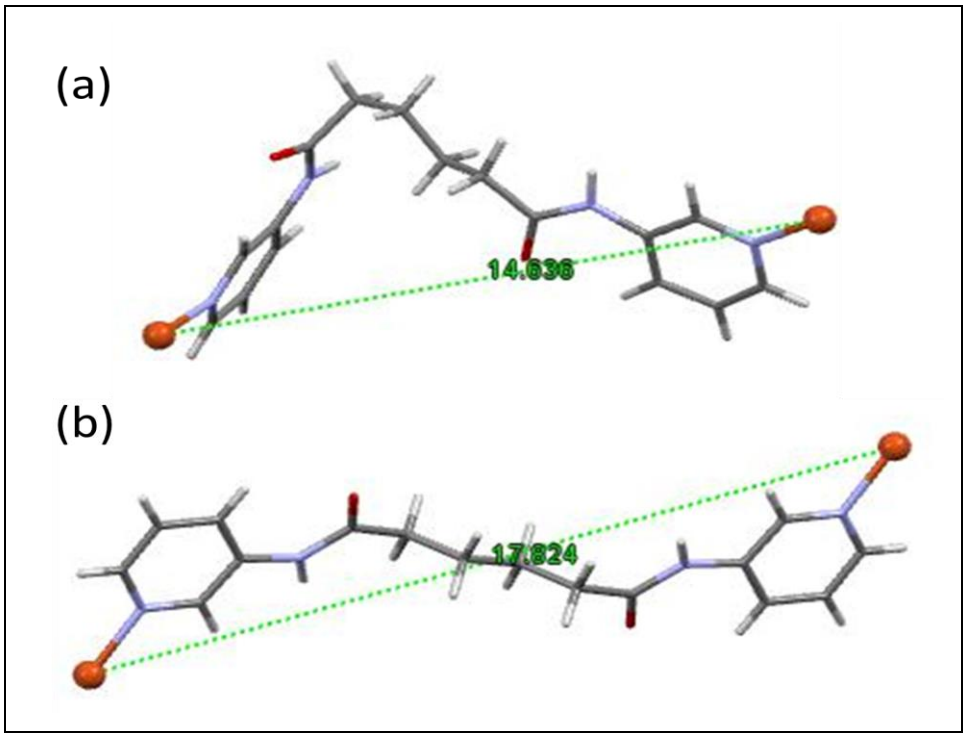

Figure 4.5: Geometry of ligand **1b** in (a) **CP3** and (b) **CP4**

The size of the metal centre is the determining factor in arranging the CPs. In **CP3**, two neighboring Cu(II) centers are separated by a distance of 14.831 Å, whereas in **CP4**, the

Cd(II) centers are separated by a distance of 17.955 Å. The flexibility of the butyl chain in **1b** resulted in changing the ligand length required for the Cu(II) and Cd(II) centre. In **CP3**, the butyl chain adopts *gauche–anti–gauche* conformation, whereas in **CP4**, it adopts an all *anti* conformation (Figure 4.5). This in turn affected the overall geometry of the CPs. In **CP4**, the ligand **1b** behaves as a longer "rigid" analogue of 3,3′-bipyridine. In **CP3**, the ligand **1b** adopts a wavy type of geometry with more of the hydrocarbon chain "clustered" in the spacer. The presence of two amide groups resulted in self-complementary amide-to-amide hydrogen bonds in both of the CPs, even in the presence of counter anions and free water molecules. Crystal structure analysis of **CP3** shows that it crystallizes in the orthorhombic space group $P2_12_12$.

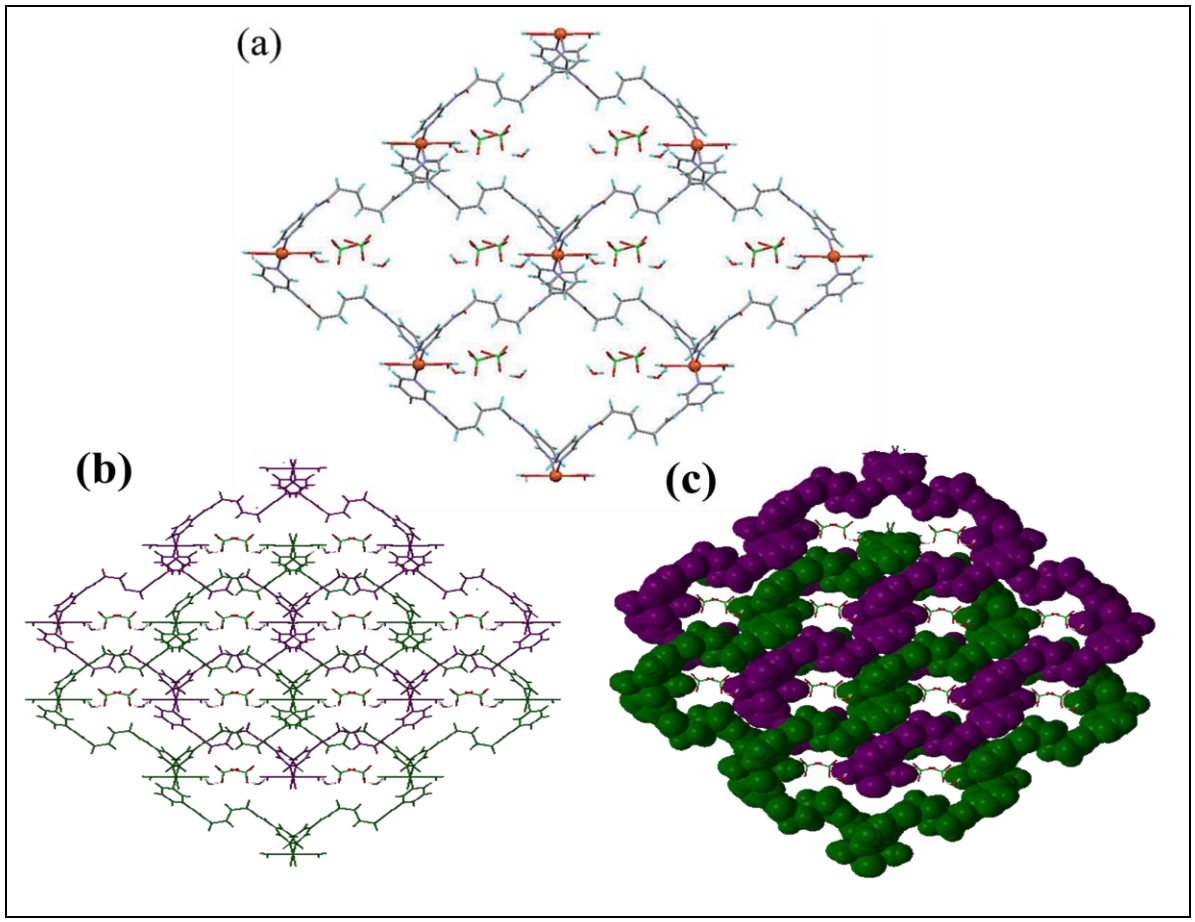

Figure 4.6 : The crystal structure of **CP3**; (a) part of the 2D-layer of (4,4) topology (C = grey; N = dark blue; O = red; Cu = brown; H = Sky blue; Cl = green)Two-fold parallel interpenetration of the layers; (b) ball and stick mode (c) space fill mode: one layer is shown in green colour and another shown in violet colour.

The Cu(II) centre adopts a distorted-octahedral geometry, in which the coordination environment of Cu(II) includes four molecules of **1b** in the equatorial position (Cu–N: 2.023

Å, 2.027 Å) and two H_2O molecules in the axial position (Cu–O: 2.480 Å). The wavy-shape of the ligand due to a *gauche–anti–gauche* conformation results in the formation of a highly corrugated 2D-network with (4,4) topology (Figure 4.6). The (4,4)-layers have rhomboidal-shaped cavities with diagonal-to-diagonal distances of 22.530 Å × 19.216 Å and the co-ordinated H_2O molecules point into the cavities. Two such (4,4)-layers interpenetrate in parallel mode (Figure 4.6).

The layers in **CP3** interact with each other *via* amide-to-amide hydrogen bonds. The hydrogen bond pattern in case of amide groups represents the synthon (Figure 4.7).

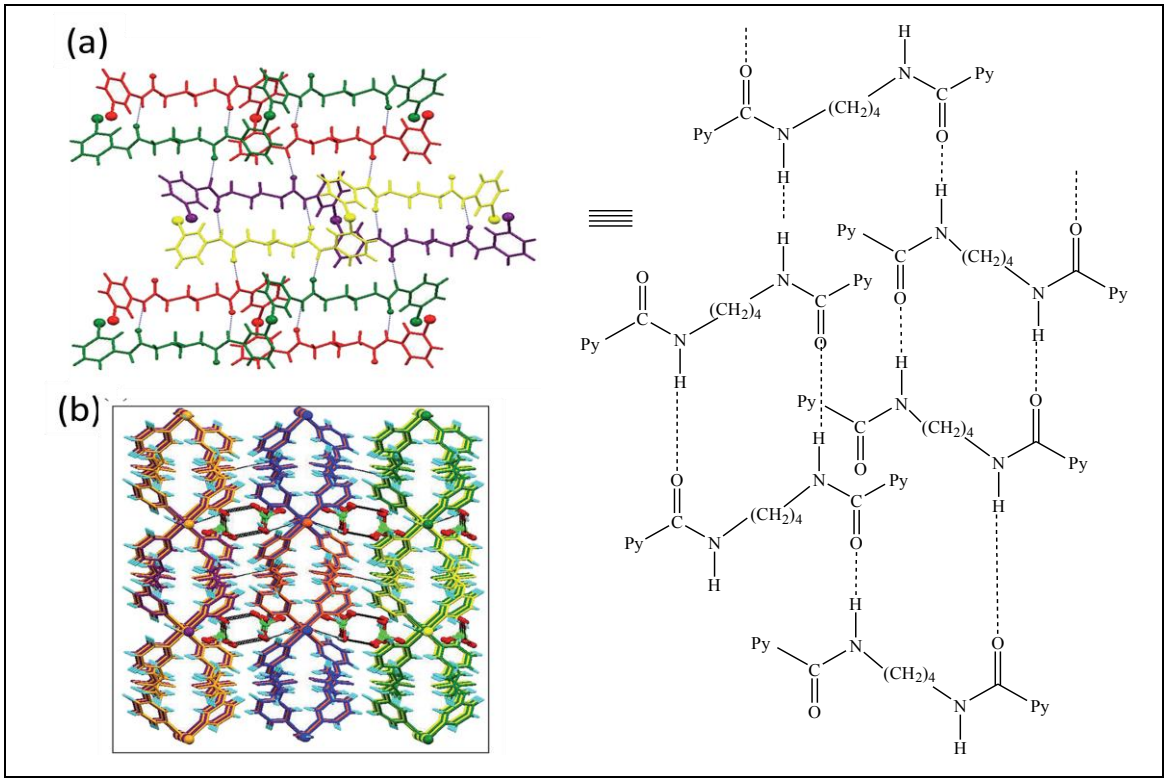

Figure 4.7: (a) Amide-to-amide hydrogen bonding pattern **(β-**Sheet + **(4,4)** - network); (b) side-view of the interpenetrated layers. (Each **(4,4)**-layer is shown in a different color; three pairs of interpenetrated layers)

Biradha *et al.* obtained a similar structure with a ligand, having reverse functional group than this ligand and $Cu(ClO_4)_2$, in which the amide-to-amide hydrogen bonds are present between the two interpenetrated layers. Note that the continuity of the amide hydrogen bonds throughout the network is hindered by water molecules and counter anions.[12] However, in **CP3**, the amide-to-amide hydrogen bond is present throughout the structure and is not affected by counter anions and H_2O molecules.

4.4.2 Looped 1D co-ordination network – the role of the metal centre

The effect of the metal centre on the geometry of the co-ordination polymers was studied by analyzing the structure of **CP4**, which crystallizes in the triclinic *P* T space group. The co-ordination environment of the Cd(II) centre includes four molecules of ligand **1b** in the equatorial sites and two H_2O molecules in the axial sites (Cd–N: 2.306 Å, 2.311 Å, 2.365 Å, 2.404 Å; Cd–O: 2.341 Å, 2.349 Å). The butyl chain spacer of **1b** adopts an *anti–anti–anti* conformation (Figure 4.5), which results in stretching the ligand **1b** to its maximum length; hence, the linear geometry of the ligand is seen.

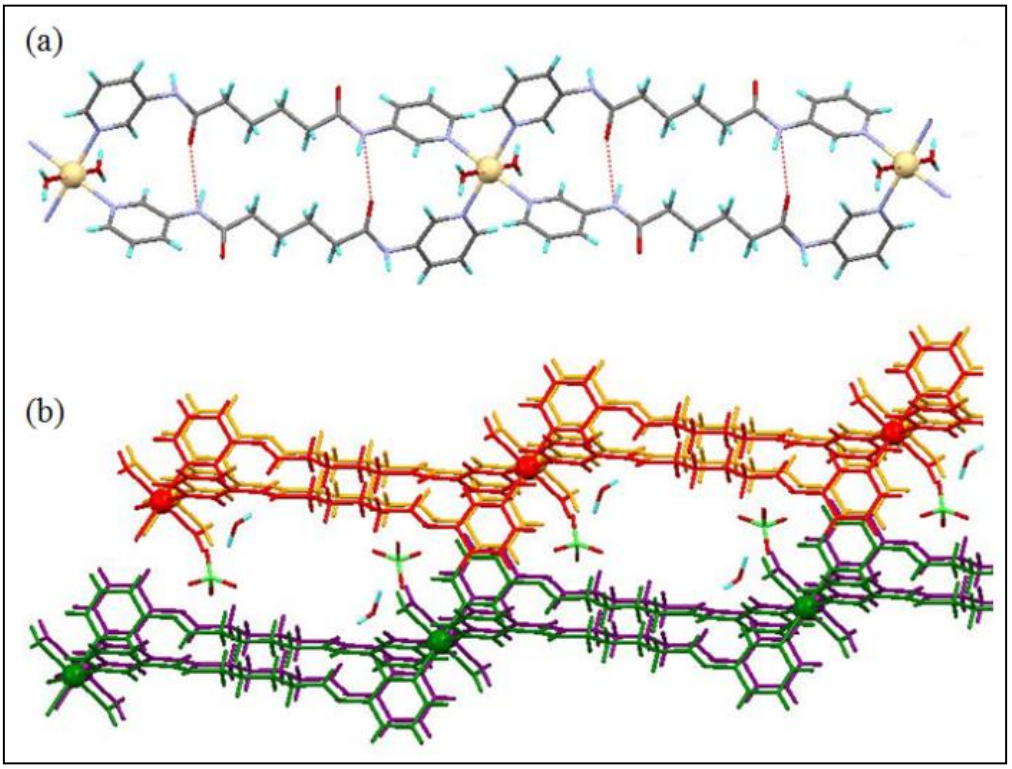

Figure 4.8 : The crystal structure of **CP4**; (a) part of the 1D-looped chain (C = grey; N = dark blue; O = red; Cd = brown; H = Sky blue; Cl = green); (b) packing of the 1D-chains *via* hydrogen bonding between the amide groups, water molecules and counter anions.

The geometry of the ligand in **CP4** is similar to that of cis-arranged 3,3′-bipyridine. The cis arranged 3,3′-bipyridine is reported to form 1D-chains with Zn(II), Co(II) and Ni(II), whereas with Hg(II), it forms a dinuclear macrocyclic structure.[13,14] The network formed in **CP4** can be described as a 1D-chain with rectangular loops. The longer length of ligand **1b** compared to that of 3,3′-bipyridine and the larger size of the Cd(II) centre resulted in generating the overall features of the reported structures (i.e. 1D looped chain). The rectangular loops in

CP4 have dimensions of 17.923 Å × 5.176 Å, in which the amide groups are involved in self-complementary hydrogen bonding. The adjacent chains are held together by the hydrogen bond interaction between the amide N–H and ClO_4^-, and between the amide C=O and H_2O (Figure 4.8). The π•••π interactions between the pyridyl groups are also responsible for holding the adjacent chains together. The 1D-looped chain with intra-chain amide-to-amide hydrogen bonds observed in the case of **CP4** is similar to the reported structures by Dastidar and co-workers, involving bis(3-pyridyl)terephthalamide with Cu(II) salts, in which the ligand has a "rigid" phenyl spacer in between the *bis*-pyridyl-*bis*-amide moieties.[15] This shows the ability of the "flexible" alkyl chain spacer of ligand **1b**, when involved in forming CPs with a larger metal center (i.e. Cd(II)), in mimicking the structural features obtained by a ligand involving a "rigid" phenyl spacer.

4.4.3 Transmetallation studies on the CPs

The response of the flexible spacer of ligand **1b** during the formation of CPs upon changing the metal centre has further prompted us to study their post-synthetic transformations. Transmetallation studies were performed on **CP3** and **CP4** to analyze whether the flexibility of the spacer will be able to change the geometry of the CPs upon changing the metal centre or the robustness of the precursor CP will not allow any modification on the skeletal structure during metal metathesis.

Figure 4.9: Crystal morphology of **CP4** on transmetallation reaction with Cu(II).

The transmetallation study on **CP4** with $Cu(ClO_4)_2$ showed complete exchange of the Cd(II) centre with Cu(II). The crystal color changed rapidly from white to blue, while the crystal morphology remained the same throughout the ion exchange process (Figure 4.9). The powder X-ray diffraction (PXRD) pattern of the resulting **CP5** is similar to that of the parent compound **CP4** (Figure 4.10). The kinetics of this transmetallation was studied with Atomic

Absorption Spectroscopy (AAS). The results further supported with Wavelength Dispersive X-Ray Fluorescence Spectroscopy (WD-XRF) Study.

4.4.4 Powder XRD

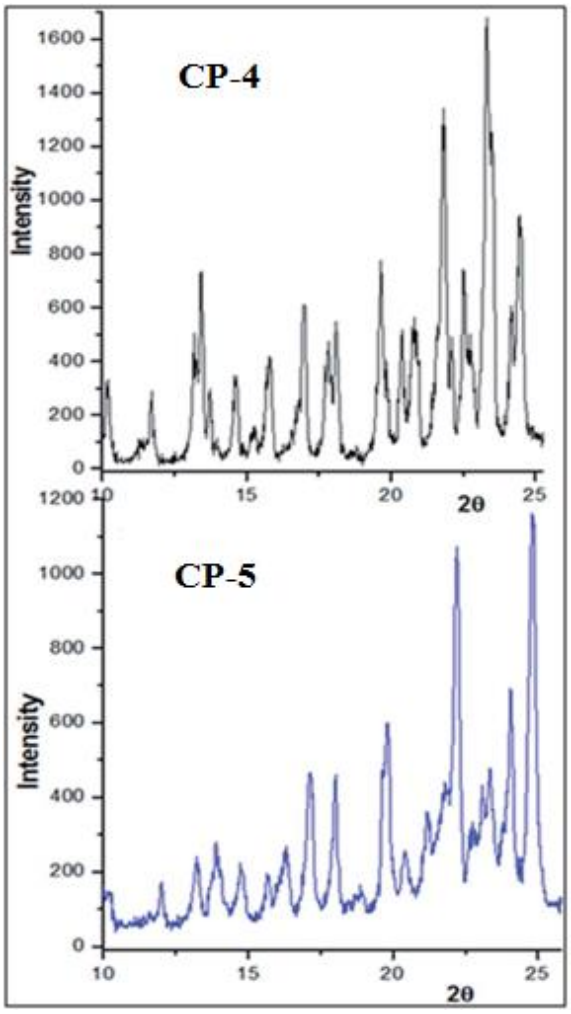

Figure 4.10: Powder X-ray diffraction profiles for the parent (**CP4**) and ion exchanged material (**CP5**) demonstrating the maintenance of the framework integrity.

The powder XRD patterns of the CPs were analyzed along with the calculated powder XRD of **CP3** and **CP4** and the similarities in both experimental and calculated supported our results. The powder XRD patterns of **CP3** and **CP5** were different. Thus structural difference of **CP3** and **CP5** is evident from these analyses. The powder XRD reflects the similarity in the structures of **CP4** and **CP5**. Therefore, we can relate that the structure of **CP5** is isomorphous to that of **CP4**. The direct reaction of ligand **1b** with that of $Cu(ClO_4)_2$ always resulted in the formation of **CP3**. The synthesis of **CP5** is only possible using the transmetallation technique.

4.4.5 Atomic Absorption Spectroscopy (AAS) Study

The kinetics of transmetallation, the ion exchange process of Cd(II) by Cu(II) was monitored by Atomic Absorption Spectroscopy (AAS). For AAS technique standard solutions of both metals copper and cadmium required. The standard solutions of cadmium were prepared with $3CdSO_4.8H_2O$ having molecular weight 769.52 gm, 337.23 gm of Cd present per mole of salt. Three standard solutions were used 0.5, 1.0, 1.5 ppm, prepared by dissolving 0.00141, 0.00282, 0.00423gm of $3CdSO_4.8H_2O$ salt for 10 ml of each solution. Five standard solutions of copper 1, 2, 3, 4, 5 ppm were prepared by dissolving 0.00380, 0.00760, 0.01440, 0.01520, 0.01900 gm of $Cu(NO_3)_2.3H_2O$ respectively for each 10 ml of the solution. The salt $Cu(NO_3)_2.3H_2O$ have molecular weight 241.6 gm, 63.5 gm of Cu present per mole of the salt. For metal metathesis, 9.4341 ≈ 9.5 gm of co-ordination polymer of **CP4** was taken and 100 ml of 0.5 M $Cu(ClO_4)_2.6H_2O$ solution poured over it. After different intervals of time, took out small amount of solid sample from it and quenched the reaction. Washed this solid with ethanol 3-4 times, untill whole surface deposited Cu removed and dried it. Took 0.001gm of this dry powder, digested it with conc. nitric acid (few drops), adding water made volume 10 ml. This is sample for AAS, directly measured the amount of Cu and Cd in ppm. Initially 0.001 gm of the **CP4** taken, the ppm value from AAS was considered as 100% Cd. Nearly 50% of the framework Cd^{2+} ions were replaced by Cu^{2+} within 1 hour, and 99% of the Cd^{2+} ions were exchanged by Cu^{2+} within 7 hours (Figure 4.11).

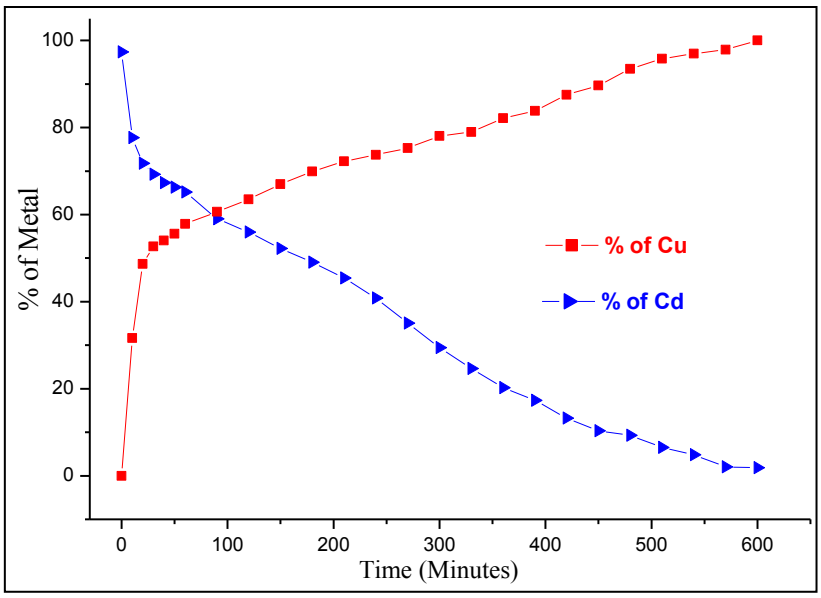

Figure 4.11: Kinetic profile of framework metal ion exchange of Cd(II) with Cu(II) from AAS.

Similar transmetallation study on **CP3** and **CP5** with $Cd(ClO_4)_2$ was also performed by our group. For that we took around 10 gm of **CP3** and **CP5** separately and 40 ml of 0.5M $Cd(ClO_4)_2$ solution poured over it. The transmetallation process was very slow; moreover, negligible exchange was observed even after three months.

4.4.6 Wavelength Dispersive X-Ray Fluorescence Spectroscopy (WD-XRF) Study

For Wavelength Dispersive X-Ray Fluorescence Spectroscopy (WD-XRF) 5 - 10 mg of the solid sample in fine powdered form required. Thus during transmetallation we collected solid sample at different intervals of time, washed with ethanol to remove surface deposited metals and powdered it. The powered samples were then analyzed with WD-XRF. We know that in WD-XRF the Cu metal shows it's peaks; Cu $K_{\alpha 1}$ at 8.047 keV and Cu $K_{\beta 1}$ at 8.904 keV and Cd at 23.047 keV.

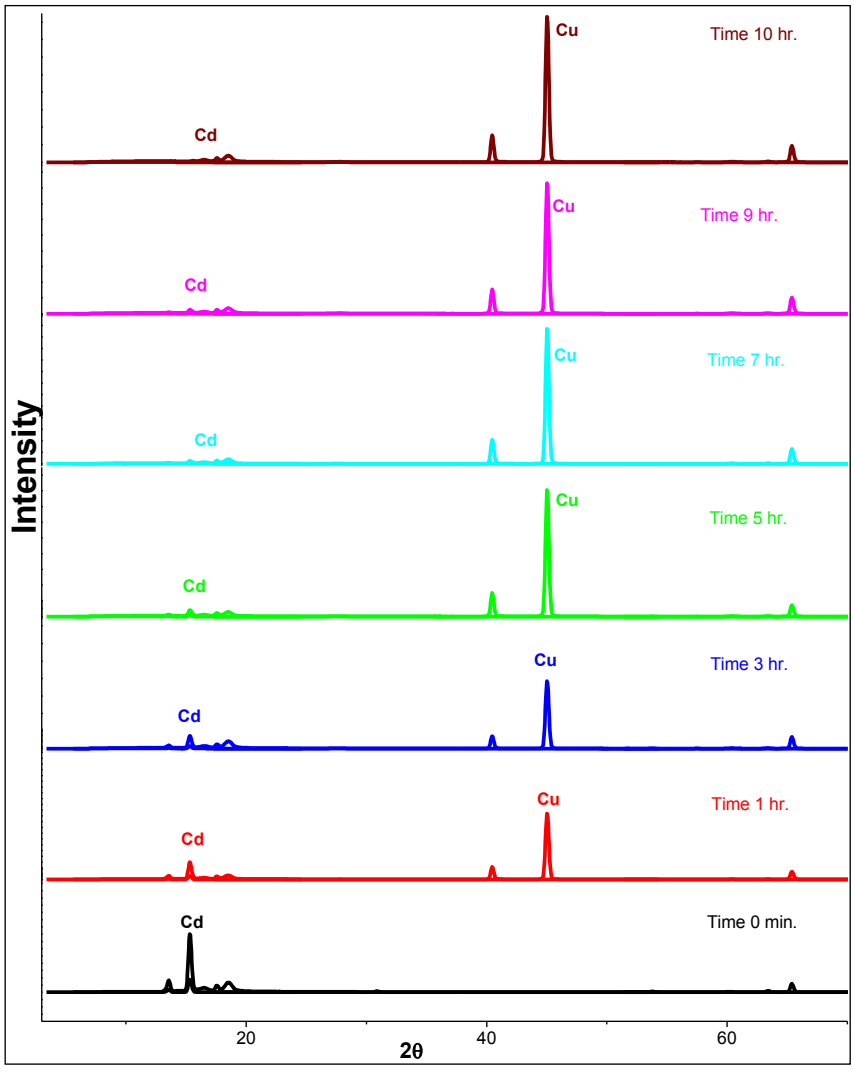

Figure 4.12: WD-XRF of the Transmetallation Reaction at various intervals (**Intensity *vs* 2θ**)

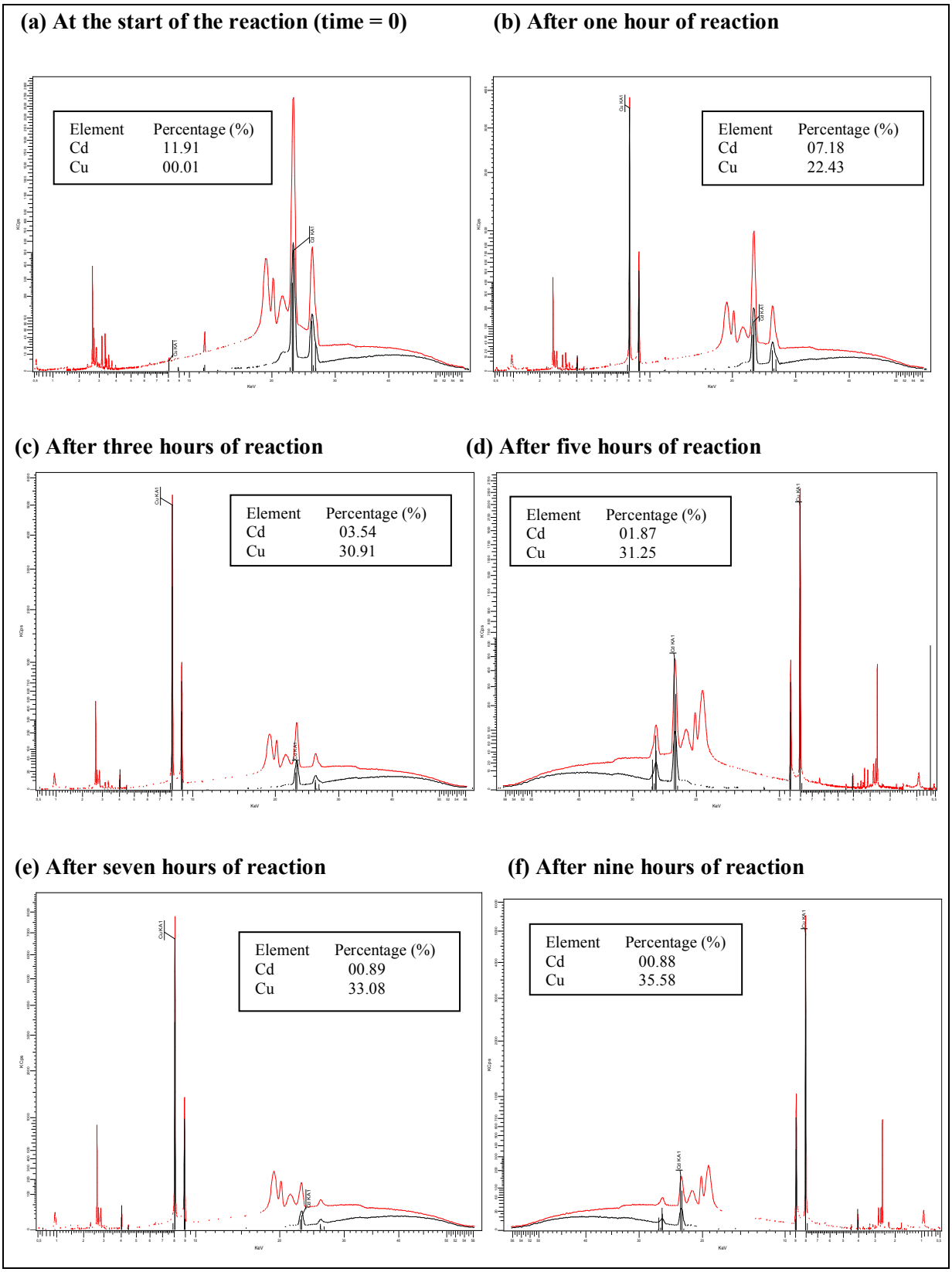

Figure 4.13: WD-XRF (Intensity *vs* Binding Energy) of the Transmetallation Reaction at various intervals [**CP4 → CP5**]

Then data's collected from WD-XRF and plotted graphs using these. Both the graphs were plotted Intensity *vs* 2θ (Figure 4.12) & Intensity *vs* binding energy (Figure 4.13), further used for quantitative estimation of Copper and Cadmium metals. Figure 4.12 (graph intensity *vs* 2θ) showed that the intensity of Cu peak increases with time while intensity the peak corresponding to Cd decreases during metal metathesis. The wavelength dispersive X-ray fluorescence (WD-XRF) shows nearly complete replacement of the framework Cd (II) ions of **CP4** with Cu(II) ions and formation of co-ordination polymer **CP5**. Both **CP4** and **CP5** have similar powder XRD pattern; proved the structure integrity only the metal ion replaced. The calculated % for both Cu(II) and Cd(II) by WD-XRF exactly matches with the % displayed by AAS study. Both WD-XRF and AAS results showed nearly whole (≈ 100%) Cd(II) exchanged with Cu(II) in case of **CP4**. But the transmetallation was irreversible in nature, exchange for **CP3** and **CP5** with $Cd(ClO_4)_2$ was negligible (≈ 0%).

4.5 Conclusions

The metal centre was shown to play an important role in assembling the components during the formation of CPs: the size of the Cu(II) and Cd(II) centre being one of the major deciding factor in adjusting the conformation of the butyl spacer of the ligand. Transmetallation studies have shown us that despite having a flexible framework, the metal exchange reaction proceeded without changing the structure of the CPs. This may be attributed to the fact that the looped-chain of **CP4** has N–H•••O hydrogen bonds within the loops, which made the network robust. Furthermore, the CP synthesized *via* postsynthetic metal exchange could not be obtained from a direct reaction of the metal centre and ligand. A framework-templating strategy was used to synthesize **CP5**. During transmetallation reaction of **CP4** with Cu(II), the CP acted as a template and pre assembled the ligands.

4.6 References:

[1] Wells, A. F. *Three-dimensional Nets and Polyhedra*, Wiley-Interscience, New York, **1977**.

[2] Lalonde, M.; Bury, W.; Karagiaridi, O.; Brown, Z.; Hupp, J. T.; Farha, O. K. *J. Mater. Chem. A* **2013**, *1* (18), 5453-5468.

[3] Yamada, T.; Kitagawa, H. *J. Am. Chem. Soc. Society* **2009**, *131* (18), 6312-6313.

[4] Song, X.; Jeong, S.; Kim, D.; Lah, M. S. *CrystEngComm* **2012**, *14* (18), 5753-5756.

[5] Irving, H.; Williams, R. J. P. *J. Am. Chem. Soc.* **1953**, (0), 3192-3210.

[6] Yao, Q.; Sun, J.; Li, K.; Su, J.; Peskov, M. V.; Zou, X. *Dalton Trans.* **2012**, *41* (14), 3953-3955.

[7] Song, X.; Kim, T. K.; Kim, H.; Kim, D.; Jeong, S.; Moon, H. R.; Lah, M. S. *Chem. Mater.* **2012**, *24* (15), 3065-3073.

[8] Mukherjee, G.; Biradha, K. *Chem. Commun.* **2012**, *48* (36), 4293-4295.

[9] Rajput, L.; Singha, S.; Biradha, K. *Cryst. Growth Des.* **2007**, *7* (12), 2788-2795.

[10] *CrysAlis PRO (oxford Diffraction),* Oxford Diffraction Ltd., Yarton, Oxfordshire, England, **2010**.

[11] Sheldrick, G. *Acta. Crystallogr. Sect. A* **2008,** *64* (1), 112-122.

[12] Sarkar, M.; Biradha, K. *Cryst. Growth Des.* **2007,** *7* (7), 1318-1331.

[13] LaDuca, R. L.; Desciak, M. P.; Rarig, R. S.; Zubieta, J. A. *Z. Anorg. Allg. Chem.* **2006**, *632* (3), 449-453.

[14] Khutia, A.; Sanz Miguel, P. J.; Lippert, B., *Bioinorg. Chem. Appl.* **2010**, *2010*.

[15] Adarsh, N. N.; Kumar, D. K.; Suresh, E.; Dastidar, P., *Inorg. Chim. Acta.* **2010**, *363*(7), 1367-1376.

Chapter 5

Role of Anions in Tailoring Co-ordination Polymers (CPs)

5.1 Introduction

In the previous chapter 4, we have discussed the effect of metal ion on geometry of co-ordination polymers (CPs) of ligand **1b**. The ligand flexibility allowed to change a 2D-interpenetrated network of Cu(II) to 1D-looped chain network of Cd(II) on requirement of the metal centre. The combined effect of the anion exchange and guest inclusion in co-ordination polymers of Cu(II) and ligand **1a** was discussed in chapter 3. Thus, it was observed that the geometry of coordination networks depended on several factors such as coordination environment of the metal centre, metal-to-ligand ratio, nature and the geometry of the ligands and the presence of solvents (guest molecule) and counter anions. Among all these factors, the role of counter anions is important as they have different shape, size and hydrogen bonding ability and coordinating ability.

In this chapter, we will discuss the effect of counter anions on the co-ordination polymers of Cu(II) with ligand **1b**. Ligand **1b** with $Cu(ClO_4)_2$ formed a 2D network having two-fold parallel interpenetration (**CP3**), with $Cu(SO_4)_2$ formed a 1D network with rectangular loops (**CP6**) and with $Cu(C_6H_5COO)_2$ resulted in a 1D chain (**CP7**). Three counter anions - ClO_4^-, SO_4^{2-}, $C_6H_5COO^-$ were chosen in the present study; ClO_4^- and SO_4^{2-} has tetrahedral geometry, but the differences lie in the charge, size and coordinating ability with the metal centre. The benzoate anion, on the other hand, with its larger size and carboxylate group can bind *via* different co-ordinating modes with the metal centre and may also participate in the framework of the CP.

In order to understand the role of anions on the network stability, the anion exchange reactions were performed. Further the reverse exchange reactions of the CPs also performed in order to check the reversibility of the exchange reactions. The reactivity of the counter anions (ClO_4^-, SO_4^{2-} and $C_6H_5COO^-$) towards the formation of the CPs was monitored through the competitive reactions, where the ligand was allowed to react with $Cu(NO_3)_2$ in the presence of all the three counter anions in one pot. Thus in this chapter, the extent of the structural changes in the network due to the nature of the anions is studied by analyzing the following features:-

(i) Effect of counter anions of same geometry (tetrahedral) but different size and charge, in the overall supramolecular structure of the CP.

(ii) Differences between weakly/non-coordinating anions and carboxylate anions, which is involved in the framework geometry; in terms of ease of formation of CP.

(iii) The structural transformation in response to anion exchange reactions.

There are large numbers of reports on anion templating of Co-ordination Polymers, where the counter anions of the CPs either acted as void filling species or co-ordinated to the metal centre in a mono-dentate or bi-dentate fashion and may or may not involve in the propagation of the network. Adonis & Stavroula converted the neutral 3D microporous Co-ordination Polymers of adipate ($^{-}OOC-(CH_2)_4-COO^{-}$) and Lanthanide (Pr^{3+}, Gd^{3+}, Sm^{3+}) to the ionic 1D polymer, where the anions NO_3^- or Cl^- acted as templates. The strong hydrogen bonding pattern between positively charged 1D lanthanide-adipate chains allowed the single-crystal-to-single-crystal transformation during the exchange of NO_3^- for Cl^- and *vice versa*.[1]

Honghan Fei *et al.* reported cationic metal–organic materials of Co(II) and Zn(II) with 4,4′-bipyridine where 1,2-ethanedisulfonate anion (EDS^{-2}) acted as template and non-covalently interacted with the cationic layers. This weak interaction encourage the anion exchange reaction with toxic oxo-metal anions (*i e.* CrO_4^{-2}, SeO_3^{2-}, AsO_4^{-3} *etc.*), it was observed that the toxic CrO_4^{-2} was trapped selectively when non-toxic anions (*e.g.,* NO_3^-, SO_4^{-2}) were present along with chromate.[2] Fang *et al.* synthesized 1D nano-sized metal–organic tubes of Ag(I) with multifunctional double-Schiff-base ligand (N,N'-Bis-(4-pyridin-4-yl-benzylidene)-ethane-1,2-diamine) incorporated with anion PF_6^-. Further they exchanged the anion PF_6^- with ClO_4^- & SbF_6^- and observed that emission intensity decreased when PF_6^- gradually replaced by ClO_4^- or SbF_6^-.[3] Shucong Ma *et al.* studied binding affinities of different anions [BF_4^-, ClO_4^-, PF_6^- and *bis*-(trifluoromethane)sulfonamide (NTf_2)] into a cationic tetrahedral Fe(II) cage; metal-organic framework of Fe(II) with di-Schiff-base ligand.[4] Dastidar *et al.* synthesized co-ordination polymers of $ZnSO_4.7H_2O$ with *N,N′*-bis(3-pyridyl)-p-phenylenebis-urea and N,N′-bis(3-pyridyl)terephthalamide under identical reaction conditions; crystallized in 2D - 2D Borromean entanglement involving 3-fold (6,3) honeycomb layers and 2D-corrugated sheet, respectively. They separated anion SO_4^{-2} from a mixture of Zn(II) salts having mixture of various counter anions such as sulfate, nitrate, perchlorate and triflate under competitive and non-competitive condition.[5]

The meta-position of pyridyl-N atom and the butyl spacer makes the ligand **1b** more flexible, a slight variation in any of the component of CP may results a wide-ranging structural

transformation. Thus collective effect of ligating topology, flexible aliphatic spacer, amide backbone and counter anions resulted in frameworks intriguing geometry and interesting properties. The conformational adjustments of the butyl spacer of the ligand **1b** in the CPs according to the requirements of the counter anions are observed in the present study. *N,N′*-(butane-1,4-diyl)dinicotinamide having more flexibility due to meta position of pyridyl-N, on reaction with $Cu(ClO_4)_2$ form 2D layer of (4,4)-topology with ClO_4^- and H_2O in the rhomboidal cavities, having parallel interpenetrated *via* β-sheet hydrogen bonding. An identical network obtained with $Cu(NO_3)_2$ but with $Cu(PF_6)_2$ an open 2D- network of (4,4)-topology with rhomboidal cavities having PF_6^- and H_2O packed *via* α-sheet hydrogen bonding pattern.[6] The anion exchange represents the greater template effect of the PF_6^- anion compared to that of the ClO_4^-, may be understood given the fact that the N-H•••F hydrogen bond is stronger than the N-H•••O hydrogen bond.

Lalit *et al.* also reported Cu(II) co-ordination polymers of ligand *N,N′*-bis(4-pyridyl)suberamide in presence of anions SO_4^{-2}, SiF_6^{-2}, NO_3^-.[7] Cheng *et al.* synthesized ten Ag(I) complexes of ligand **1b** with different anions (ClO_4^-, BF_4^-, NO_3^-, PF_6^-, $CF_3SO_3^-$, p-TsO^- *i.e* p-toluenesulfonate) using different solvents- DMF, methanol, acetonitrile etc.[8] On using acetonitrile solvent the octahedral PF_6^- anion form 1D concavo-convex chain whereas tetrahedral BF_4^- and ClO_4^- anions and the triangular NO_3^- anions form 1D polymeric pairs of zigzag chains, supported by weak Ag•••Ag and π•••π stacking interactions. Ligand **1b** with $AgClO_4$ and acetonitrile solvent, 1D polymeric pair involving acetonitrile obtained however in methanol 1D zig-zag chain produced, undergo reversible single-crystal to single-crystal transformation on removal and uptake of acetonitrile.

The butyl spacer has AAA (*anti-anti-anti*) confirmation in both networks only difference is in orientations of two pyridyl-N - *syn-syn* and *anti-anti* confirmation respectively. Ag(p-TsO) and ligand 1b in CH_3CN solvent form zero-dimensional (0D) dinuclear metallocycle which undergo irreversible SCSC transformation on removal of acetonitrile resulted a two-dimensional (2D) pleated grid with a $\{4,8^2\}$ topology. The networks are same in orientations of two pyridyl-N atoms - *anti-anti* but differ by the butyl confirmation, having AGG (*anti-gauche-gauche*) and AGA (*anti-gauche-anti*) respectively. Finally the authors concluded that flexibility of the ligand **1b,** nature of counter anion and solvent were essential in determining the structural type of any network and the structural transformations were accompanied by

the changes in the conformation of ligand **1b**, which in turn adopted the conformation that maximize the intra- and intermolecular forces.

5.2 Experimental Section

5.2.1 Synthesis of CP6, $\{[Cu(1b)_2(SO_4)]\bullet 3(H_2O)\}_n$

The ligand **1b** (596 mg, 2.0 mmol) dissolved in 20 ml of 1:1 mixture of water-ethanol was layered over a 10 ml aqueous solution of copper sulphate (370.1 mg, 1.0 mmol). Blue-colored crystals were formed after 8-10 days in 85% yield. Anal. Calcd (%) for $C_{32}H_{42}CuN_8O_{11}S$: C, 47.43 %; H, 5.22 %; N 13.83 % Found: C, 47.360 %; H, 5.325 %; N, 13.652 % FT-IR (KBr, cm^{-1}): 3964(w).3928(m), 3903(m), 3842(s), 3811(w), 3744(s), 3611(m), 3270(w), 3232(vs), 3868(m), 3147(w), 3085(vs), 2970(w), 1705(s), 1612(w), 1558(vs), 1489(s), 1427(w), 1373(w), 1296(s), 1242(w), 1134(vs), 1033(s), 964(w), 802(m), 694(w), 648(w), 624(w) (Appendix-1 Figure 28). PXRD pattern of the co-ordination polymer **CP6** was shown in (Appendix-1 Figure A29)

5.2.2 Synthesis of CP7, $\{[Cu(1b)(C_6H_5COO)_2]\}_n$

To the ligand **1b** (596 mg, 2.0 mmol) dissolved in 15 ml of 1:1 mixture of water-ethanol, 5 ml aqueous potassium benzoate was added. Then 10 ml ethanolic solution of $Cu(NO_3)_2.3H_2O$ (241.6 mg, 1.0 mmol) was layered over it slowly. Blue-colored crystals were formed after one week in 60% yield. Anal. Calcd (%)for $C_{30}H_{28}CuN_4O_6$: C, 59.64; H, 4.67; N 9.27 Found: C, 59.003; H, 4.881; N, 9.593 (Figure S6) FTIR (KBr, cm^{-1}): 3302(w), 3256(m), 3186(s), 3132(s), 3074(vs), 2947(s), 2860(s), 2538(m), 1967(m), 1921(m), 1867(w), 1821(w), 1697(vs), 1597(s), 1551(vs), 1485(s), 1404(vs), 1311(s), 1242(s), 1203(s), 1117(vs), 1065(s), 1018(w), 933(s), 849(s), 810(s), 764(s), 717(s), 668(s), 555(s) (Appendix-1 Figure 30). PXRD pattern of the co-ordination polymer **CP7** was shown in (Appendix-1 Figure 31)

5.2.3 Anion Exchange Reactions of CP6 with ClO_4^-

The anion exchange reaction was performed by keeping (810.34 mg, 1 mmol) of crystalline **CP6** in an aqueous solution of $NaClO_4$ (140.46 mg, 10 mmol). and resulted sample characterized by FT-IR and PXRD. FT-IR: 3564 (s), 3278 (s), 3201 (w), 3101 (w), 2931 (w), 2862 (w), 1674 (s), 1612 (w), 1589 (w), 1550 (vs), 1488 (m), 1427 (s), 1365 (w), 1296 (m), 1242 (w), 1195 (w), 1103 (vs), 956 (w), 918 (w), 810 (m), 702 (m), 624 (m), 555 (w)

(Appendix A-1 Figure 32). After anion exchange reactions PXRD pattern of the co-ordination polymer **CP6** was shown in (Appendix-1 Figure 33)

5.2.4 Anion Exchange Reactions of CP6 with $C_6H_5COO^-$

The procedure is similar to that of above. The crystalline **CP6** (810.34 mg, 1 mmol), was taken for the reaction and kept in aqueous solution of potassium benzoate (160.21 mg, 10 mmol). The resulted powder was characterized by FT-IR and PXRD. IR: 3302(w), 3256(m), 3186(s), 3132(s), 3074(vs), 2947(s), 2860(s), 2538(m), 1967(m), 1921(m), 1867(w), 1821(w), 1697(vs), 1597(s), 1551(vs), 1485(s), 1404(vs), 1311(s), 1242(s), 1203(s), 1117(vs), 1065(s), 1018(w), 933(s), 849(s), 810(s), 764(s), 717(s), 686(s),617(w), 555(s) (Appendix A-1 Figure 34). After anion exchange reactions PXRD pattern of the co-ordination polymer **CP6** was shown in (Appendix-1 Figure 35)

5.2.6 Competitive Reactions

The ligand **1b** (0.5 mmol) was allowed to react with $Cu(NO_3)_2$ (0.25 mmol) in the presence of different ratios of $NaClO_4$, Na_2SO_4, and C_6H_5COOK, condition I to VIII. After 10-15 days, the resulted crystals were characterised by FT-IR and PXRD for each every condition. The FT-IR and PXRD pattern for condition IV were shown in Appendix-1 Figure 36 and Appendix-1 Figure 37.

5.3 Single Crystal X-ray Diffraction

Initial crystal evaluation and data collection were performed on a Kappa APEX II diffractometer equipped with a CCD detector (with the crystal-to-detector distance fixed at 60 mm) and sealed-tube monochromated MoKα radiation using the program APEX2.[21] By using the program SAINT[21] for the integration of the data, reflection profiles were fitted, and values of F^2 and $\sigma(F^2)$ for each reflection were obtained. Data were also corrected for Lorentz and polarization effects. The subroutine XPREP[1] was used for the processing of data that included determination of space group, application of an absorption correction (SADABS)[21], merging of data, and generation of files necessary for solution and refinement. The crystal structures were solved and refined using SHELX 97.[22] In each case, the space group was chosen based on systematic absences and confirmed by the successful refinement of the structure. For **CP6**, attempts to solve it in higher symmetry system were not successful. Positions of most of the non-hydrogen atoms were obtained from a direct methods solution.

Several full-matrix least-squares/difference Fourier cycles were performed, locating the remainder of the non-hydrogen atoms.

Table 5.1: Crystal structure data of co-ordination polymers **CP6** & **CP7**

CP	CP6	CP7
Empirical formula	$C_{32}H_{42}CuN_8O_{11}S$	$C_{30}H_{28}CuN_4O_6$
Formula Wt.	810.34	604.1
Temperature (K)	100(2)	296(2)
Wavelength (Å)	0.71073	0.71073
Crystal system	Monoclinic	Monoclinic
Space group	$P2_1/c$	$P2_1/n$
a(Å)	17.2590(12)	13.3810(10)
b(Å)	11.5261(9)	5.8873(5)
c(Å)	18.0883(14)	18.7769(18)
α (°)	90	90
β (°)	90.438(4)	100.016
γ (°)	90	90
Volume ($Å^3$)	3597.6(5)	1456.7(2)
Z	4	2
Density (g/cm^3)	1.496	1.377
Absorption coefficient (mm^{-1})	0.736	0.799
Theta(°) range for data collection	1.18 to 25.05°	1.73 to 25.01°
F(000)	1692	626
Reflections collected	26847	8246
Independent reflections	6330	2563
Reflection with $I > 2\sigma(I)$	5603	1678
R_{int}	0.0413	0.0616
No. of parameters refined	484	187
Goodness-of-fit on F^2	1.19	1.012
Final R1/wR2 (with $I > 2\sigma(I)$)	0.1294/0.2965	0.0529/0.1122
Weighted R1/wR2 (all data)	0.1361/0.2992	0.0944/0.1298
Largest diff. peak and hole ($eÅ^{-3}$)	1.845 and -1.137	0.428 and -0.456

Data were collected for **CP6** at 298 K as well. The results presented here for **CP6** at 100 K are the best out these two sets. Although the highest residual electron density is close to one

oxygen atoms (O6) of the sulphate group which has very similar thermal parameters compared to other oxygen atoms, an attempt to consider any disorder of did not provide any improvement in the structure. All non-hydrogen atoms were refined with anisotropic displacement parameters. All hydrogen atoms were placed in ideal positions and refined as riding atoms with individual isotropic displacement parameters. The crystal data and structure refinement parameters of co-ordination polymers **CP6** and **CP7** summarized in Table 5.1.(CCDC 1478590 and 1478591)

5.4 Results and Discussion

5.4.1 Structural Description of the Co-ordination Polymers

The crystal structure analysis of **CP3**, **CP6, CP7** was done in terms of the type of the counter anion involved, effect of structure and hydrogen bonding ability of the counter anions on the geometry of the ligand and finally how the hydrogen bonding ability and the presence of the amide group in the ligand is affecting the overall geometry of the CPs.

5.4.2 Structural features of CP3

The co-ordination polymer **CP3**, showed a two-dimensional network of (4,4)-topology and have two-fold parallel interpenetration, discussed in chapter 4. The Cu(II) centre in **CP3** has a distorted-octahedral geometry with four units of ligand **1b** occupying the equatorial positions and two H_2O molecules occupying the axial positions (Cu-O: 2.480Å). The butyl chain of the ligands in **CP3** adopted *gauche-anti-gauche* conformation which finally resulted in the formation of a highly corrugated 2D-network with (4,4) topology (Figure 5.1).

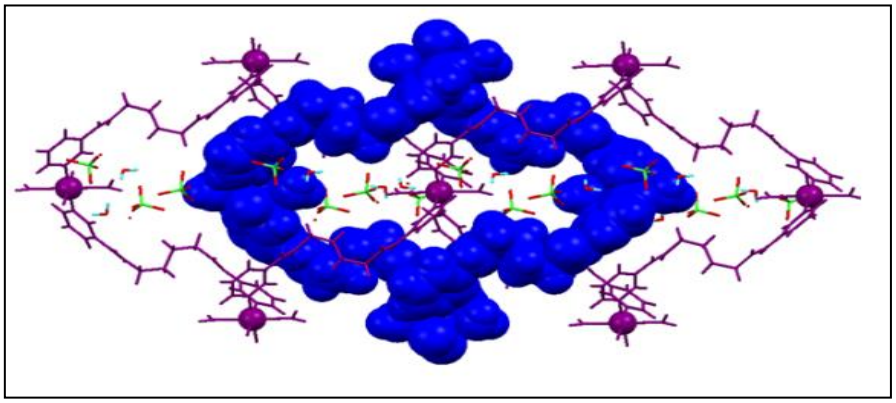

Figure 5.1: Illustrations of the crystal structure of **CP3**: 2D layer of (4,4) topology having two-fold parallel interpenetration (Blue layer interpenetrated with violet layers); Notice the ClO_4^- anions are present in rhomboidal cavity, atoms colour (Cl in green and O in red colour).

The (4,4)-network has rhomboidal-shaped cavities with diagonal-to-diagonal distances of 22.530Å × 19.216Å. The layers in **CP3** have shown a two-fold parallel interpenetration and ligands interact with each other *via* amide-to-amide hydrogen bonds which are present throughout the structure and are not interfered by counter anions and H_2O molecules as discussed in chapter 4.

5.4.3 Structural features of CP6

CP6 has crystallized in monoclinic $P2_1/c$ space group. The crystal structure analysis showed that the Cu(II) center in **CP6** forms a distorted square pyramidal geometry, where four units of the ligand **1b** form the base while the SO_4^{2-} occupy the apical position (Cu-N: 2.058 Å, 2.042 Å, 2.027 Å, 2.036 Å; Cu-O: 2.156 Å) (Figure 5.2). To accommodate the steric requirements of the co-ordinated SO_4^{2-}, the ligand **1b** adopts an arc-like geometry where the butyl chain conformation becomes *anti-anti-gauche*. The four ligand **1b** units connected to the Cu(II) centre and forms upward arc and downward arc, alternately. This results in the formation of a 1D looped chain. The looped chains have rectangular cavities with dimension of 12.848 Å × 4.285 Å (Figure 5.3). It is interesting to observe that within the loops, the two C=O groups of different ligand units are arranged in anti parallel manner with centroid-to-centroid distance of 3.471Å (Figure 5.2).

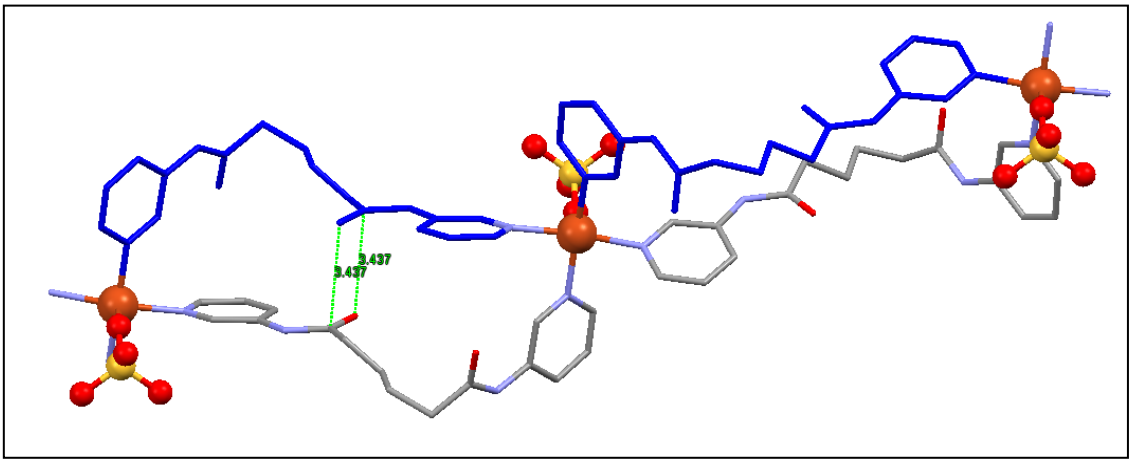

Figure 5.2: Illustrations of the crystal structure of **CP6**: 1D chain, notice the distorted square pyramidal geometry of Cu(II) centre with four units of ligand **1** and one SO_4^{2-} and parallel positioning of C=O within the loop.

The 1D looped chains are arranged in an offset fashion *via* aromatic π•••π interactions (centroid-to-centroid distance of 3.668 Å) and N-H•••O(SO_3^{2-}) (1.954Å, 2.820Å, 167.65º)

hydrogen bonding interactions to form layers (Figure 5.3(a)). Each 2D layers are further stacked upon one another *via* H-bond between SO_4^{2-}, NH, CO and H_2O to extend the network in 3D (Figure 5.3(b)). The 2D layers stack over one another (in an ABAB….. manner) and the adjacent planes are oriented at an angle of 53.71° (Figure 5.4).

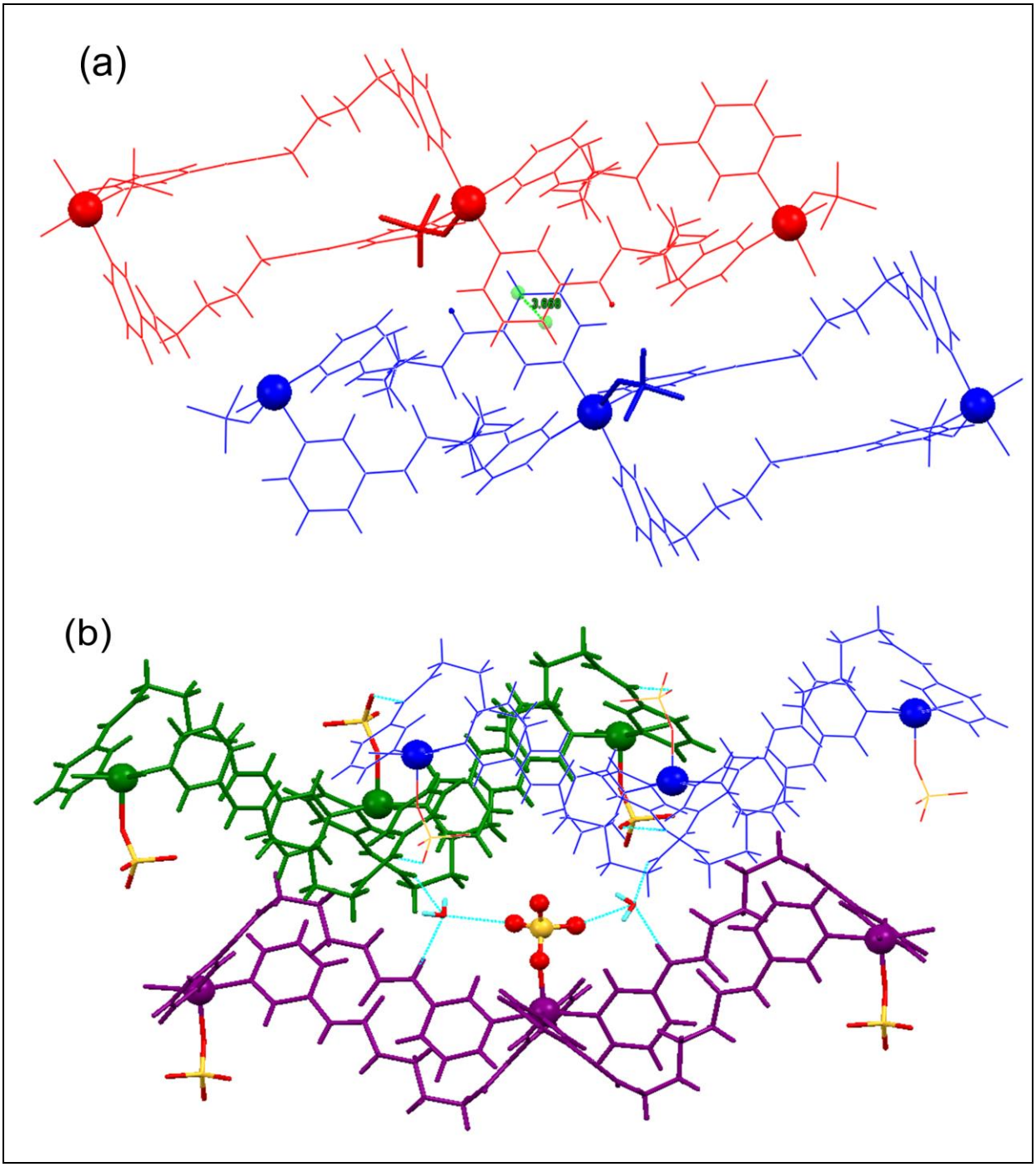

Figure 5.3: Packing of the looped chains *via* (a) aromatic π•••π interactions and (b) N-H•••O(SO_3^{2-}) hydrogen bonding interactions to form layers.

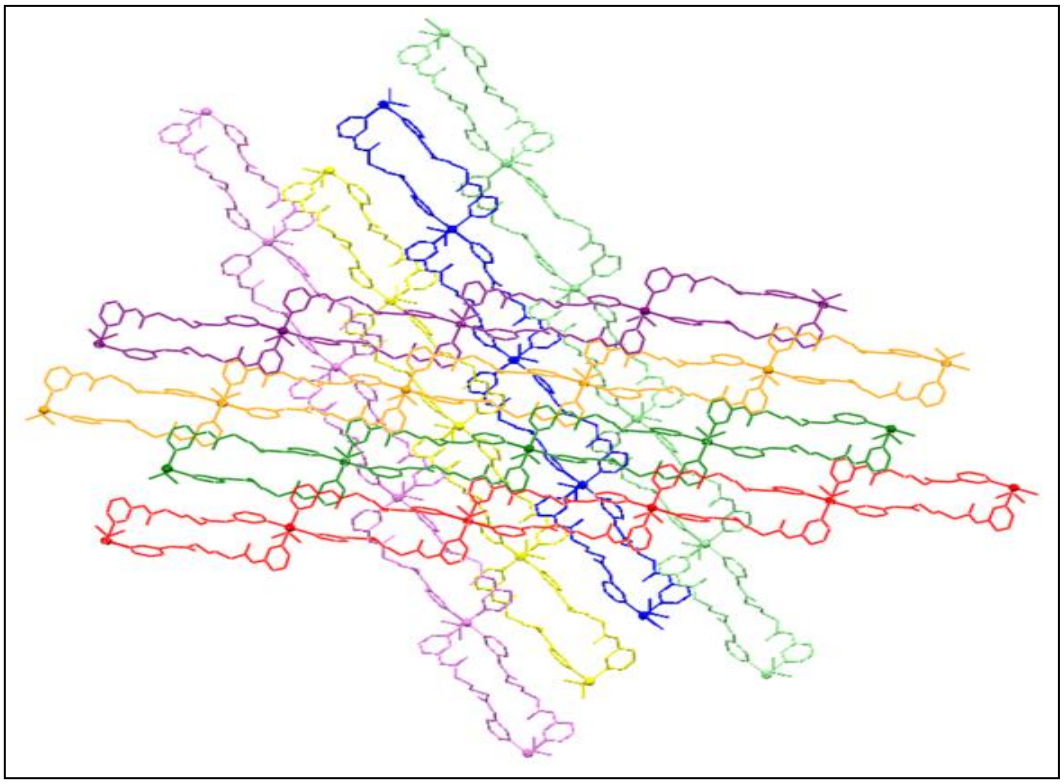

Figure 5.4: Stacking of the layers to form 3D extended network; with the orientation of the layers one over another.

5.4.4 Structural features of CP7

The asymmetric unit of **CP7** consists of half unit of ligand and one benzoate anion coordinated to Cu(II) centre (Figure 5.5(a)).

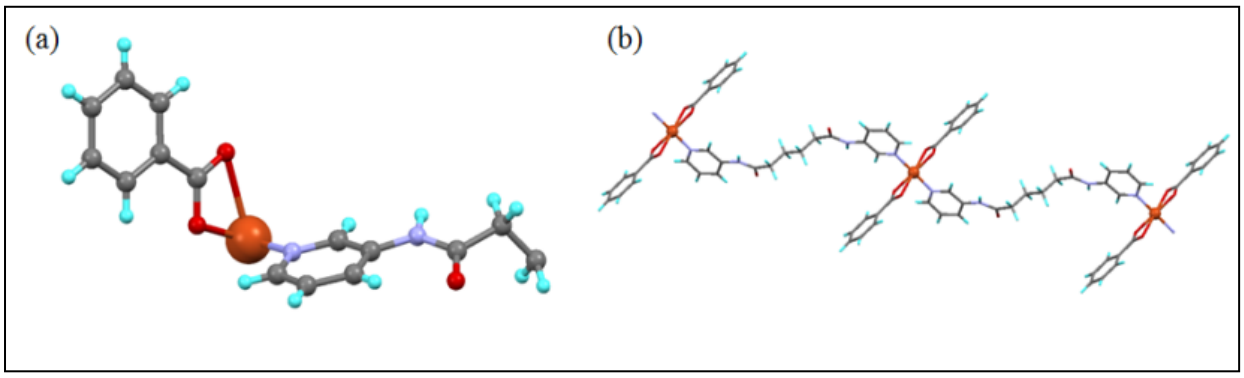

Figure 5.5: Illustrations of the crystal structure of **CP7**: (a) Asymmetric unit; (b) 1D chain network.

The coordination environment of Cu(II) has an distorted-octahedral geometry, where the two benzoates occupy the equatorial positions through chelating binding mode and apical positions are satisfied by the two moieties of the ligand. The butyl spacer of ligand **1b** in **CP7**

adopts all *anti* conformation and the overall structure can be viewed as 1D chain extended *via* ligand **1b** (Figure 5.5(b)).

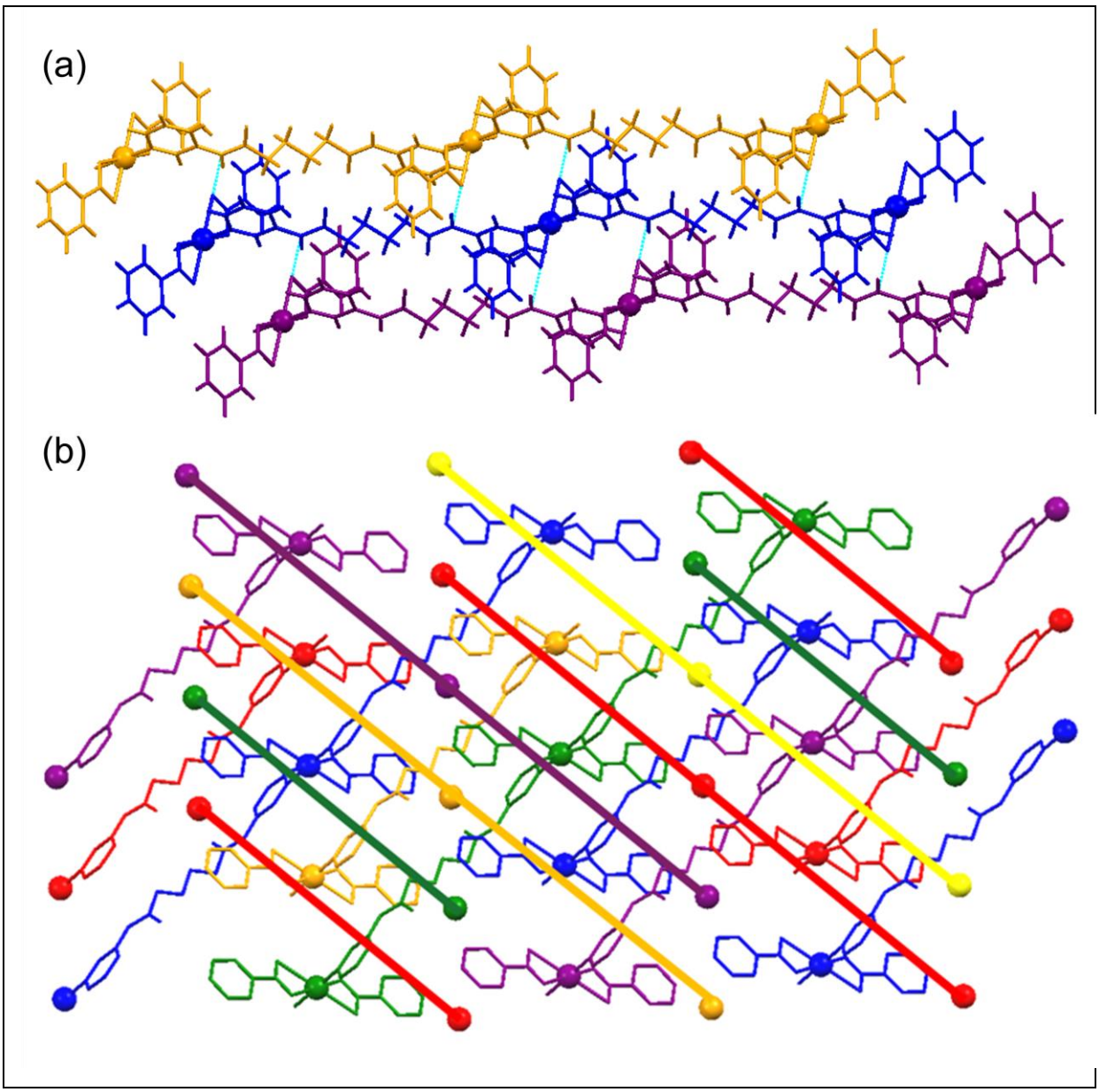

Figure 5.6: (a) Packing of the chains *via* aromatic and N-H•••O(CO-) hydrogen bonding interactions to form layers; (b) Stacking of the layers to form 3D. Notice the arrangement of the chains in the adjacent layers (H atoms are removed for clarity; ligands are shown as straight lines in the top layer)

The presence of benzoate anion blocks most of the coordination sites, there by restricting the geometry of **CP7** to simple 1D chain. The 1D chains were packed *via* aromatic and N-H•••O(CO-) hydrogen bonding interactions to form 2D layers (Figure 5.6(a)). The 1D chains are further arranged in criss-cross fashion to given a 3D extended network (Figure 5.6 (b)).

5.4.5 Effect of Anions on the geometry of CPs

The geometry observed in **CP3**, **CP6** and **CP7** can be rationalized in terms of the counter anions involved. Although ClO_4^- and SO_4^{2-} have tetrahedral shapes, but the resultant coordination polymers from these have completely different geometries.

(i) Co-ordination environment of Cu(II) centre

The coordination environment of Cu(II) centre in **CP3** is an octahedral environment with four units of ligand **1b** and two water molecules whereas distorted square pyramidal geometry of Cu(II) centre with four units of ligand **1b** and one SO_4^{2-} is observed with **CP6**. In **CP7**, Cu(II) has an octahedral geometry with benzoate groups satisfying four sites.

(ii) Conformation of butyl spacer of ligand 1b

Gauche-Anti-Gauche conformation in **CP3**, while *Anti-Anti-Gauche* conformation in **CP6**. In **CP7**, all *anti* conformation of butyl chain is observed.

(iii) Amide groups of ligand 1b

In **CP3**, all amide groups involved in self-complementary amide-to-amide hydrogen bonding, but in **CP6**, amide-to-amide hydrogen bonds are absent. The amide groups form hydrogen bond with SO_4^{2-} and H_2O molecules. In **CP7**, amide groups are involved in hydrogen bond interaction with the benzoates.

(iv) Overall geometry

The network observed in **CP3** is a two-dimensional one with (4,4)-topology. The layers in **CP3** have shown two-fold parallel interpenetration. One-dimensional looped chain is observed in case of **CP6**. Within the loops, the amide C=O are involved in π•••π interactions. The benzoate anion (carboxylate anions) has a greater binding affinity towards the metal centre and can have various binding modes. The presence of benzoate anion in **CP7** has resulted in assembling of the ligand **1b** in 1D chain.

5.4.6 Competitive Reactions of Anions

In order to study the effect of the anions affinity in the formation of CPs, a number of competitive experiments were conducted, wherein Ligand **1b** was reacted with $Cu(NO_3)_2$ (in

2:1 ratio of ligand to metal) in presence of different ratios of ClO_4^-, SO_4^{2-} and benzoate (Scheme 5.2; Table 5.2). The formation of CPs in each reaction was verified by IR and powder XRD.

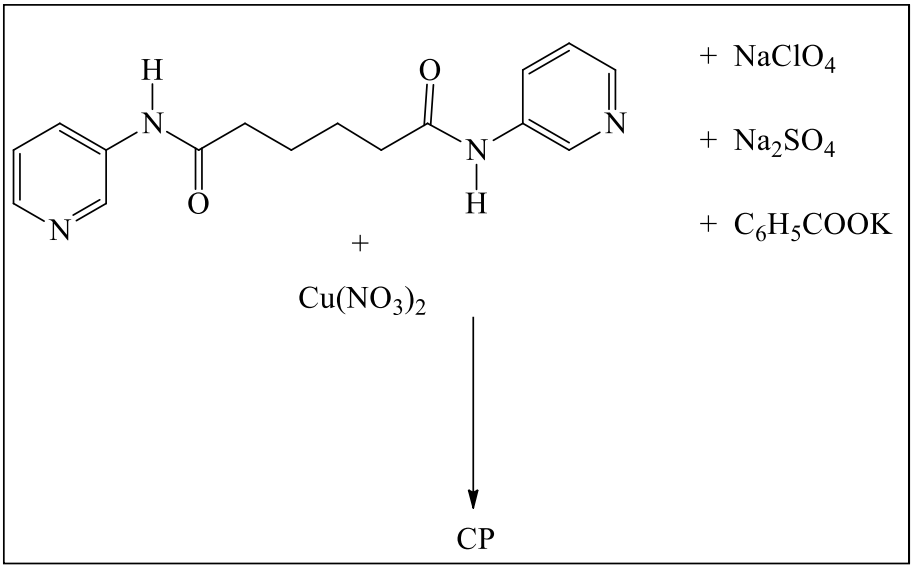

Scheme 5.1: Reactions of Ligand **1b** and $Cu(NO_3)_2$ in 2: 1 molar ratio in the presence of different anions (ClO_4^-, SO_4^{2-} and $C_6H_5COO^-$ in the molar ratio of p : q : r respectively)

In the present experiment, it was observed that the SO_4^{2-} anion showed the highest preference for forming the co-ordination polymer followed by benzoate anion; while ClO_4^- showed least affinity of forming the CP in presence of other anions.

Table 5.2: CPs obtained in different competitive experiments.

Reaction No.	**$NaClO_4$** **p**	**Na_2SO_4** **q**	**C_6H_5COOK** **r**	**Co-ordination Polymer obtained**
I	2	1	2	**CP6**
II	3	1	2	**CP6**
III	2	1	2	**CP6**
IV	2	1	3	**CP6 & CP7**
V	2	2	2	**CP6**
VI	3	2	2	**CP6**
VII	2	2	2	**CP6**
VIII	2	2	3	**CP6 & CP7**

The anion ClO_4^- have poor co-ordinating ability for Cu(II) centre, thereby, in **CP3**, ClO_4^- act as the counter anion to balance the charge and act as template in building up the network. The SO_4^{2-} and benzoate, on the other hand, have good coordinating ability with the metal centre and in the present case, SO_4^{2-} and benzoate are involved within the network in **CP6** and **CP7**, respectively. The observations of the competitive reaction is the direct consequence of the affinity of the counter anions towards Cu(II) centre. The reactivity of the reaction of Cu(II), ligand **1b** and SO_4^{2-} proceeds with the fastest rate as SO_4^{2-} has good co-ordinating affinity, while the same reaction with ClO_4^- has a slower rate due to poor affinity of the counter anion with Cu(II).

5.4.7 Anion Exchange Reactions

The anion exchange reactions were carried out by immersing the crystals of the CPs (**CP3**, **CP6** or **CP7**) in ethanolic solution of sodium or potassium salts of the ClO_4^-, SO_4^{2-} or $C_6H_5COO^-$.

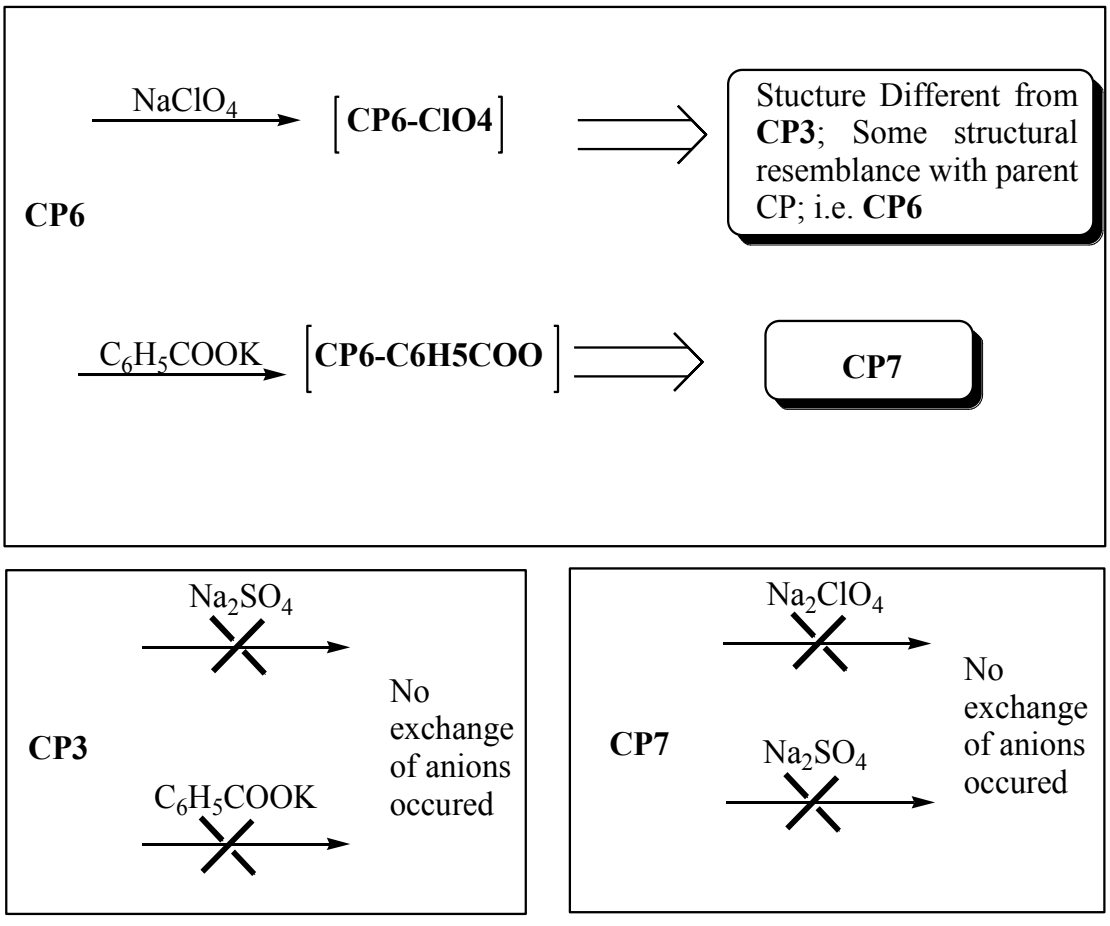

Scheme 5.2: Schematic showing anion exchange reactions of different co-ordination polymers

After 10-15 days, the crystals were taken out from the solution to analyze their powder XRD and IR spectra. Scheme 5.2 summarizes the observations of anion exchange reactions.

5.4.8 Anion exchange reactions of CP6 with benzoate

The anion exchange reaction of **CP6** with benzoate resulted in complete exchange of SO_4^{2-} with benzoate anions. The IR spectra of the benzoate exchanged crystals of **CP6** showed the presence of peaks at 1551 cm^{-1} & 1404 cm^{-1}, characteristic of benzoate and complete disappearance of peaks at 1134 cm^{-1} corresponding to SO_4^{2-} groups (Figure 5.7).

The powder XRD spectra of **CP6** and the benzoate exchanged crystals of **CP6** showed completely different pattern, which confirms the structural transformation during anion exchange (Figure 5.8). On comparing the powder XRD spectra of the **CP6** exchanged was compared with **CP7** and it was observed that the anion exchange reaction has resulted in this case also the formation of **CP7**.

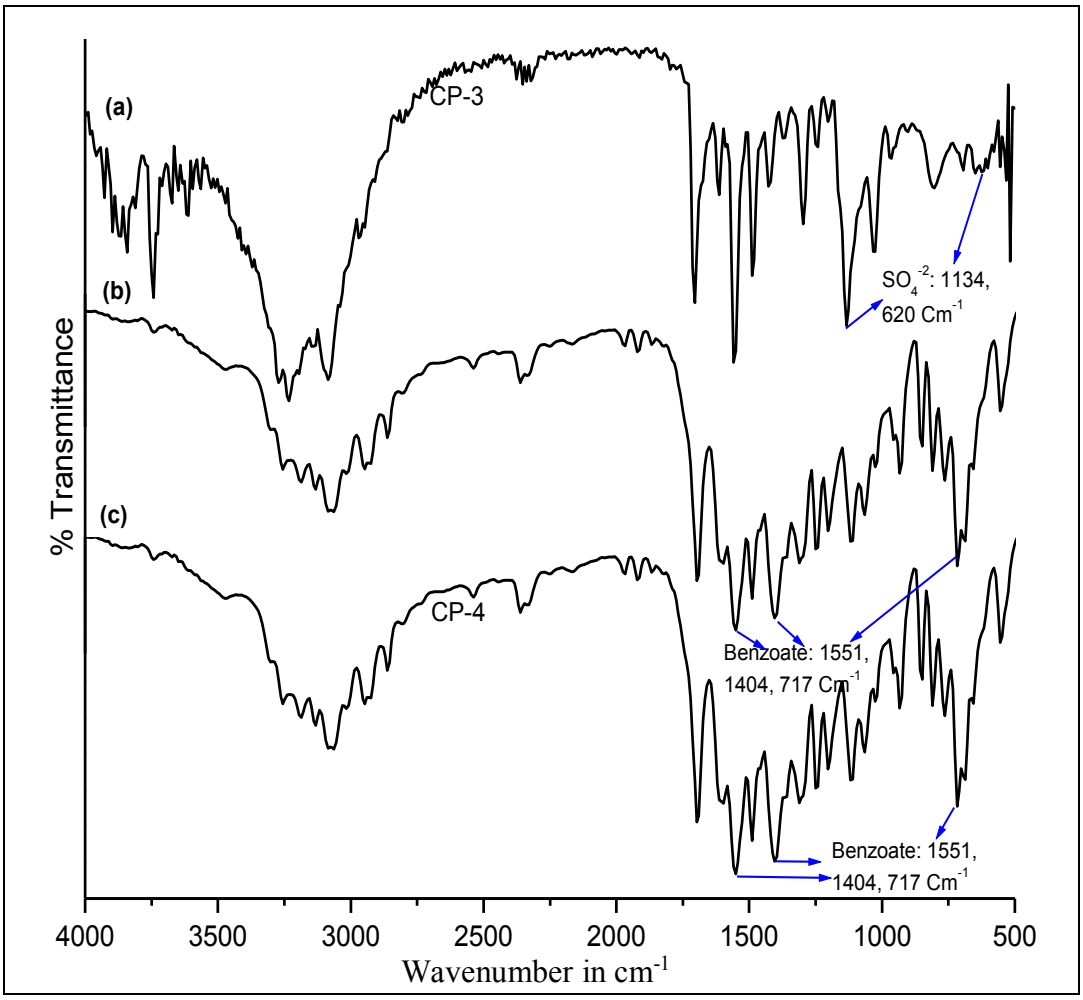

Figure 5.7: IR spectra of (a) **CP6**; (b) **CP6** on anion exchange with Benzoate; (c) **CP7**.

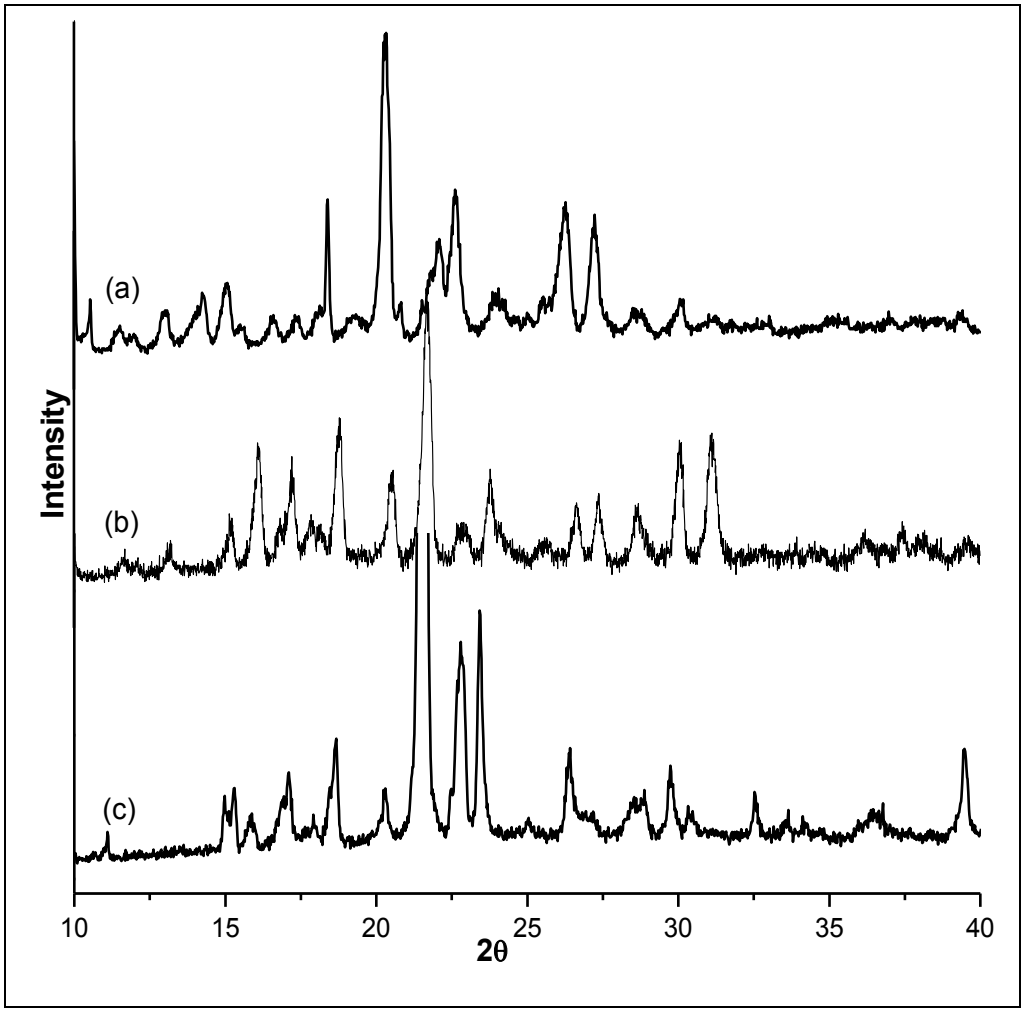

Figure 5.8: Powder XRD Spectra of (a) **CP6**; (b) **CP6-C6H5COO**; (c) **CP7.**

5.4.9 Anion exchange reactions of CP6 with ClO_4^-

The anion exchange reaction of **CP6** with sodium per chlorate resulted in complete exchange of SO_4^{2-} with ClO_4^-. In co-ordination polymer **CP6,** anion SO_4^{2-} co-ordinated with Cu(II) and showed peaks at 1134 cm^{-1} corresponding to the sulphate group. The IR spectra of **CP6** showed the presence of peaks at 1103 cm^{-1}, characteristic of ClO_4^- and complete disappearance of peaks at 1134 cm^{-1} corresponding to SO_4^{2-} groups (Figure 5.9).

The powder XRD spectra of **CP6** and **CP6-ClO4** showed some similarities which indicated that some of the structural features of the parent CP was intact (Figure 5.10). The powder XRD spectra of **CP6-ClO4** did not show any resemblance with **CP3**; so the structure

obtained from the anion exchange reaction was completely different from that obtained by direct reaction of ligand **1b** and $Cu(ClO_4)_2$.

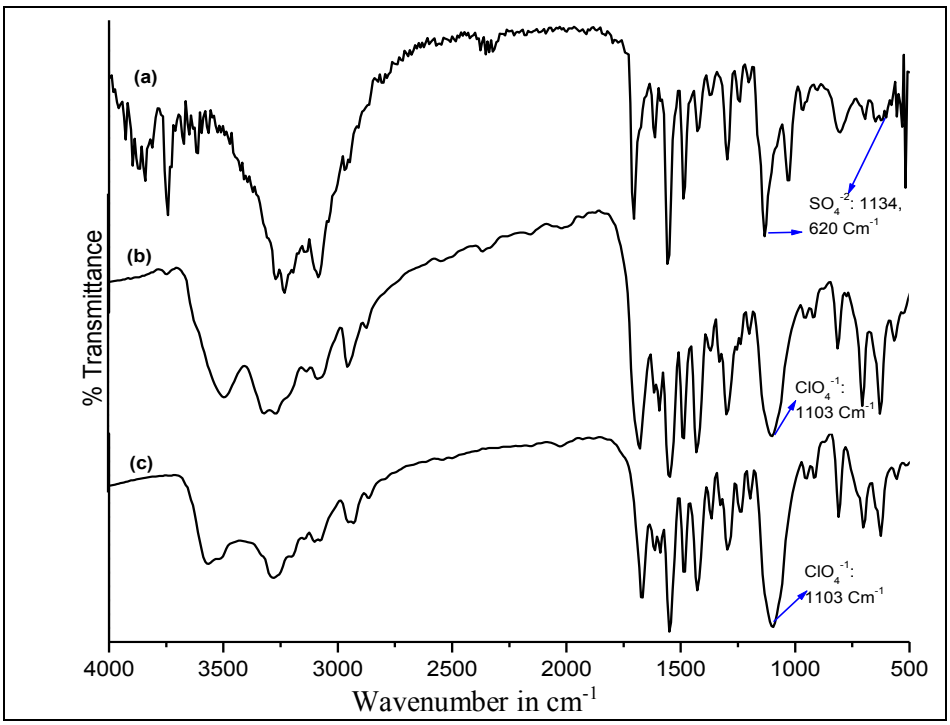

Figure 5.9: IR spectra of (a) **CP6**; (b) **CP6** on anion exchange with ClO_4^-; (c) **CP3**

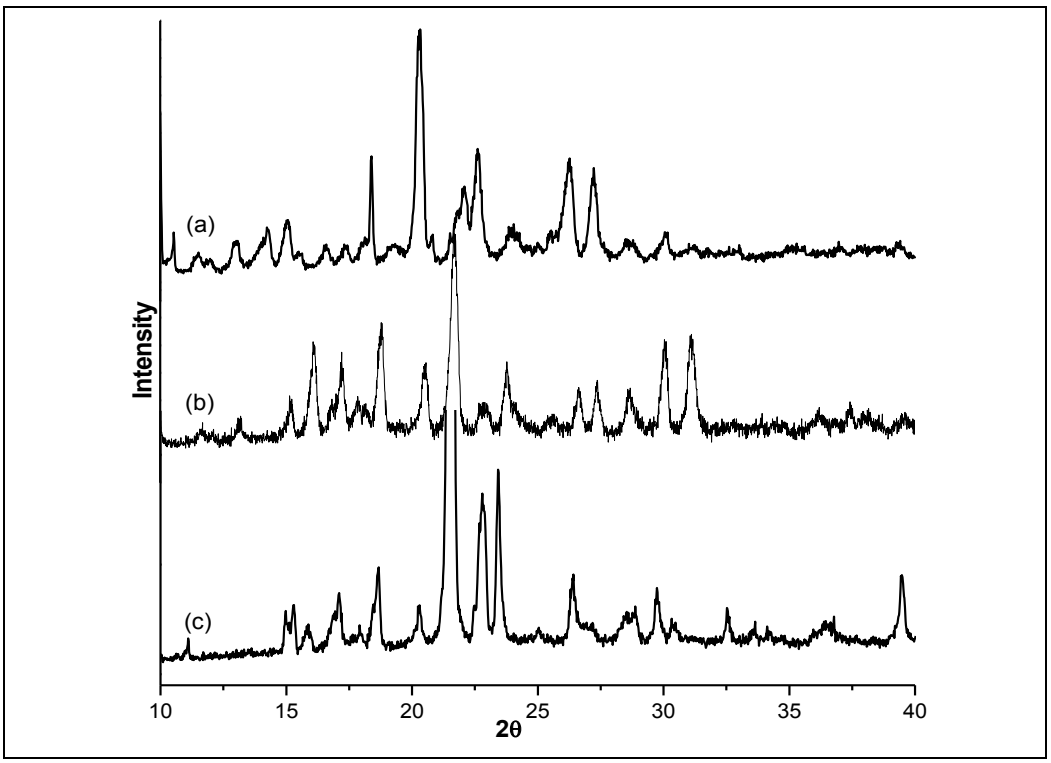

Figure 5.10: Powder XRD Spectra of (a) **CP6**; (b) **CP6-ClO4**; (c) **CP3**

5.5 Conclusions

Based on the analysis of the structural features of **CP3**, **CP6** and **CP7**, it is observed that the flexibility of *bis*-pyridyl-*bis*-amide resulted in achieving diversities in the network. The role of different types of anions in forming CPs was also seen. The benzoate and SO_4^{2-} were involved in the network framework, so reacted and rapidly formed CPs compared to ClO_4^-, which acted as non-coordinating anion. Further, the network stability was also observed during the anion exchange reaction. **CP3** being an interpenetrated network is not affected when reacted with different anions.

5.6 References

[1] Michaelides, A.; Skoulika, S. *Cryst. Growth Des.* **2009**, *9* (5), 2039-2042.

[2] Fei, H.; Han, C. S.; Robins, J. C.; Oliver, S. R. J. *Chem. Mater.* **2013**, *25* (5), 647-652.

[3] Fang, C.; Liu, Q.-K.; Ma, J.-P.; Dong, Y.-B. *Inorg. Chem.* **2012**, *51* (7), 3923-3925.

[4] Ma, S.; Smulders, M. M. J.; Hristova, Y. R.; Clegg, J. K.; Ronson, T. K.; Zarra, S.; Nitschke, J. R. *J. Am. Chem. Soc.* **2013**, *135* (15), 5678-5684.

[5] Adarsh, N. N.; Dastidar, P. *Cryst. Growth Des.* **2010**, *10* (2), 483-487.

[6] Sarkar, M.; Biradha, K. *Cryst. Growth Des.* **2007**, *7* (7), 1318-1331.

[7] Rajput, L.; Biradha, K. *Cryst. Growth Des.* **2009**, *9* (9), 3848-3851.

[8] Cheng, P.-C.; Yeh, C.-W.; Hsu, W.; Chen, T.-R.; Wang, H.-W.; Chen, J.-D.; Wang, J.-C. *Cryst. Growth Des.* **2012**, *12* (2), 943-953.

Chapter 6

Thermal, Photo-Physical & Photo-catalytic Properties of Co-ordination Polymers (CPs)

6.1 Introduction

In the previous chapters, we have discussed the synthesis, characterisation and structural analysis of the co-ordination polymers (CPs). In general, the solid state arrangement of the molecules, decides the properties of a co-ordination polymer. The crystal structure analysis will provide detailed information on arrangement of the molecules. Role of central metal ion, alkyl spacer length, counter anion and the effect of anion exchange, guest inclusion and metal metathesis is studied and analyzed. It was observed that the geometry of co-ordination networks depend on several factors such as coordination environment of the metal centre, metal-to-ligand ratio, nature, the geometry of the ligands, the presence of solvents (guest molecule) and counter anions and a slight variation or modification in any of these will have extensive effect on the overall geometry.

In this chapter, we will discuss properties of the co-ordination polymers (CPs) discussed in the previous chapters. The thermal properties of all co-ordination polymers (CPs) were analysed using Thermogravimetric Analysis (TGA). It was observed that co-ordination polymers (CPs) were thermally stable up to 200 ºC. The co-ordination polymers **CP1 – CP7** can be utilized up to temperature 200 ºC for any application. The results obtained from TGA permitted us to obtain information, which will relate the structure of CPs to the degradation process on increasing temperature. The presence of lattice (unco-ordinated) and co-ordinated water molecules in co-ordination polymers and their removal on increasing temperature were investigated by the (TG/DTG) technique. The exothermic and endothermic processes were associated with dehydration, melting, decomposition and crystallisation. Wang *et al.* studied thermal behaviour of Cu(II) co-ordination polymer of ligand **1a,** ligand **1b** along with different aromatic polycarboxylates.[1]

Ligand **1a** and 1,4 – benzenedicarboxylate formed a co-ordination polymer with Cu(II), where the lattice water molecules extended the supramolecular architecture to 3D *via* hydrogen bonding. The lattice water molecules were removed first at 107 ºC, followed by removal of ligand **1a** at 150 – 464 ºC, while at the end 15.27 % residue of CuO remained. In another co-ordination polymer of Cu(II) with ligand **1a** and 1,4- naphthalene dicarboxylic acid, three lattice water molecules were present. The thermal analysis showed that water molecules were removed in the range of 40 -140 ºC, followed by degradation of organic ligands. A co-ordination polymer of ligand **1b** and 1,4 – benzenedicarboxylate with Cu(II)

degraded in the range of 140 - 474 °C, leaving behind CuO residue. In the CP of ligand **1b** and 1,3,5 – benzenetricaboxylate with Cu(II), loss of water molecule started at 101 °C, while degradation of organic ligands occurred between 323−543 °C.

Gong *et al.* reported the thermal analysis of Zn(II) co-ordination polymer of 4-pyridyl analogue of **1b** and 2,6-naphthalenedicarboxylate, where unco-ordinated dimethyl amine molecules were present in the network. These dimethyl amine molecules were removed easily from the network and the host framework was stable up to 170°C.[2] Biradha *et al.* thermally analysed co-ordination polymers of ligand **1a** and ligand **1b** with $Cu(SCN)_2$, where DMF molecules were co-ordinated with Cu(II) and also present as unco-ordinated guest molecule.[3] They observed that the CPs looses DMF molecules at 170°C and from 170°C onwards degradation of ligand started. In one of their co-ordination polymers, both DMF and nitrobenzene were present as unco-ordinated guest molecules. TGA suggested that both the guest molecules were removed at 185°C and beyond 185 °C ligand degradation started. Lin *et al.* studied thermal behaviour of Cd(II) co-ordination polymer of ligand **1a** and 5-aminoisophthalic acid (5-H_2AIP), where one co-ordinated water molecule and two lattice water molecules were present. The first weight loss of 10.83% in the range of 139 - 212 °C was equivalent to the elimination of the co-ordinated water and lattice water molecules. The second weight loss was observed in the range of 220 - 360°C corresponding to the decomposition of organic ligands.[4]

The structural diversity of co-ordination polymers (CPs): well-defined orientation of organic ligands in the lattice, porous nature and host-guest interactions encourage attractive luminescent properties in these materials.[5,6] Thermally stable CPs based on d^{10} metal canters; Zn(II) or Cd(II) and π-conjugated organic ligands have been investigated because of their tunable fluorescent properties.[7,8] The d^{10} metal center ions are difficult to oxidize & reduce, their luminescent properties are originated mainly from the organic ligand (*i.e.* intra-ligand charge transfer fluorescent emission), but ligand-to-metal charge transfer (LMCT) transitions also permits to obtain tunable fluorescent properties.[9,10,11]

Wang *et al.* reported the fluorescent properties of ligand **1a**, ligand **1b** and Cu(II) co-ordination polymers of these ligands along with aromatic polycarboxylates.[1] The free ligand **1a** and **1b** display intense emission bands with the maxima at 447 nm and 385 nm upon excitation at 320 nm, respectively. The co-ordination polymer of Cu(II) with Ligand **1a** and

1,4- naphthalene dicarboxylic acid and the co-ordination polymers of Cu(II) with Ligand **1a** and 1,2 – benzenedicarboxylic acid showed emission bands with maxima at 399 nm upon excitation at 320 nm. In both the cases, the absorption bands were blue-shifted by 48 nm compared to the free ligand **1a**. The Cu(II) co-ordination polymers of ligand **1b** along with 1, 2 – benzenedicarboxylic acid and Cu(II) co-ordination polymer of ligand **1b** along with 1, 3, 5 – benzenetricarboxylic have emission bands with maxima at 404 nm and 400 nm, respectively, upon excitation at 320 nm, which are red-shifted by 19 nm and 15 nm, respectively, compared to the free ligand **1b**. It was suggested that the carboxylate ligands have no significant contribution towards the fluorescent properties of co-ordination polymers and the emission was associated only with N-donor ligands.[12]

Lin *et al.* reported photo-luminescence of Cd(II) co-ordination polymer of ligand **1a** along with 5-aminoisophthalic acid (5-H_2AIP), where the emission bands showed maxima at 386 nm when excited at 300 nm. The emission bands were blue-shifted by 14 nm compared to free ligand **1a**.[4] Cheng *et al*. studied photo-luminescence of co-ordination polymers of d^{10} metal centers : Zn(II) and Cd(II) with ligand **1b** along with polycarboxylates.[10] Both red and blue shift of the emission bands compared to ligand **1b** were observed due to the different conformations of butyl spacer and co-ordination modes adopted by the ligand **1b** in the CP.[12] In the co-ordination polymers of Cu(II), the luminescence may be attributed due to the coupling of ligand-to-ligand charge transfer (LLCT) and ligand-to-metal charge transfer (LMCT).[13]

The porous nature of some CPs and/or the presence of catalytically active transition-metal centers are seen a suitable as candidate for size- and shape-selective catalytic applications of co-ordination polymers.[14] The application of CPs in UV-light driven photo catalysis is still in its infancy. Some groups have demonstrated the use of co-ordination polymers (CPs) as efficient photo-catalysts on the green degradation of organic pollutants.[15,16,17] This development of photo-catalysis may be applied in removal of organic pollutant from waste-water under UV-light. Wang *et al.* reported that the photo-catalytic activity of Cu(II) co-ordination polymer of ligand **1a** and ligand **1b** was dependent on spacer length.[1]

Further the literature studies suggested that increase in the spacer length may support the transport of excited holes/electrons to the surface to initiate the photocatalytic decomposition reaction of organic dyes/pollutants.[18-20] Wang *et al.* reported Co(II) Co-ordination Polymer

of ligand **1a** and **1b** along with aromatic polycarboxylates, which, degraded Methylene Blue (MB), organic dye by 90% under UV-light.[21] Lin *et al.* studied photo-catalytic behaviour of co-ordination polymer of Cd(II) with ligand **1a** along with 5-aminoisophthalic acid (5-H_2AIP). It was observed that the decomposed 45 % of MB under UV-light.[4] In the present chapter, we will discuss the following properties of co-ordination polymers **CP1** to **CP7**:

(i) Thermal Analysis

(ii) Photo physical properties

(iii) Photo catalytic studies

6.2 Results and Discussion

6.2.1 Thermogravimetric Analysis (TGA)

The thermal properties of the Co-ordination Polymers **CP1** to **CP7** were investigated by Thermogravimetric Analysis (TGA). In TGA, the sample weight loss is measured as a function of temperature. The weight loss associated with a thermal reaction is measured between the inflection points of the TG curve. The most important uses of TG involve measurement of a material's thermal stability and composition during heating and followed by cooling. For TGA, 5-10 mg of the CPs were heated at a rate of 5°C / min under N_2 atmosphere up to a temperature 800°C. The degradation of all CPs started with the removal of lattice water, followed by the release of co-ordinated water and then decomposition of ligand backbone in fragments, which involved a multi-step decomposition process and finally resulted the formation of metal oxides as the residue.

6.2.1.1 TGA of Co-ordination Polymer CP1

The crystal structure of **CP1** showed that the asymmetric unit contain one ligand **1a**, one co-ordinated water, half Cu(II) and one PF_6^-. The molecular formula derived from the structural data of is **$[Cu(1a)_2.2H_2O].2PF_6$** and the resultant molecular weight is 930.10 g/mol. The central metal ion, Cu(II), has a distorted octahedral geometry with four **1a** units occupying equatorial positions & two H_2O occupying the axial positions.

For TGA, 4.3689 mg of **CP1** was taken and heated at a rate of 5 °C/min under N_2 atmosphere up to a temperature 500°C. At a temperature 190.12ºC, 0.23 mg of weight loss was observed which is equal to 3.81 %. This may correspond to the loss of two co-ordinated water

molecules (Calculated: 3.87 %). After 190ºC, in the temperature range of 190ºC - 271.08ºC, degradation of the co-ordination polymer started and weight loss of 2.7789 gm equal to 59.4 % is due to the loss of two ligands (Calculated: 58.06 %) (Figure 6.1).

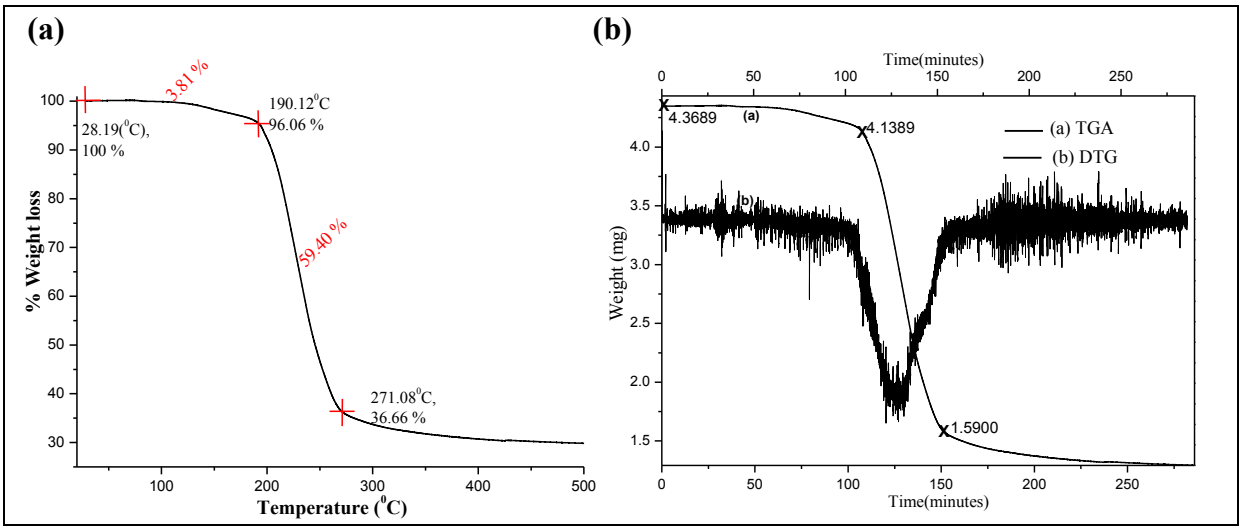

Figure 6.1: (a) TG **(b)** TG/DTG graph of co-ordination polymer **CP1.**

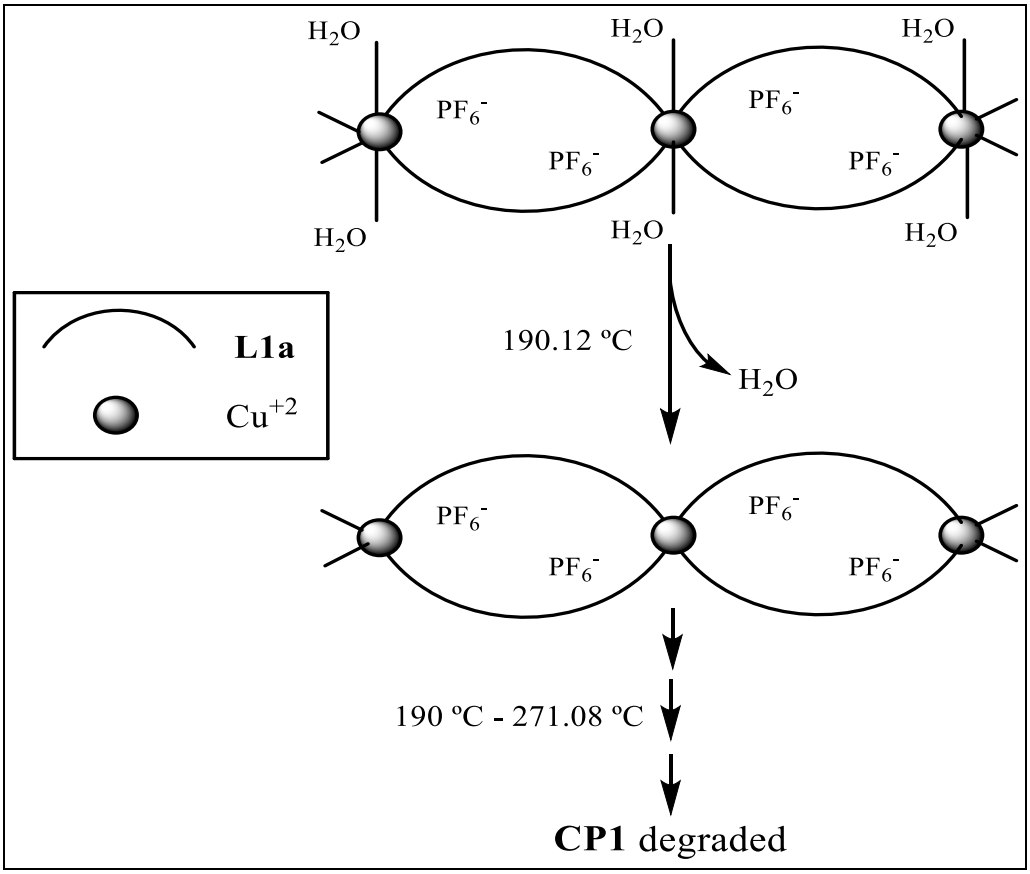

Scheme 6.1: Schematic showing thermal degradation of co-ordination polymer **CP1**

6.2.1.2 TGA of Co-ordination Polymer CP3

From single crystal XRD structural analysis, molecular formula of Co-ordination Polymer **CP3** was found to be **$\{[Cu(1b)_2(H_2O)_2](ClO_4)_2.2(H_2O)\}_n$**. This resulted molecular weight 931.19 g/mol. In the structure, Cu(II) centre adopted a distorted-octahedral geometry, in which the coordination environment of Cu(II) includes four molecules of **1b** in the equatorial position and two H_2O molecules in the axial position. The ClO_4^- anions are present as unco-ordinated anions while two non-coordinating water molecules are also present in the network.

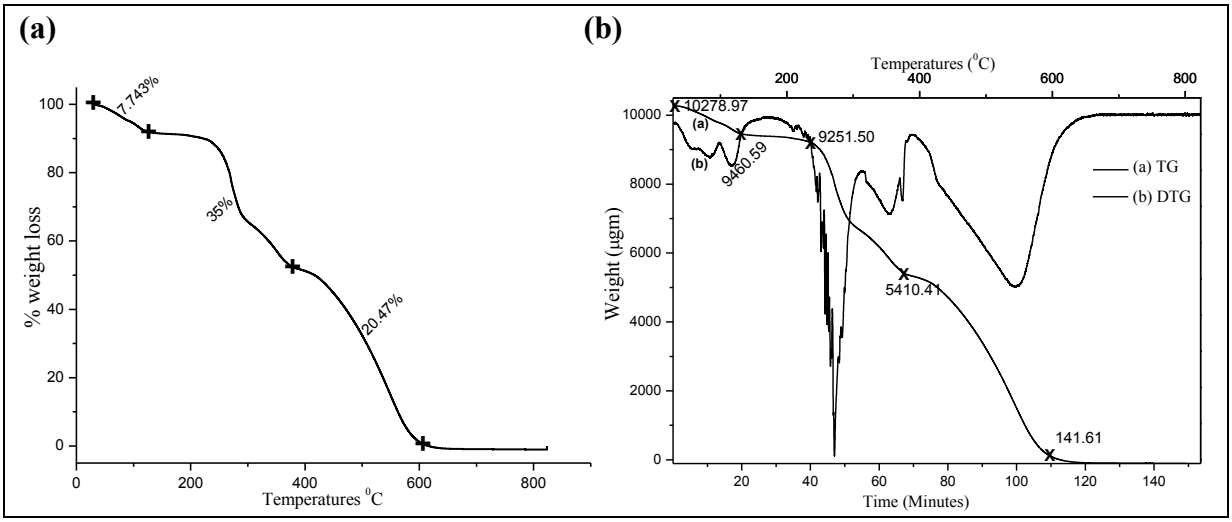

Figure 6.2: (a) TG **(b)** TG/DTG graph of co-ordination polymer **CP3.**

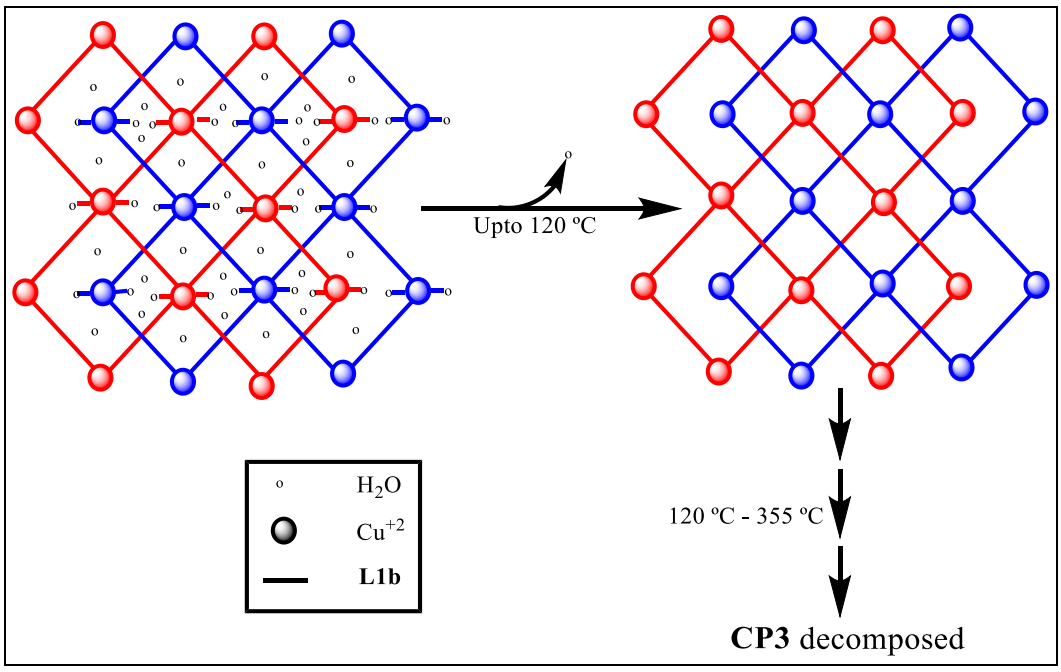

Scheme 6.2: Schematic showing thermal degradation of co-ordination polymer **CP3**

For TGA, 10278.97 µg of **CP3** was taken. It was observed that till 120ºC, 818.38 µgm of weight loss was observed which is equal to 7.743 %. This corresponds to the loss of two unco-ordinated water molecules and two co-ordinated water molecules (Calculated: 7.74 %). In the DTG, the stepwise loss of water molecules is observed, which clearly indicates the different type of water molecules. From 120ºC - 355ºC, weight loss of 35 %, corresponding to the decomposition of the organic ligand **1b** (Calculated: 32.04 %) (Figure 6.2).

6.2.1.3 TGA of Co-ordination Polymer CP4

From single crystal XRD, molecular formula of **CP4** was found to be **$\{[Cd(1b)_2(H_2O)_2](ClO_4)_2.2(H_2O)\}_n$** which corresponds to a molecular weight of 980.05 g/mol. The co-ordination environment of the Cd(II) centre includes four molecules of **1b** in the equatorial sites and two H_2O in the axial sites. The network also has two unco-ordinated water molecules.

For thermal analysis, initially, 5.174 g of **CP4** was heated in inert atmosphere of N_2 at the rate of 5°C/min. Weight loss of 0.135 mg of sample was observed below 100°C which is equal to 3.32 %. This corresponds to two unco-ordinated water molecules. Within a temperature range of 100 - 120°C, weight loss of 0.154 mg was observed which is equal to 3.56 %. Thus weight loss of 8 % observed up to 220ºC corresponds to the loss of two unco-ordinated water molecules and two co-ordinated water molecules (Calculated: 7.34 %).

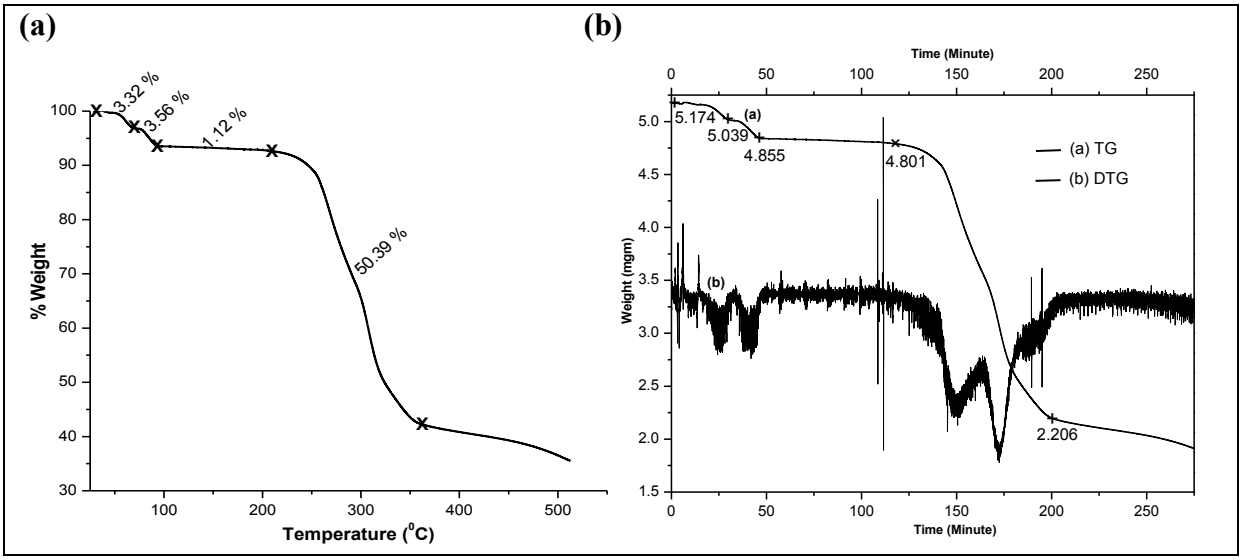

Figure 6.3: (a) TG **(b)** TG/DTG graph of co-ordination polymer **CP4.**

The anhydrous sample remained stable up to ≈ 250ºC without any weight loss. After 250ºC degradation of organic ligand started and up to a temperature of 355ºC, weight loss of 51.51 %, corresponding two organic ligands (Calculated: 60.81 %) was observed.

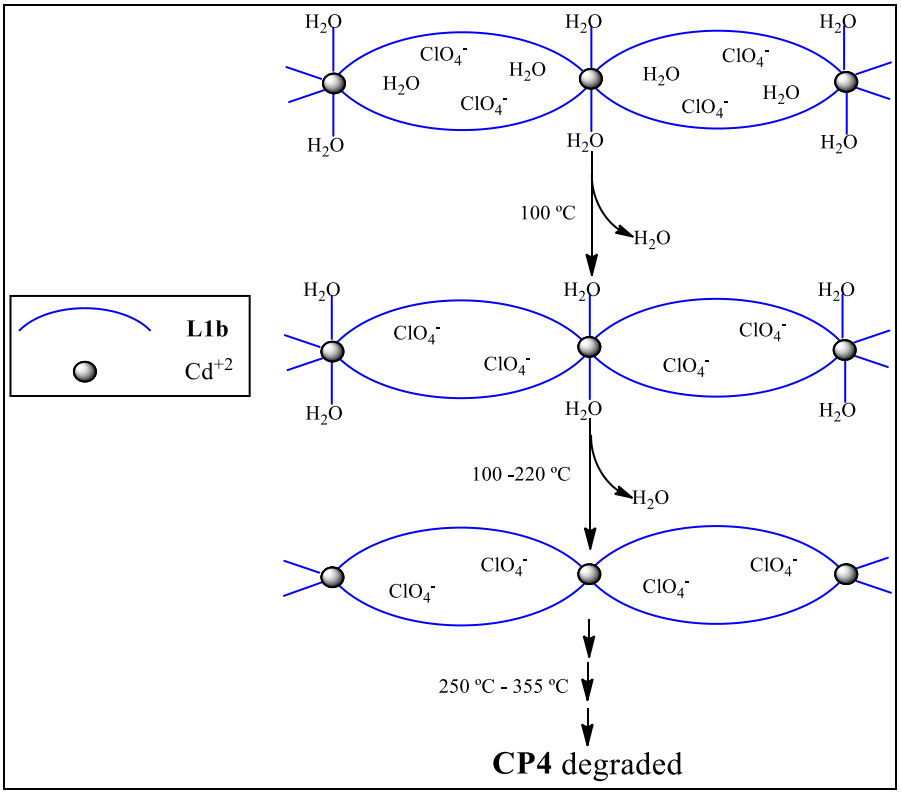

Scheme 6.3: Schematic showing thermal degradation of co-ordination polymer **CP4**

6.2.1.4 TGA of Co-ordination Polymer CP5

The co-ordination polymer **CP5** synthesized using transmetallation on **CP4.** The crystal quality of **CP5** was not good enough to give crystal structure. The PXRD of **CP5** showed similarities with that of **CP4** and during metal metathesis Cd^{+2} in **CP4** is replaced by Cu^{+2}, while the framework remained intact. **CP3** and **CP5** are Cu(II) co-ordination polymers of ligand **1b**, but structural difference arises as a result of different synthetic methodology. The difference in TGA plots of **CP3** and **CP5** also suggest that they have different crystal structures which resulted in different thermal properties.

Initially 10587.22 µg of **CP5** taken for Thermogravimetric Analysis (TGA), weight loss of 1048.2 µg (equal to 6.28 %) was observed up to 220ºC. This corresponds to loss of two unco-ordinated water molecules and two co-ordinated water molecules (Calculated: 6.34 %). This occurred in three steps, first the water molecules present in the lattice may be released as

they are unco-ordinated, followed by the removal of co-ordinated water molecules on increasing temperature to 220 ºC. From 220 ºC to 355ºC, weight loss of 48.84 % is due to the loss of one and half organic ligands (Calculated: 60.81 % for two **1b**) (Figure 6.4).

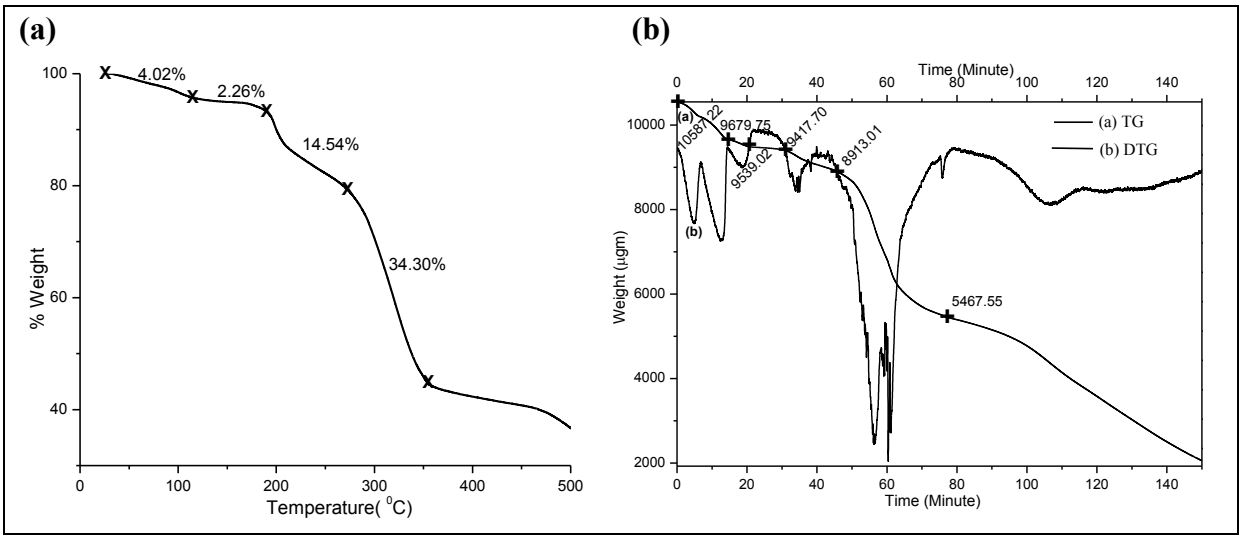

Figure 6.4: (a) TG **(b)** TG/DTG graph of co-ordination polymer **CP5.**

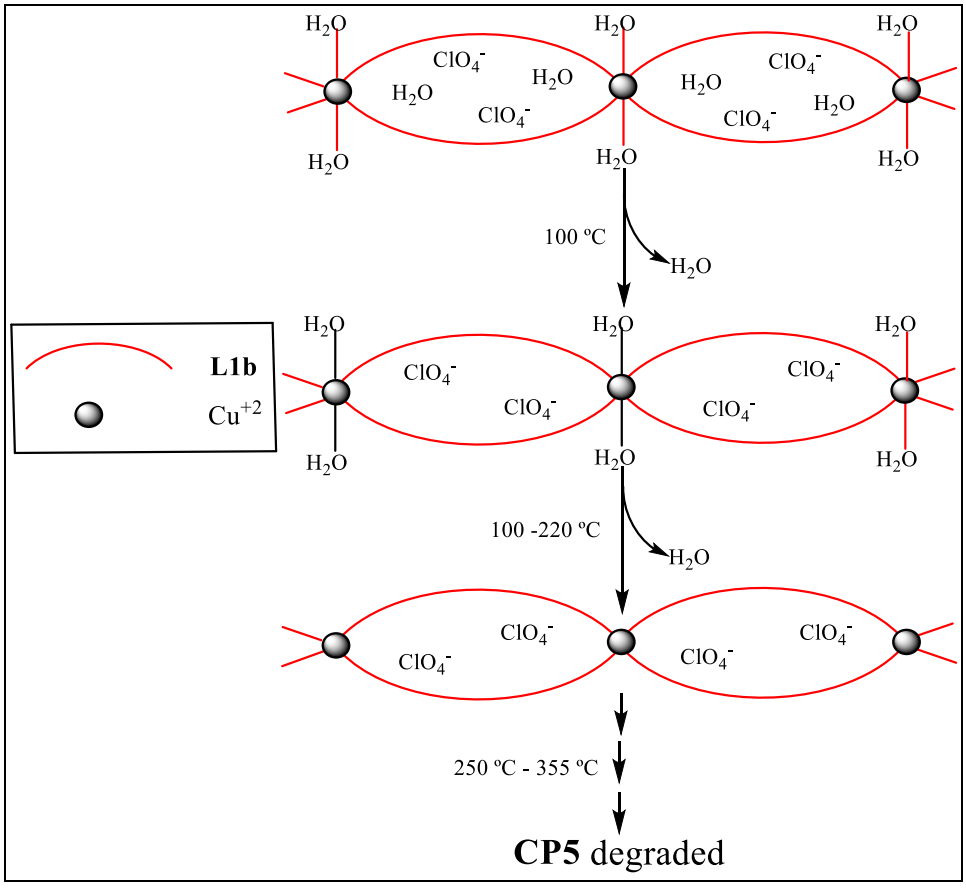

Scheme 6.4: Schematic showing thermal degradation of co-ordination polymer **CP5**

6.2.1.5 TGA of Co-ordination Polymer CP6

The crystal structure analysis showed that the Cu(II) center in **CP6** forms a distorted square pyramidal geometry, where four units of the ligand **1b** form the base while the SO_4^{2-} occupy the apical position.

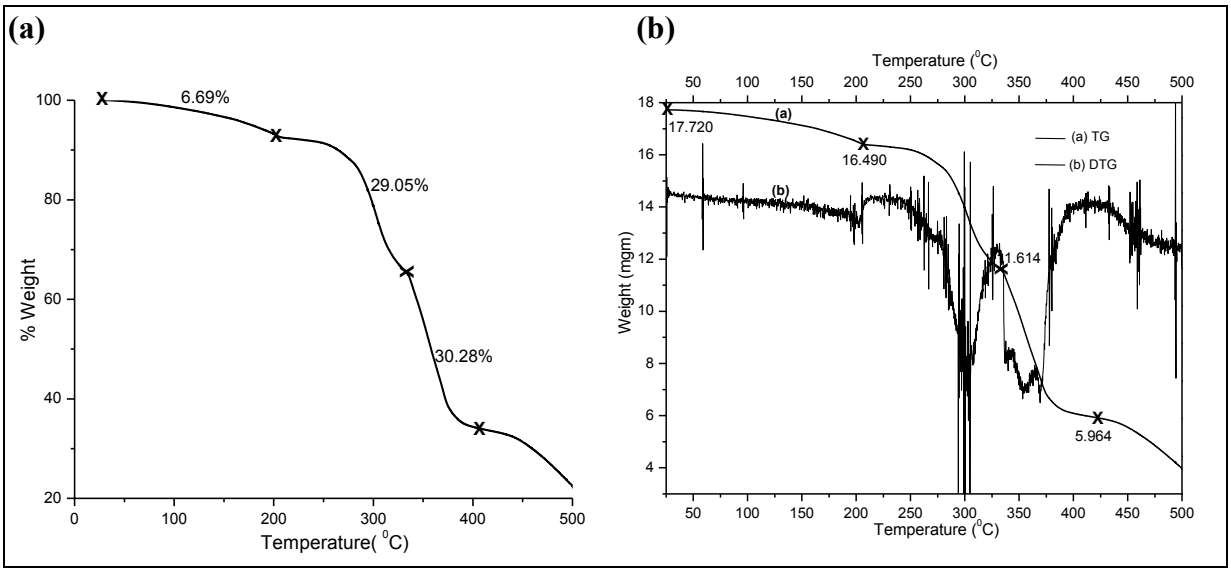

Figure 6.5: (a) TG **(b)** TG/DTG graph of co-ordination polymer **CP6.**

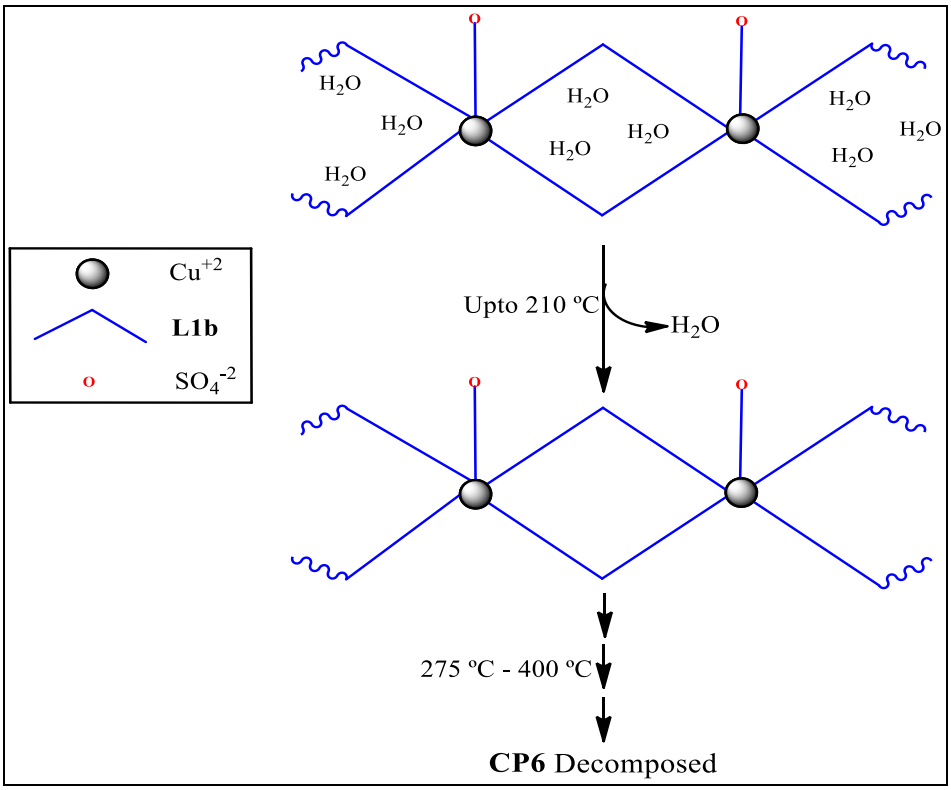

Scheme 6.5: Schematic showing thermal degradation of co-ordination polymer **CP6**

Molecular formula of co-ordination polymer **CP6** was found to be **{[Cu(1)$_2$(SO$_4$)]•3(H$_2$O)}$_n$** which resulted in molecular weight of 810.34 g. The unco-ordinated H_2O molecules are present in the network which helps in extending the network to 3D-network.

For TGA, initially 17.720 mg weight of **CP6** was taken. Weight loss of 1.23 mg (equal to 6.69 %) up to 210ºC corresponds to the loss of three water molecules present in lattice (Calculated: 6.66 %). The anhydrous network is stable up to 275ºC after that decomposition of the organic components began, weight loss is 59.33 % due to the loss of two organic ligands (Calculated: 60.81 %) (Figure 6.5).

6.2.1.6 TGA of Co-ordination Polymer CP7

The coordination environment of Cu(II) has an octahedral geometry, where the two benzoates occupy the equatorial positions through chelating binding mode and apical positions are satisfied by the two moieties of the ligand **1b**.

Molecular formula of co-ordination polymer **CP7** was found to be **{[Cu(1b)(C$_6$H$_5$COO)$_2$]}$_n$** which resulted in molecular weight of 604.1 g. The network of co-ordination polymer **CP7** was stable up to 190ºC, after it began to lose both benzoate anions and ligand **1b.** Weight loss of 7.74 % observed up to 250ºC corresponds to the loss of CO_2 molecules (Calculated: 7.28 %). From 250ºC to 300ºC, weight loss of 41.79 % is due to the loss of two benzoate anions (Calculated: 40.06 %) (Figure 6.6)

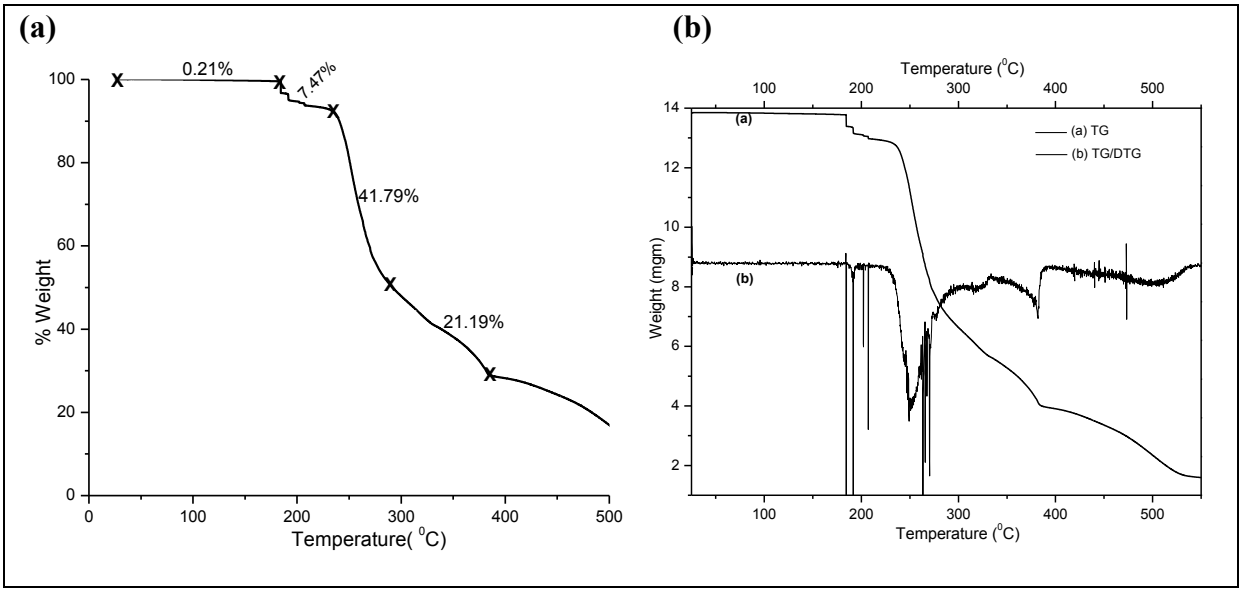

Figure 6.6: (a) TG **(b)** TG/DTG graph of co-ordination polymer **CP7.**

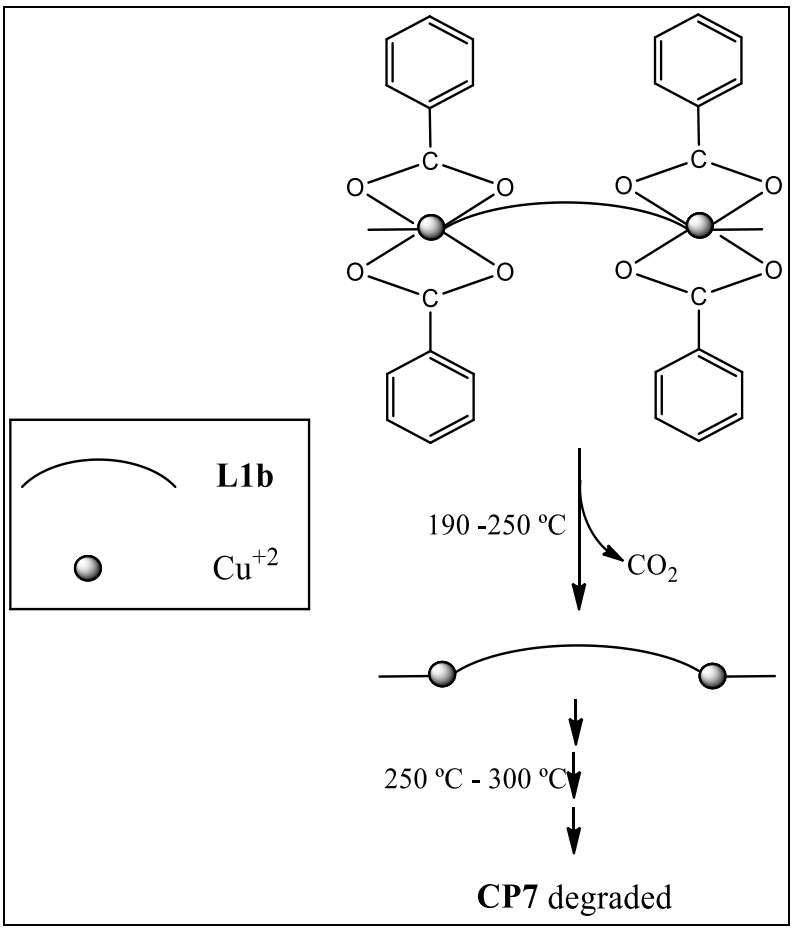

Scheme 6.6: Schematic showing thermal degradation of co-ordination polymer **CP7**

6.2.2 Photo-Physical Properties of CPs

6.2.2.1 UV-Vis Absorption Spectra

The solid state UV-Vis absorption spectra of the free organic ligand **1a**, **1b** and all co-ordination polymers (CPs) were recorded at room temperature. Both free ligands **1a** and **1b** exhibits absorption in the range of 200 - 310 nm. The absorption maxima for ligand **1a** at 200 nm, 250 nm and 290 nm while for ligand **1b** have at 224 nm, 244 nm, 281 nm and a shoulder at 305 nm were observed.

The 200 nm peak of **1a** and 224 nm peak of **1b** was due to $\pi \rightarrow \pi^*$ transition. It can be observed that $\pi \rightarrow \pi^*$ transition in ligand **1b** is red shifted when compared to ligand **1a**. The maxima at 250 and 290 nm in **1a** and 244, 281 and 305 nm in **1b** corresponds to $n \rightarrow \pi^*$ transition (Figure 6.7). Here also red –shift in peak positions were observed for **1b** compared to **1a**. The crystal structure of **1a** and **1b** are reported by Biradha *et al.* where it was observed

that both have similar supramolecular architecture.[22] So the small shift in the peak position may be attributed to the difference in the spacer length.

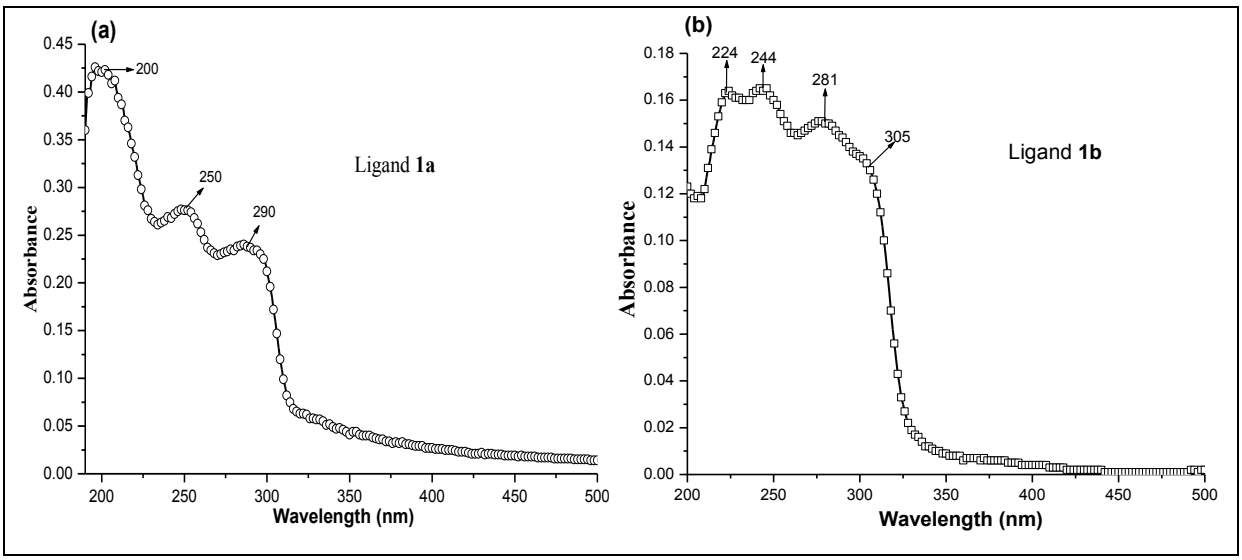

Figure 6.7 Solid state UV absorption spectra of the 'free' organic (a) ligand **1a** and (b) ligand **1b**.

In case of octahedral co-ordination polymers of Cu(II) (t_{2g}^6 e_g^3), the Laporte forbidden d (t_{2g}^6) → d(e_g^3) transition resulted in the absorption wavelength visible region, which is responsible for blue colour of **CP1, CP2, CP3, CP5, CP6, CP7** co-ordination polymer.

The UV-Vis absorption spectra of **CP1** showed absorption peak at 198 nm and weak absorptions in the range 250–400 nm with peak maxima at 292 and 360 nm (Figure 6.8(a)). The apohost **CP2** exhibited an absorption peak at 200 nm and weak absorptions in the range 250–400 nm with peak maxima at 295 and 375 nm (Figure 6.8(b)).

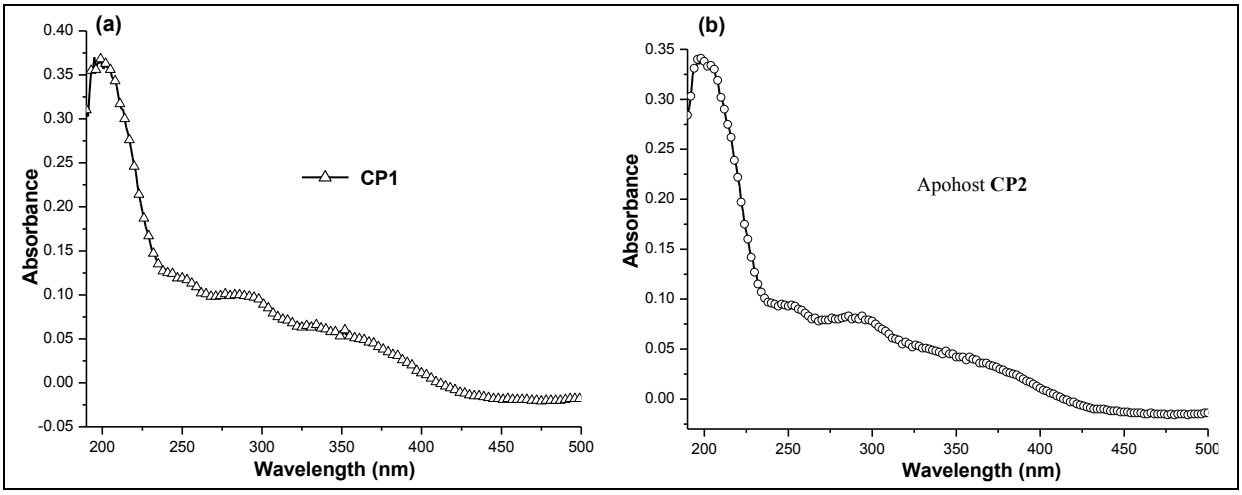

Figure 6.8: Solid state UV absorption spectra (a) **CP1**, (b) Apohost **CP2**

The **CP2a** showed intense peak at 254 nm (Figure 6.9(a)), which was due to the presence of nitrobenzene in the network ("free" nitrobenzene shows a strong absorption band at 262 nm). The presence of benzonitrile in **CP2b** is also confirmed by the solid state UV-VIS spectra, where the presence of intense peaks at 219 nm, 258 nm, 274 nm and 297 nm (Figure 6.9(b)) were observed ("free" benzonitrile having peaks at 240 nm, 264 nm, 278 nm and 300 nm).

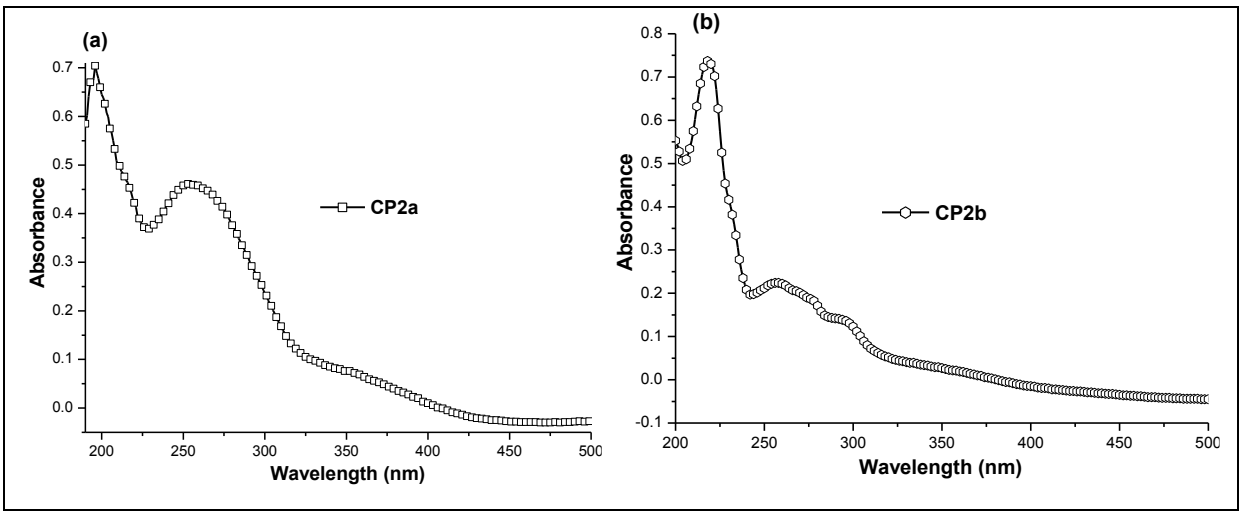

Figure 6.9: Solid state UV absorption spectra of (a) **CP2a** and (b) **CP2b.**

The co-ordination polymers **CP3**, **CP4** and **CP5** showed absorption peaks at 250 nm, 290 nm corresponding to $n \rightarrow \pi^*$ transition and were red-shifted in comparison to ligand **1b**. **CP3** and **CP5** have absorption hump at 390 nm in the ultra-violet region and a strong absorption band in visible region (corresponding to blue colour) because of metal-to-ligand charge-transfer (MLCT) and Laporte forbidden d (t_{2g}^6) $\rightarrow$ d(e_g^3) transition of Cu(II) metal ion (Figure 6.10 (a) and (c)).

The co-ordination polymer **CP5** has absorption peak at 209 nm corresponding $\pi \rightarrow \pi^*$ transition of the π- electrons of ligand **1b**. This peak was absent in both **CP3** and **CP4** showed the structural difference of **CP5** from **CP3**. The absorption hump at 390 nm was absent in **CP4** as MLCT is not possible in Cd(II) metal ion (Figure 6.10(b)).

The co-ordination polymers **CP6** showed absorption peaks at 205 nm, 252 nm, 284 nm and absorption band in visible region responsible for blue colour of the **CP6.** The absorption peak at 205 nm was corresponding to $\pi \rightarrow \pi^*$ transition of the π- electrons of ligand **1b**. Peaks at 252 nm and 284 nm were corresponding to $n \rightarrow \pi^*$ transition and were red-shifted in comparison to ligand **1b** (Figure 6.11(a)).

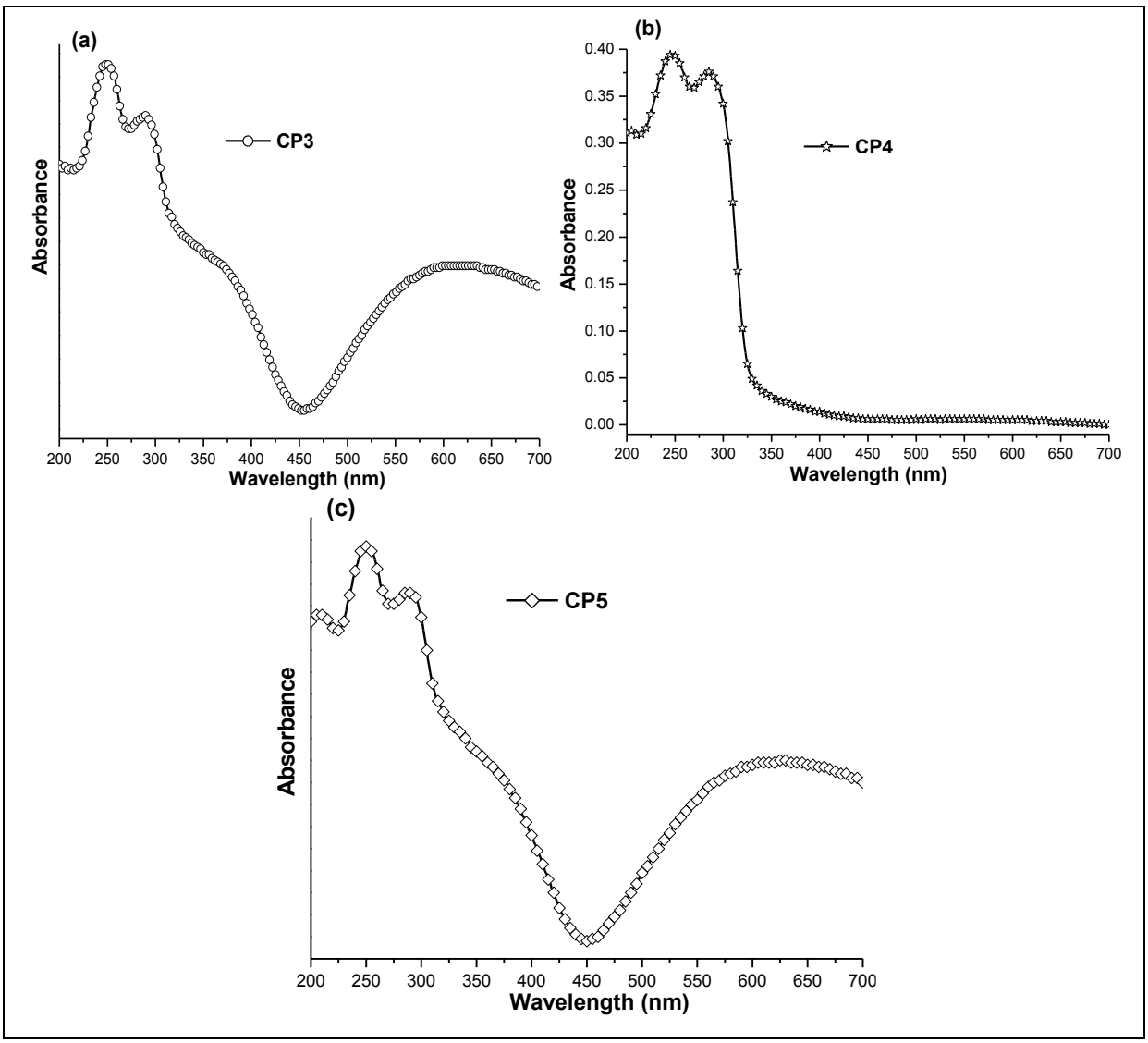

Figure 6.10: Solid state UV absorption spectra of (a) **CP3,** (b) **CP4,** (c) **CP5**

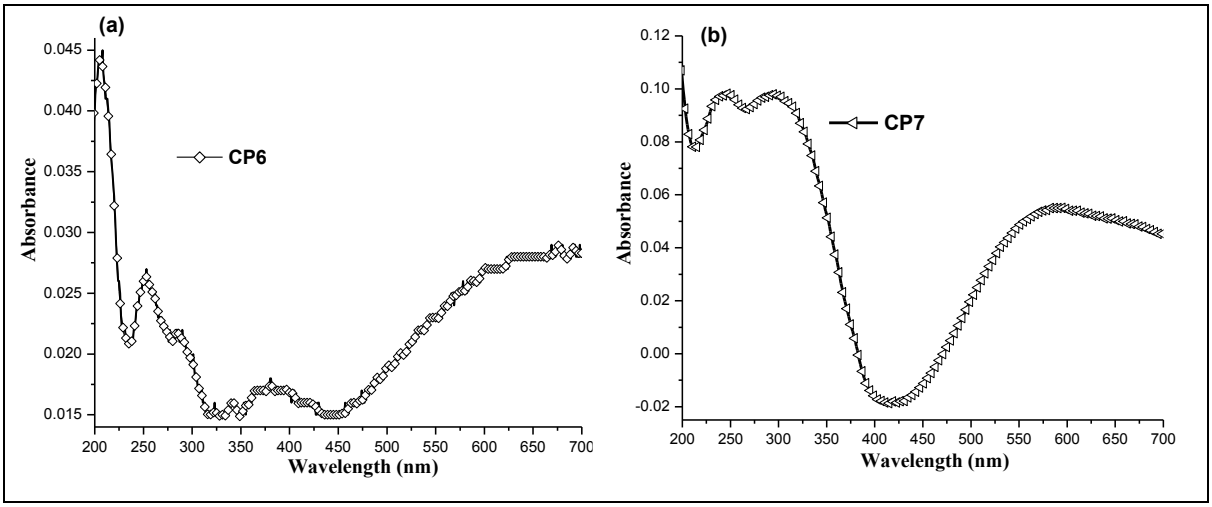

Figure 6.11: Solid state UV absorption spectra of co-ordination polymer (a) **CP6** and (b) **CP7.**

The **CP7** showed absorption peaks at 194 nm, 246 nm and 298 nm, hump and absorption band in the visible region. The absorption peak at 194 nm was due to of $\pi \rightarrow \pi^*$ transition of the co-ordinated benzoate and ligand **1b.** There was broadening in 250-300 nm region because of two types of ligands are present in **CP7**, which resulted in ligand-to-ligand charge-transfer (LLCT). The peak at 252 nm and 284 nm corresponds to $n \rightarrow \pi^*$ transition and were red shifted in comparison to ligand **1b** (figure 6.11(b)).

6.2.3.2 Photoluminescence

Photoluminescence properties of all co-ordination polymers (CPs) have been investigated in the solid state at room temperature together with the free ligands **1a** and **1b.** The organic ligands **1a** and **1b** have small chromophoric moieties separated by ethyl and butyl spacer, respectively.

The crystal structures of **1a** and **1b,** reported by Biradha *et al.*, showed that both of the organic compounds are iso-structural.[22] The molecules are packed *via* C-H•••N hydrogen bonding, which results in the formation of herringbone arrangement (Figure 6.12). The angle between amide and pyridyl plane was equal to zero, which further support the favourable π-conjunctions leading to chromophoric properties of ligands.

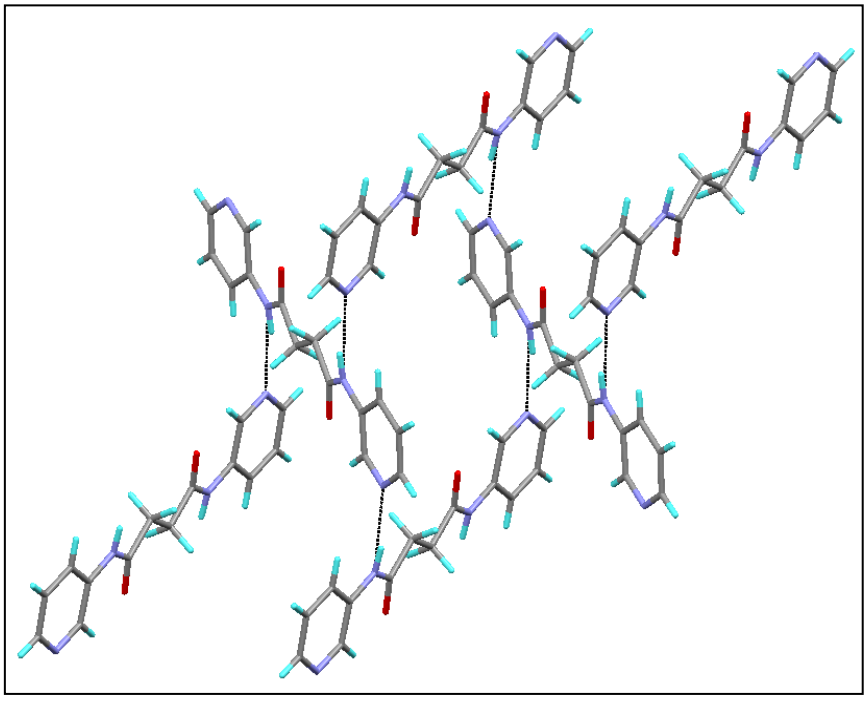

Figure 6.12: Crystal Structure of Ligand **1a**; Notice the Herringbone Arrangement of the molecules: **1a** and **1b** are iso-structural; Structure is generated from cif obtained from CCDC 650273.

The emission spectra of these ligands in solid states and DMF solution were recorded. In solid state, ligands **1a** and **1b** exhibit fluorescent emission peaks at 373 nm and 475 nm (λ_{ex} = 320 nm) respectively (Figure 6.13).

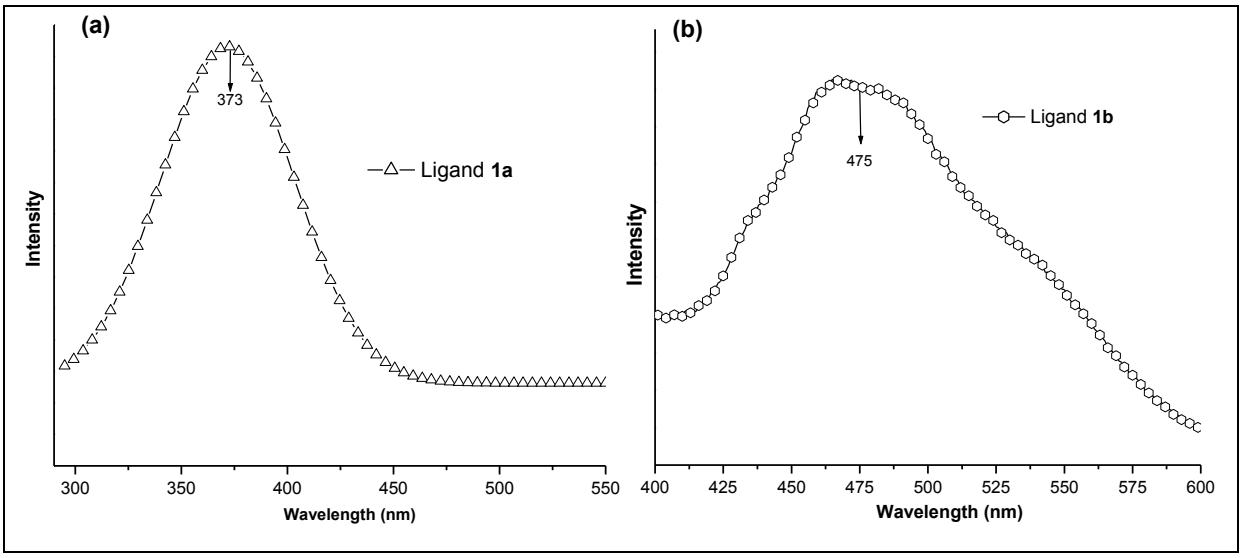

Figure 6.13: Solid state emission spectra of (a) ligand **1a** and (b) ligand **1b.**

For dilute solution (1×10^{-5}M) the emission maxima were at 358 nm, red-shifted by 15 nm compared to solid state but the intensity was very low. On increasing the concentration, red-shift in the emission maxima was observed along with increase in intensity. Ligand **1a** and **1b** showed Aggregation Induced Emission (AIE) behaviour. The quenching of PL peaks on dilution may be resulted due to the non - radiative decay processes such as rotational motion *etc*.

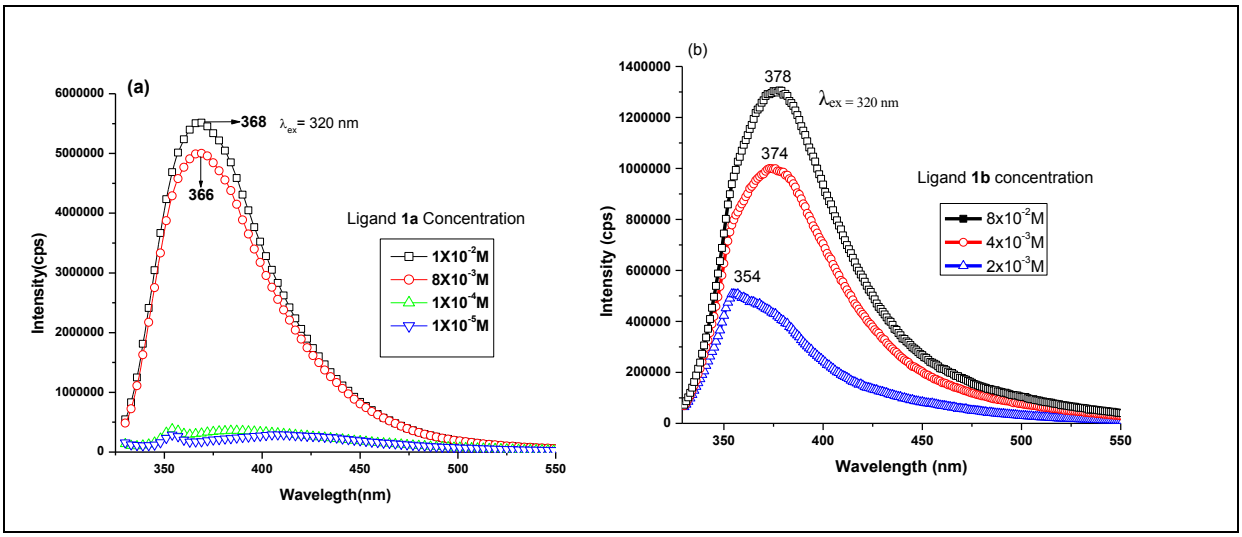

Figure 6.14: Emission spectra at different concentration of (a) ligand **1a** and (b) ligand **1b**.

On increasing the concentration, the self-complementary amide-to-amide hydrogen bond formation will lead to restriction of intra-molecular motion and hence PL intensity increasing. In the solid state, the molecules of ligand **1a** and **1b** has rigid structure leading to enhanced emission compared to dilute solution. The emission maxima were at 366 nm for 8 $\times 10^{-3}$M and 368 nm for 1 $\times$ 10^{-2}M for ligand **1a** (Figure 6.14(a)) but at 374 nm for 4 $\times$ 10^{-3}M and 378 nm for 8 $\times 10^{-3}$ M for ligand **1b** (Figure 6.14(b)).

For co-ordination polymers **CP1** the emission band was observed at 347 nm (blue-shifted by 26 nm compared to 'free' ligand 1a) (Figure 6.16(a)). The crystal structure of **CP1** showed that it is a 1D-looped chain with elliptical cavities. The amide moieties are involved in hydrogen bonding N-H•••F (PF_6^-) and C=O•••H (H_2O). The geometry of ligand **1a** in **CP1** is twisted, where the pyridyl plane and amide planes are at an angle of 28˚. This twisting of the chromophoric moiety resulted in blue-shifted emission band compared to **1a** (Figure 6.15).

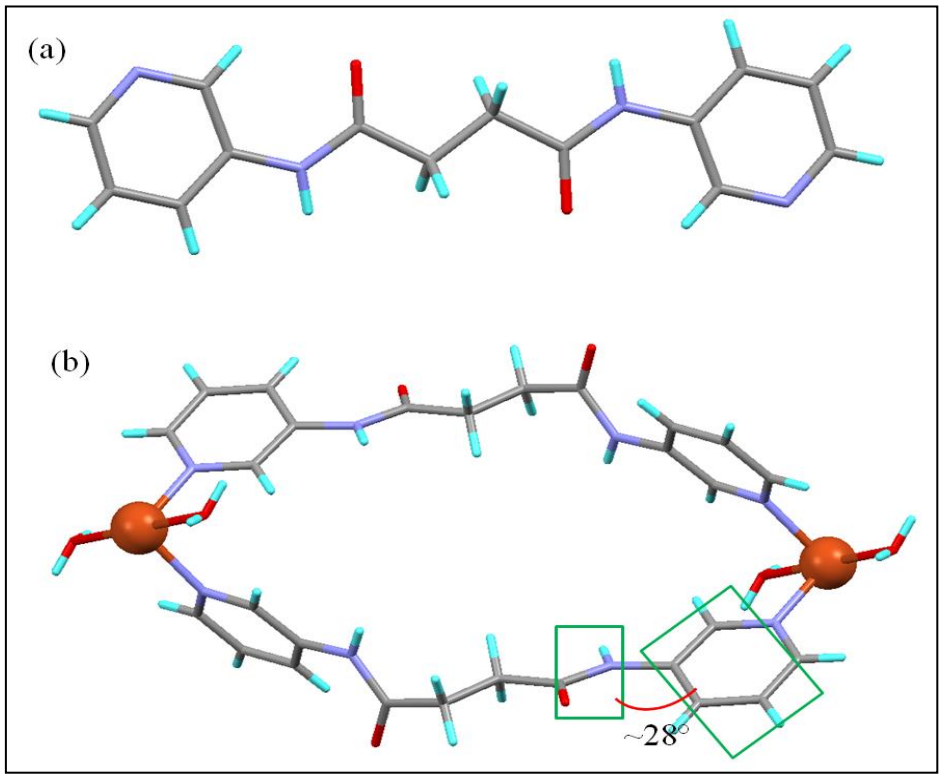

Figure 6.15: Comparison of geometry of free Ligand **1a** and **1a** in **CP1**: (a) Crystal Structure of **1a**; Notice the planar geometry; Structure is generated from cif obtained from CCDC 650273; (b) Crystal Structure of CP1; Notice the twisted geometry of **1a.**

For co-ordination polymer **CP2** the emission band was observed with emission maximum at 354 nm when excited at 320 nm (blue-shifted by 19 nm compared to 'free' ligand **1a)** (Figure 6.16(b)). The ethyl spacer of ligand **1a** has *Anti* confirmation in **CP1**, while *Gauche* in **CP2**.

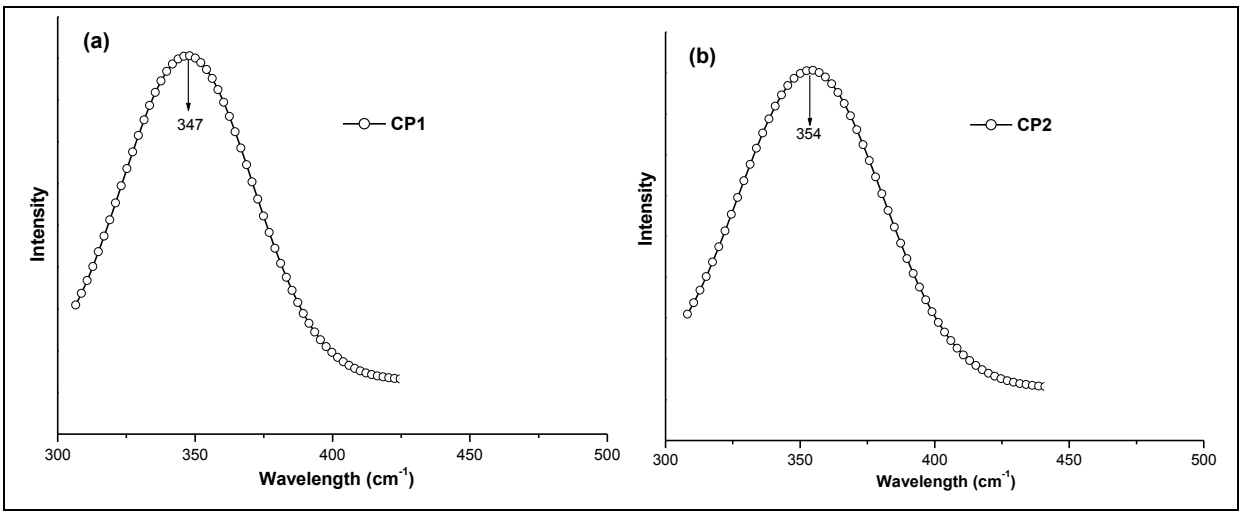

Figure 6.16: Solid state emission spectra of co-ordination polymer (a) **CP1** and (b) **CP2.**

The co-ordination polymers **CP3** have emission bands at emission maxima at 442 nm (blue-shifted by 33 nm compared to 'free' ligand **1b**) (Figure 6.17(a)).

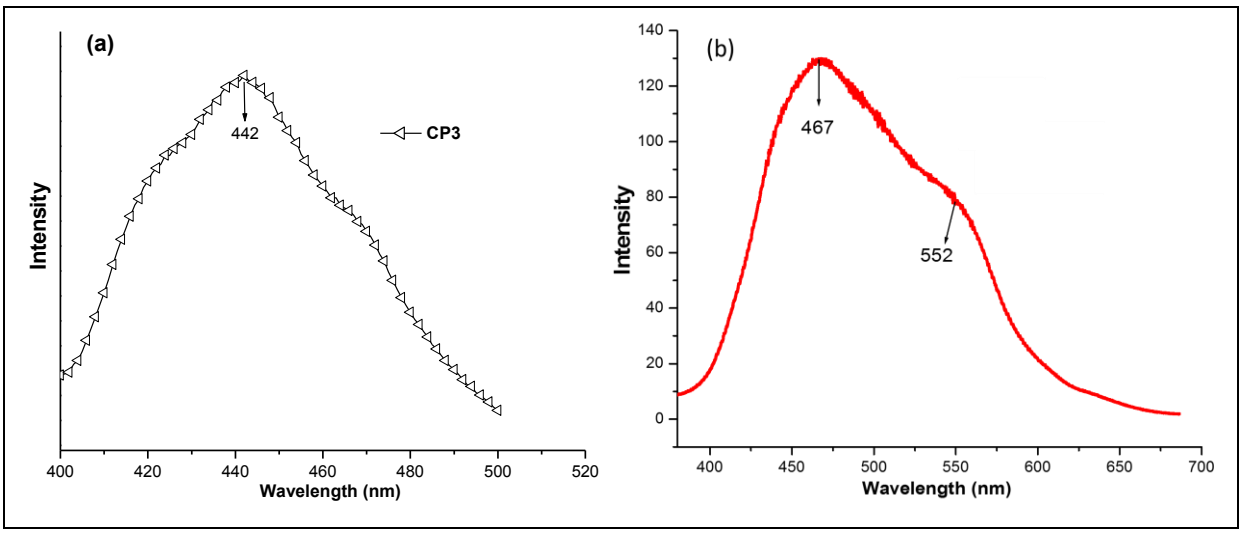

Figure 6.17: Solid state emission spectra of co-ordination polymer (a) **CP3** and (b) **CP4.**

The crystal structure of **CP3** is 2D parallel interpenetrated network of (4,4)- topology, where the butyl spacer have *Gauche-Anti-Gauche* confirmation (Figure 6.18(b)). The amide groups are extensively involved in self-complementary hydrogen bonding. Further the geometry of **1b** in **CP3** is non-planar, which explain the blue-shifted emission band. Co-ordination polymer **CP4** has Cd(II) metal ion (d^{10} system), where d-d transition is not possible. The crystal structure of **CP4**, showed that it is 1D-chain with rectangular loops having π•••π interactions, C=O•••H (H_2O) and N-H•••O (ClO_4^-), where the butyl spacer have *Anti-Anti-*

Anti confirmation . As d^{10} Cd(II) metal centre will not contribute to the emission, the photoluminescence (PL) in **CP4** is mainly due to the geometry of ligand **1b.** The emission maxima observed in **CP4** is at 467 nm, while a hump at 552 nm was observed due to metal-to-ligand charge transfer (MLCT) from metal ion Cd(II) to ligand **1b** (Figure 6.17(b)).

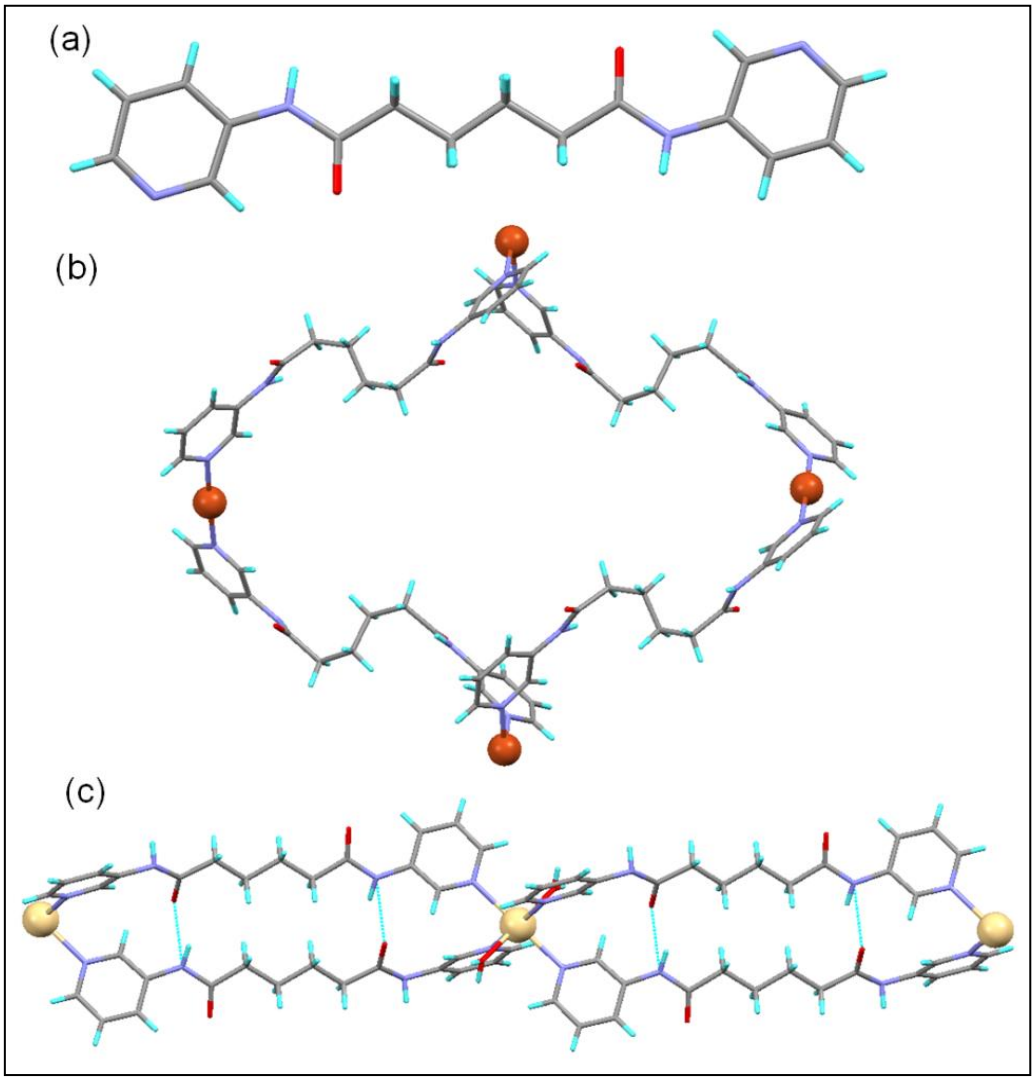

Figure 6.18: Comparison of geometry of free Ligand **1b** and **1b** in **CP3** and **CP4**: (a) Crystal Structure of **1b**; Notice the planar geometry; Structure is generated from cif obtained from CCDC 650274; (b) Crystal Structure of **CP3**; Notice the twisted geometry of **1b** (c) Crystal Structure of **CP4**; Notice the twisted geometry of **1b**

The co-ordination polymers **CP5** have emission bands at emission maxima at 426 nm (blue-shifted by 49 nm compared to 'free' ligand **1b**) (Figure 6.19(a)). The structure of **CP5** is different from **CP3**, which is also evident from their different PL spectra. The co-ordination polymer **CP6** has emission band with emission maximum at 469 nm (blue-shifted by 6 nm compared to 'free' ligand **1b**).

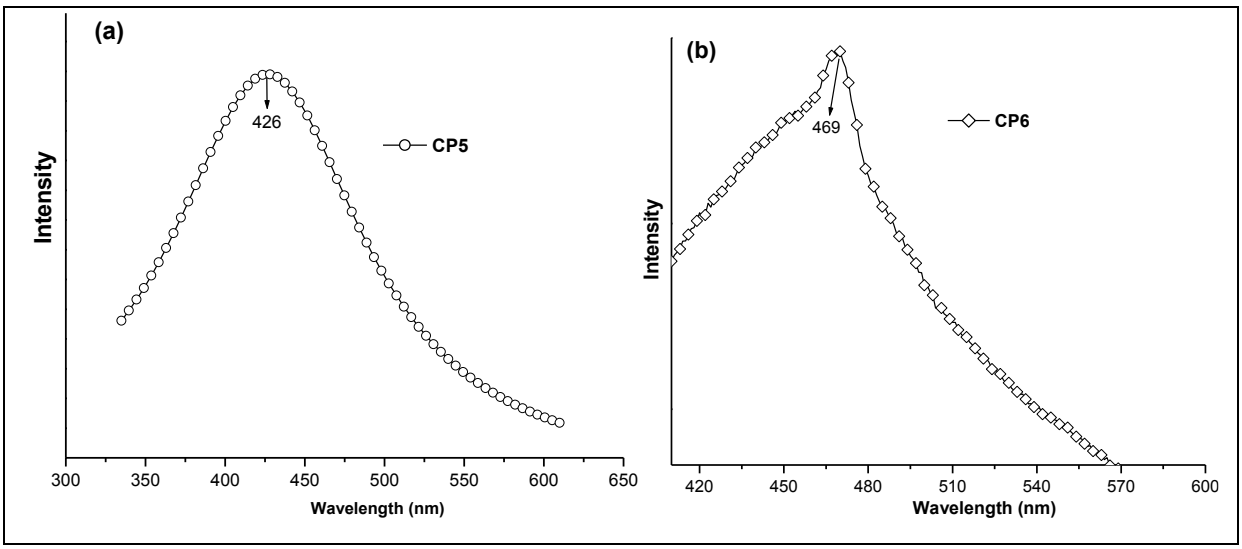

Figure 6.19: Solid state emission spectra of co-ordination polymer (a) **CP5** and (b) **CP6.**

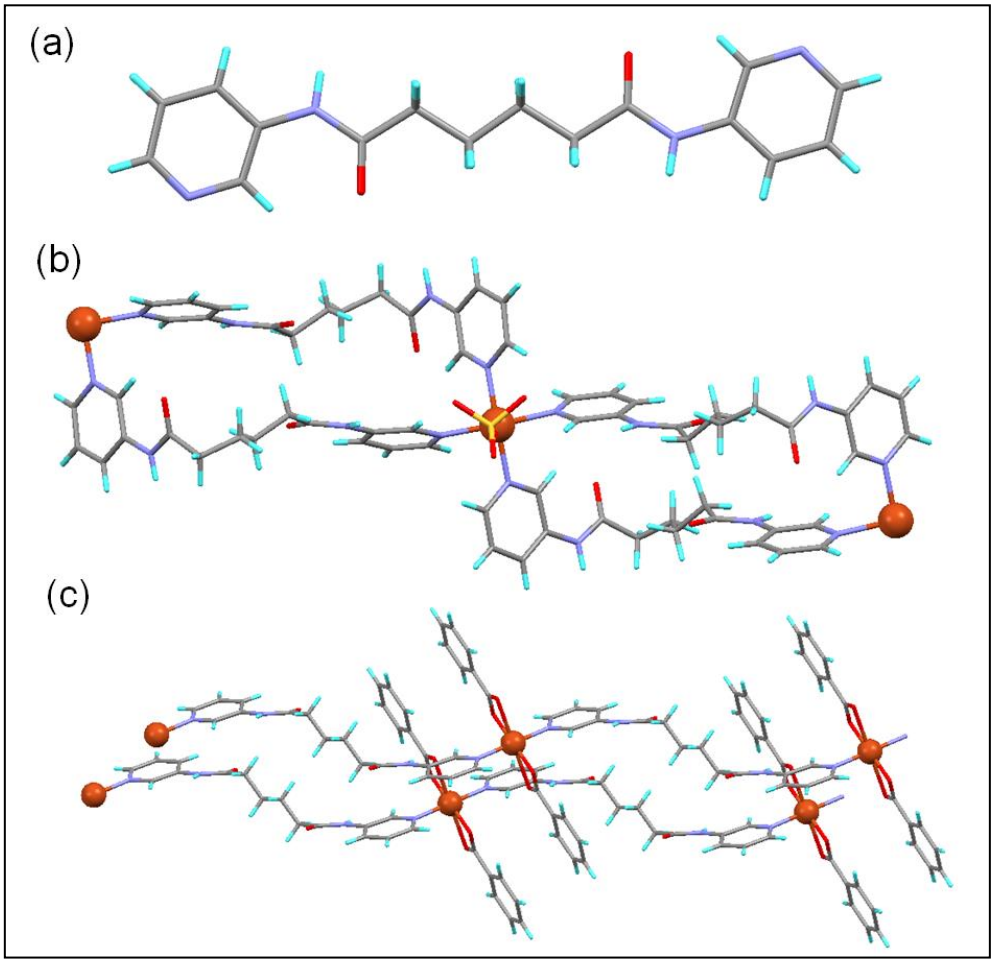

Figure 6.20: Comparison of geometry of free Ligand **1b** and **1b** in **CP6** and **CP7**: (a) Crystal Structure of **1b**; Notice the planar geometry; Structure is generated from cif obtained from CCDC 650274; (b) Crystal Structure of **CP6**; Notice the planar nature (Py-NH-C=O) of **1b** (c) Crystal Structure of **CP7**; Notice benozoate rings are arranged in parallel manner.

From crystal structure of **CP6**, 1D-looped chains are packed *via* π•••π interactions, N-H•••O(SO_3^{2-}) hydrogen bonding interactions and form layers. The butyl spacer in the **CP6** have *Anti-Anti-Gauche* confirmation and the C=O group of amide was, not involved in any type of hydrogen bonding (Figure 6.20 (b)). Although the ligand **1b** in **CP6** is non-planar but the chromophoric unit Py-NH-C=O adopts almost planar geometry. So the observed blue-shift compared to**1b** is less than other CPs.

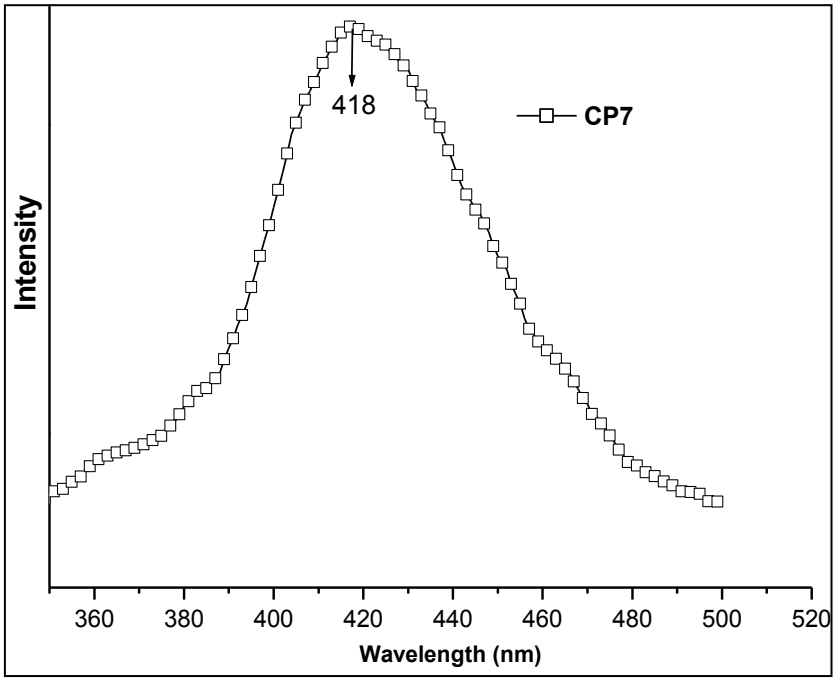

Figure 6.21: Solid state emission spectra of co-ordination polymer **CP7.**

The co-ordination polymer **CP7** have emission bands with emission maxima at 418 nm (blue-shifted by 57 nm compared to 'free' ligand **1b**) (Figure 6.21), highest amongest all CPs of ligand **1b**. Also the PL peak intensity are very less. In **CP7** the 1D chains are arranged in a parallel manner such that each benzoate units is in close proximity to neighbouring benzoates (Figure 6.20(c)). The overall arrangement of 1D chains may result in exciplex formation due to which PL is quenched for **CP7**.

6.2.3 Photo-Catalytic Properties of CPs

All the synthesized Cu(II) and Cd(II) co-ordination polymers derived from the flexible *bis*-pyridyl-*bis*-amide ligands **1a** and **1b**, exhibited significantly photocatalytic activities to degrade organic dyes. *i.e.* Methylene Blue (MB). The photo-catalytic activity of any co-ordination polymers was influenced by number of co-ordinated water molecules, the extent of

the conjugation in organic ligands, co-ordination environments of the central metal ion and the sizes of the metal-oxygen clusters formed in CPs.[16-20]

To compare the photo-catalytic activities, we investigated the decomposition of MB with 'free' ligands, with copper salts and $Cd(ClO_4)_2$ in presence of UV-light. To study the photo-catalysis of **CP1 - CP7**, 150 mg powder of CPs was dispersed in the 100 ml solution of Methylene Blue (MB) (Strength = 10.0 mg/L). For ligand **1a**, ligand **1b**, **CP1** and **CP2**, 100 ml solution of Methylene Blue (MB) (Strength = 20.0 mg/L) was used. These solutions were stirred in the dark for 30 minutes to establish an adsorption/desorption equilibrium of the working solutions, then exposed to UV – light.

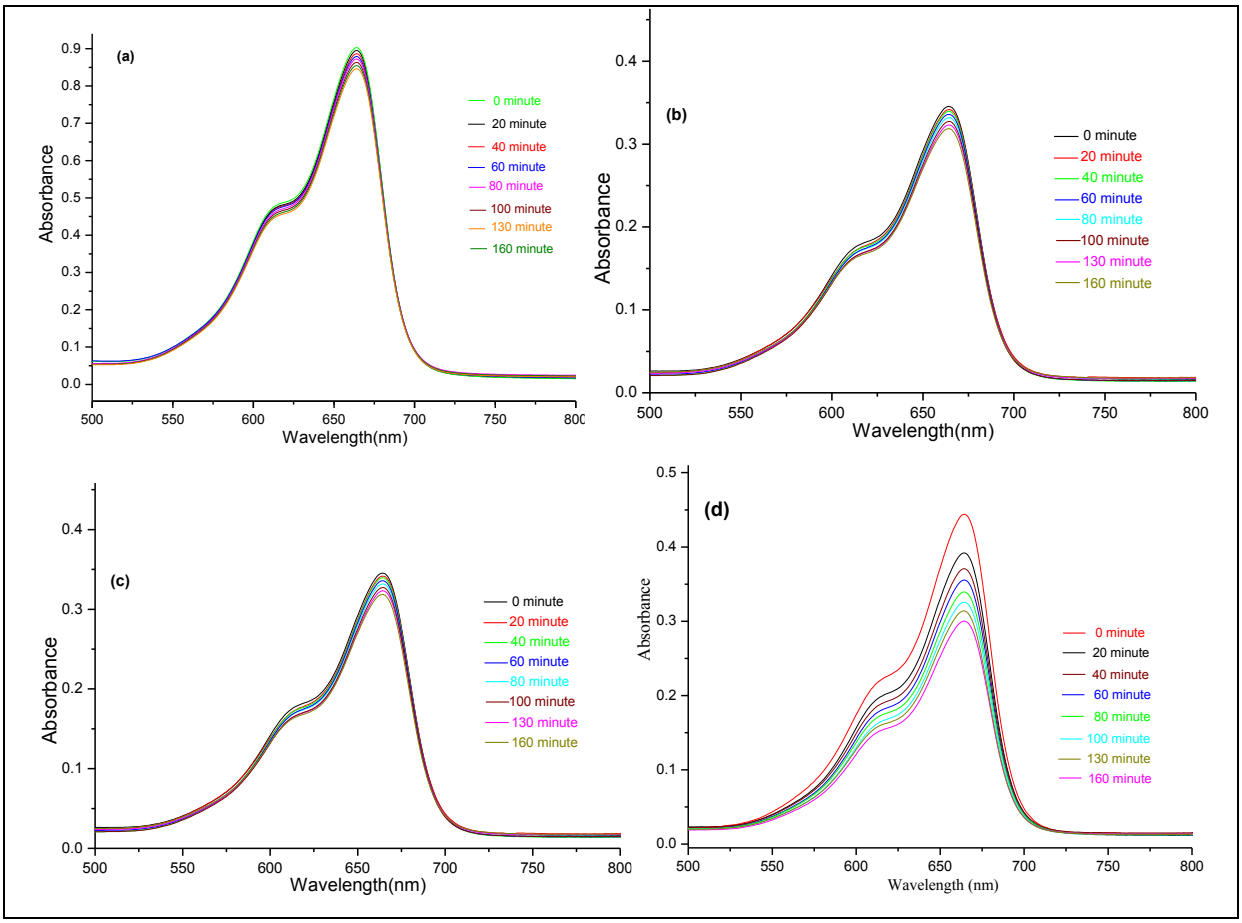

Figure 6.22: Decmposition of MB dye in presence of (a) UV-light (b) ligand **1a** (c) ligand **1b** (d) co-ordination polymer **CP1**

After certain time intervals (20 minute), UV-spectra was recorded to determine the amount of MB. Absorbance was recorded *vs* wavelength for each samples at different intervals of time (Figure 6.22 and 6.23). The intensity of absorption peaks of MB (609 nm and 668 nm),

decreased with time which confirmed the degradation of MB. The degradation process was monitored for 160 minutes for each sample.

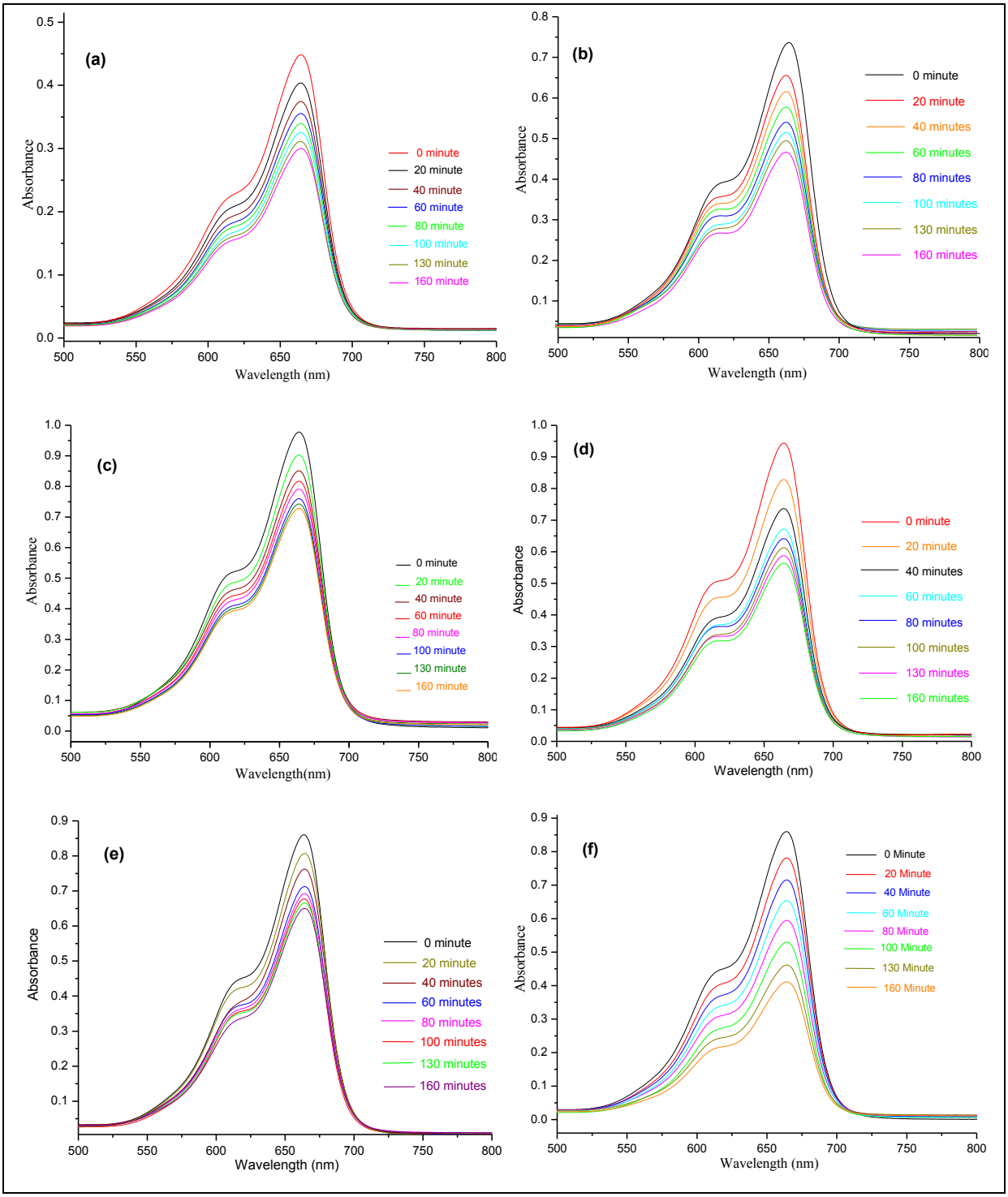

Figure 6.23: Decmposition of MB dye in presence of co-ordination polymer (a) **CP2** (b) **CP3** (c) **CP4** (d) **CP5** (e) **CP6** (f) **CP7**

During the photo-catalysis reactions, in the catalyst, electron is transferred from the highest occupied molecular orbital (HOMO) to the lowest unoccupied molecular orbital (LUMO) in the presence of UV-light. The HOMO is mainly contributed by 2p bonding orbitals of oxygen or nitrogen of ligand **1a** and **1b** (valance band) and LUMO is the empty Cu(II) d-orbitals (conduction band). On UV-light (photo excitation) exposure, charge/electron transfer takes place from oxygen or nitrogen of ligand **1a** and **1b** to Cu(II).[17] The electron is captured from water molecules and converted it into the free radical (·OH), very reactive species, this free radical, ·OH cleaved MB effectively (Figure 6.24).[18]

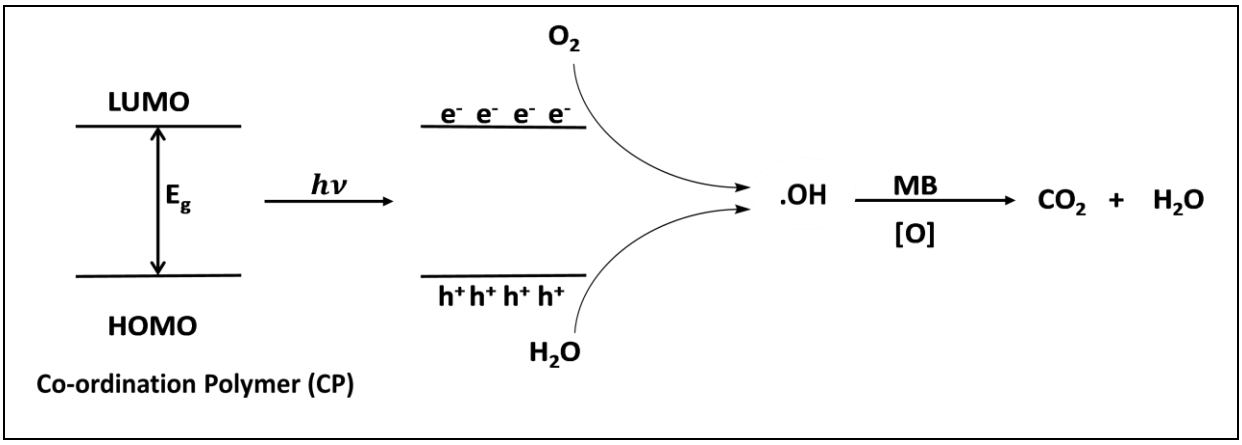

Figure 6.24: Schematic showing Photo degradation of MB using co-ordination polymer.

Further, the percentage decomposition of MB *vs* time also plotted to compare photo-catalytic activity of free ligands and the co-ordination polymers (CPs). The percentage decomposition of MB after 160 minutes in presence of UV - light is 6.21 % while in visible light it 3.8 %. For free ligand **1a** and **1b,** it is nearly same equal to 7.88 % and 7.90 % , respectively. The percentage decomposition of MB was 31.89 % for **CP1** and 33.74 % for **CP2**, (Figure 6.25) both the CPs have same composition except the anion; means the anion perchlorate increases the photo-catalytic activity.

The co-ordination polymer of Cu(II) **CP3** decomposed 36.52 % of MB while Cd(II) **CP4** decomposed 25.76 % ; both having same anion perchlorate, differ by metal ion. Thus Cu(II) co-ordination polymer have more photocatalytic activities than Cd(II) co-ordination polymers. Both **CP5** and **CP6** were Cu(II) co-ordination polymers decomposed 40.25 % and 23.72 % of MB. Thus again their photocatalytic activity was anion dependent, co-ordination polymer **CP5** have pechlorate anion good photocatalyst than **CP6** having sulphate anion.

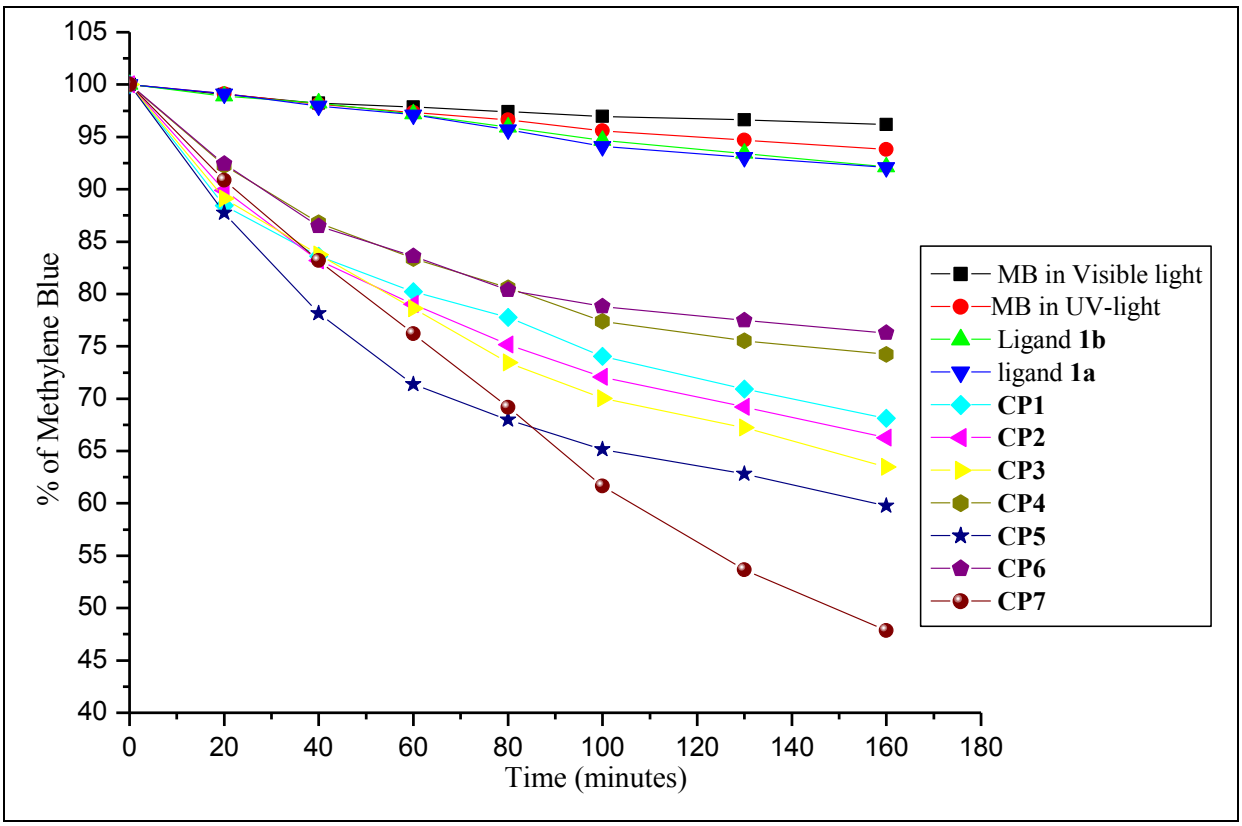

Figure 6.25: Percentage (%) decomposition of MB.

The co-ordination polymer **CP7** having hightest photo-catalytic activity among all co-ordination polymers , decomposed 52.15 % of MB in 160 minutes time period. This may be because **CP7** has two types of organic ligands; ligand **1b** and the benzoate anion which acts as chelating ligand and occupies two position of octahedra, may increases its photo-catalytic activity. Thus all these co-ordination polymers can be used as photo-catalyst in degradation of other organic dyes: Rodahamein, Methylene Orange (MO) *ect.*, which are acting as organic water pollutants.

6.3 References

[1] Wang, X.-L.; Luan, J.; Sui, F.-F.; Lin, H.-Y.; Liu, G.-C.; Xu, C. *Cryst. Growth Des.* **2013,** *13* (8), 3561-3576.

[2] Gong, Y.; Li, J.; Qin, J.; Wu, T.; Cao, R.; Li, J. *Cryst. Growth Des.* **2011,** *11* (5), 1662-1674.

[3] Rajput, L.; Biradha, K. *New J. Chem.* **2010**, *34* (11), 2415-2428.

[4] LIN, H.; LU, H.; LE, M.; LUAN, J.; WANG, X.; LIU, G. *J. Chem. Sci.* **2015**, *127* (7), 1275-1285.

[5] Uemura, K.; Kitagawa, S.; Kondo, M.; Fukui, K.; Kitaura, R.; Chang, H.-C.; Mizutani, T. *Chem. Eur. J.* **2002**, *8* (16), 3586-3600.

[6] Wang, H.; Cheng, F.; Zou, C.; Li, Q.; Hua, Y.; Duan, J.; Jin, W. *CrystEngComm* **2016**, *18* (30), 5639-5646.

[7] Zheng, S.-L.; Yang, J.-H.; Yu, X.-L.; Chen, X.-M.; Wong, W.-T. *Inorg. Chem.* **2004**, *43* (2), 830-838.

[8] Zhu, L.; An, Z. *Synth. React. Inorg. Met.-Org. Nano-Metal Chem.* **2016**, *46* (7), 1065-1068.

[9] Wang, X.-L.; Bi, Y.-F.; Lin, H.-Y.; Liu, G.-C. *Cryst. Growth Des.* **2007**, *7* (6), 1086-1091.

[10] Cheng, P.-C.; Kuo, P.-T.; Liao, Y.-H.; Xie, M.-Y.; Hsu, W.; Chen, J.-D. *Cryst. Growth Des.* **2013,** *13* (2), 623-632.

[11] Ma, L.-F.; Wang, L.-Y.; Hu, J.-L.; Wang, Y.-Y.; Yang, G.-P. *Cryst. Growth Des.* **2009,** *9* (12), 5334-5342.

[12] Chen, S.-S.; Zhao, Y.; Fan, J.; Okamura, T.-a.; Bai, Z.-S.; Chen, Z.-H.; Sun, W.-Y. *CrystEngComm* **2012**, *14* (10), 3564-3576.

[13] Cui, Y.; Yue, Y.; Qian, G.; Chen, B. *Chem. Rev.* **2012**, *112* (2), 1126-1162.

[14] Zhang, H.; Liu, G.; Shi, L.; Liu, H.; Wang, T.; Ye, J. *Nano Energy* **2016**, *22*, 149-168.

[15] Mahata, P.; Madras, G.; Natarajan, S. *J. Phys. Chem. B* **2006**, *110* (28), 13759-13768.

[16] Li, D.-X.; Ren, Z.-G.; Young, D. J.; Lang, J.-P. *Eur. J. Inorg. Chem* **2015**, *2015* (11), 1981-1988.

[17] Dai, M.; Li, H.-X.; Lang, J.-P. *CrystEngComm* **2015**, *17* (26), 4741-4753.

[18] Kan, W.-Q.; Liu, B.; Yang, J.; Liu, Y.-Y.; Ma, J.-F. *Cryst. Growth Des.* **2012**, *12* (5), 2288-2298.

[19] Chen, Y.-Q.; Liu, S.-J.; Li, Y.-W.; Li, G.-R.; He, K.-H.; Qu, Y.-K.; Hu, T.-L.; Bu, X.-H. *Cryst. Growth Des.* **2012**, *12* (11), 5426-5431.

[20] Yang, H.; Liu, T.; Cao, M.; Li, H.; Gao, S.; Cao, R., *Chem. Commun.* **2010**, *46* (14), 2429-2431.

[21] Wang, X. L.; Sui, F. F.; Lin, H.Y.; Zhang, J.W .; Liu, G. C. *Cryst. Growth Des.* **2014**, *14* (7), 3438-3452.

[22] Rajput, L.; Singha, S.; Biradha, K. *Cryst. Growth Des.* **2007**, *7* (12), 2788-2795.

[23] Lin, H.; Maggard, P. A. *Inorg. Chem.* **2008**, *47* (18), 8044-8052.

Chapter 7

Rationalization of the Results and Conclusions

7.1 Role of Ligands 1a and 1b in the Formation of CP1 – CP7

The work discussed in chapters 3-5 analyzed the nature of the ligands **1a** and **1b** (Scheme 7.1) and their coordination ability to form flexible CPs. The ligands are equipped with hydrogen bond functionality and amide-to-amide hydrogen bond interactions were present in some networks, while in some cases they were interfered by counter anions and water. In short the co-ordination networks formed by ligand **1a** & **1b** in the present thesis include 1D chain, 1D looped chain, 2D interpenetrated networks.

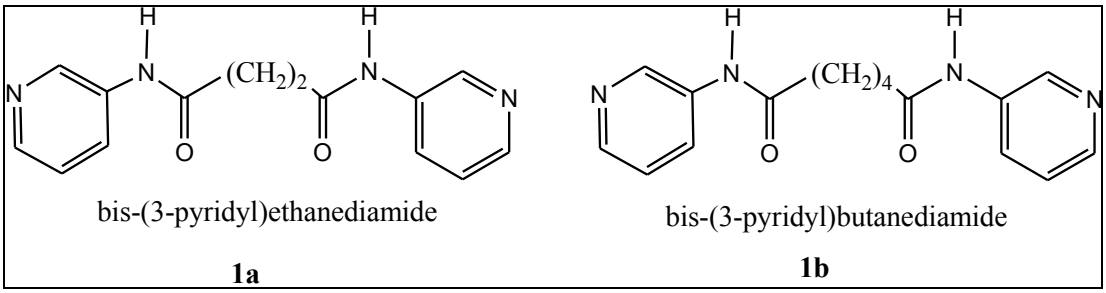

Scheme 7.1: Ligands used in present work

The synthesis of CPs with **1a** and **1b** was carried out with Co(II), Ni(II), Zn(II), Cd(II) and Cu(II) metal salts, but Cu(II) and Cd(II) resulted in formation of crystalline compounds. Out of seven CPs of **1a** and **1b**, which are synthesized for this thesis, six belongs to Cu(II) salts. In this chapter, the rationalization of the results obtained and future outlook of **1a** and **1b** in the preparation of co-ordination polymers have been discussed.

Table 7.1 CPs of ligands **1a** and **1b**

Co-ordination polymers (CPs)	Ligand; Metal salt	Type of Network	Interactions in CPs	Conformation of alkyl spacer
CP1	**1a**; $Cu(PF_6)_2$	1D- Looped Chain with elliptical cavities	C=O•••H (H_2O) and N-H•••F (PF_6^-) shrink the cavity size	*Anti*
CP2a	**1a**; $Cu(ClO_4)_2$	1D-Chain with Nitrobenzene in cavities*	C=O•••H (H_2O) and N-H•••O (ClO_4^-)	*Gauche*
CP2b	**1a**; $Cu(ClO_4)_2$	1D-Chain with Benzonitrile in cavities*	C=O•••H (H_2O) and N-H•••O (ClO_4^-)	*Gauche*
CP2c	**1a**; $Cu(ClO_4)_2$	1D-Chain with p-Xylene in cavities*	C=O•••H (H_2O) and N-H•••O (ClO_4^-)	*Gauche*
Apohost CP2	**1a**; $Cu(ClO_4)_2$	1D-Chain without any guest molecules*	C=O•••H (H_2O) and N-H•••O (ClO_4^-)	*Gauche*

CP3	**1b**; $Cu(ClO_4)_2$	Two-fold parallel interpenetration of (4,4) corrugated layers	β-sheet hydrogen bonding (amide-to-amide), form 2D layers	*Gauche-Anti-Gauche*
CP4	**1b**; $Cd(ClO_4)_2$	1D-chain with rectangular loops	π•••π interactions, C=O•••H (H_2O) and N-H•••O (ClO_4^- anion)	*Anti-Anti-Anti*
CP5	**CP4**; $Cu(NO_3)_2$	1D-chain with rectangular loops*	π•••π interactions, C=O•••H (H_2O) and N-H•••O (ClO_4^- anion)	*Anti-Anti-Anti*
CP6	**1b**; $CuSO_4$	1D looped chain with rectangular cavities	π•••π interactions, N-H•••O(SO_3^{2-}) hydrogen bonding interactions to form layers	*Anti-Anti-Gauche*
CP7	**1b**; $Cu(C_6H_5COO)_2$	simple 1D chain arranged in criss-cross fashion	N-H•••O(CO^-) hydrogen bonding interactions to form layers	*Anti-Anti-Anti*

***** Crystal structure couldn't be confirmed by single crystal XRD. The powder XRD suggested the mentioned structure.

7.2 Effect of Hydrogen Bonding in Assembling the Coordination Networks

Both the ligands **1a** & **1b** have two amide functional groups in their backbone, responsible for amide-to-amide hydrogen bonding. In case of co-ordination polymer **CP3**, the β-sheet hydrogen bonding is present throughout the network and is not affected by counter anions (*i.e.* ClO_4^-) and water molecules. In some CPs, self-complementary amide-to-amide hydrogen bondings disturbed by counter anions, guest molecules. In co-ordination polymer **CP1**, anion PF_6^- involved in hydrogen bonding simultaneously with two N-H of same loop and resulted interference in self complementary amide-to-amide hydrogen bonding. The co-ordination polymer **CP4**, within the loop self-complementary hydrogen bonding present called intra-chain hydrogen bonding while the adjacent chains are held together *via* hydrogen bonding between the amide N-H…O(ClO_3^-) and amide C=O and water. The intra-chain hydrogen bonding is responsible for network stability and metal exchange led to the formation of co-ordination polymer **CP5**. In co-ordination polymer **CP6**, the SO_4^{-2} anion involved in hydrogen bonding and the 1D-looped chains are arranged in an offset fashion *via* N-H…..O(SO_3^{-2}) hydrogen bonding interactions to form 2D layers. Further each 2D-layer stacked upon one another *via* SO_4^{-2} and N-H, C=O and H_2O to extend the network in 3D. In

the co-ordination polymer **CP7**, the 1D-chains packed *via* N-H….O(CO^-) hydrogen bonding interactions and form layers.

7.3 Effect of Counter Anions on Network Stability of Co-ordination Polymers (CPs)

In chapter 3 and 5 we have discussed the effect of counter anion on network geometry of co-ordination polymers. The counter anions used; PF_6^-, ClO_4^-, SO_4^{-2}, $C_6H_5COO^-$ influenced the occurrence of amide-to-amide hydrogen bonds in the co-ordination polymers of Cu(II). The interference in amide-to-amide hydrogen bond formation by the counter anions was observed to be more in case of PF_6^- anions compared to the other anions. In case of PF_6^-, the N-H···F hydrogen bond is stronger than the N-H···O (amide-to-amide) hydrogen bond. Hence the interference in the amide-to-amide hydrogen bonds could be occurred more frequently in the complexes of PF_6^- anions. Whereas the strengths of N-H···O(amide), N-H···O(ClO_3^-) hydrogen bonds are almost similar and hence the interference of anion found to be relatively less in case of ClO_4^- anions as discussed in chapter 3. The SO_4^{-2} and $C_6H_5COO^-$ are acting as co-ordinating anions and involved in network formation while ClO_4^- is a non-co-ordinating anion, present in the cavities of networks. The SO_4^{-2} co-ordinated to Cu(II) in mono-dentate fashion, while the $C_6H_5COO^-$ co-ordinated as chelating ligand and occupy two co-ordinating sites of Cu(II). Thus anions SO_4^{-2} and $C_6H_5COO^-$ interfered in amide-to-amide hydrogen bonding because the N-H of amide involved in hydrogen bonding with SO_4^{-2} (*i.e.* N-H….O(SO_3^{-2}) in **CP6** and with $C_6H_5COO^-$ (*i.e.* N-H….O(CO^-) in case of **CP7** co-ordination polymers. The anions of same geometry (tetrahedral *i.e.* ClO_4^-, SO_4^{-2}) but different size and charges showed their effect on the overall supramolecular structure of the CPs. The competitive and anion exchange reactions confirmed the binding order and networks stability in presence of different anions.

7.4 Effect of Alkyl Spacer Conformation on Co-ordination Polymers (CPs)

The flexibility of alkyl spacer is foremost structure directing factor in co-ordination polymers. We have discussed in chapter 3, the ethyl spacer of ligand **1a** attuned its conformation on requirement *i.e.* anion exchange and guest inclusion. In co-ordination polymer **CP1**, the functional group amide involved in hydrogen bonding with anion PF_6^- *i.e.* N-H….F (PF_6^-) and ethyl spacer has *anti* conformation and shrinks the cavity, cannot accommodate the aromatic guest molecules. On anion exchange, the ethyl spacer have *gauche* conformation, swell the cavity and accommodate the aromatic guest molecules in co-

ordination polymers **CP2a, CP2b, CP2c** and anion ClO_4^- not involved in hydrogen bonding. In Cu(II) co-ordination polymer **CP3** the butyl spacer has *Gauche-Anti-Gauche* conformation whereas in case of Cd(II) co-ordination polymer **CP4** has *Anti-Anti-Anti* conformation, butyl spacer change its conformation on requirement of metal centre. In case of co-ordination polymer **CP6**, the butyl spacer having *Anti-Anti-Gauche* conformation while in **CP7** has *Anti-Anti-Anti* conformation. Thus we observed that the butyl spacer change it's conformation on requirement of bigger size co-ordinated SO_4^{-2} anion in **CP6** and chelating benzoate anion in **CP7.**

7.5 Effect of Metal centre in assembling of Co-ordination Polymers (CPs)

In chapter 4 we have discussed that the metal centre also plays essential role while assembling the co-ordination polymers. The ligand **1b** form two different co-ordination polymers **CP3** and **CP4** with Cu(II) and Cd(II) respectively although other conditions - temperature, pressure, solvent, anion ClO_4^-, metal to ligand ratio kept similar throughout the reaction. Thus metal ion is the structure directing in co-ordination polymers **CP3** which is perpendicular interpenetrated 2D network of (4,4)-topology and **CP4** is 1D-chain with rectangular loops. The smaller size Cu(II) is responsible for interpenetration of network while in case of the Cd(II) the ligand **1b** stretched to maximum length and form 1D looped chains.

7.6 Future Scope of Present Works

- Novel network yet to be realised.

  The ligands *bis*-pyridyl-*bis*-amides and reverse *bis*-pyridyl-*bis*-amides, although explored to a great extent, are capable of forming novel architectures by tuning the reaction conditions. Many geometries of 2D (Bilayer, Honeycomb) and 3D networks of these ligands are not much explored.

- CPs with other transition metals, lanthanides and actinides can be explored.

  Present work mentioned the CPs of Cu(II) and Cd(II). The other transition metals- Ni(II), Co(II), Zn(II) can also be used for CP synthesis. As lanthanides show interaeting fluorescent, its CPs can be explored for various photophysical applications.

- CPs with other ligands like carboxylates and other pyridyl based ligands along

with bis pyridyl bis amides can be explored further which can show novel geometries and various non covalent interactions.

- Application based on porous nature of CP can be explored.

  The co-ordination polymers synthesized by us are porous in nature. We have studied the photo-catalytic degradation of Methylene Blue (MB) using our CPs in UV – light. But many other applications based on photo physical properties and gas storage yet to be explored.

- Synthesis of disulphonamide ligands (analogous of diamides) and the hydrogen bonding patterns in their structure can be studied.

Appendices

Figure A1: IR Spectra of ligand **1a**

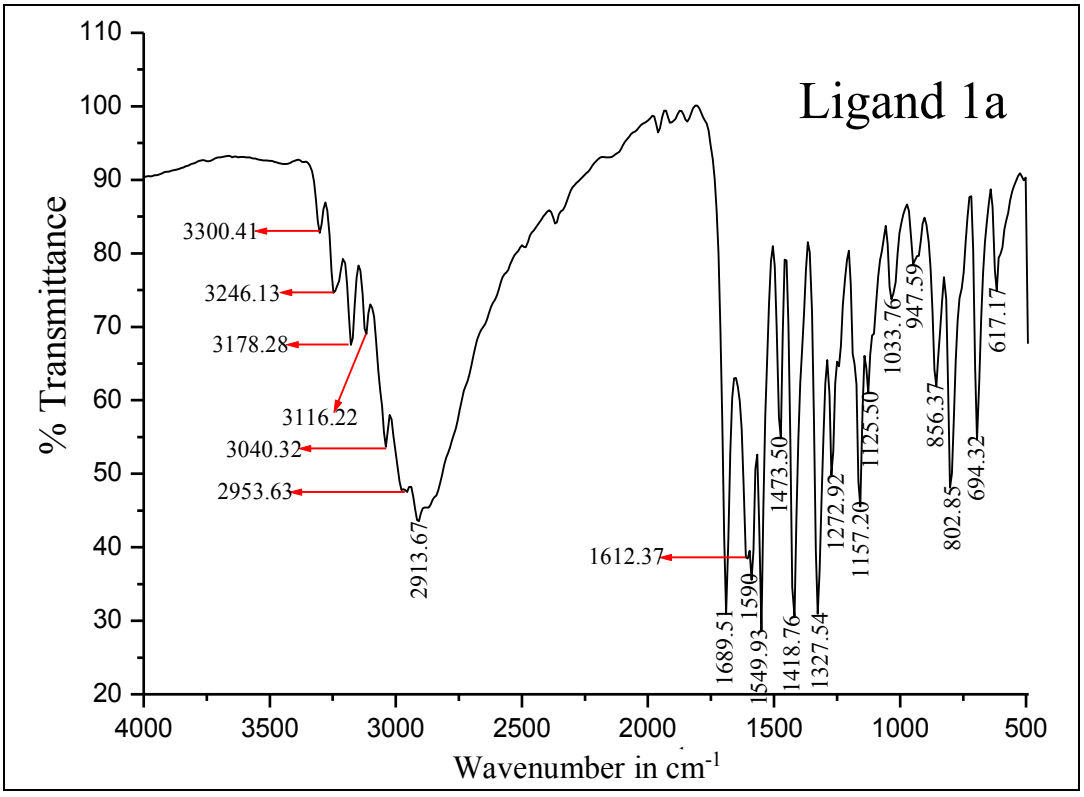

Figure A2: IR Spectra of Co-ordination Polymer **CP1**

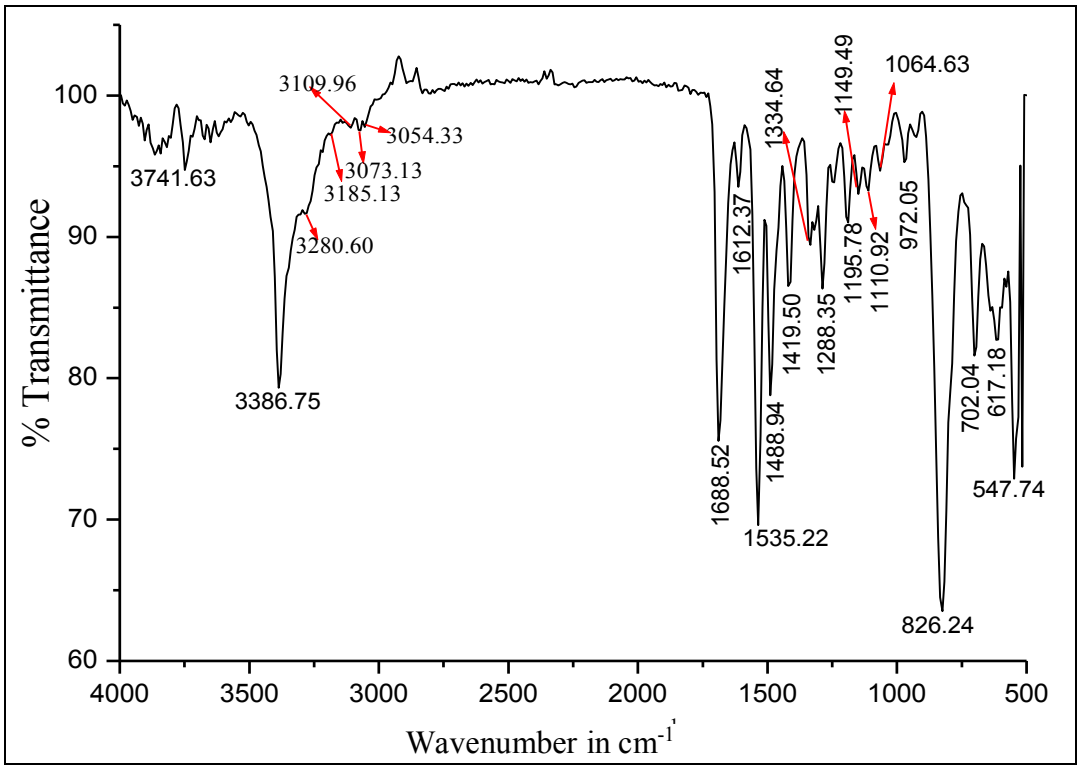

Figure A3: PXRD of Co-ordination Polymer **CP1**

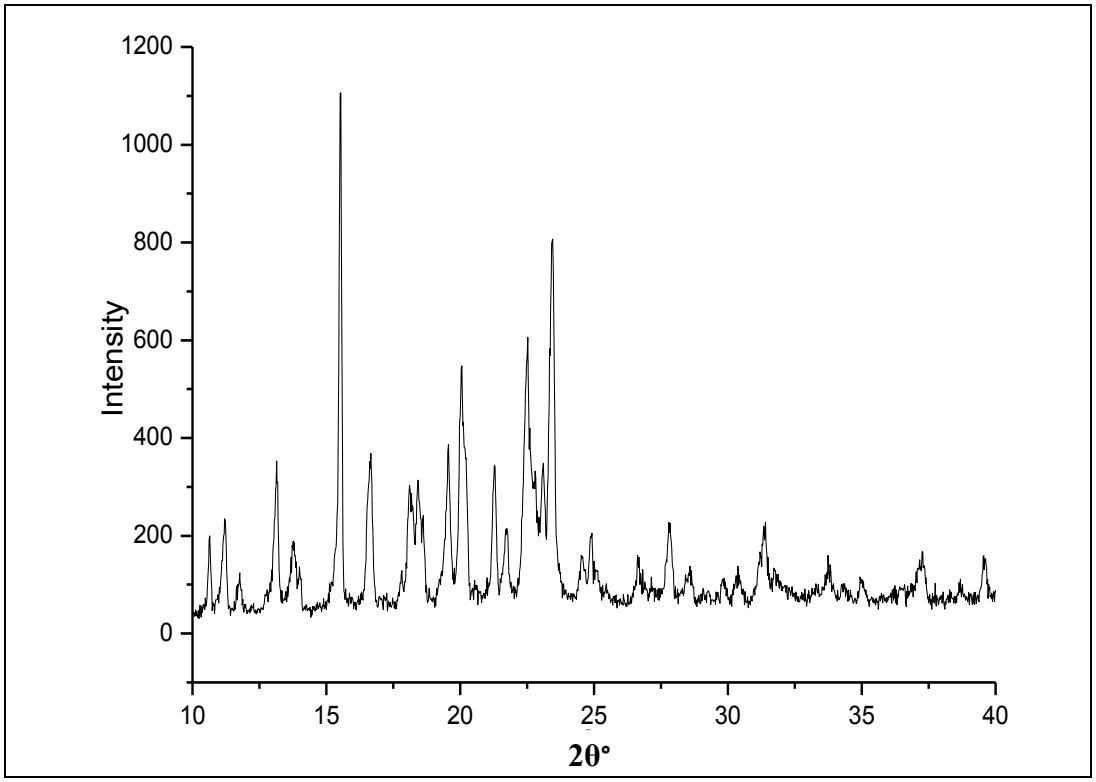

Figure A4: IR Spectra of Co-ordination Polymers **CP2a**

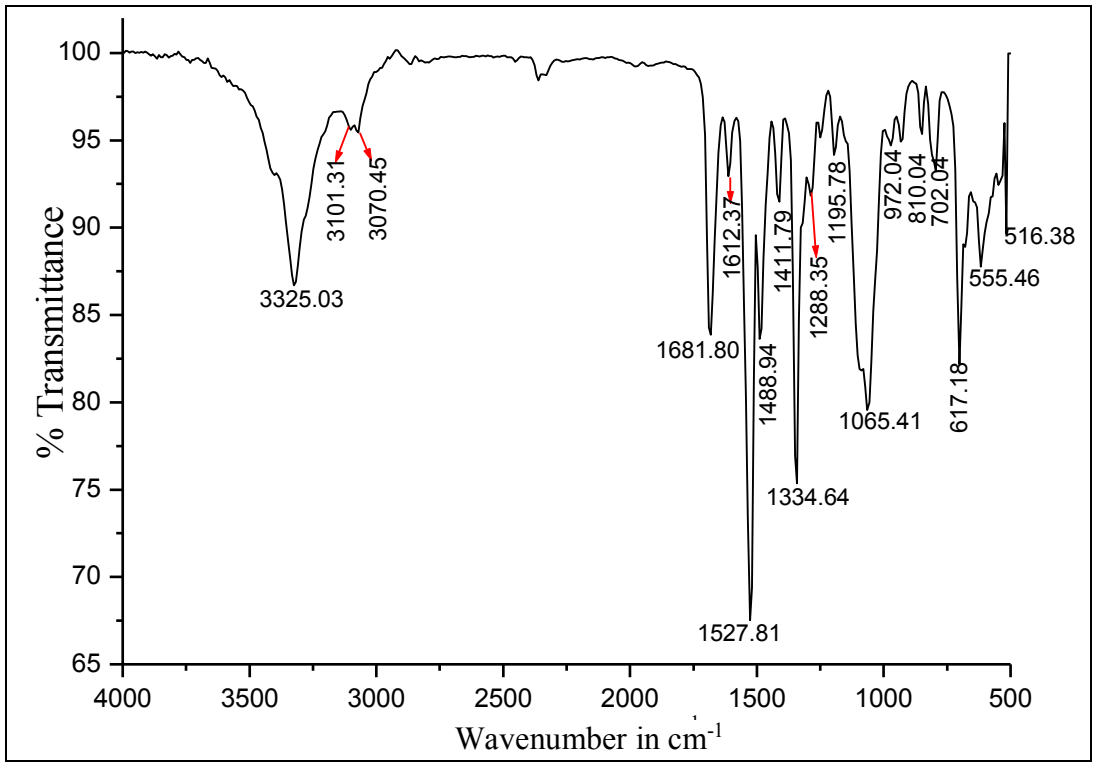

Figure A5: PXRD of Co-ordination Polymer **CP2a**

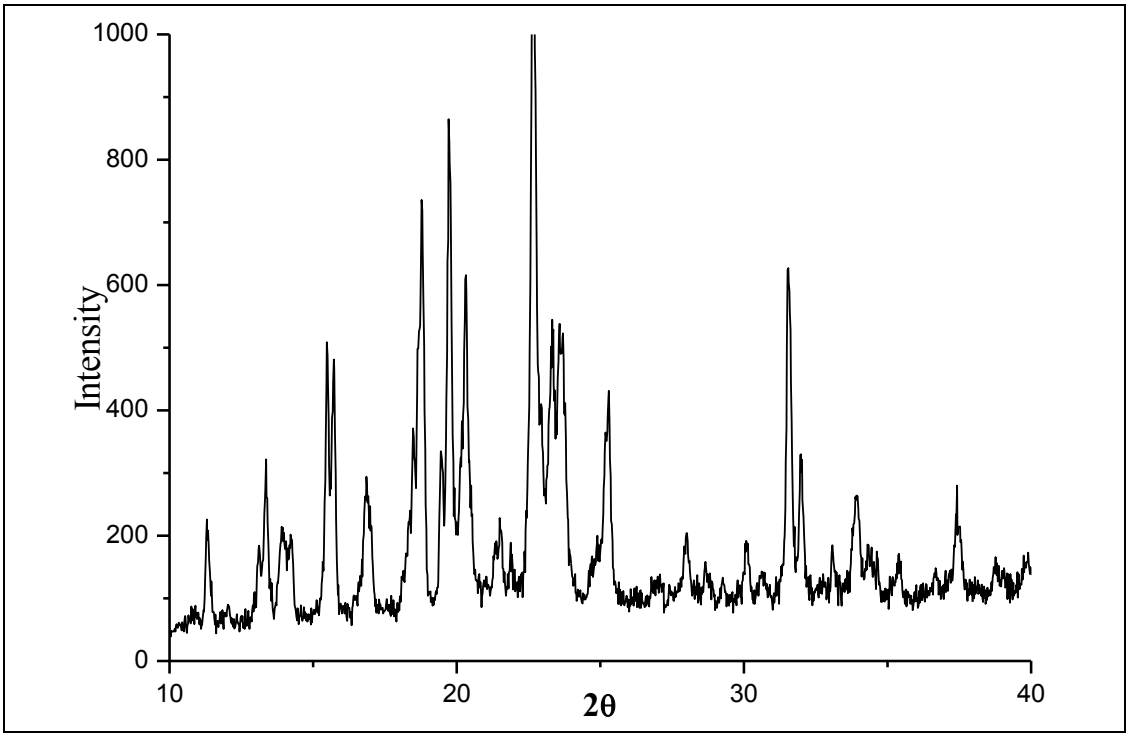

Figure A6: IR Spectra of Co-ordination Polymer **CP2b**

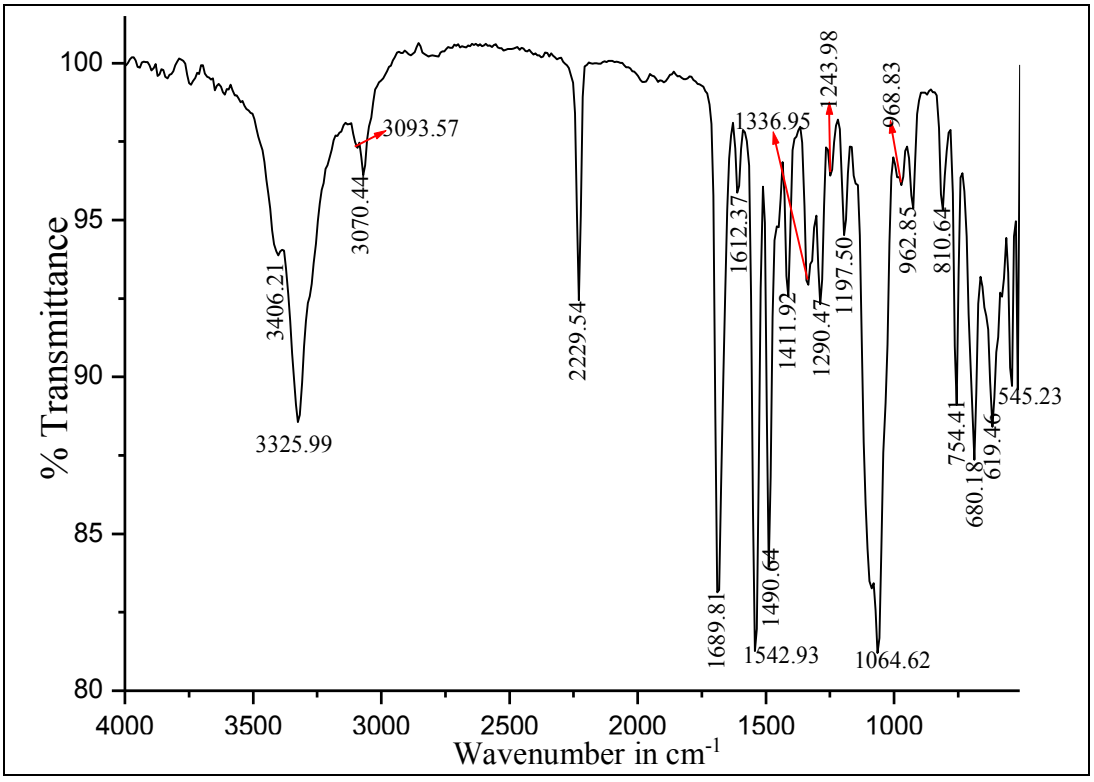

Figure A7: PXRD of Co-ordination Polymer **CP2b**

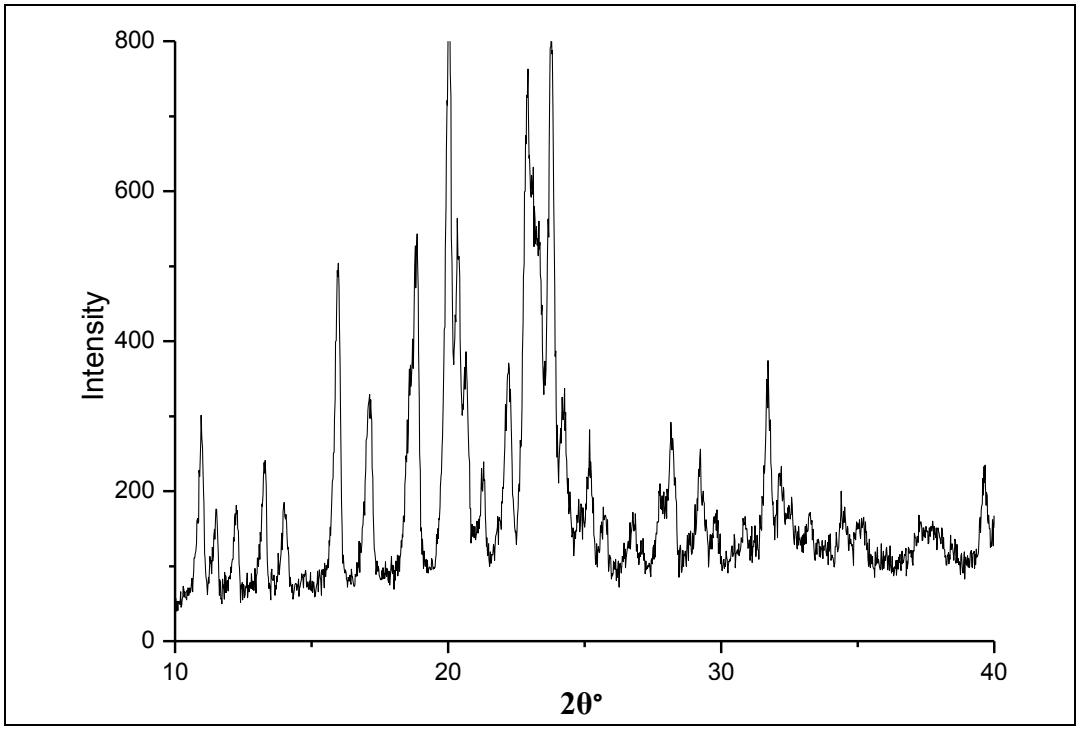

Figure A8: IR Spectra of Co-ordination Polymer **CP2c**

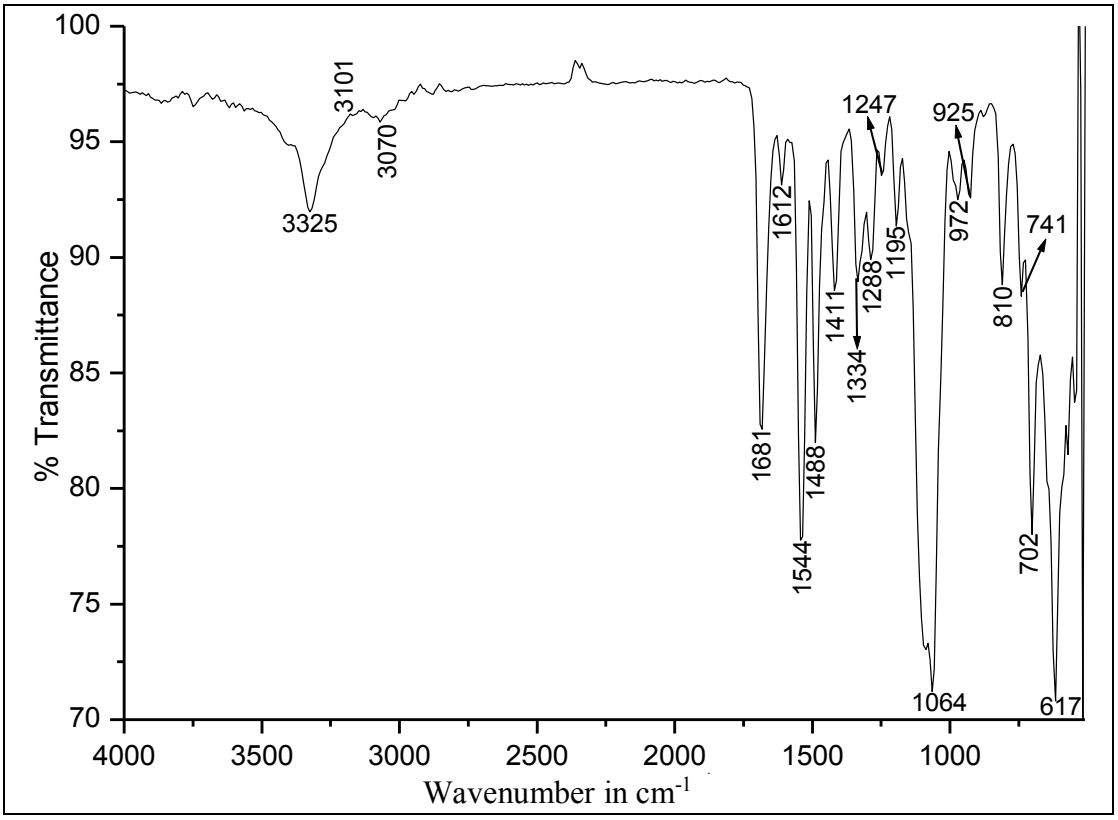

Figure A9: PXRD of Co-ordination Polymer **CP2c**

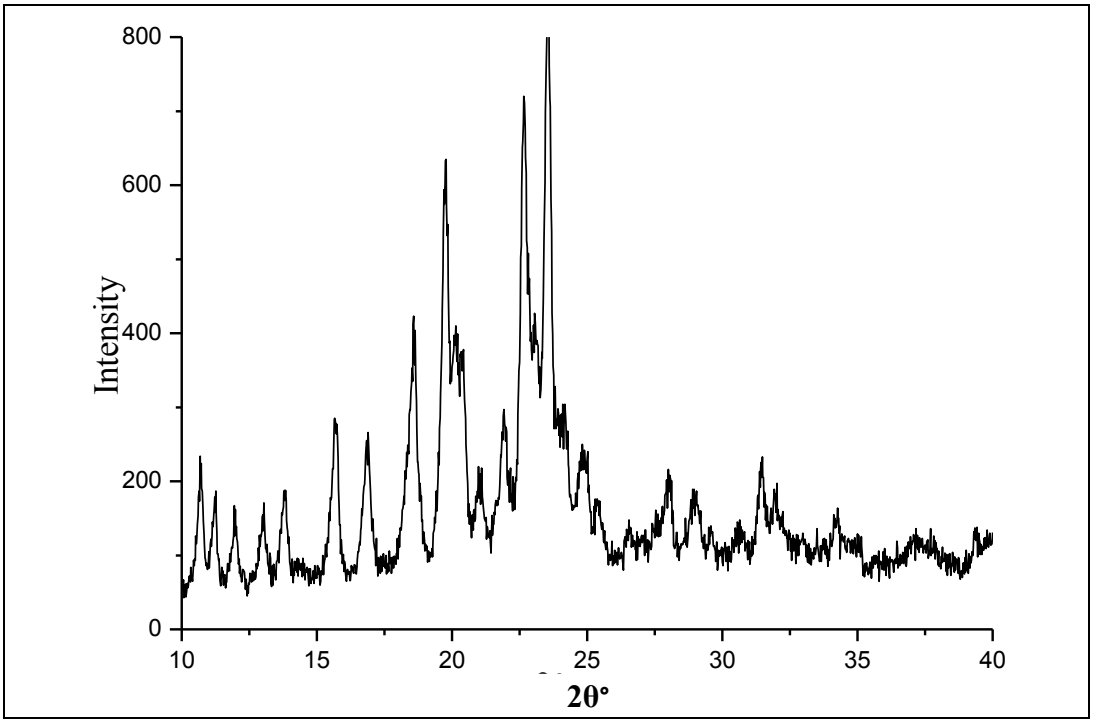

Figure A10: FT-IR Spectra of Co-ordination Polymer **Apohost CP2**

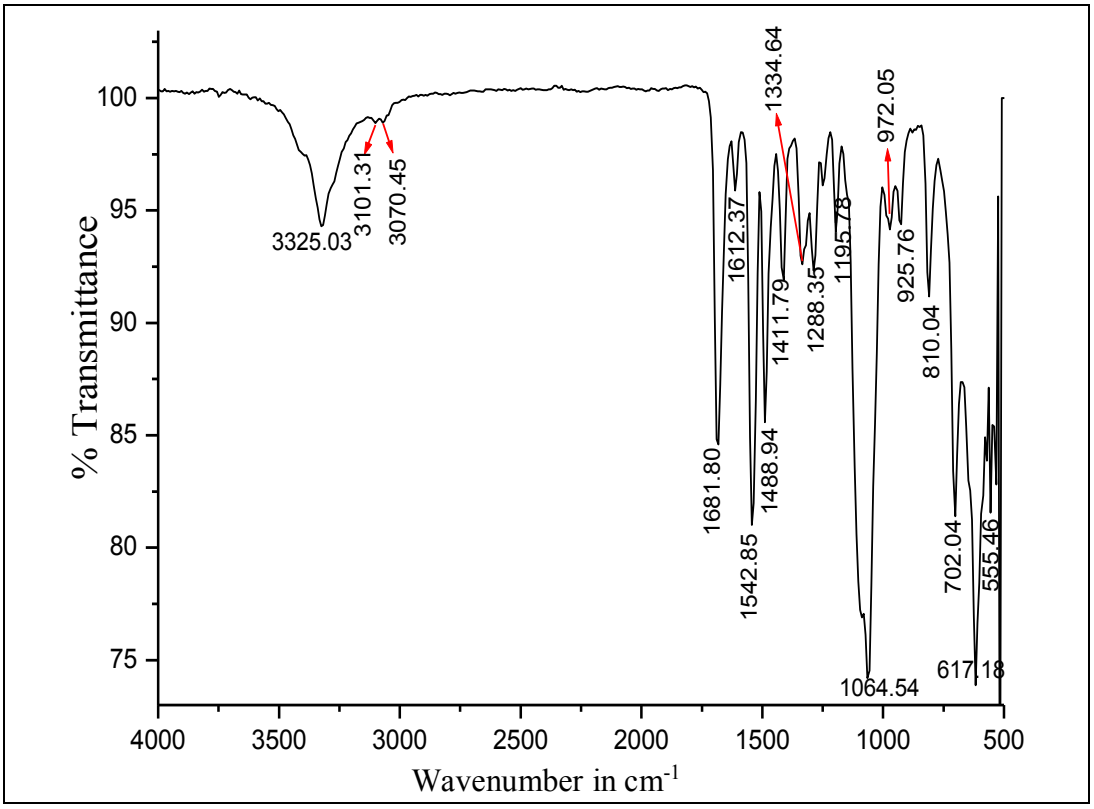

Figure A11: PXRD of Co-ordination Polymers **Apohost CP2**

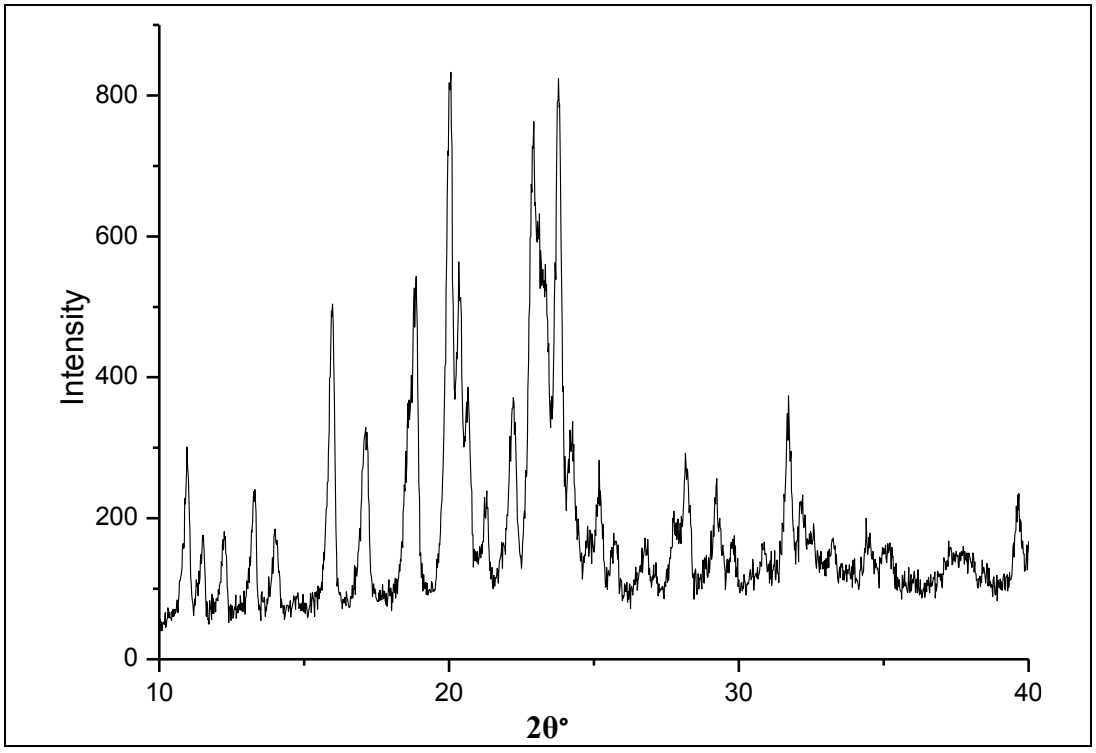

Figure A12: IR Spectra of Co-ordination Polymers **CP2a** after Anion Exchange

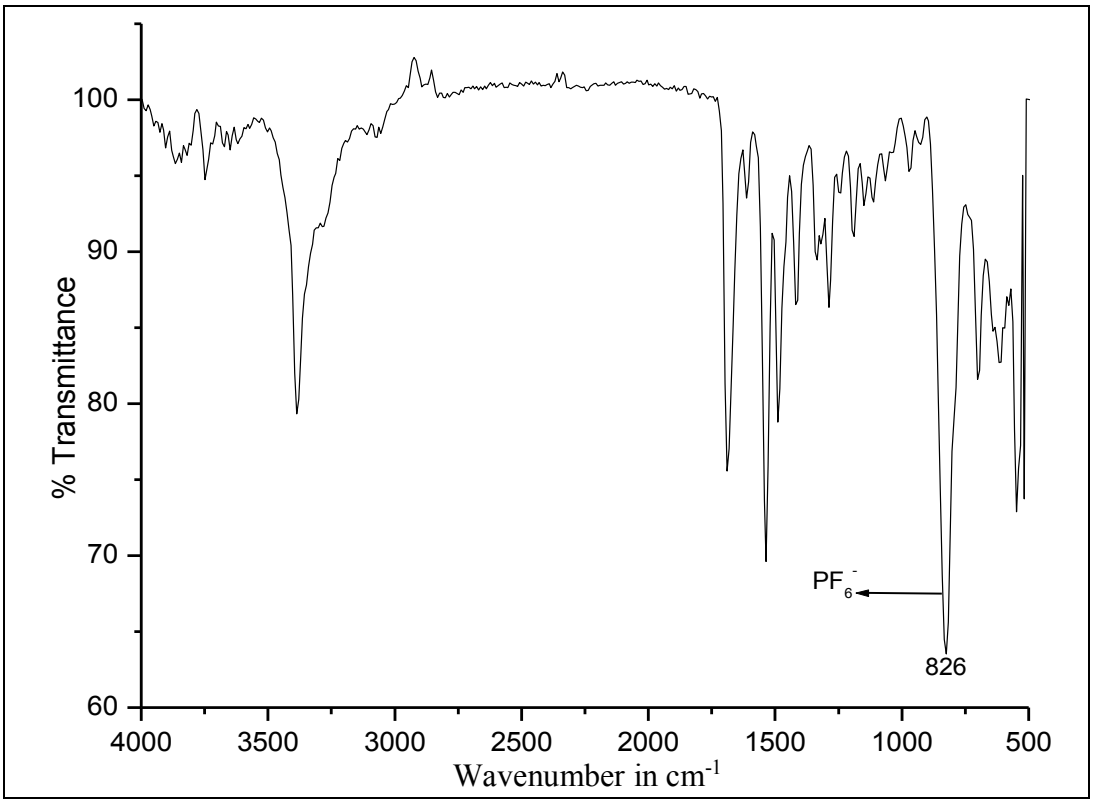

Figure A13: IR Spectra of Co-ordination Polymer **CP2b** after Anion Exchange

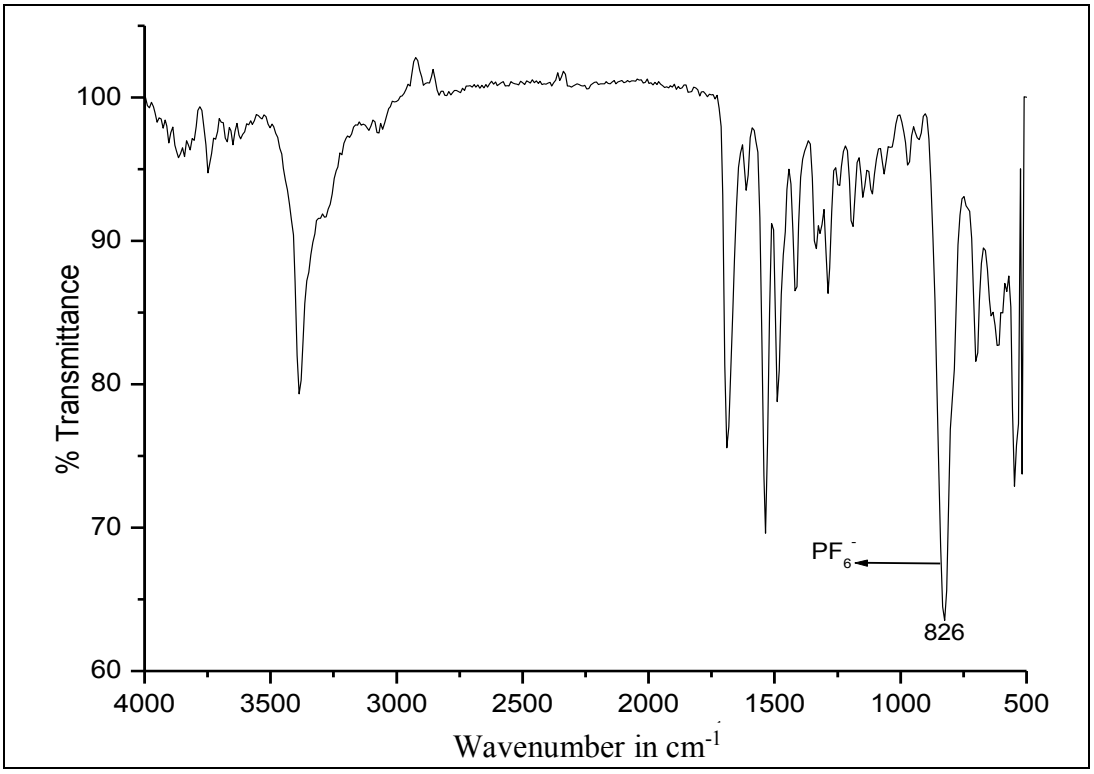

Figure A14: IR Spectra of Co-ordination Polymer **CP2c** after Anion Exchange

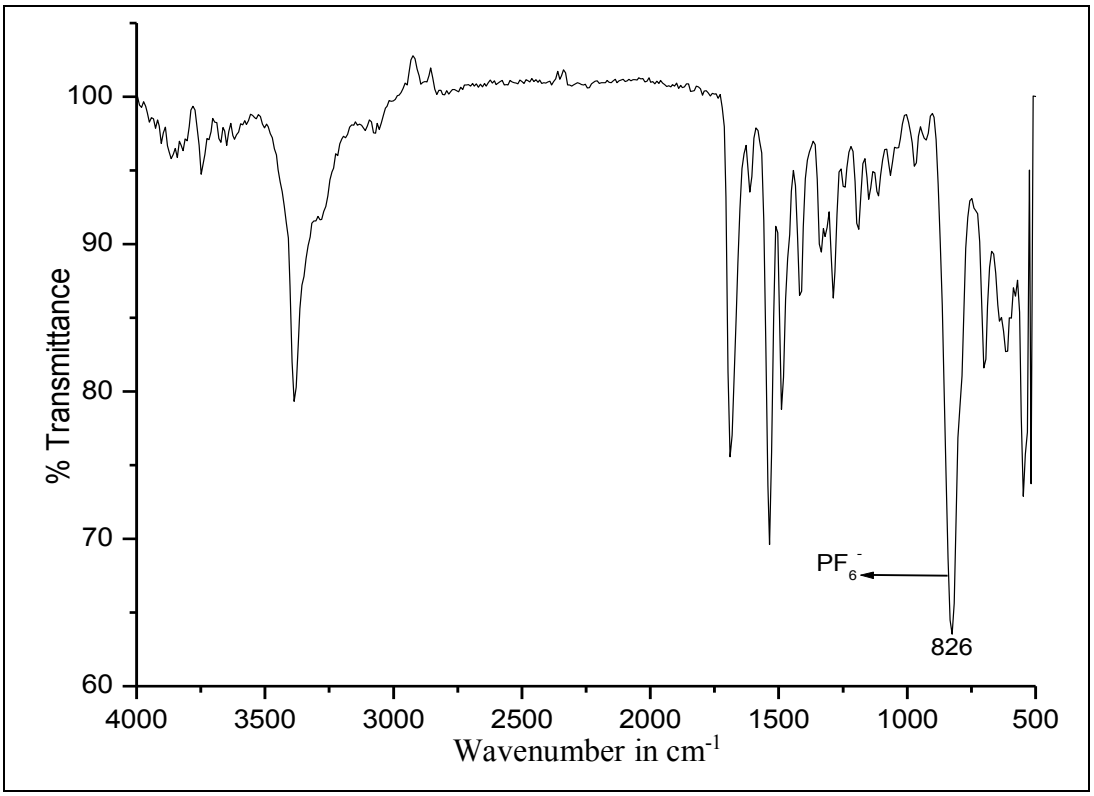

Figure A15: PXRD of Co-ordination Polymer **CP2a** after Anion Exchange

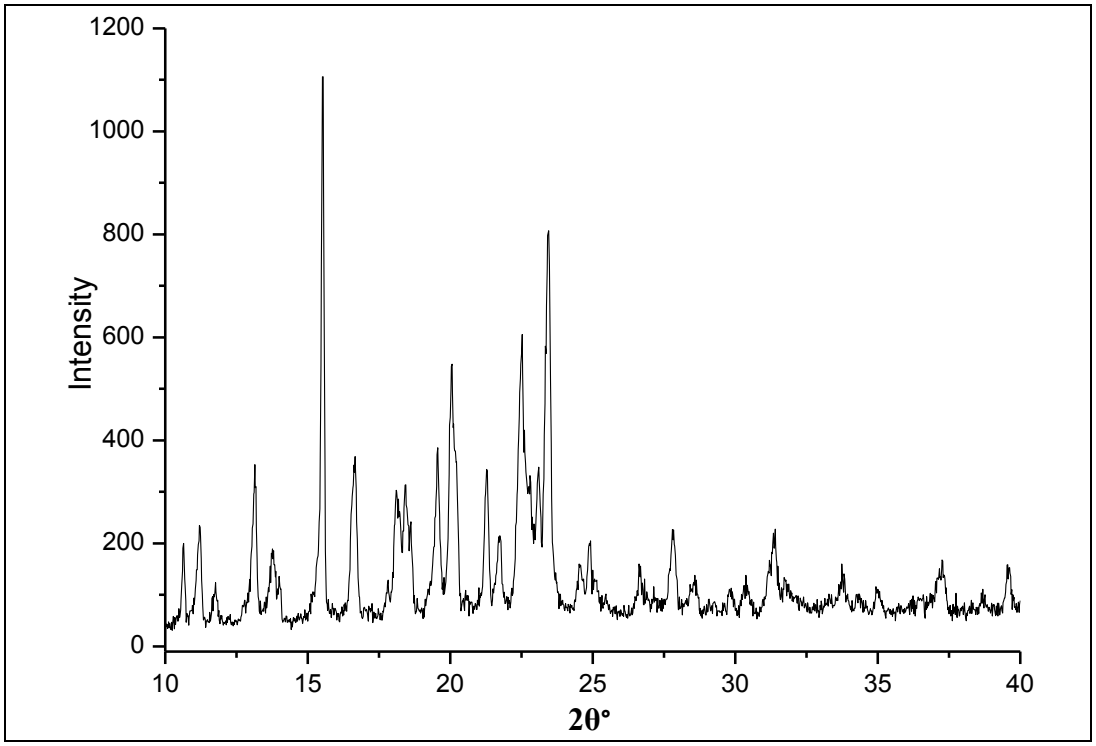

Figure A16: PXRD of Co-ordination Polymer **CP2b** after Anion Exchange

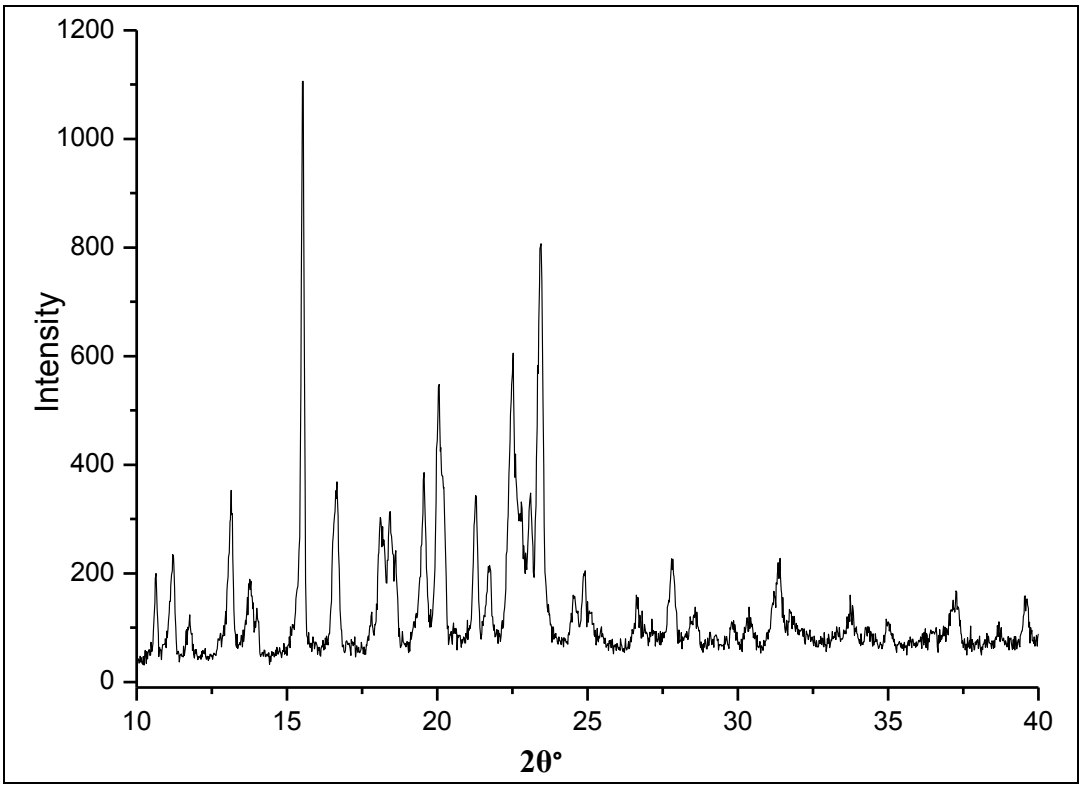

Figure A17: PXRD of Co-ordination Polymer **CP2c** after Anion Exchange

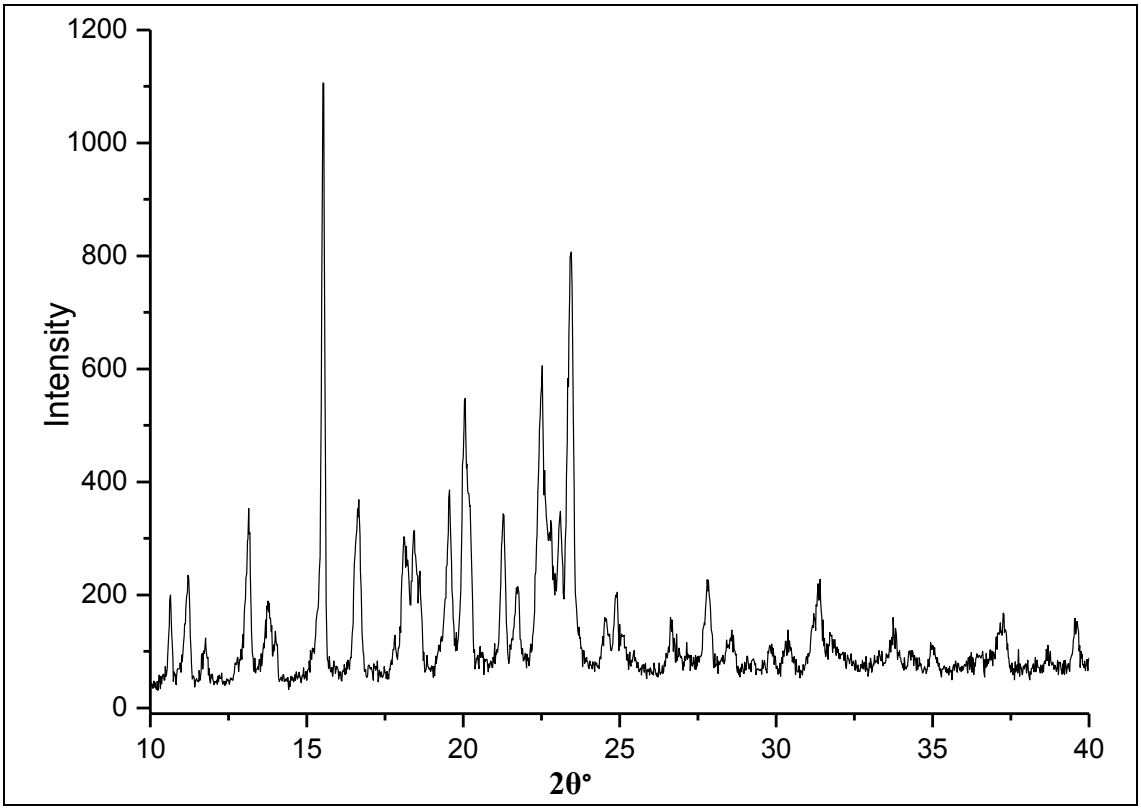

Figure A18: ORTEP of Co-ordination Polymer **CP1**

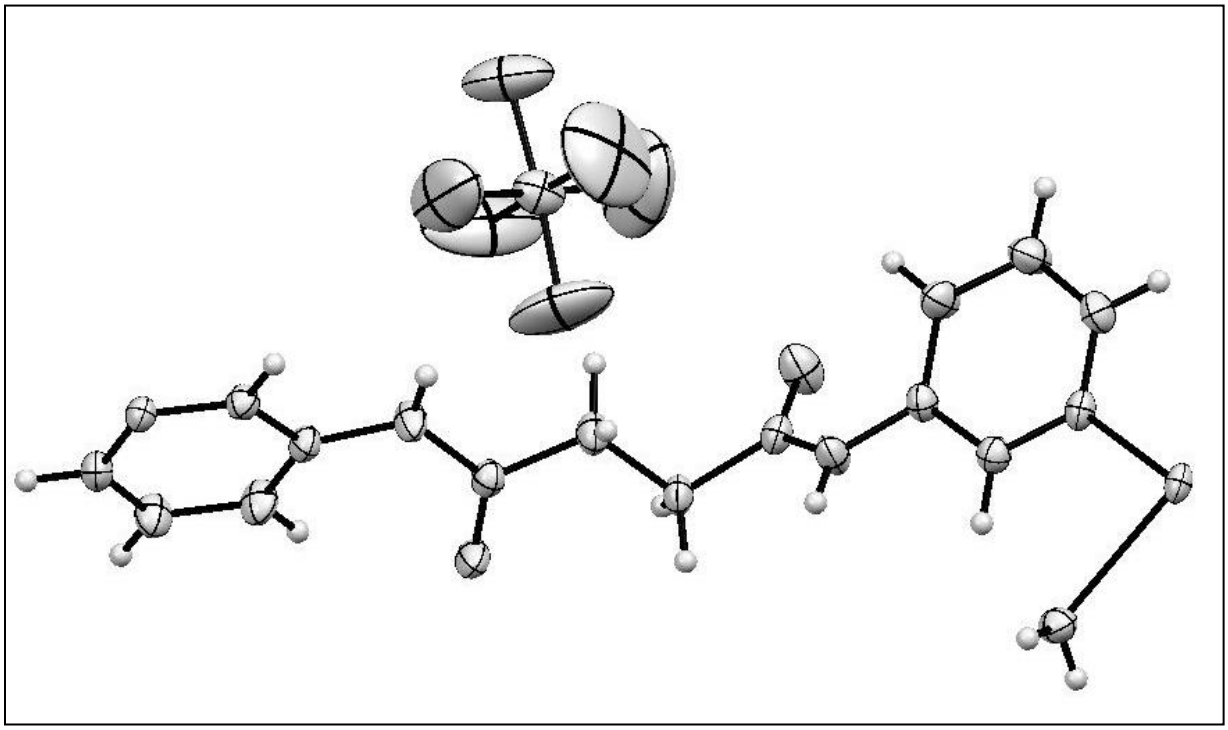

Figure A19: IR Spectra of Ligand **1b**

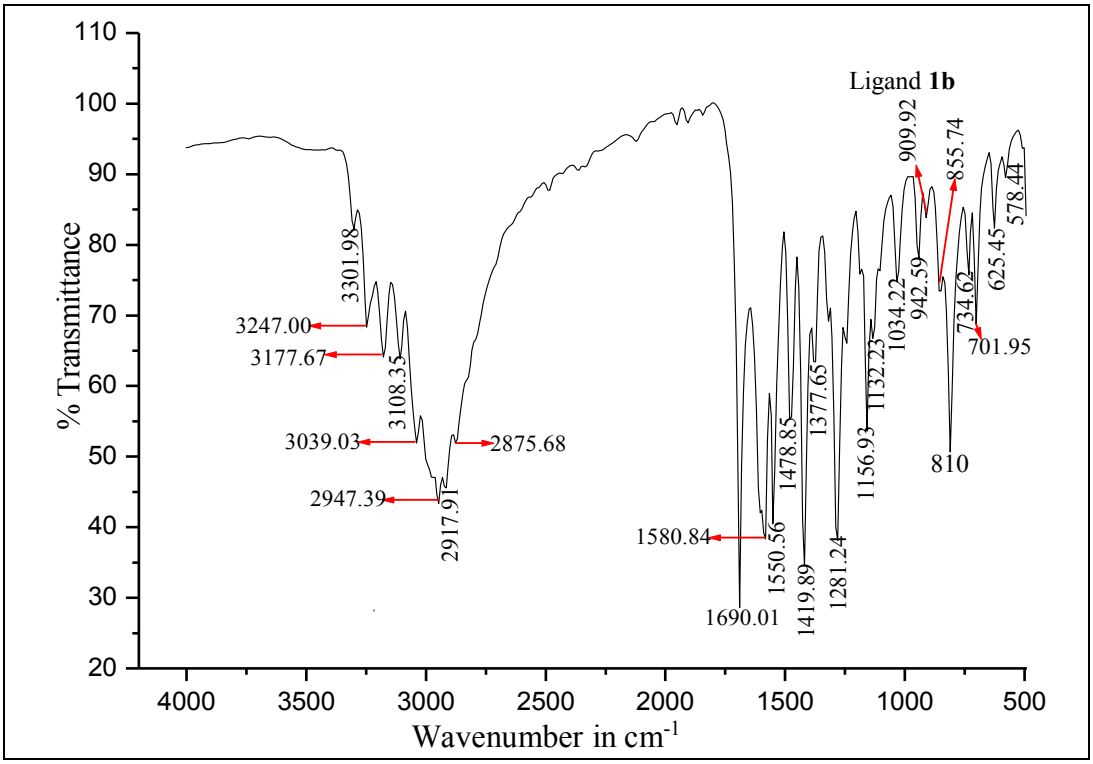

Figure A20: IR Spectra of Co-ordination Polymer **CP3**

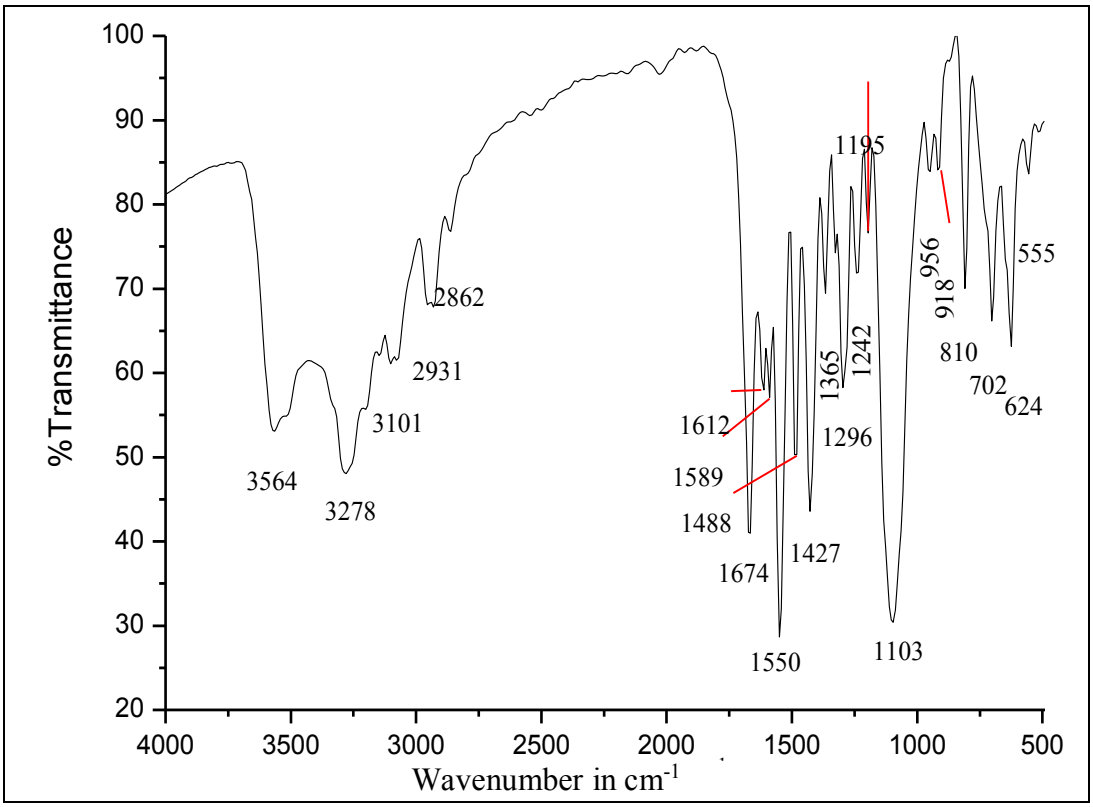

Figure A21: PXRD of co-ordination polymer **CP3**

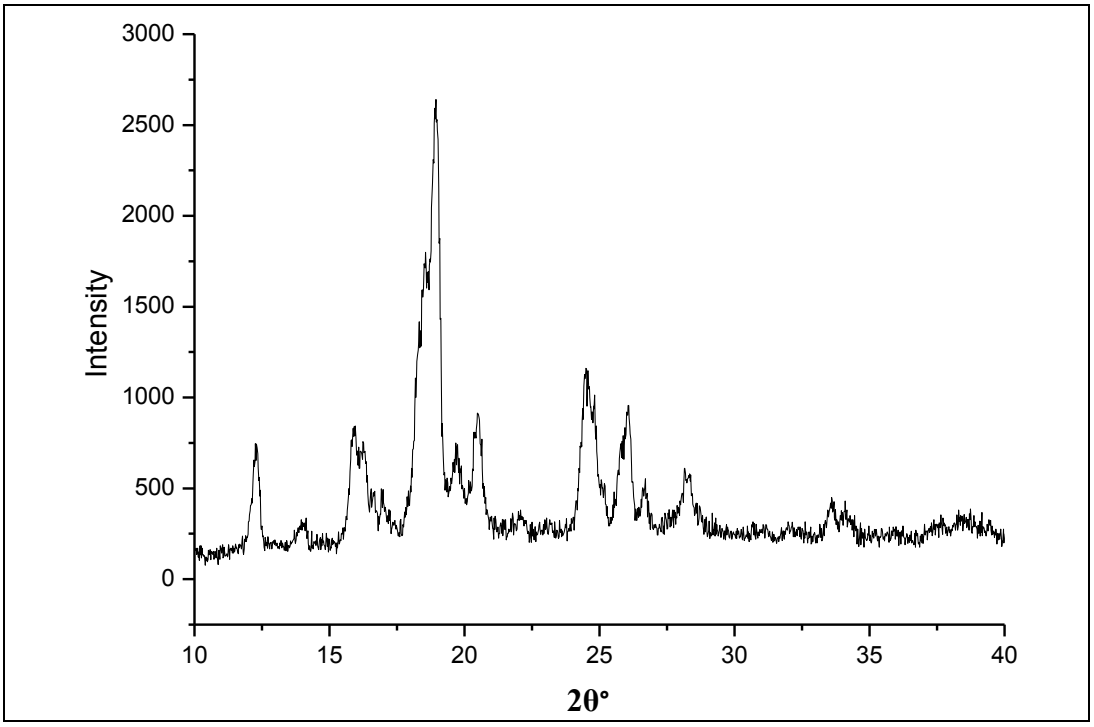

Figure A22: IR Spectra of co-ordination polymer **CP4**

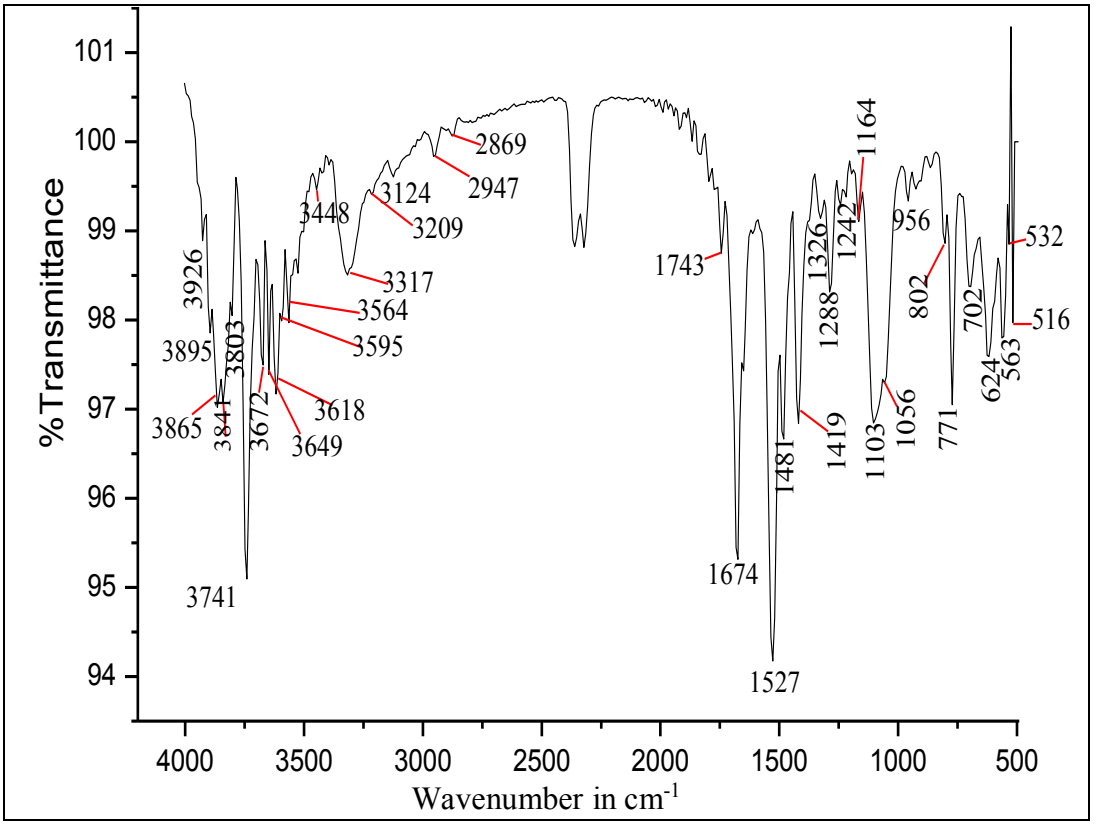

Figure A23: PXRD of co-ordination polymer **CP4**

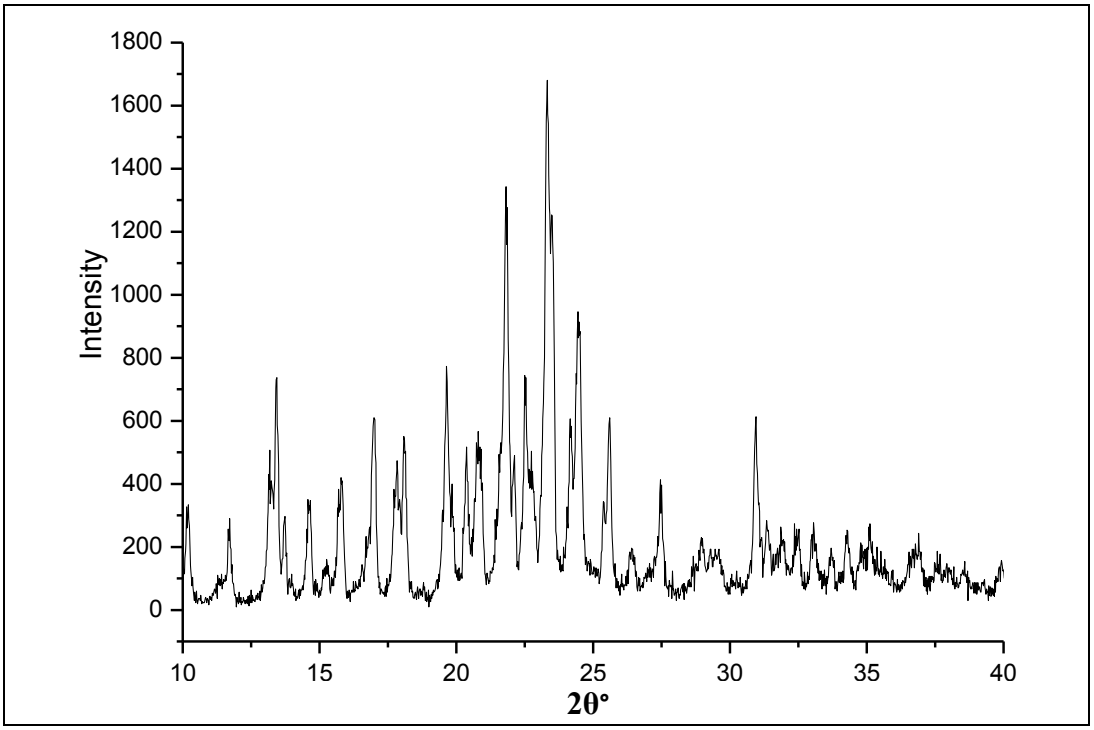

Figure A24: IR Spectra of co-ordination polymer **CP5**

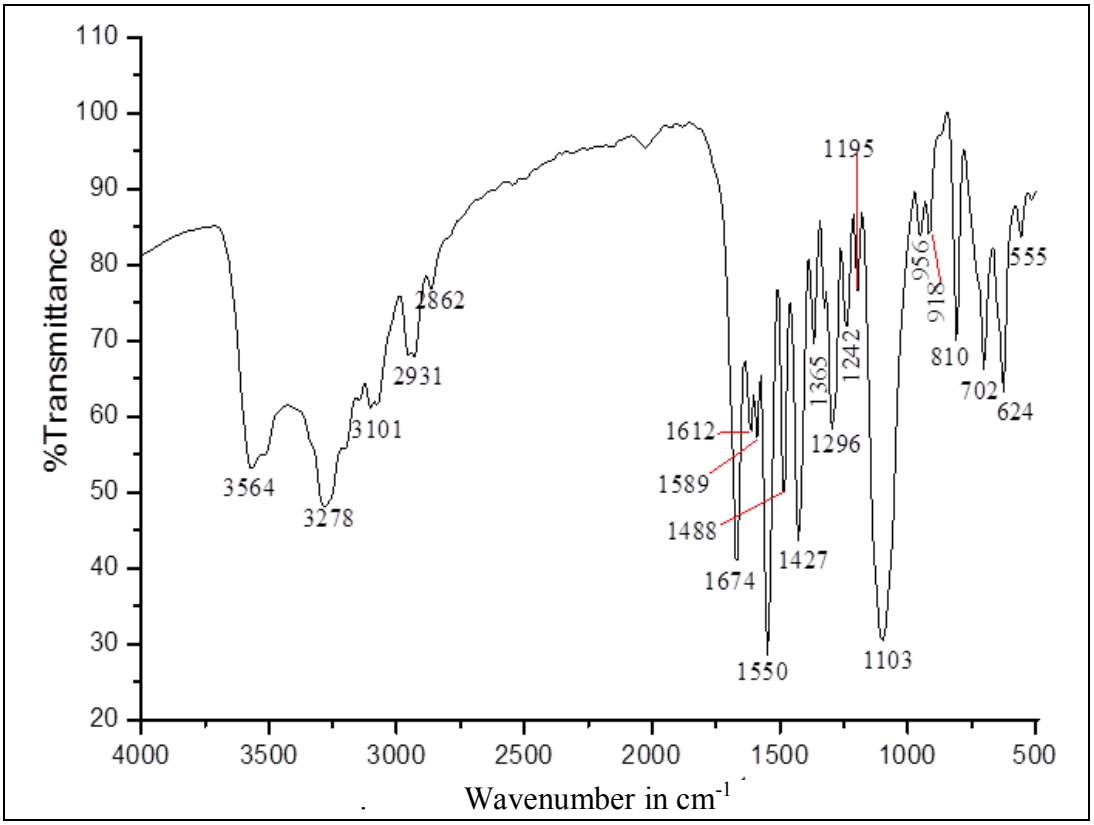

Figure A25: PXRD of co-ordination polymer **CP5**

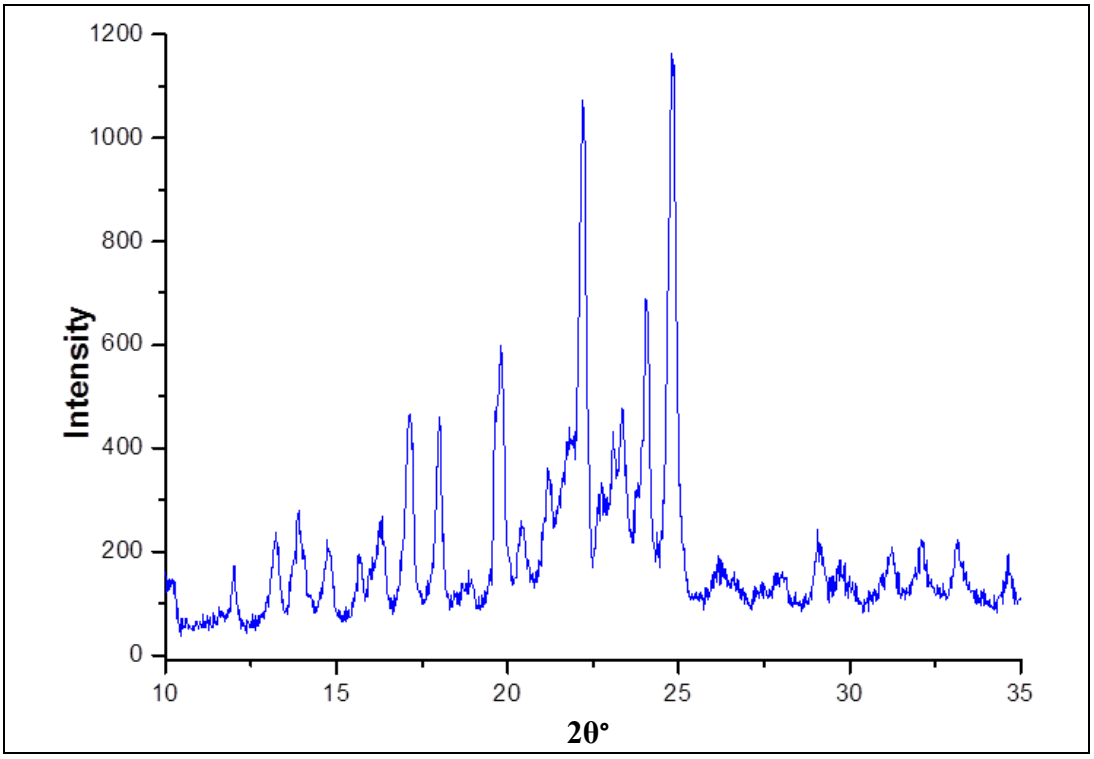

Figure A26: ORTEP of co-ordination polymer **CP3**

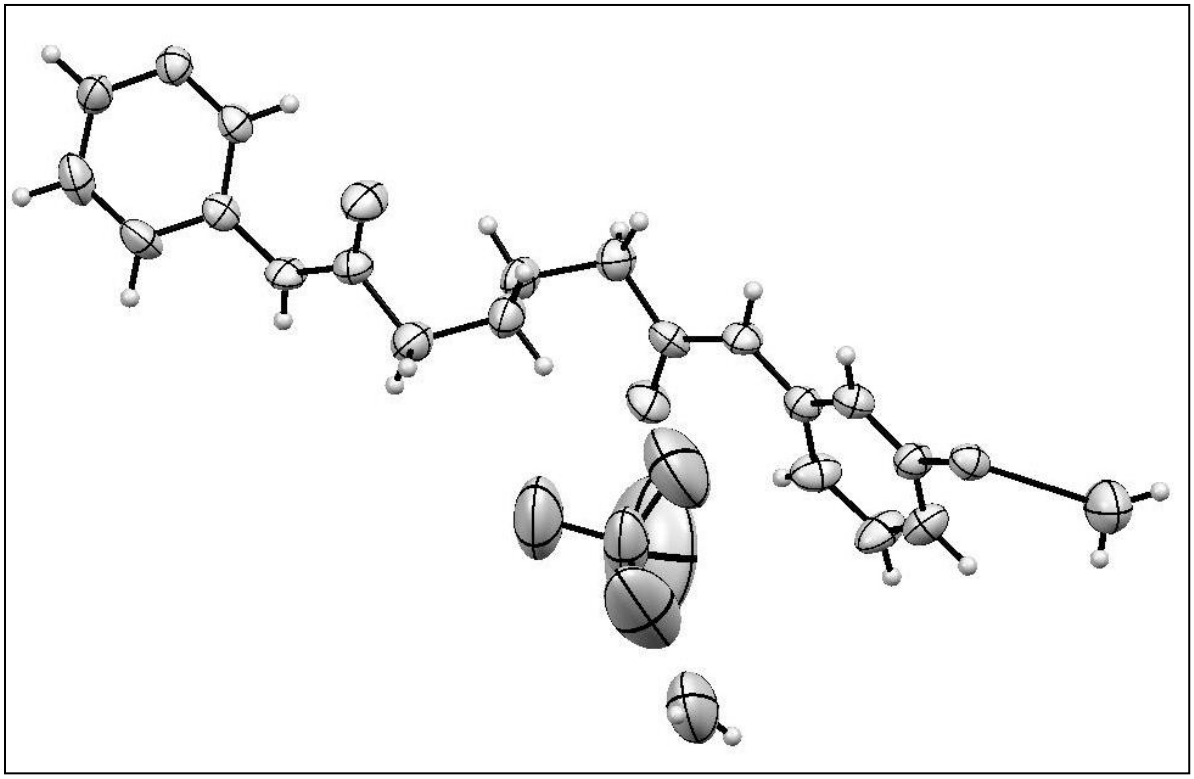

Figure A27: ORTEP of co-ordination polymer **CP4**

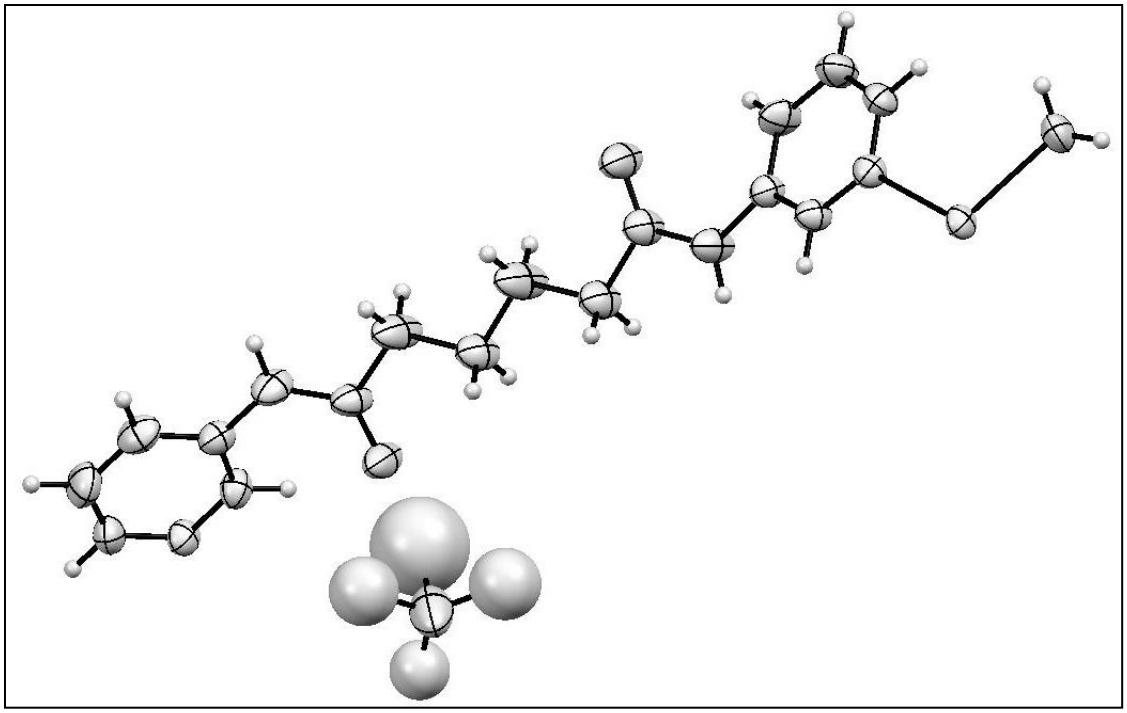

Figure A28: IR Spectra of co-ordination polymer **CP6**

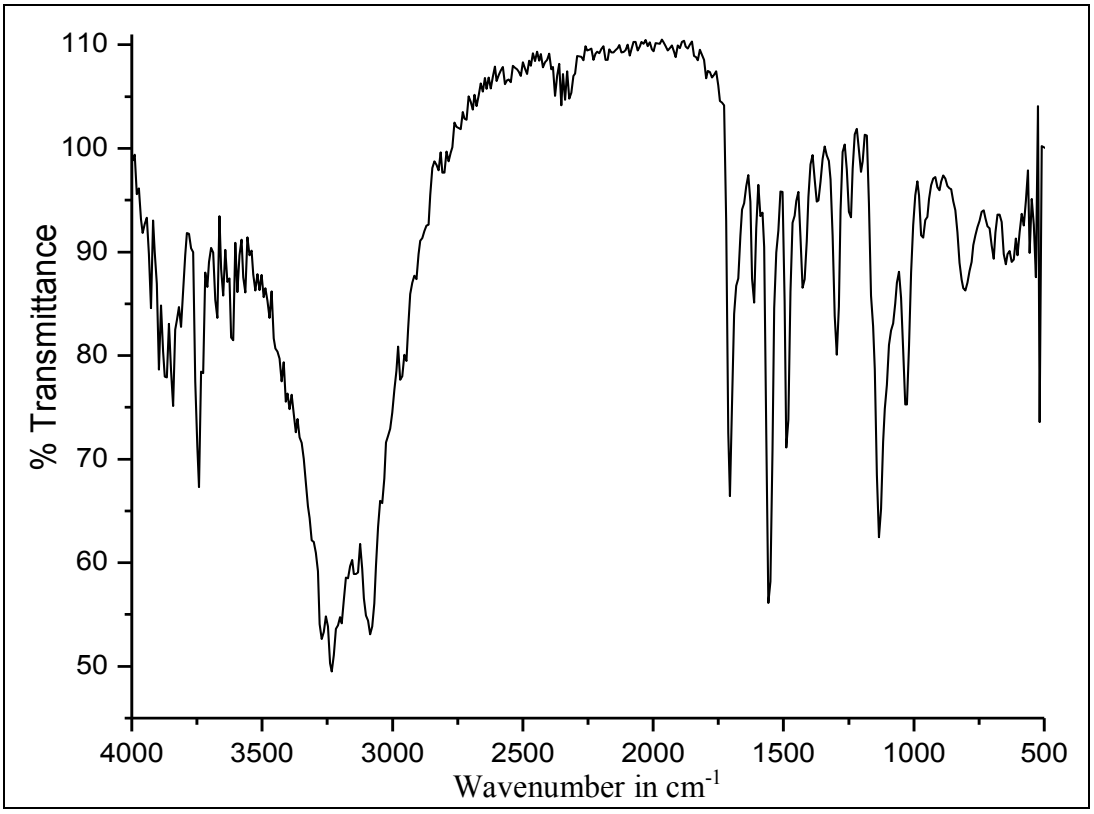

Figure A29: PXRD of co-ordination polymer **CP6**

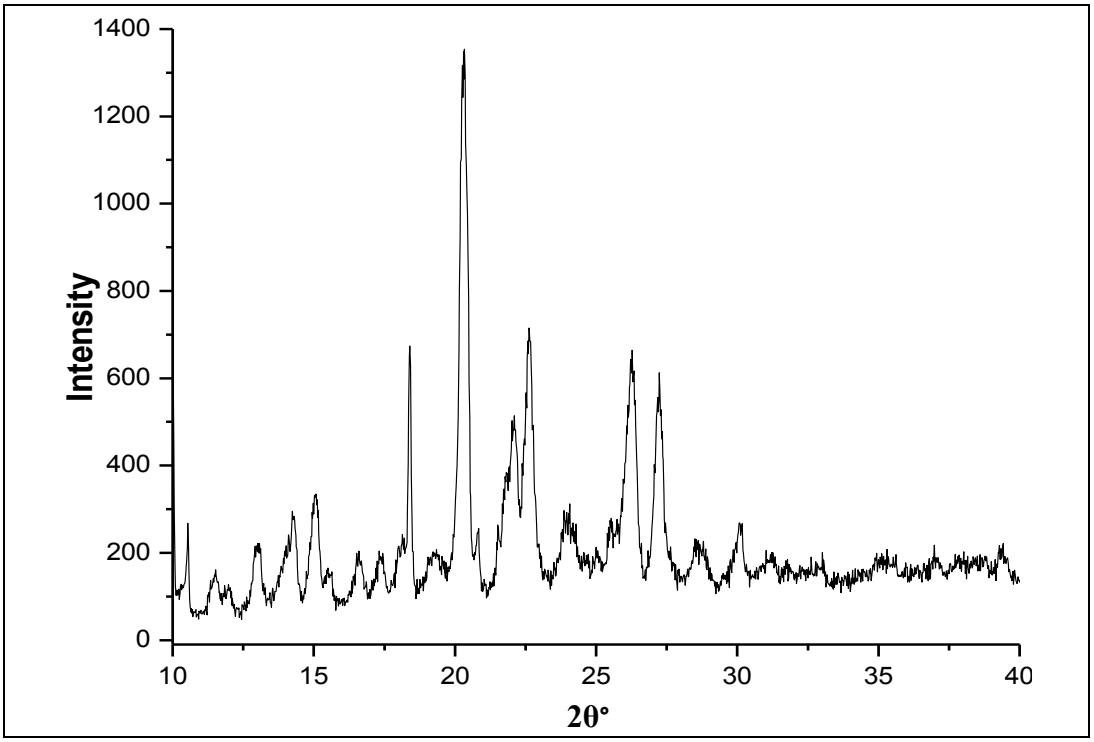

Figure A30: IR Spectra of Co-ordination Polymers **CP7**

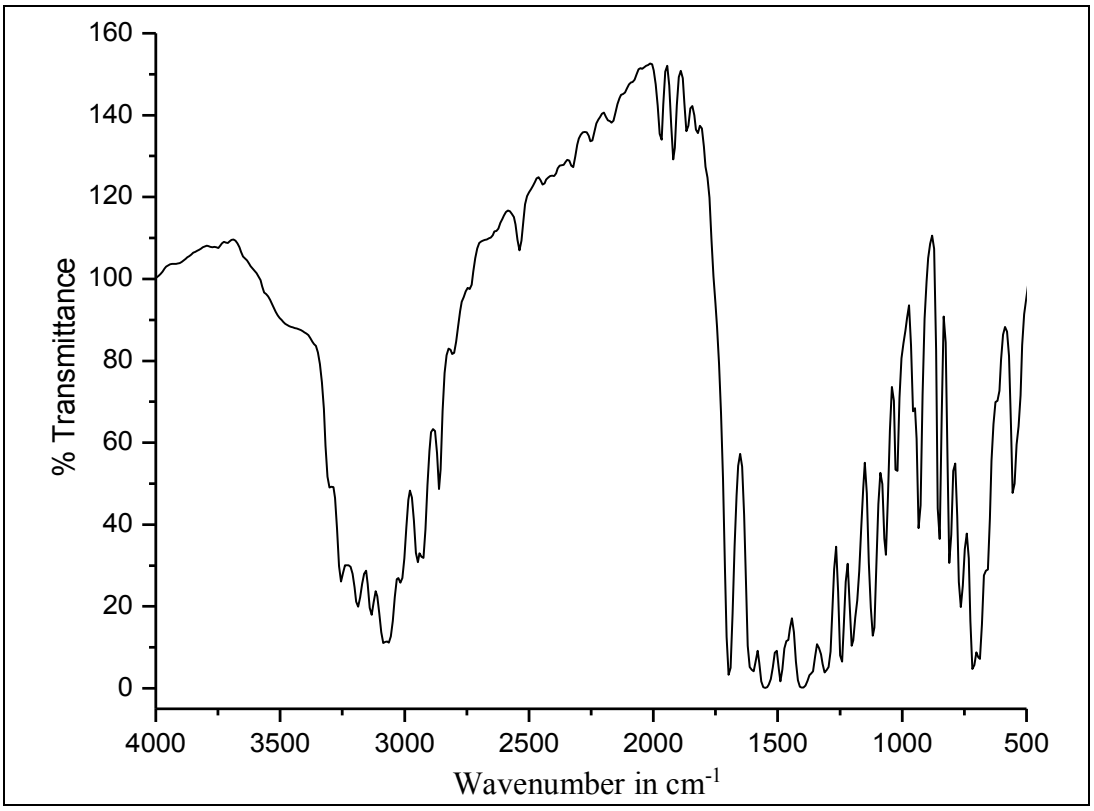

Figure A31: PXRD of Co-ordination Polymer **CP7**

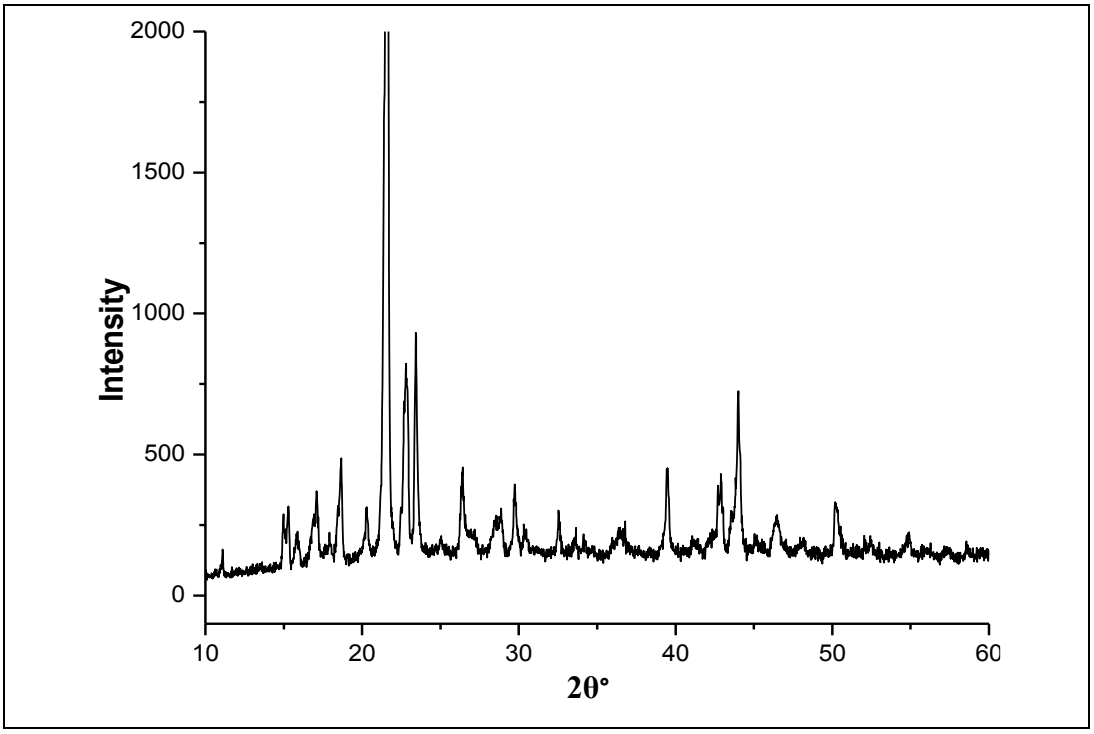

Figure A32: IR Spectra of (a) **CP6**, (b) **CP6** anion SO_4^{-2} exchanged with ClO_4^{-1}, (c) **CP3**

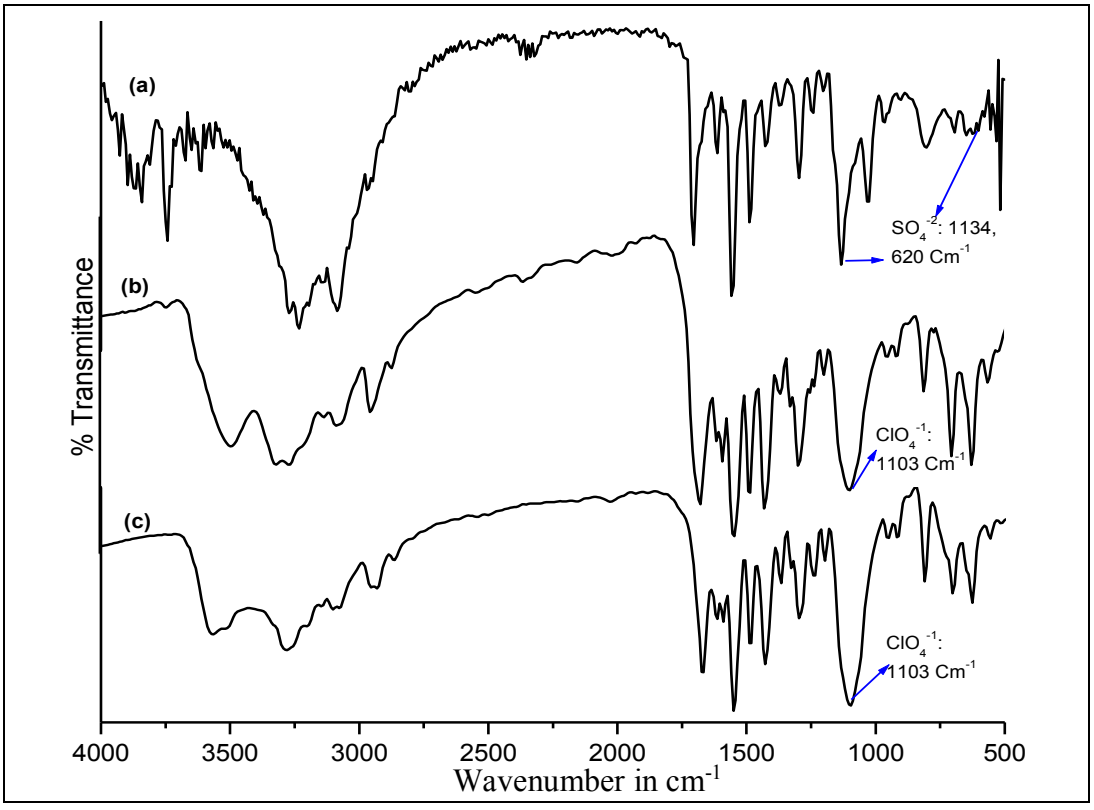

Figure A33: PXRD of (a) **CP6**, (b) **CP6** anion SO_4^{-2} exchanged with ClO_4^{-1}, (c) **CP3**

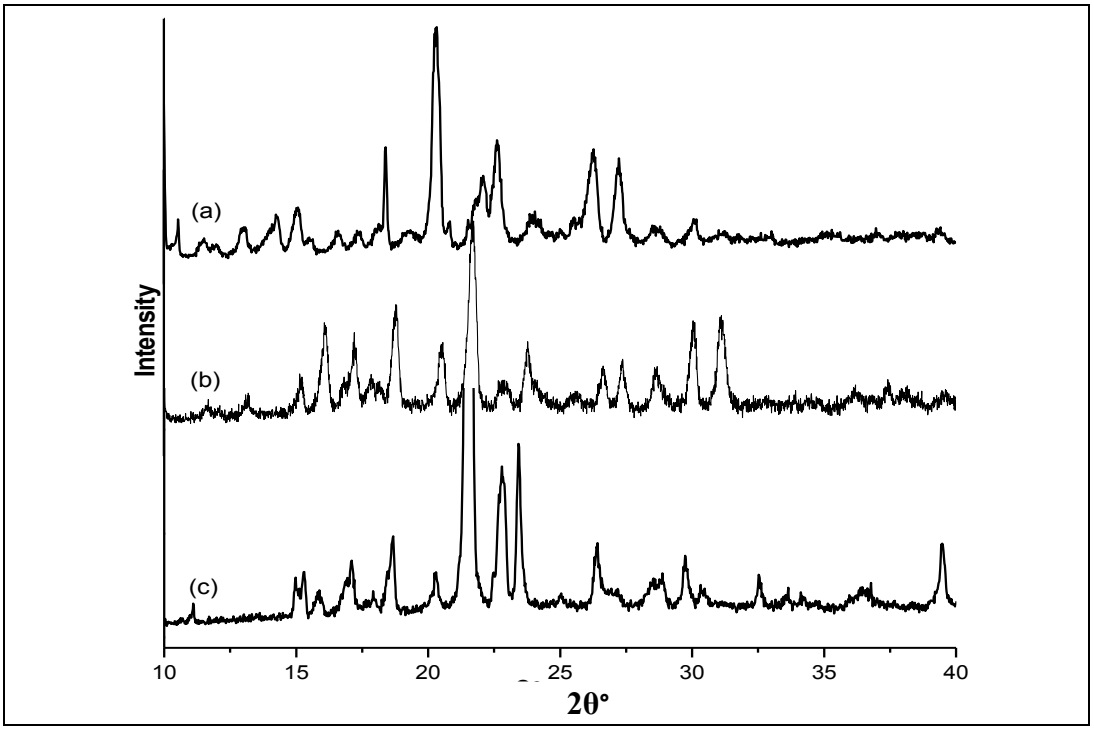

Figure A34: IR of (a) **CP6**, (b) **CP6** anion SO_4^{-2} exchanged with $C_6H_5COO^{-1}$, (c) **CP7**

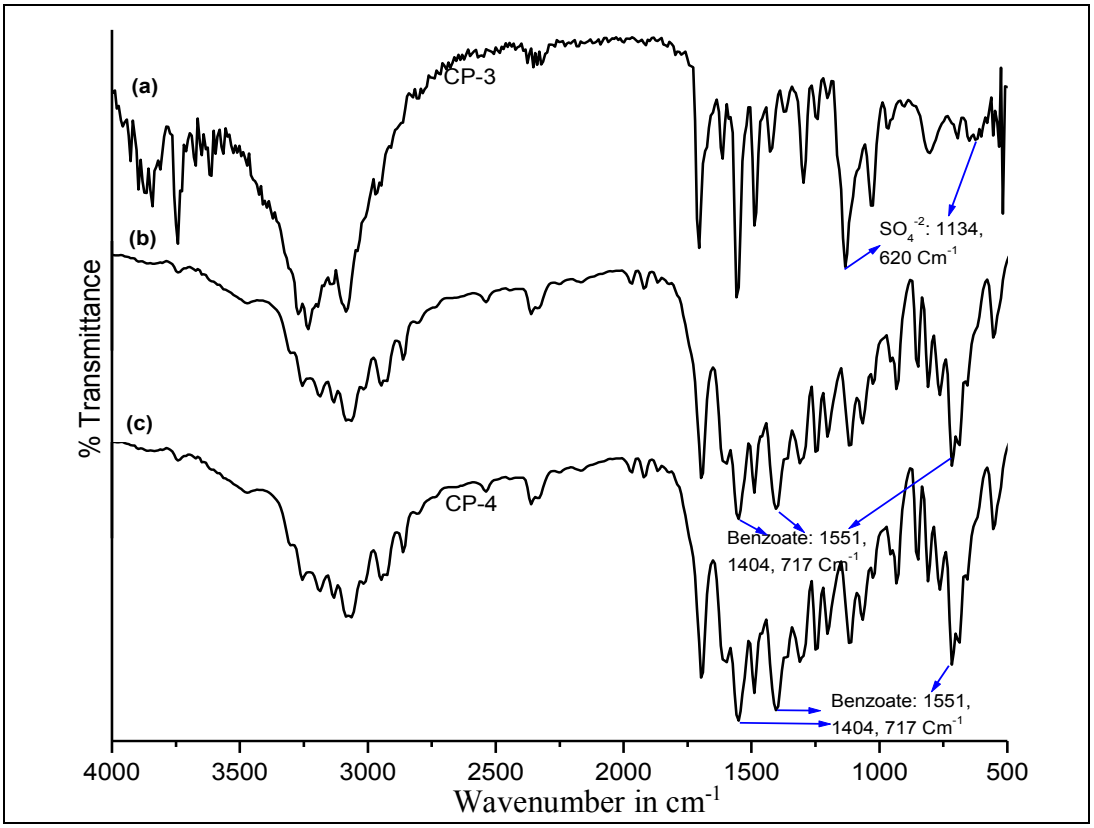

Figure A35: PXRD of (a) **CP6**, (b) **CP6** anion SO_4^{-2} exchanged with $C_6H_5COO^{-1}$, (c) **CP7**

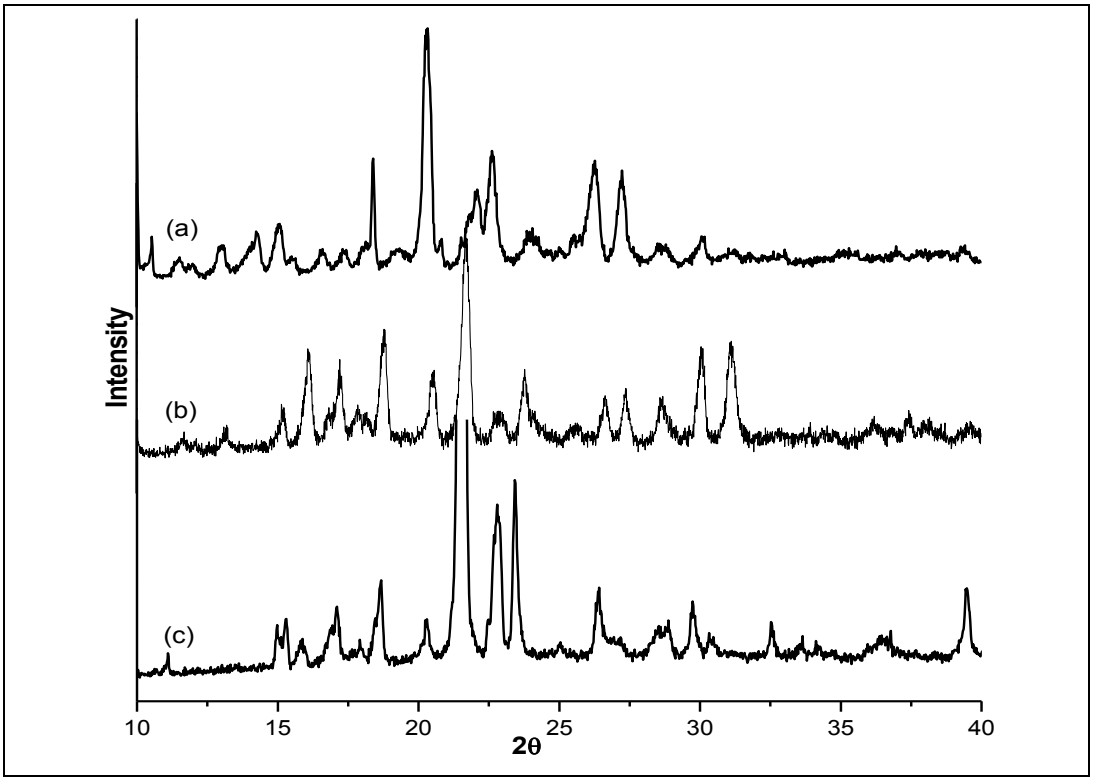

Figure A36: IR Spectra of Competitive Reaction Condition IV

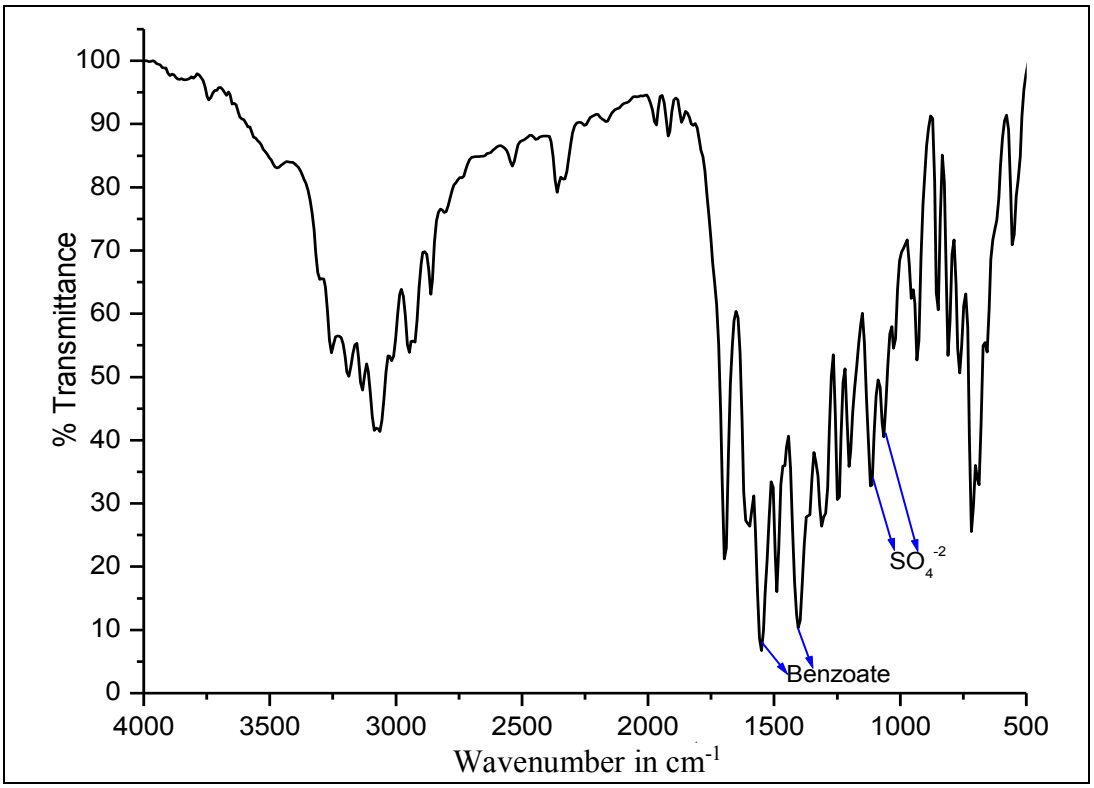

Figure A37: Powder XRD of Competitive Reaction Condition IV

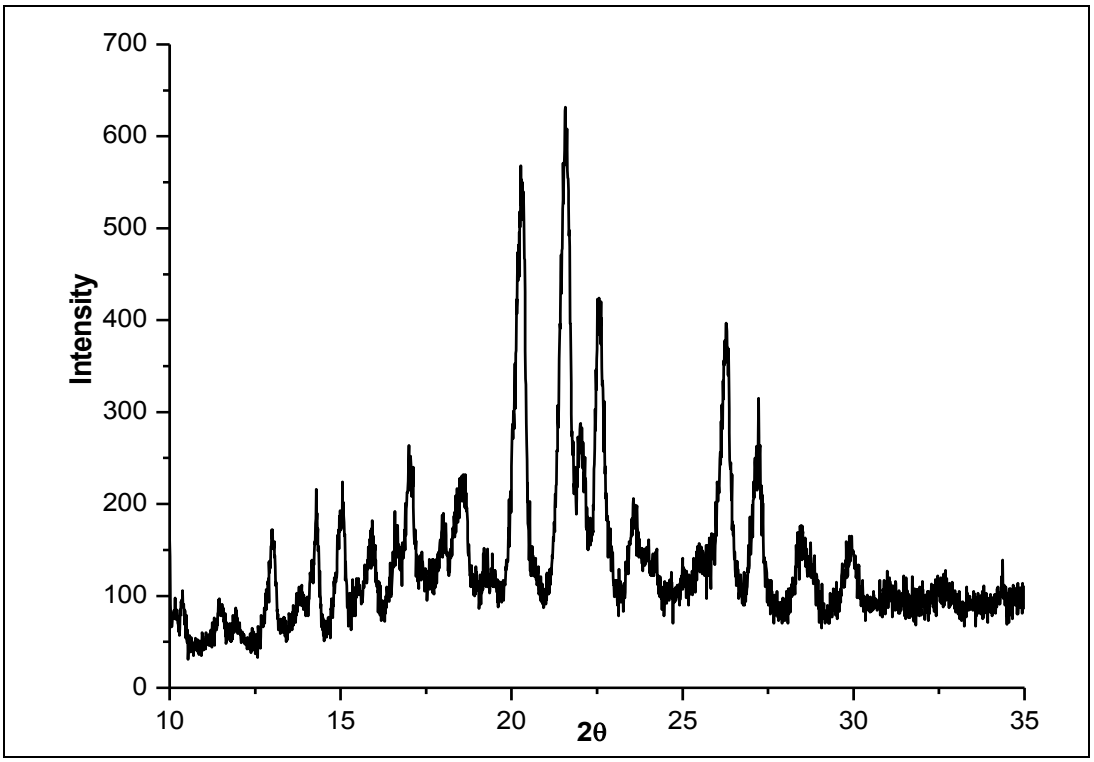

LIST OF PUBLICATIONS

1. **Suman, K.**; Rajnikant; Gupta, V. K.; Sarkar, M., Cooperative effect of "flexible" interaction and "flexible" framework in reversible intake and removal of aromatic guest molecules. *Dalton Transactions* **2013,** *42* (23), 8492-8497.

2. **Suman, K.**; Baig, F.; kant, R.; Gupta, V. K.; Mandal, S.; Sarkar, M., Is metal metathesis a framework-templating strategy to synthesize coordination polymers (CPs)? Transmetallation studies involving flexible ligands. *RSC Advances* **2014,** *4* (69), 36451-36457.

3. **Suman, K.**; Khullar, S.; Mandal, S. K.; Sarkar, M., Role of Anions in Assembling the Coordination Polymers of *bis*-pyridyl-alkanediamides. *Chemistry Select* **2016,** DOI: 10.1002/slct.201601249

4. **Suman, K.**; Sarkar, M., Analysis of Structure Properties Relationship of Co-ordination Polymers of Amide based Compounds. (manuscript under preparation)

LIST OF PAPERS PRESENTED IN CONFERENCES/SYMPOSIUMS

1. **Suman K**.; Sarkar, M. "Guest Exchange Dynamics of Porous Co-ordination Polymers (CPs)" at the Conference on Advances in Chemistry, Organized by Department of Chemistry at Birla Institute of Technology and Science, Pilani Campus, Pilani. (26th March, **2011**).

2. **Suman K.;** Sarkar, M. "Effect of Counter Anions & Guest Molecules in Assembling Metal-Organic-Frameworks (MOFs): A Case Study on the MOFs formed by amide-Based *Exo*-Bidentate Ligand" at National Symposium *On* Recent Trends in Chemical Science & Technology Organized by Department of Chemistry at Indian Institute of Technology, Patna. (3rd – 4th March, **2012**)

3. **Suman,K.**; Sarkar, M. "Interference of Pyridyl Moiety in Formation of Amide-to-Amide Hydrogen Bonds: A Case Study on the Crystal Structures of *Mono*-pyridyl-*mono*-amidealkanes and *Bis*-pyridyl-*bis*-amidealkanes" at 19th International Conference on Chemical Biology for Discovery: Perspectives and Challenges Organized by the Indian Society of Chemists & Biologists (ISCBC-2013) at Department of Chemistry, Mohanlal Sukhadia University, Udaipur. (2nd – 5th March, **2013**).

4. Baig, F.; **Suman, K**.; Sarkar, M. "Is hydrogen bonding along with flexible alkyl chain a way to generate dynamic coordination polymers? A case study on coordination polymers derived from *bis*-pyridyl-diamide ligands" at National conference on Recent developments in Chemical Sciences NCRDCS-14). (25th – 26th Febrary, **2014**).

5. **Suman, K**.; Sarkar, M. "Study on the Structrual Transformations of Coordination Polymers derived from *Bis*-Pyridyl Diamide Ligands on Exchange of Metal Centre and Counter Anions" at A National Conference on NANO- And FUNCTIONAL MATERIALS, Organized by Department of Chemistry at Birla Institute of Technology and Science, Pilani Campus, Pilani. (7th – 8th November, **2014**).

6. Baig, F.; **Suman, K**.; Sarkar, M. "Post Synthetic Studies on Coordination Polymers Derived from Bis-pyridyl Diamide Ligands" at 2nd Indo-German Workshop on Supramolecular Chemistry, conducted by University of Delhi. (30th March, **2015**)

7. **Suman,K**.; Sarkar, M. "Effect of Anions on Coordination Polymers (CPs) of Bis-pyridyl-alkanediamides" at International conference on Nascent Developments in Chemical Sciences, Organized by Department of Chemistry at Birla Institute of Technology and Science, Pilani Campus, Pilani. (16th – 18th October, **2015**).

8. Baig, F.; **Suman, K**.; Sarkar, M. "Structural transformations of coordination polymers on the counter anion exchange and metal-metathesis" at 44th National Seminar on Crystallography (NSC-2016), organized by NCCS, IISER Pune, and NCL Pune, Pune. (10th – 13th July-2016)

BRIEF BIOGRAPHY OF THE SUPERVISOR

Dr. Madhushree Sarkar is an Assistant Professor in Department of Chemistry, Birla Institute of Technology and Science Pilani (BITS Pilani), Pilani Campus. She had done her B.Sc. Department of Chemistry, St. Stephens College, University of Delhi, India (1997-2000) and M.Sc. from Department of Chemistry, Indian Institute of Technology, Kanpur, India (2000-2002). She received her Ph.D. from Department of Chemistry, Indian Institute of Technology, Kharagpur, India (2003-2007) under the supervision of Prof. Kumar Biradha. During her doctoral studies she worked on "Supramolecular Chemistry and Crystal Engineering" which involves understanding various Intermolecular Interactions, Molecular Recognitions, "Host-Guest" Chemistry and will ultimately lead to design and synthesize advanced materials for practical purposes (molecular sensing, storage, separation, catalysis).

Dr. **Madhushree Sarkar** joined BITS Pilani in as Assistant Professor in 2009. She has around nine years of research experience and six years of teaching experience. She is supervising three Ph.D students, as a result of her research accomplishment she has published 13 research papers in peer reviewed journals, presented papers and delivered lectures in several national and international conferences. She has completed two research project as PI.

BRIEF BIOGRAPHY OF THE CANDIDATE

Kumari Suman completed her B.Sc. from F. C. College (Hisar), Kurukshetra University, Kurukshetra , India (2003-2006) and M.Sc. from Department of Chemistry, Ch. Devi Lal University (Sirsa), India(2007-2009). During her Master Degree she did a project work entitled 'Aqueoustic study of DMSO in Benzene', using Interferometer under guidance of **Dr. H.K. Mudgil**.

In January 2011, she joined the Department of Chemistry, BITS Pilani for her doctoral research under the supervision of **Dr. Madhushree Sarkar**. During her doctoral studies, she received fellowship from BITS Pilani and in April 2012, she received assistantship from a UGC, UGC-BSR Fellowship. In December 2013, she has been appointed as PGT Chemistry (HES-II) in Department of School Education, Haryana. She has published three research articles, communicated one manuscript in peer reviewed international journals and presented papers in eight conferences/symposiums. Her research interest lies in designing and developing advanced materials (Super Molecules), can be used for practical purposes (molecular sensing, storage, separation, and catalysis).